ELECTROCATALYTIC CYCLING OF NICOTINAMIDE COFACTORS BY *RALSTONIA EUTROPHA* SOLUBLE HYDROGENASE

ZULKIFLI IDRIS

WADHAM COLLEGE

UNIVERSITY OF OXFORD

TRINITY TERM 2012

A thesis submitted to the
Board of the Faculty of Physical Sciences,
for the degree of
Doctor of Philosophy,
University of Oxford

Acknowledgements

This Thesis would have never been completed without the help and expert supervision of Kylie. I thank her for all her enthusiasm, encouragement, excellent advice, fruitful discussion, never-tired spirit and wonderful years in Oxford. I will always remember that she is the person that showed me around London when I first arrived in the UK, and the one that managed to nicely ask a Wadham College's Scout to give me a Wadham water bottle at the first conference I attended. I extend my gratitute to Dr Oliver Lenz and Lars Lauterbach, of Humboldt University Berlin for supplying the protein samples I have used in this Thesis.

I would also like to extend my sincere appreciation and thanks to Holly Reeve, Kate Simpson-Wells and Tommy Lyle for helping me with experiments-without whom I would have ended up doing 365 days of experiments each year! Holly should be credited for her help in proof reading and her excellent thesis formatting skills. Phil should also be thanked for his expertise in IR and in getting me wonderful spectra of pyruvate/lactate. I also thank Ian for his help with proof reading my chapters and Dan for his assistance with FPLC.

Juan Liu is specially thanked for her endless advice and discussion on the SH. The meals at selected restaurants in Oxford will always be remembered. I thank all the members of the Vincent group, past and present for friendship, in particular Adam (I vividly remember when we had our first group dinner at a Lebanese Restaurant), Pong, Min-Wen, Gary, Jonathan, Charlie, Robert and all the Part IIs.

Big thanks should go to Jon for his moral support. I appreciate the generosity of the Malaysian government for financing my studies in Oxford. Also, Wadham College for travel and living-out grants.

I thank my mother for always being there listening to me and for her support throughout all my studies at University.

I thank someone who said this to me:

'Hey Zul. I think you should stop freaking out.'

Electrocatalytic cycling of nicotinamide cofactors by *Ralstonia eutropha* Soluble Hydrogenase

Zulkifli Idris, Wadham College, University of Oxford
A thesis submitted for the degree of Doctor of Philosophy, Trinity Term 2012

Nicotinamide cofactors in their reduced and oxidised forms are important redox agents in biology. Of about 3000 dehydrogenases available to date, many require these cofactors for their activity. Dehydrogenases are of interest to chemists as they offer asymmetric catalysis to yield chiral products. The requirement of dehydrogenases for nicotinamide cofactors necessitates research into finding the best way of recycling the oxidised or reduced forms of these cofactors. Electrocatalytic NAD(P)H oxidation and $NAD(P)^+$ reduction on standard electrodes is problematic due to unwanted side reactions and high overpotential requirements, but in Nature efficient enzyme catalysts are available to facilitate these reactions.

The focus of this Thesis, the Soluble Hydrogenase of *R. eutropha* (SH) is a multimeric bidirectional hydrogenase that couples H_2 oxidation to the reduction of NAD^+ to NADH. Protein Film Electrochemistry (PFE) has been employed to study NAD^+-reducing catalytic moieties of the SH for the first time. It is shown that SH subunits on an electrode are able to catalyse NADH oxidation and NAD^+ reduction efficiently with minimal overpotential, which is significant because *in vivo*, NAD(H) cycling is coupled to $2H^+/H_2$ cycling and these reactions are closely spaced in potential. Substrate affinities and inhibition constants for the SH, determined using PFE are discussed in the context of the SH function and the related catalytic domains of respiratory Complex I. A range of molecules that are known to inhibit the related Complex I have been investigated for their ability to inhibit the SH moieties: the

similarity between inhibition constants is consistent with structural and functional similarity between the SH and Complex I. The ability of the SH moieties to sustain NAD(H) catalysis in the presence of O_2 is also demonstrated and is consistent with the requirement for the SH to function under aerobic conditions and to reactivate the inactivated hydrogenase moiety by supplying low potential electrons from NADH.

Engineered variants of the SH, designed to enhance the affinity towards $NADP^+$, were investigated for the first time, using PFE. Electrochemical characterisation of the variants is presented and results are discussed alongside findings on the wild-type SH. The variants are shown to exhibit $NADP^+$ reduction, and to have higher affinity towards $NADP^+$ than the wild-type SH. The first efficient $NADP^+$ reduction and NADPH oxidation is observed for one of the variants on a graphite electrode and the best variant showed a K_M of 1.7 mM for $NADP^+$.

This Thesis also provides evidence for the ability of moieties of the SH to be used in cofactor regeneration systems. Two novel systems are demonstrated. The first involves H_2-driven NADH recycling based on the NAD^+-reducing moiety of the SH immobilised on graphite particles together with a hydrogenase or platinum, with electrons from H_2 passed from the hydrogenase through the graphite to the NAD^+-reducing moiety. The second involves an electrode modified with the NAD^+-reducing moiety of the SH, and is demonstrated as an electrochemical NADH recycling system coupled with NADH-dependent pyruvate reduction to lactate by lactate dehydrogenase. The ability of variants of the SH to catalyse $NADP^+$ reduction suggests that it may also be possible to use these systems for recycling NADPH for catalysis of important biotransformation reactions by NADPH-dependent dehydrogenases.

Abbreviations

A. aeolicus	*Aquifex aeolicus*
ADP	adenosine diphosphate
ADP-Ribose	adenosine diphosphate ribose
A. fulgidus	*Archaeoglobus fulgidus*
AMP	adenosine monophosphate
ATP	adenosine triphosphate
A. vinosum	*Allochromatium vinosum*
C. pasterianum	*Clostridium pasterianum*
DCPIP	2,6-dichlorophenolindophenol
D. gigas	*Desulfovibrio gigas*
E. coli	*Escherichia coli*
E(NAD^+/NADH)	Potential for NAD^+/NADH
EPR	electron paramagnetic resonance spectroscopy
FAD	Flavin adenine dinucleotide
FMN	Flavin mononucleotide
FT-IR	Fourier transform infra-red spectroscopy
GDH	Glutamate dehydrogenase
IR	Infrared spectroscopy
LDH	Lactate dehydrogenase
MBH	Membrane bound hydrogenase
NAD^+	nicotinamide adenine dinucleotide (oxidised form)
NADH	nicotinamide adenine dinucleotide (reduced form)
$NADP^+$	nicotinamide adenine dinucleotide phosphate (oxidised form)
NADPH	nicotinamide adenine dinucleotide phosphate (reduced form)
PFE	protein film electrochemistry
PGE	pyrolytic graphite 'edge'
R. eutropha	*Ralstonia eutropha*
Rh. opacus	*Rhodococcus opacus*
RH	regulatory hydrogenase
R. metallidurans	*Ralstonia metallidurans*
SCE	saturated calomel electrode
SH	soluble hydrogenase
SHE	standard hydrogen electrode
T. thermophilus	*Thermus thermophilus*

Table of Contents

Chapter 1: Introduction 1

1.1 Global redox cycles 2

1.2 Hydrogen cycling in *Ralstonia eutropha* H16 5

1.3 Common biological redox centres 7

1.3.1 Iron-Sulphur clusters 7
1.3.2 $NAD(P)^+$/NAD(P)H 10
1.3.3 Flavins 12
1.3.4 Quinones 15

1.4 Hydrogenases: Classification on the basis of active site metals 16

1.4.1 Fe hydrogenase 16
1.4.2 FeFe hydrogenase 18
1.4.3 NiFe hydrogenase 20

1.5 Classification of NiFe hydrogenases on the basis of biological functions 21

1.6 The Soluble Hydrogenase of *Ralstonia eutropha* H16 22

1.6.1 Relationship between the SH and Complex I 25
1.6.2 The NADH binding site 30
1.6.3 FeS clusters composition in the SH 32
1.6.4 Other Soluble Hydrogenases 34

1.7 Applications of Soluble Hydrogenases in cofactor recycling 35

1.8 NAD(H) cycling on electrode 36

1.9 Protein Film Electrochemistry for studying redox enzymes 40

1.10 Applications of enzymes on electrodes 41

1.10.1 Enzyme electrodes for H_2/O_2 fuel cells 41
1.10.2 Biosensors 43

1.11 Aims and structure of this Thesis 44

1.11.1 Understanding NAD^+/NADH cycling 44
1.11.2 Exploring $NADP^+$/NADPH cycling 44
1.11.3 Developing a cofactor regeneration system 45

Chapter 2: Electrochemical Theory and Experimental Methods 46

2.1 Introduction 47

2.2 Electrode surfaces and protein binding 48
2.2.1 Film loss and selected film stabilisation strategies 52
2.3 Methods of potential control 54
2.3.1 Chronoamperometry 55
2.3.2 Cyclic Voltammetry 56
2.3.3 Non-Faradaic current contributions 57
2.3.4 Faradaic current contributions from adsorbed species 58
2.4 Electrochemical apparatus 65
2.4.1 Electrochemical cell setup 65
2.4.2 Glove box 68
2.5 Enzymes and preparation of enzyme films 68
2.5.1 Purification of *Ralstonia eutropha* SH HoxFU moiety 68
2.5.2 Membrane Bound Hydrogenase (MBH) 70
2.5.3 Lactate dehydrogenase 70
2.6 Solutions and gases 70
2.6.1 Electrochemical buffers 70
2.6.2 Substrate purification 71
2.6.3 Gases 76
2.7 Graphite particles 76
2.8 Michaelis-Menten kinetics 77
2.8.1 Ways of analysing enzyme affinity constants 81
2.9 Enzyme inhibition 83
2.10 Relation of this Chapter to other Chapters 87

Chapter 3: Electrochemical Characterisation of Diaphorase Moiety of Soluble Hydrogenase *Ralstonia eutropha* H16 89

3.1 Introduction 90
3.2 Electrocatalytic NAD^+/NADH cycling on a bare graphite electrode 91
3.3 Investigation of electrocatalytic NAD^+/NADH cycling by HoxFU 93
3.3.1 Interpreting an electrocatalytic cyclic voltammogram for HoxFU 93
3.3.2 The Effect of pH and temperature on catalytic activity 98
3.3.3 Potential-dependent inactivation 103
3.4 The effect of substrate on catalytic activity 109
3.4.1 K_M for NADH oxidation 110

3.4.2 K_M for NAD^+ reduction 114
3.4.3 Enzyme activation 116
3.5 The effect of potentials on K_M values 119
3.5.1 NADH oxidation 120
3.5.2 NAD^+ reduction 122
3.6 Does HoxI have any effect on HoxFU activity? 124
3.6.1 NADH catalysis 125
3.6.2 Inactivation at low potentials 126
3.7 Summary 127

Chapter 4: Inhibition 128

4.1 Product inhibition of HoxFU 129
4.1.1 NADH oxidation 129
4.1.2 NAD^+ reduction 137
4.1.3 Analysing HoxFU product inhibition assuming worst case scenario film loss. 142
4.1.4 Discussion of product inhibition results 144
4.2 Investigating the effect of Complex I inhibitors on HoxFU 145
4.2.1 Adenosine Diphosphate (ADP) 146
4.2.2 Adenosine Monophosphate (AMP) 148
4.2.3 Adenosine Triphosphate (ATP) 150
4.2.4 Adenosine Diphospho-Ribose (ADP-Ribose) 153
4.2.5 5,5'-dithiobis-(2-nitrobenzoic acid) (DTNB) 156
4.2.6 General discussion on the inhibition of HoxFU by Complex I inhibitors 158
4.3 HoxFU turnover in the presence of O_2 160
4.3.1 NADH oxidation 160
4.3.2 NAD^+ reduction 161
4.3.3 Discussion: Observations of Superoxide ($O_2^{\cdot-}$) production in solution assays of HoxFU 167
4.4 Final summary of HoxFU inhibition implications for SH catalysis 168
4.4.1 Direction of catalysis and possible control mechanisms 169
4.4.2 Potential-dependent effects on activity and FMN release 171
4.4.3 Ability of the SH to function under aerobic conditions 173
4.4.4 Towards applications in the supply of NADH to NADH-dependent dehydrogenases 174

Chapter 5: Towards $NADP^+$/NADPH cycling 176

5.1 Introduction 177

5.2 Electrocatalytic activity of wild type HoxHYFU 180

5.2.1 Interpreting an electrocatalytic cyclic voltammogram for HoxHYFU 180

5.2.2 Quantifying substrate affinity for NAD^+ and NADH 184

5.2.3 Potential dependent inactivation 186

5.3 Are $NADP^+$ and NADPH substrates or inhibitors for HoxFU, $HoxFUI_2$ and HoxHYFU? 188

5.3.1 $NADP^+$ reduction and NADPH oxidation 188

5.3.2 Investigation of $NADP^+$ and NADPH as inhibitors 191

5.3.3 Quantifying substrate affinity for $NADP^+$ and NADPH 193

5.4 Site-directed mutagenesis designed to increase affinity for $NADP^+$/NADPH 198

5.4.1 HoxHYFU D401K 202

5.4.2 Overall electrochemical data for variants 213

5.4.3 HoxHYFU D401K/D340A 216

5.5 Summary 217

Chapter 6: Applications 219

6.1 Introduction 220

6.2 Particles for H_2-driven cofactor recycling 224

6.2.1 The thermodynamics of the reaction 224

6.2.2 Using HoxFU and Platinised Particles 228

6.2.3 Finding Suitable Enzymes and Conditions for NADH Regeneration 232

6.2.4 Using graphite particles with MBH and HoxFU for NADH regeneration 237

6.2.5 NADH regeneration in the presence of O_2. 240

6.3 Electrochemical NADH regeneration for coupling HoxFU and Lactate Dehydrogenase on electrode 242

6.3.1 Regeneration of NADH for lactate dehydrogenase 242

Chapter 7: Summary 253

References 259

Appendix 1 I

Appendix 2 VII

Appendix 3 XIV

Appendix 4 XXI

Chapter 1: Introduction

1.1 Global redox cycles

Life on planet Earth is believed to have started 3.8 billion years ago, and has since evolved and responded to changes in the planetary environment. The early atmosphere was reducing and rich in H_2 and methane.[1-3] Somewhere between 3.2 and 2.4 billion years ago, O_2 begins to accumulate with the emergence of photosynthetic organisms such as cyanobacterial microbes.[4] It is predicted that the partial pressure of O_2 at the atmospheric level of Earth back in 3.2 billion years ago used to be 10^{-12}-fold lower than the present value. The lower atmosphere now comprises 21 % O_2, together with 0.000055 % H_2. Figure 1 illustrates the major cycles for carbon, hydrogen and oxygen on our planet.[4] Carbon in the atmosphere exists mainly in the form of carbon dioxide, CO_2. This gas is captured by plants during photosynthesis and this process releases O_2 and generates biomass that is eventually further utilised by animals and microbes, or buried in organic sediments. Respiration harnesses the energy from biomass, at the same time releasing CO_2 back to the atmosphere. Human industrial processes such as combustion add to the total volume of CO_2 in the atmosphere which contributes to the increasing level of greenhouse gases.

Chemists have become increasingly interested in understanding the biogeochemical cycling of C, N, O and H both because of its importance to climate issues but also because we may be able to learn from the chemistry occurring in microorganisms. In the next Section, discussion on the ability of microbes to use H_2 as a fuel is presented.

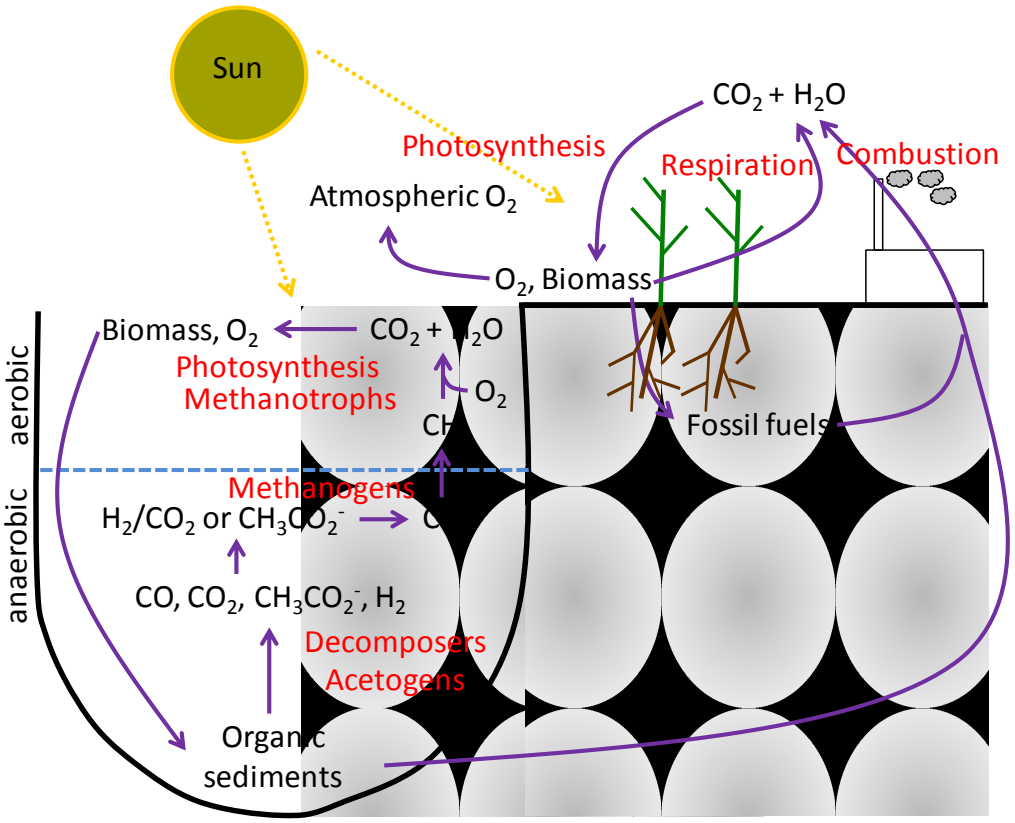

Figure 1. Global biogeochemical cycles for carbon, hydrogen and oxygen on earth. This picture was constructed according to reference[4].

Hydrogen as a fuel in biology

Hydrogen gas is often regarded as a possible energy carrier in a future clean green economy by chemists and technologists. In biology, many microorganisms exploit H_2 as an energy source, the highest energy yield being provided by the oxidation of H_2 by O_2.[5] Figure 2 shows an illustration of H_2 cycling in aquatic systems, such as pond or wetland soil.

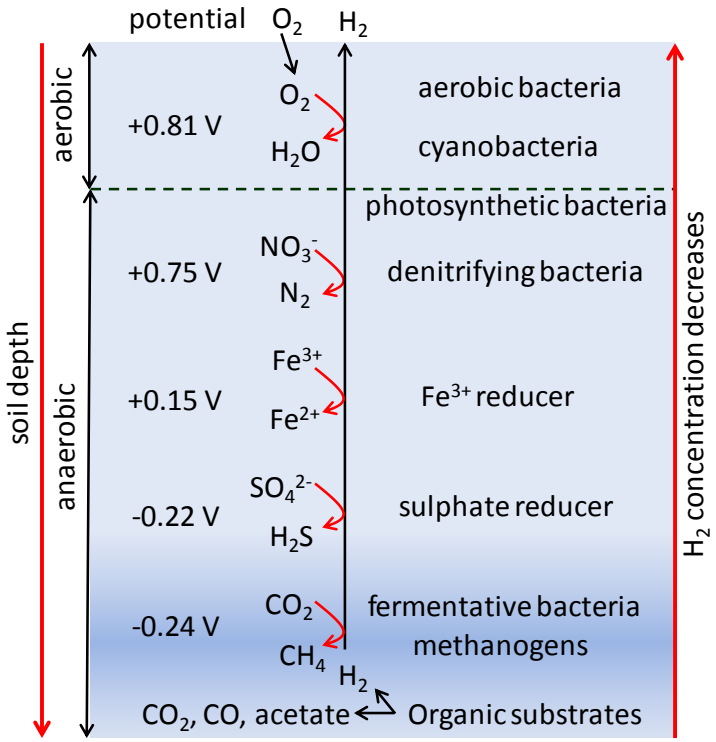

Figure 2. A schematic representation of certain redox reactions which contribute to production and consumption of H_2 in submerged wetland soil. Adapted from refs[1, 6].

At the bottom of the hierarchy (the anoxic sediment), fermentation of organic matter by fermentative bacteria takes place and H_2 and CO_2 are excreted as waste products which are subsequently utilised by methanogens for the reduction of CO_2 to methane.[7, 8] The remaining biologically produced H_2 is then used as reducing power by other organisms such as the sulphate reducing bacteria. Species like *Desulfovibrio* and *Desulfomicrobium* reduce sulphate, SO_4^{2-} to sulphide, H_2S.[9] Further up the anaerobic environment, families of Fe^{3+} reducers such as *Geobacter* use electrons from H_2 oxidation for the reduction of Fe^{3+} to Fe^{2+}.[10] It has also been reported that these species can utilise nitrate and oxygen as alternative electron acceptors. Levels of H_2 are further depleted by denitrifying bacteria that use H_2 as an energy source for reduction of nitrate to dinitrogen.[11] Close to the soil surface, the conditions are now aerobic due to contact with air and also because of O_2 production from photosynthesis by species like

cyanobacteria.[12] Aerobic bacteria such as *Ralstonia* are thus equipped to encounter O_2 and to use H_2 to reduce O_2 to water.[13, 14] Oxidation of H_2 by oxidants shown in Figure 2 produces energy which is recovered, for example in the form of ATP by oxidative phosphorylation. Conrad and coworkers found that the H_2 concentration at atmospheric conditions (0.5 ppm) was too low for H_2 uptake by most microorganisms, postulating that microbes may rely on H_2 supplemented by geological or other biological activity.[6] However, recently they reported that *Streptomyces* hydrogenase extracted from soil is able to oxidise atmospheric H_2, suggesting a very high affinity for H_2.[15]

1.2 Hydrogen cycling in *Ralstonia eutropha* H16

As discussed earlier, most H_2 gas produced by anaerobic fermentation is consumed in the anoxic environment by archea, sulphate reducers and anoxygenic phototrophs.[6] Therefore, only a small percentage of H_2 enters the aerobic environment and microbes living in this environment have adapted their H_2 oxidising systems to the small percentage of H_2 available and to exposure to O_2. An example of a class of microbe that has successfully adapted to this environment is the group of facultative chemolithoautotrophic Knallgas bacteria.[13, 14] They are known as Knallgas bacteria due to their ability to scavenge H_2 and survive exposure to O_2. One well-studied Knallgas bacterium is *Ralstonia eutropha* H16.[13] This β-proteobacterium hosts at least three NiFe hydrogenases: a periplasmic Membrane Bound Hydrogenase (MBH), a cytoplasmic Soluble Hydrogenase (SH) and a H_2-sensing Regulatory Hydrogenase (RH) as shown in Figure 3.[13, 16]

The MBH is composed of two subunits; the large subunit which harbours the NiFe active site is called HoxG and a small subunit, HoxK contains three FeS clusters which act as electron relay centres.[17, 18] The MBH is anchored to the membrane via the

hydrophobic C-terminal domain of HoxK and linked to the respiratory chain via a di-heme cytochrome *b*, HoxZ.[19] This hydrogenase is primarily involved in H_2 oxidation thus generating a H^+ gradient, driving the formation of ATP while the electrons from H_2 oxidation are transferred to the quinone pool, and eventually used for reduction of O_2 to H_2O.[13]

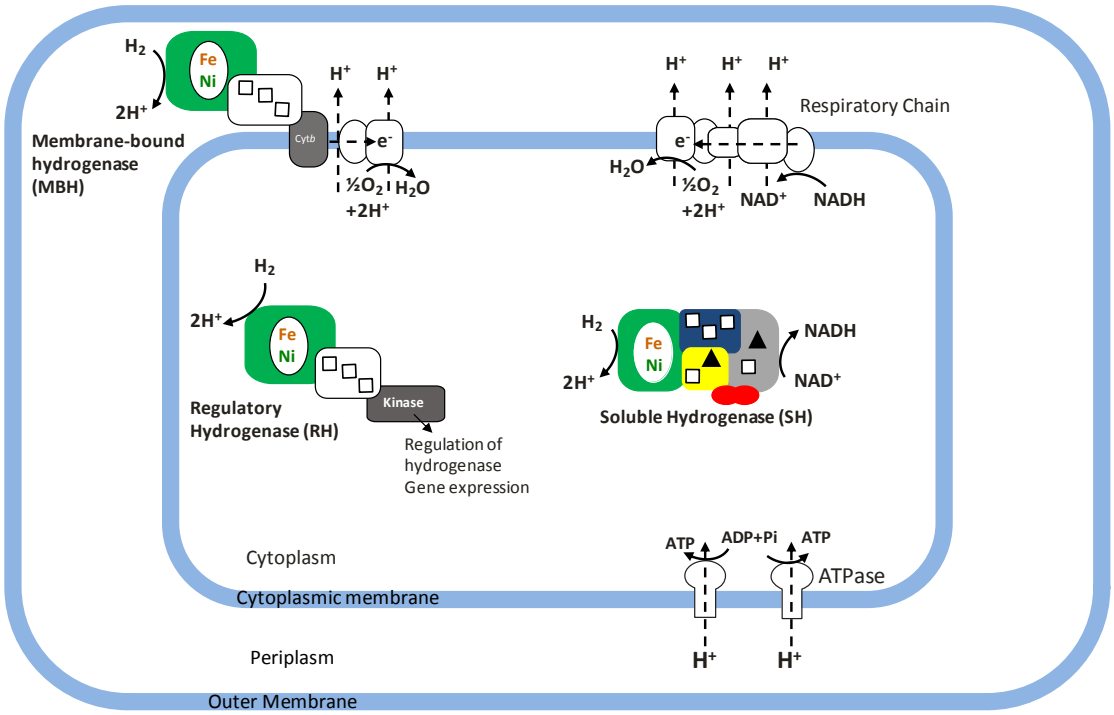

Figure 3. The roles of hydrogenases in *Ralstonia eutropha* H16. ADP: adenosine diphosphate, ATP: adenosine triphosphate, NAD: nicotinamide adenine dinucleotide. FeS clusters are shown as white squares and FMN cofactors are shown as triangles. The original figure was kindly provided by Dr Oliver Lenz and has been adapted accordingly.[13]

The second hydrogenase in *R. eutropha* resides in the cytoplasm and is called the SH. It is composed of two catalytic moieties: the hydrogenase and diaphorase moieties.[20-22] The SH catalyses H_2 oxidation and transfer the electrons for formation of NADH which is used for CO_2 fixation and other important biological processes.

The low availability of H_2 in the surrounding environment in which *R. eutropha* thrives requires this microbe to efficiently regulate hydrogenase expression for optimal

energy conservation. The H_2 sensing hydrogenase, also known as the RH, controls hydrogenase gene expression via a protein kinase.[23, 24] It detects the presence of H_2 in the environment and transmits the signal to a response regulator, thus triggering the expression of MBH and SH. This NiFe hydrogenase is also capable of oxidising H_2, albeit at a much lower rate than that observed for the SH and MBH.[25, 26]

1.3 Common biological redox centres

A cofactor is a chemical entity that is necessary together with biological macromolecules such as proteins to perform a biological function.[27] In redox enzymes, a cofactor can serve a number of purposes. For example, they can participate in the reaction by channelling electrons from a donor to the active site or from active site to an acceptor, or by transferring a H^- ion which can be considered as $2e^- + H^+$.[28] A brief description of biological redox centres relevant to the enzymes investigated in this Thesis will now be discussed.

1.3.1 Iron-Sulphur clusters

Iron-sulphur clusters are ubiquitous in biology, found in most kingdoms of life from archaea to plants and animals. This prosthetic group is largely used in electron transfer proteins as their redox potentials can be finely tuned over a range of values in the fairly reducing region.

The crystal structure of a 2Fe2S cluster (cluster N1b from subunit Nqo3) from *Thermus thermophilus* Complex I is shown in Figure 4.[29] Two iron atoms are coordinated by two bridging sulphide ligands and four cysteine residues. The distance between the two iron atoms of this protein is 3.02 Å with the charge of the FeS cluster varying from +1 ($Fe^{II}Fe^{III}$) to +2 ($Fe^{III}Fe^{III}$).[30, 31] In the case of cluster N1b of

T. thermophilus Complex I, a mid-point potential of around -0.24 ± 0.02 V was measured.[31] Although generally the iron atom is bound by cysteines from the protein structure, variations have been found in several classes of FeS proteins such as Rieske proteins, in which histidine residues are coordinated to one of the iron atoms instead of cysteines.[32] The 2Fe2S cluster of *Escherichia coli* succinate dehydrogenase has one aspartate-oxygen coordinated to the iron atom.[33]

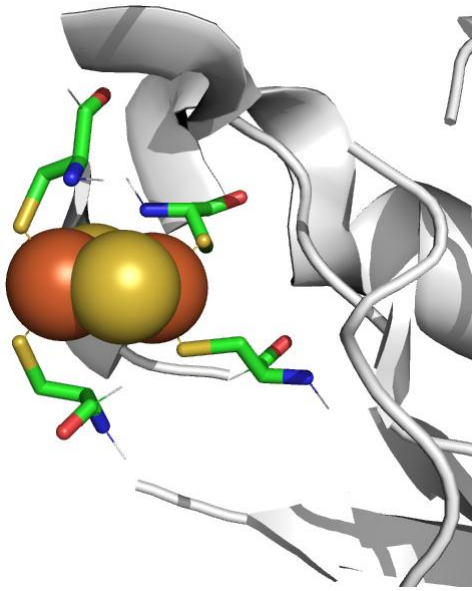

Figure 4. The 2Fe2S cluster, known as N1b cluster conserved in subunit Nqo2 of *T. thermophilus* Complex I showing the Fe atoms are coordinated to cysteine residues (sticks). PDB code: 3IAM.[29, 34]

The most ubiquitous FeS cluster in biology is the cubane structure, shown in Figure 5A. The basic structure is a distorted cube with alternating iron and sulphur atoms at the corners. Generally, four cysteine residues coordinate the cube at the four iron corners forming a distorted tetrahedral geometry at each Fe atom. However, there are cases where one cysteine residue is replaced with histidine (as in the case of 2Fe2S clusters). For example, in *T. thermophilus* Complex I, the 4Fe4S cluster, called the N5 cluster positioned in subunit Nqo3 is coordinated by a histidine, His^{115} and three

cysteine residues as shown in panel B.[29, 31] Similar types of clusters have also been found in *Clostridium pasterianum* I FeFe-hydrogenase (called FS4C cluster) and in nitrate reductase A (called FS0).[35, 36]

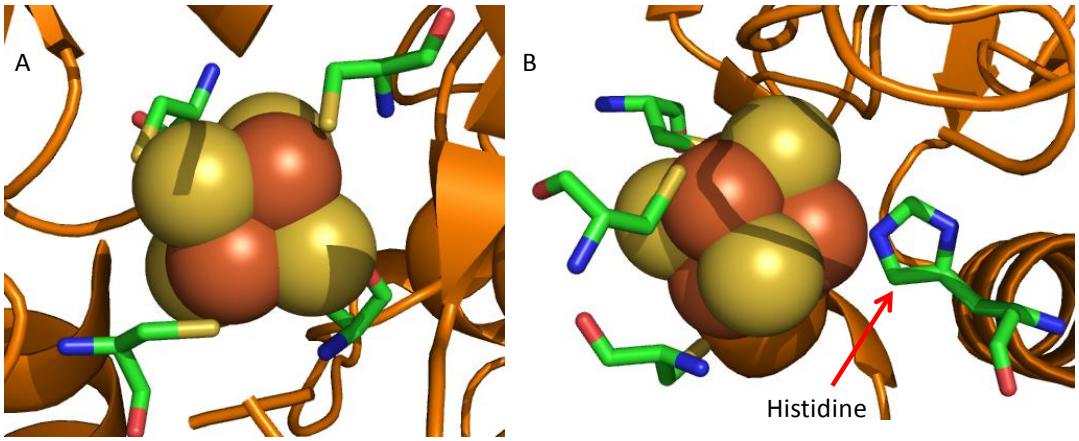

Figure 5. Panel A shows a typical 4Fe4S cluster, with four cysteine residues ligated to the iron atoms. The picture was constructed using N4 cluster of subunit Nqo3 of *T. thermophilus* Complex I. Panel B shows a case where one of the cysteine residues is replaced with a histidine residue, constructed using N5 cluster of subunit Nqo3 from *T. thermophilus* Complex I. PDB code: 3IAM.[29, 34]

The 3Fe4S cluster shown in Figure 6 is also common. It can be described as a cubane that is lacking one of the iron atoms, thus only three cysteine ligands are required for coordinating the cluster. This type of FeS cluster has been observed for the medial cluster of several NiFe hydrogenases such as the MBH from *R. eutropha*, *Desulfovibrio gigas* or *Allochromatium vinosum* and Hyd1 of *E. coli*.[18, 37-40]

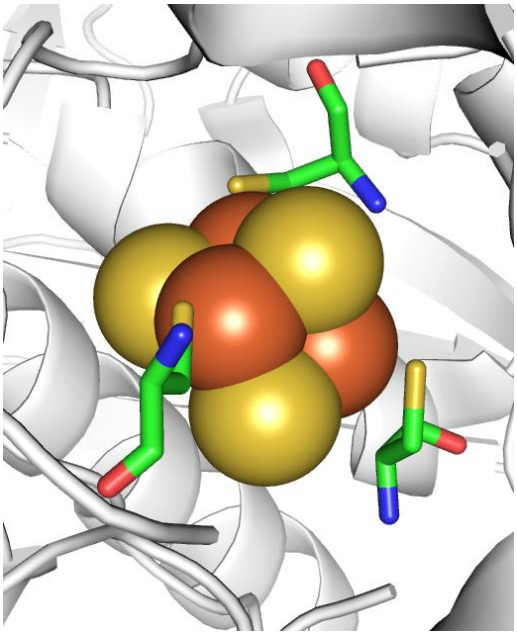

Figure 6. The medial 3Fe4S cluster of the MBH from *R. eutropha* showing the iron atoms are coordinated by three cysteine residues. The picture was constructed in Pymol, PDB code: 3RGW.[18]

1.3.2 NAD(P)$^+$/NAD(P)H

Nicotinamide adenine dinucleotide (NAD(H)) and nicotinamide adenine dinucleotide phosphate (NADP(H)) are also ubiquitous redox cofactors used in biological reactions. These nicotinamide cofactors act as a hydride carrier by transferring a hydride ion from or to the carbon atom in position 4 of the nicotinamide ring in a stereospecific way (Figure 7). Despite their great similarity (NADH differs from NADPH only in the absence of a phosphate group esterified to the 2'-hydroxyl group of the ribose at the adenine end) significant biochemical differences exist between the functions of NADH and NADPH within living cells. For example, exclusively NADH is involved in oxidative degradations that produce ATP while NADPH is involved with reactions of reductive biosynthesis.[27, 41]

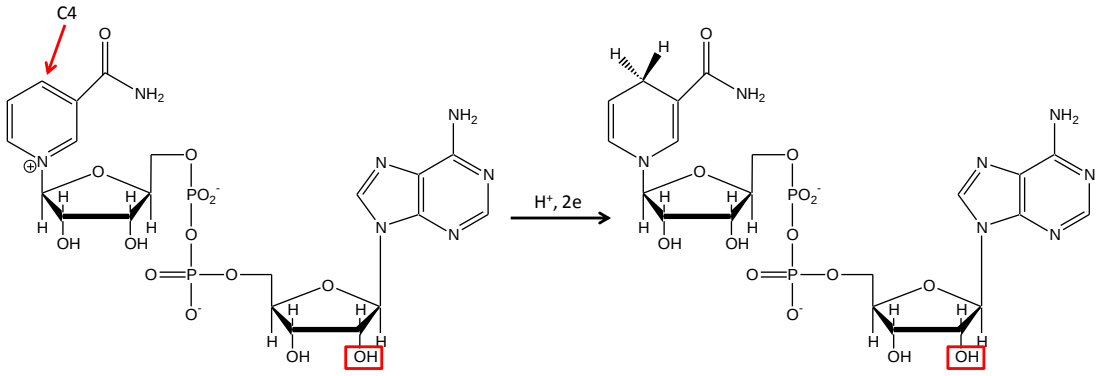

Figure 7. The structures of NAD(H) showing reduction of oxidised nicotinamide adenine dinucleotide (NAD^+) to NADH. Addition of a hydrogen atom occurs at position C4 of the nicotinamide ring, shown as a red arrow. The red boxes indicate the position where the hydroxyl group in NAD(H) is replaced with a phosphate group in NADP(H).

Most NAD(P)-dependent enzymes show a preference for one of these two cofactors. For example, a family of glutamate dehydrogenases (GDH) has been shown to exhibit cofactor specificity ranges from strictly NADH to strictly NADPH *e.g.* GDH from *Clostridium symbiosum* uses only NADH for oxidative deamination of glutamate to 2-oxoglutarate, while GDH from *Salmonella typhimurium* only uses NADPH to catalyse the same reaction.[42, 43] Several research groups have demonstrated that enzymes that discriminate NADH over NADPH often have aspartate or glutamate residues close to the active site, and these negatively charged residues form hydrogen bonds to the diol group of the ribose near the NADH adenine moiety.[44-47] Meanwhile NADPH-enzyme complexes are often stabilised by an arginine side chain that faces the NADPH adenine plane and is hydrogen bonded to the phosphomonoester.[44-49] The fact that a small structural difference makes a large impact on the affinity of enzymes for these cofactors provides an excellent example of molecular recognition in biological chemistry.

Although NADH and NADPH perform different functions, the close similarity of these two molecules means that the redox potentials of the two couples are very

similar. The redox potential for the NAD^+/NADH and $NADP^+$/NADPH couples is -0.32 V vs SHE at pH 7.0, 25 ^oC. Since the oxidation of a molecule of NADH involves two electrons and one proton, the thermodynamic potential for this reaction shifts by 0.0295 V for each unit change in pH at 25 ^oC, illustrated in Figure 8.

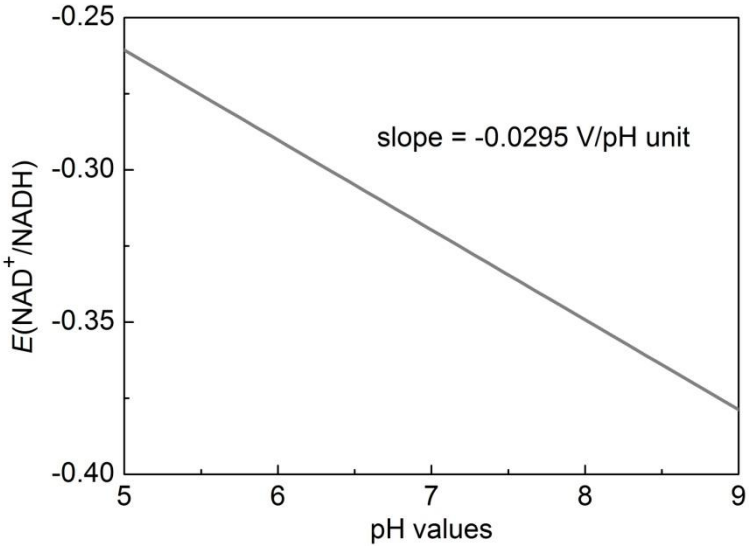

Figure 8. Plot showing the dependence of E(NAD^+/NADH) on pH values at 1:1 ratios of NAD^+:NADH, 25 ^oC according to the Nernst equation.

1.3.3 Flavins

Two common types of flavin cofactor are synthesised from dietary riboflavin (vitamin B2): flavin mononucleotide, FMN and flavin adenine dinucleotide, FAD as shown in Figure 9. The difference between FMN and FAD lies at the presence of additional phosphate, ribose and adenosine groups attached to the phosphate chain in FAD.[41] These extra groups, however, do not conjugate to the redox active part of the molecule (the isoalloxazine ring), hence the redox potential of the couple does not change *i.e.* all have $E^{o'}$ of -0.21 V at pH 7.

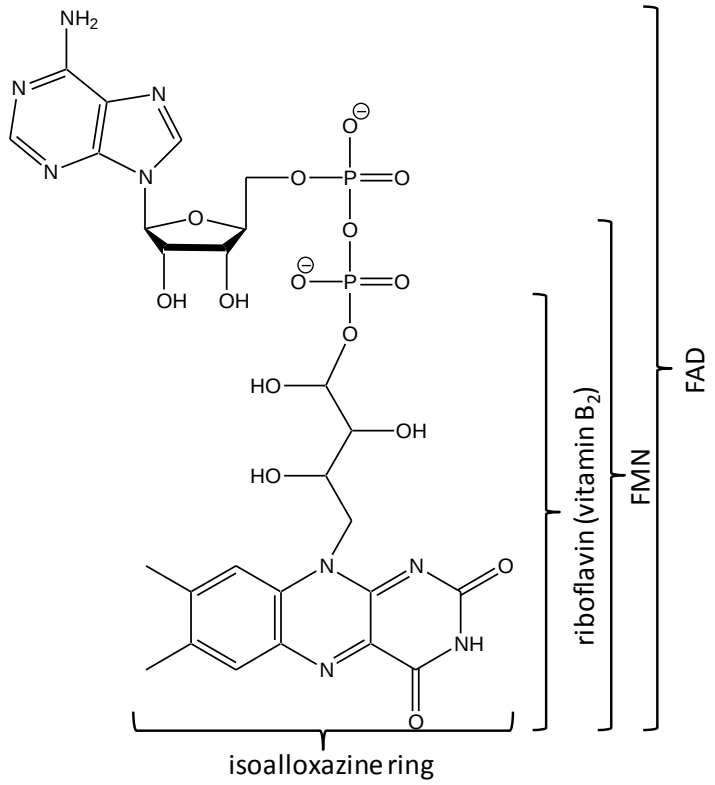

Figure 9. Structure of isoalloxazine, riboflavin, FMN and FAD.

Flavins undergo reversible redox conversions as shown in Figure 10, with the overall reduction accompanied by binding of two protons to the nitrogen atom of the isoalloxazine ring (position N1 and N5).[50] The process can occur via one-electron steps with formation of intermediates such as the semiquinone free radical as shown in Figure 10.

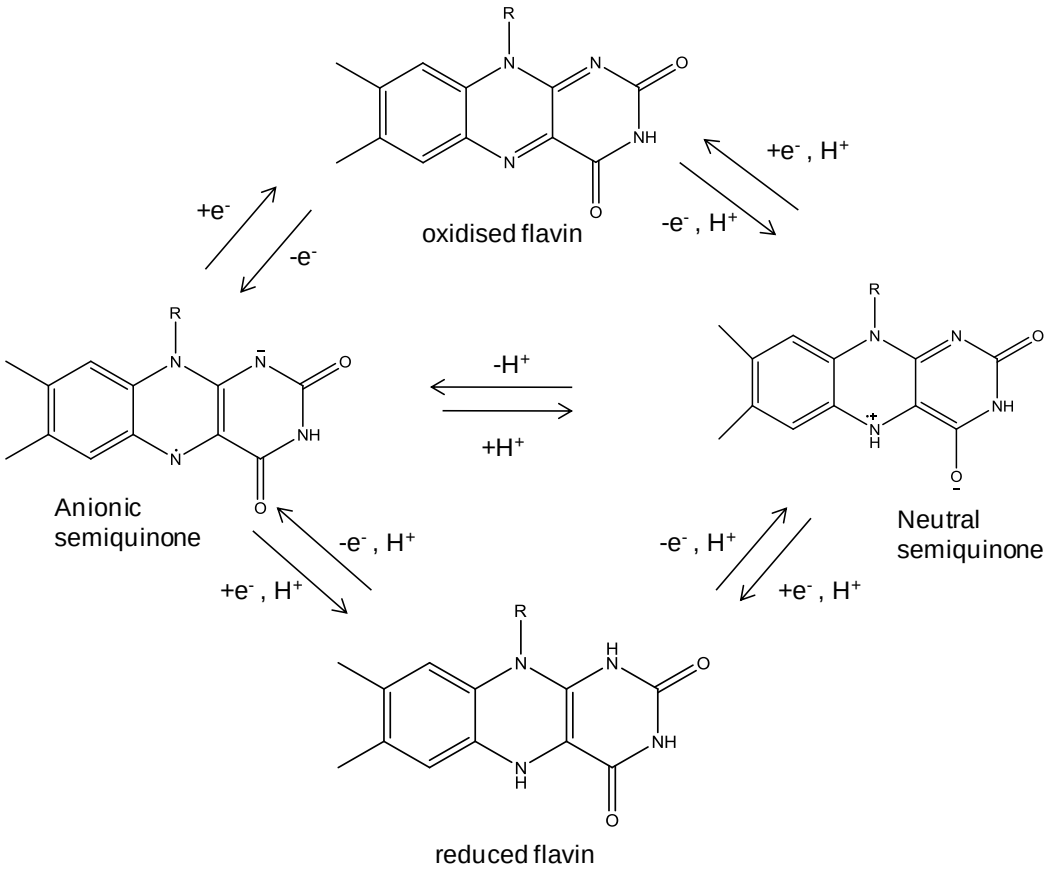

Figure 10. The redox reactions of flavins.

As shown in Figure 10, flavins can couple one and two electron reactions between substrates and different electron carriers; they can convert between a two-electron reaction and one-electron reaction in a relay. Flavins thus play a substantial role in biology. For example, FMN and FAD participate in a wide variety of enzyme-catalysed reactions such as dehydrogenation, electron transfer and disulphide reduction.

As mentioned earlier, the reduction potential for free flavins is around -0.21 V, yet when flavins are bound in the enzyme environment, the reduction potential may vary between -0.4 and 0.1 V.[51] In *T. thermophilus* Complex I, the reduction potential of the FMN in subunit Nqo1 is found to be -0.38 V.[52]

1.3.4 Quinones

Quinones are cyclic organic molecules with a long isoprenoid chain which makes them lipid soluble so that they can freely diffuse in the lipid membrane.[41] Quinones (oxidised forms) can either be reduced in a single two-electron reaction or two one-electron reactions yielding quinols (Figure 11). Quinones are hydrogen atom carriers and are involved in energy transduction: one example is the coupling of electron transport between photosystem II and the cytochrome *bf* complex. Since the redox reactions of quinones involve electrons and protons, the redox couple for quinone is pH dependent, shifting by 0.059 V per pH unit.

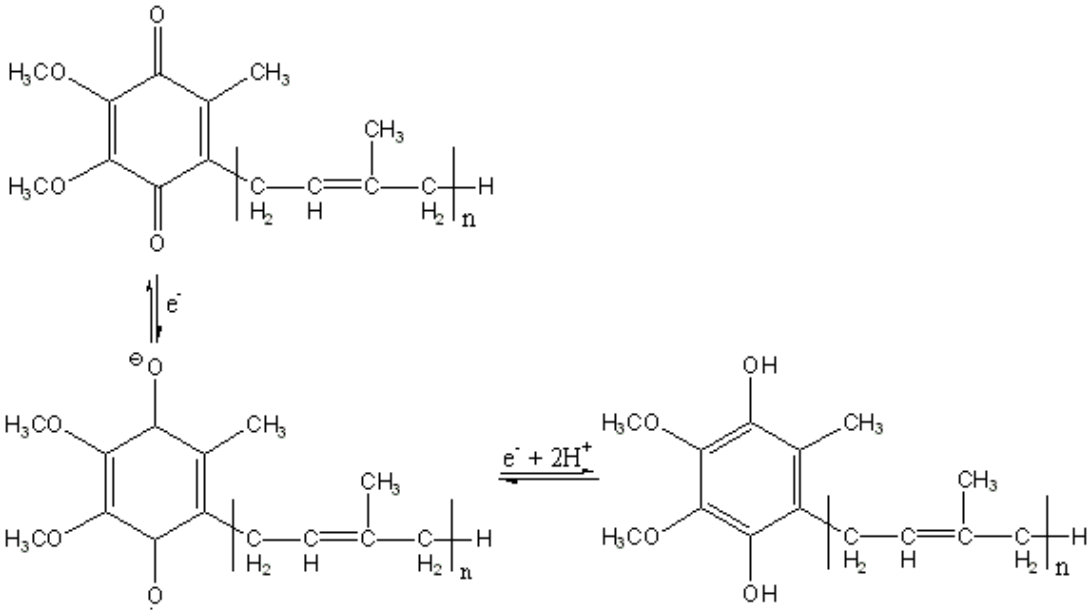

Figure 11. Reduction of quinone to quinol.

This thesis deals with an enzyme that couples H_2 oxidation to the storage of reducing equivalents as NADH. In the next Section, discussion of the enzyme used throughout this Thesis will be presented.

1.4 Hydrogenases: Classification on the basis of active site metals

Hydrogenases exist in a wide variety of organisms, both prokaryotic and eukaryotic.[1, 5, 53] They catalyse the reversible cleavage of H_2 into H^+ and electrons as shown in equation [1].[1]

$$H_2 \leftrightarrow 2H^+ + 2e^- \qquad [1]$$

Hydrogenases can be classified into three distinct groups based on the metal composition of their active sites. Most known hydrogenases comprise a bimetallic catalytic centre: a Ni and an Fe atom (in NiFe hydrogenases), or two Fe atoms (in FeFe hydrogenases).[54-56] Although hydrogenases can work in both directions, they often tend to operate in one direction under physiological conditions. The FeFe hydrogenases are generally found in roles involving H_2 evolution while NiFe hydrogenases tend to be associated with H_2 oxidation.[56, 57]

Another type of hydrogenase, only harbouring one Fe atom at the active site, is called the Fe hydrogenase[58-60] and functions as H_2-forming methylenetetrahydromethanopterin dehydrogenase, Hmd.

1.4.1 Fe hydrogenase

Shima, Ermler and coworkers first reported the crystal structure of *Methanocaldococcus jannaschii* and *Methanopyrus kandleri* Fe hydrogenase apoenzymes in 2006.[58] These enzymes were discovered in some methanogens and they reversibly catalyse the hydride transfer to N^5,N^{10}-methenyltetrahydromethanopterin from H_2 to give N^5,N^{10}-methylenetetrahydromethanopterin which is an intermediate

step in methanogenesis to CO_2. During the reaction, N^5,N^{10}-methenyltetrahydromethanopterin accepts a hydride ion from H_2 stereospecifically at a carbon atom at position 14a as shown in Figure 12A.[60] Later, in 2008, the crystal structure of the holoenzyme of *Methanocaldococcus jannaschii* was made available by the same group.[61] The enzymes are composed of two identical subunits, with no FeS cluster and contain two Fe atoms for each homodimer.[59, 61] The Fe active site has been shown to be coordinated by two CO ligands, one sulphur ligand provided by a cysteine residue and a pyridone derivative, linked to a guanosine base by phosphodiester bond. Analysis of the crystal structure of this enzyme revealed that its N-terminal domain shares structural similarity with the binding site of various NAD(P)-dependent dehydrogenases which agrees well with the proposed structure of this hydrogenase: a mononucleotide cofactor is bound to the Fe atom (Figure 12B).[58] Although these enzymes do not catalyse H_2 oxidation or H^+ reduction,[62] they engage in hydride transfer which is similar to reactions of NAD(P)-dependent enzymes.

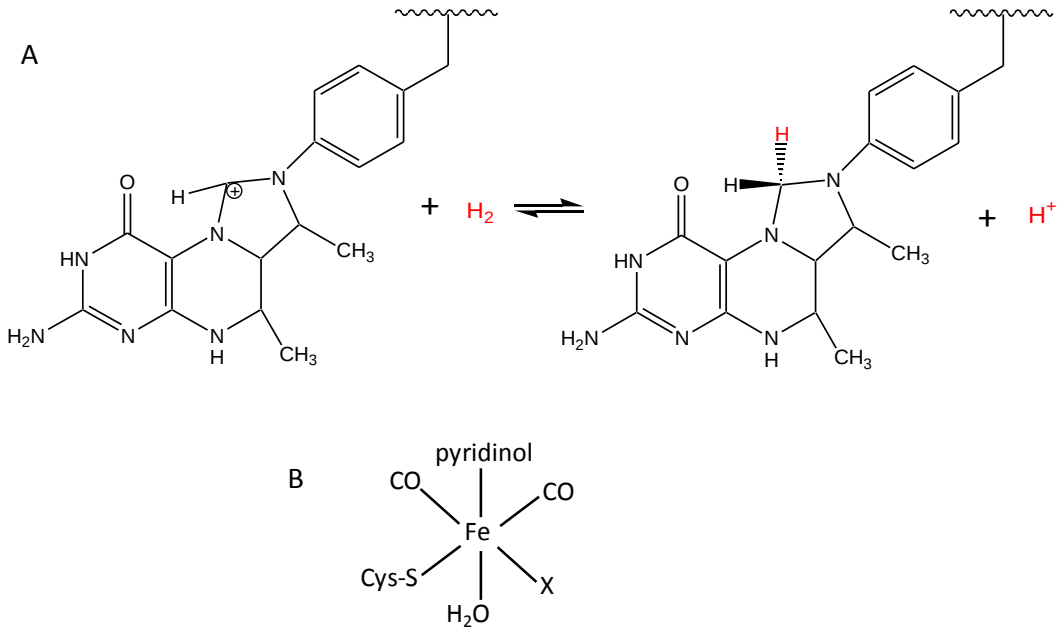

Figure 12. Panel A: The hydride transfer reaction catalysed by Fe hydrogenase. Panel B: the active site of the Fe hydrogenase. X refers to an unknown ligand.

1.4.2 FeFe hydrogenase

Figure 13 shows the crystal structure of an FeFe hydrogenase from *Clostridium pasterianum*.[35] The enzyme is composed of several FeS clusters, one of which is coordinated to the active site via a cysteine ligand and termed as the H-cluster. The binuclear FeFe centre is coordinated with CO and CN ligands, suggested to be important in tuning the electronic structure of the active site. The Fe atoms are also ligated to a bidentate five atom dithiolate ligand, probably a di(thiomethyl)amine molecule. The distances between all cofactors are in the range of 10 Å: within the 14 Å limit for electron tunnelling at biologically relevant rates as proposed by Dutton and coworkers.[63] This finding indicates that these clusters form a molecular wire to efficiently transfer electrons to and from the buried active site.

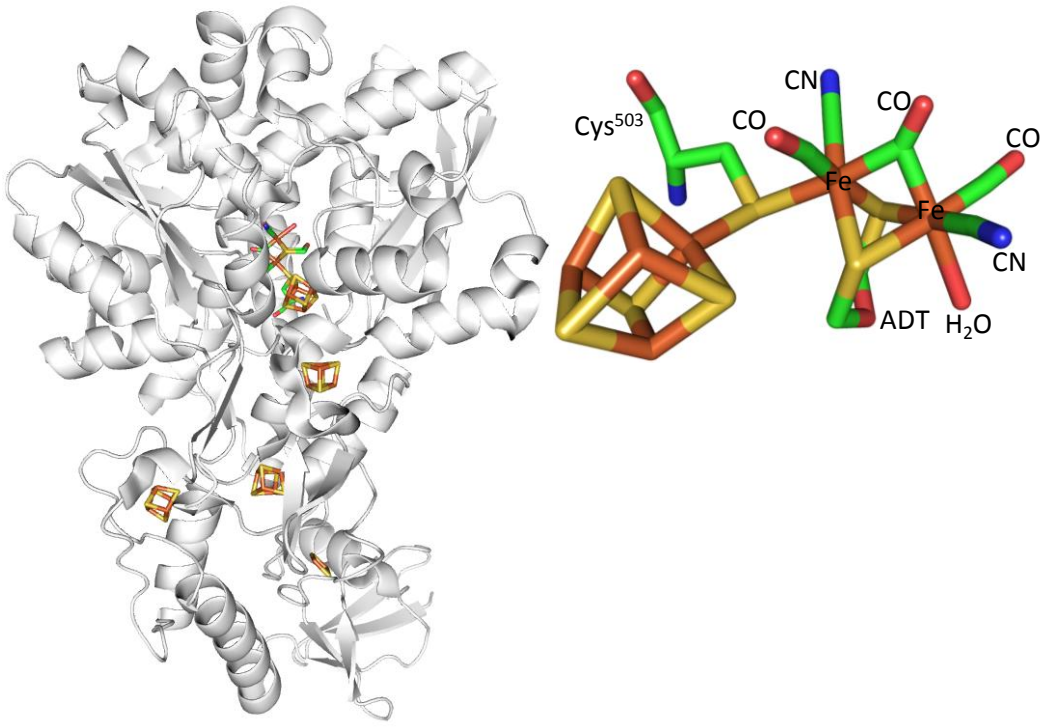

Figure 13. The crystal structure of the oxidised form of *C. pasterianum* FeFe hydrogenase. ADT refers to a di(thiomethyl)amine molecule. Picture was constructed using Pymol, PDB code 3C8Y.[35]

Analysis of the sequence identity of N-terminal part of *C. pasterianum* FeFe hydrogenase (residues 1 to 240) and N-terminal part of *T. thermophilus* Complex I subunit Nqo3 (residues 1 to 206), shown in Figure 14 indicates that these parts of the proteins are quite similar: they share 19 % sequence identity. As can be seen from Figure 13, the *C. pasterianum* FeFe hydrogenase has five conserved FeS clusters while in contrast, only four FeS clusters are conserved in subunit Nqo3 of *T. thermophilus* Complex I.[29, 35] The 4Fe4S cluster proximal to the H-cluster of the FeFe hydrogenase is missing in subunit Nqo3, although as argued by Sazanov and co-workers, the residues responsible for coordinating this FeS cluster are conserved in *T. thermophilus*.[29] The absence of one FeS cluster in Nqo3 does not, however, affect electron transfer as the distance between this cluster to the nearest FeS clusters is still in the range of 14 Å. The similarities between these proteins are an example of Nature recycling units of proteins for different functions.

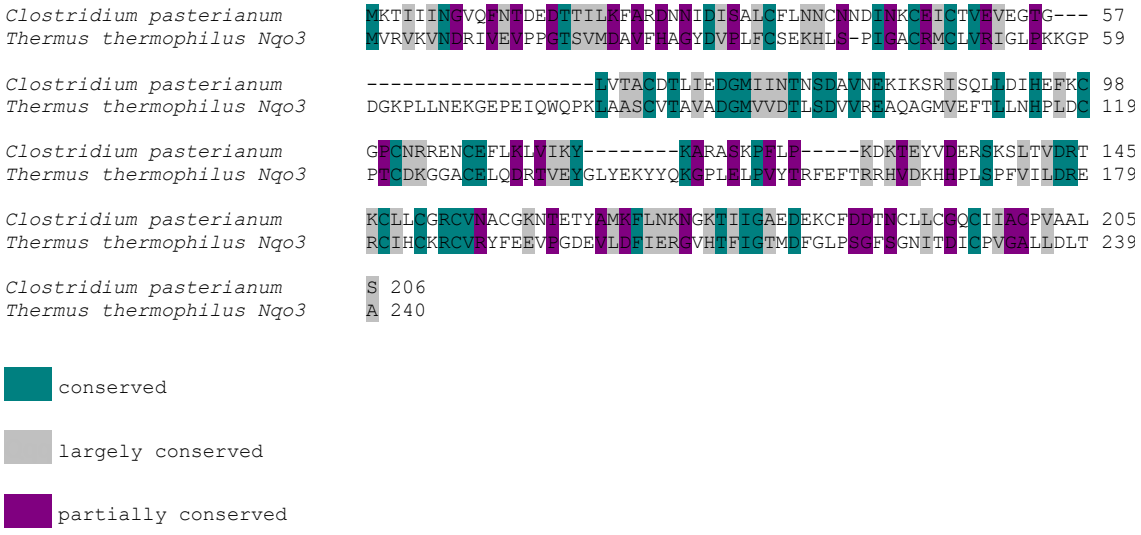

Figure 14. Amino acid sequence comparison between N-terminal part of *C. pasterianum* FeFe hydrogenase and N-terminal part of *T. thermophilus* Complex I subunit Nqo3 generated using ClustalW software (available online at www.ebi.ac.uk/clustalw/#). The amino acid sequences were obtained from www.uniprot.org and used without any modification.

1.4.3 NiFe hydrogenase

A number of crystal structures for NiFe hydrogenases have been resolved[37, 38, 40, 64-70] and Figure 15 shows the crystal structure for the Membrane Bound NiFe Hydrogenase from *Ralstonia eutropha*.[18] The NiFe active site is deeply buried in the large subunit and two bridging cysteine ligands (Cys^{78} and Cys^{600}) link these two atoms together. Two CN and one CO ligands are coordinated to the Fe atom, while two terminal cysteine ligands (Cys^{75} and Cys^{597}) are coordinated to the Ni atom. There are three FeS clusters conserved in the small subunit: one 4Fe3S (proximal), one 3Fe4S (medial) and one 4Fe4S (distal). Similar to that of *C. pasterianum* FeFe hydrogenase, all cofactors in *R. eutropha* MBH are wired in a distance of around 10 Å for efficient electron transfer.

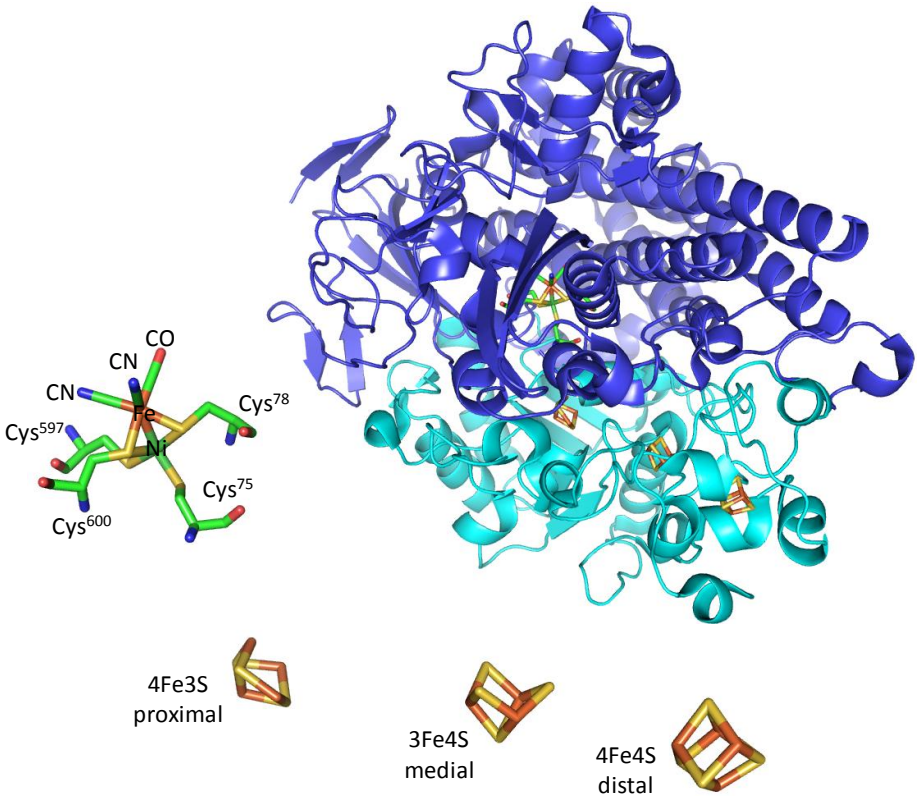

Figure 15. Crystal structure of the membrane bound NiFe hydrogenase from *Ralstonia eutropha*. Picture was constructed using Pymol, PDB code 3RGW.[18]

The NiFe hydrogenases often consist of just two subunits; the large subunit (approximately 60 kDa in size) harbours the bimetallic active site while a chain of FeS clusters are conserved in the small subunit (approximately 30 kDa in size). A number of multimeric NiFe hydrogenases are also known, and these are further discussed in the next Section.[71, 72]

1.5 Classification of NiFe hydrogenases on the basis of biological functions

Numerous NiFe hydrogenases have been studied using biochemical, spectroscopic and electrochemical techniques. Vignais and Billoud have analysed the complete amino acid sequences of the subunits of these hydrogenases and have grouped them into eight phylogenetic classes (Table 1-1).[5]

Table 1-1. Characterisation of NiFe hydrogenase groups according to Vignais and Billoud.[5]

Group	Function	Example
1	Membrane bound H_2 uptake hydrogenases	*R. eutropha* H16 MBH
2a	Cyanobacterial uptake hydrogenases	*Nostoc punctiforme* PCC73102
2b	H_2-sensing hydrogenases	*R. eutropha* H16 RH
3a	F_{420}-reducing hydrogenases	*Methanococcus voltae* DSM 1537/PS
3b	Bifunctional (NADP) hydrogenases	*Pyrococcus furiosus* DSM 3638
3c	Methyl viologen-reducing hydrogenases	*Syntrophotobacter fumaroxidans* MPOB
3d	Bidirectional NAD(P)-linked hydrogenases	*R. eutropha* H16 SH
4	Membrane bound H_2 evolving hydrogenases	*E. coli* hydrogenase 536

It should be mentioned here that *in vitro*, most NiFe hydrogenases are bidirectional in the sense that they are able to function in both directions: performing either H_2 oxidation or H^+ reduction. However, the so-called bidirectional NiFe hydrogenases (group 3) are thought to operate in both directions *in vivo*.

The NiFe hydrogenase investigated in this Thesis, the soluble hydrogenase (SH) of *R. eutropha* belongs to group 3d: bidirectional NAD(P)-linked hydrogenases. In this class of hydrogenase, the dimeric hydrogenase moiety is coupled with other subunits that bind soluble cofactors, NAD(P)(H). These bidirectional hydrogenases are found in bacteria and cyanobacteria and they share similarity to the soluble domain of Complex I. In Section 1.6 of this Chapter, the SH, soluble domain of Complex I and related bidirectional hydrogenases will be discussed.

1.6 The Soluble Hydrogenase of *Ralstonia eutropha* H16

One of the hydrogenases expressed by the Knallgas β-proteobacterium *Ralstonia eutropha* is the Soluble Hydrogenase (SH) which is also a member of the Group 3d NiFe hydrogenases. Figure 16 represents the structure of the SH, showing that this multimeric bidirectional hydrogenase consists of six subunits $HoxHYFUI_2$, containing a NiFe $2H^+/H_2$ cycling centre, five FeS clusters and two flavin mononucleotide (FMN) cofactors.[13, 20, 21, 73] In the cell, the SH catalyses H_2 oxidation at the NiFe active site in HoxH, transferring electrons via a chain of FeS clusters to the FMN-b centre in HoxF for reduction of nicotinamide adenine dinucleotide, NAD^+. The SH has been shown to be closely related to Complex I.[13, 29, 71, 74, 75] The similarities will be discussed further in the next Section. The reduction of NAD^+ at the FMN catalytic centre is postulated to occur via a hydride transfer, as shown for Complex I.[29] Apart from producing NADH,

which is used for CO_2 fixation in the Calvin cycle, the SH has also been reported to function in the reverse direction under specific cellular conditions especially when the NAD^+/NADH pool has become too reduced *i.e.* coupling NADH oxidation to H^+ reduction.

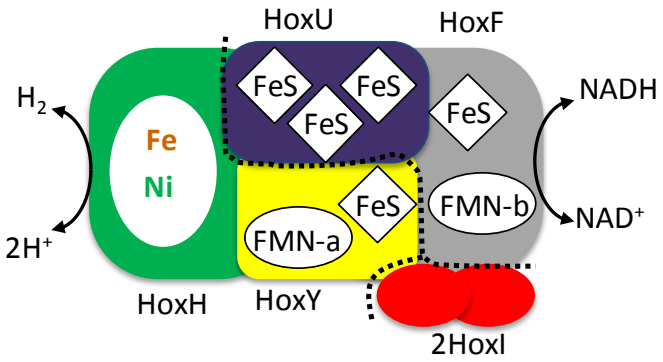

Figure 16. A schematic representation of *Ralstonia eutropha* Soluble Hydrogenase.

The ligands coordinating the NiFe active site in the HoxH subunit are now known from spectroscopic experiments to be similar to those of standard NiFe hydrogenases; four cysteine residues attached to the Ni with two of them acting as bridging ligands to the Fe atom that also coordinates one carbon monoxide and two cyanide ligands, Figure 17.[76, 77]

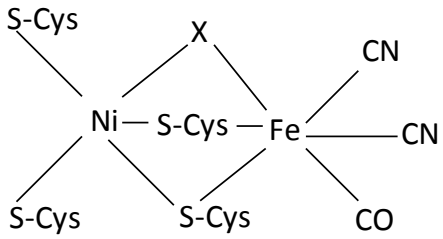

Figure 17. The proposed active site structure of the hydrogenase moiety of the SH. The nature of the bridging ligand, X depends on the redox state.[20, 76, 77]

The SH was first described as a heterotetrameric enzyme, HoxHYFU, however, Friedrich and coworkers discovered that two additional subunits, termed HoxI, are associated with the SH.[78] The attachment of the HoxI subunits is sensitive to pH and salt concentration during the purification process, and high ionic strength and pH result in the dissociation of HoxI.[78] These extra subunits have been postulated to accommodate an extra binding site for molecules of NADPH. This is on the basis of biochemical experiments in which the hydrogenase activity of the as-isolated hexameric SH was shown to be activated by a small concentration of NADPH, whilst the as-isolated tetrameric enzyme requires a significantly higher NADPH concentration for activation. An affinity chromatography-based approach was used to determine the position of HoxI subunits within the hexameric complex of the SH. The fact that the HoxI subunits do not copurify with the hydrogenase moiety indicates that HoxI interacts primarily with HoxFU and must be in close proximity to the diaphorase moiety.

As mentioned earlier, the SH contains two FMN cofactors; one is located in HoxY and the other one is in HoxF. The FMN found in HoxY, called FMN-a has been associated with the H_2 oxidation activity of the SH. Albracht and coworkers reported that the as-isolated inactive enzyme can be catalytically activated in the presence of NADH.[79] However, prolonged exposure of the SH to NADH resulted in a decrease in catalytic activity, and they attributed this behaviour to the dissociation of FMN-a from the HoxY subunit. The hydrogenase activity can be restored by addition of excess FMN to the reduced SH (an increase in H_2:NAD^+ catalytic activity was recorded) suggesting that FMN-a is essential for electron transfer between the NiFe active site to the nearest FeS cluster and HoxF for NADH formation. Although FMN-a is loosely bound, the NADH:$K_3Fe(CN)_6$ activity was unaffected during the course of the biochemical experiments performed by Albracht and coworkers suggesting that the non-covalently

bound FMN-b (residing in HoxF) was retained. The FMN-b is therefore associated with the NADH catalytic activity, presumably acting as a hydride carrier for the reaction.

Selective introduction of affinity tags and selective deletion of genes has made it possible to separate this hexameric hydrogenase into different catalytic moieties, the hydrogenase moiety, HoxHY and the diaphorase moiety HoxFU (shown separated by a dotted black line in Figure 16). The hydrogenase moiety of the SH is a heterodimer harbouring the NiFe active site, one FeS cluster and one FMN cofactor (FMN-a). The HoxFU diaphorase moiety consists of two subunits, incorporating four FeS clusters (three 4Fe4S and one 2Fe2S) and one FMN cofactor, FMN-b. Experiments described in this Thesis will focus on the catalytic activity of the diaphorase moiety of the SH.

1.6.1 Relationship between the SH and Complex I

Complex I, also known as NADH:ubiquinone oxidoreductase is regarded as an entry point for electrons into the respiratory system of mammalian mitochondria and aerobic micro-organisms.[80] It is one of the largest membrane proteins assemblies and contributes about 40 % of proton motive force required for the synthesis of ATP.[31, 74, 81, 82] Many human neurodegenerative diseases have been associated with mutations in the subunits of Complex I.[83-86] The complex has also been suggested to be a source of reactive oxygen species in mitochondria[87], which can harm mitochondrial DNA and be one of the origin of Parkinson's disease[88] and ageing.[89] Complex I has an L-shape with two major domains; the hydrophobic domain is situated within the membrane while the hydrophilic domain protrudes into the inner mitochondrial space. A complete crystal structure of *T. thermophilus* Complex I has recently been resolved by Sazanov and coworkers.[29, 34, 90, 91] The hydrophobic domain participates in proton translocation with

four protons suggested to be involved in this reaction. Under physiological conditions, the hydrophilic domain catalyses NADH oxidation and reduction of quinone.[29]

Figure 18A shows a cartoon representation of the hydrophilic domain of *T. thermophilus* Complex I. Panel B shows a schematic representation of the domain, colour-coded with respect to subunits found to have analogues in the *R. eutropha* SH (Figure 16).

Sazanov and coworkers established the electron transfer pathway from NADH oxidation to flavin mononucleotide (FMN) and then through seven conserved FeS clusters to the quinone binding site, situated at the interface of the membrane domain (Figure 18C).[29] In summary, the reaction of one molecule of NADH generates one molecule of reduced quinone and pumps four protons across the membrane as shown in equation [2].

$$\mathrm{NADH} + \mathrm{Q} + 5\mathrm{H}^{+} \rightarrow \mathrm{NAD}^{+} + \mathrm{QH}_2 + 4\mathrm{H}^{+} \qquad [2]$$

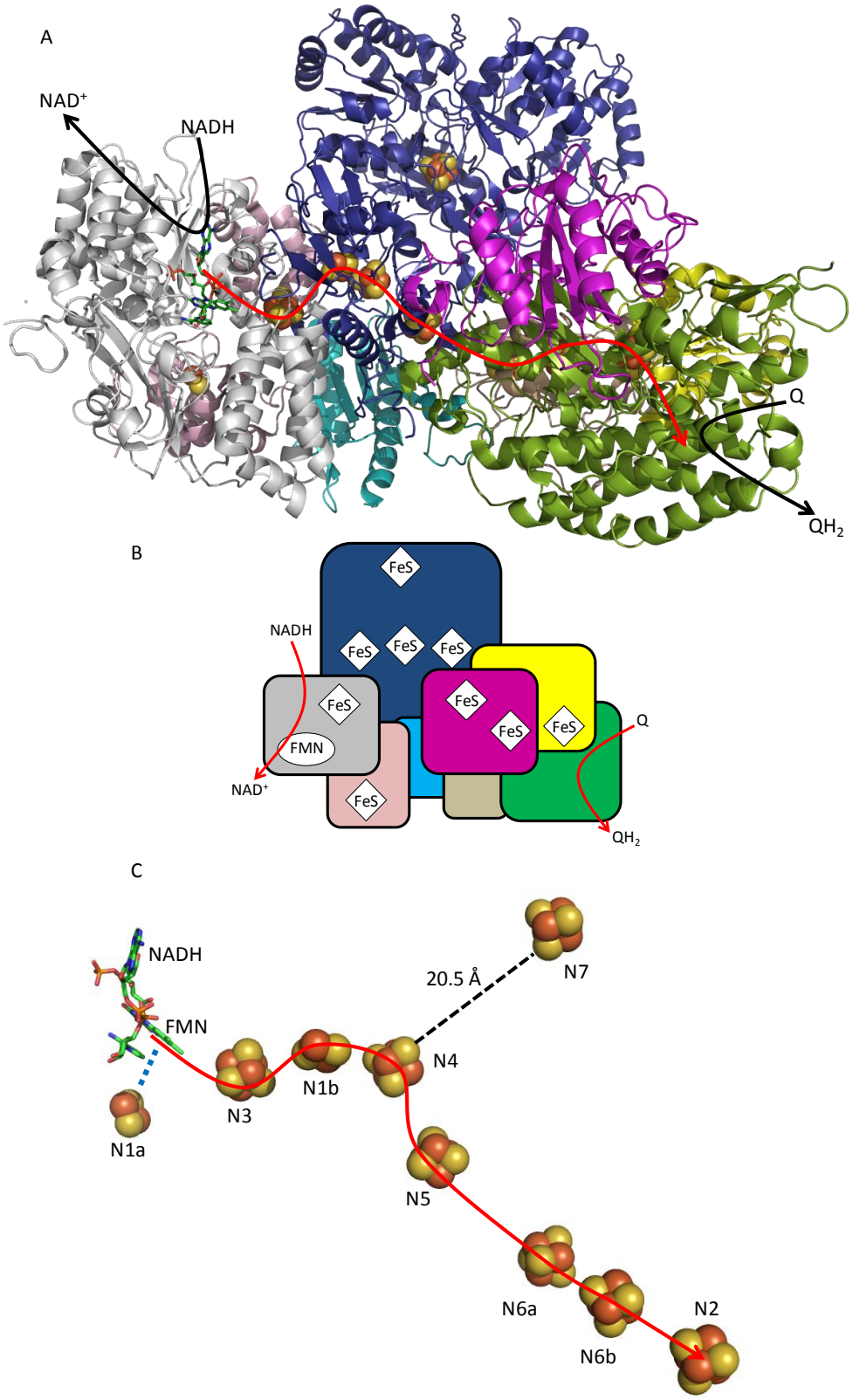

Figure 18. The crystal structure of the hydrophilic domain of *T. thermophilus* Complex I with bound NADH in a stacking position with FMN cofactor. In panel A, each subunit is coloured differently. The red arrow indicates the proposed electron pathway to the quinone binding site from flavin catalytic centre. Panel B shows a schematic representation of the hydrophilic domain of *T. thermophilus* Complex I, coloured according to panel A and subunits of the SH in

Figure 16. Subunit Nqo1, similar to subunit HoxF in the SH is coloured in grey. Subunit Nqo2 is coloured as light pink. Subunit Nqo3 which is similar to HoxU is coloured in dark blue. Subunit Nqo4, similar to HoxH is green, and subunit Nqo5 is in wheat. Subunit Nqo6, similar to HoxY is in yellow. Subunits Nqo9 and Nqo15 are coloured in magenta and light blue. Panel C shows the arrangement of the redox centres. A dotted blue line indicates a possibility of electron diversion to the N1a cluster. Clusters N4 and N7 are separated by 20.5 Å edge to edge distance. NADH and FMN are shown as sticks. Cluster N1a resides in subunit Nqo2; N3 and FMN are in Nqo1; N1b, N4, N5 and N7 are in Nqo3; N6a/b are in Nqo9 and N2 in Nqo6. The picture was constructed using Pymol (PDB code: 3IAM).[29, 34]

Subunits of the SH, apart from HoxI share sequence identity with the subunits of the hydrophilic domain of *T. thermophilus* Complex I. Table 1-2 illustrates the extent of similarities between these subunits.

Table 1-2. Amino acid residues comparison between subunits of the SH and Complex I.

R. eutropha Soluble Hydrogenase	*T. thermophilus* Complex I	Score (% identity)
HoxH	Nqo4	7
HoxY	Nqo6	18
HoxF	Nqo1	36
HoxU	Nqo3	23

Subunits HoxH and HoxY of the SH, which make up the $2H^+/H_2$ cycling moiety share similarities with subunits Nqo4 and Nqo6 of Complex I (Figure 18A and B). The core difference between Complex I and the hydrogenase moiety of the SH is that in Complex I, subunit Nqo4 which harbours the quinone binding site is replaced with the NiFe active site in HoxH. Sazanov *et al* showed that the Ni-binding site in the *D. gigas* NiFe hydrogenase is conserved in subunit Nqo4 of Complex I.[29, 92] Although no direct structural comparison can be obtained between subunits Nqo4 and HoxH of the SH due to no crystal structure being available for the SH, it is likely that the Ni-binding site in HoxH is conserved in subunit Nqo4 of Complex I.

As shown in Table 1-2, the diaphorase moiety of the SH also shares high sequence similarity with Complex I. Subunit HoxF, which harbours the NAD^+/NADH binding site and a 4Fe4S cluster is well conserved in Nqo1 (Figure 19) and is discussed in the next Section.

Figure 19. Amino acid sequence comparison between *R. eutropha* SH subunit HoxF and *T. thermophilus* Complex I subunit Nqo3 generated using ClustalW software (available online at www.ebi.ac.uk/clustalw/#). The amino acid sequences were obtained from www.uniprot.org and used without any modification.

1.6.2 The NADH binding site

A sequence alignment comparing the amino acid residues between subunits Nqo1 of *T. thermophilus* Complex I and *R. eutropha* HoxF to identify regions of similarity is shown in Figure 19. Based on the resolved crystal structure of the soluble domain of Complex I with NADH bound reported by Sazanov and co-workers,[29, 34] the amino acid residues taking part in NADH binding are shown as red letters in Figure 20. Comparing these to amino acid residues of HoxF, it can be concluded that most of the residues responsible for NADH binding in Complex I are conserved. Only Aspartic acid at position 184 of Nqo1 is not conserved in HoxF; however, a similar negatively charged amino acid group (Glu-340) is present in the SH. The presence of these amino acid residues thus indicates that the SH and Complex I are likely to share a similar NADH binding mode.

```
R. eutropha HoxF              LLLKPEQVIETIVDSRLRGRGGAGFSTGLKWRLCRDAESEQKYVICNADE 250
T. thermophilus Nqo1          ----PDEVIEEVKRSGLRGRGGAGFPTGLKWSFMPKDDGKQHYLICNADE 95

R. eutropha HoxF              GEPGTFKDRVLLTRAPKKVFVGMVIAAYAIGCRKGIVYLRGEYFYLKDYL 300
T. thermophilus Nqo1          SEPGSFKDRYILEDVPHLLIEGMILAGYAIRATVGYIYVRGEYRRAADRL 145

R. eutropha HoxF              ERQLQELREDGLLGRAIGGRAGFDFDIRIQMGAGAYICGDESALIESCEG 350
T. thermophilus Nqo1          EQAIKEARARGYLGKNLFG-TDFSFDLHVHRGAGAYICGEETALMNSLEG 194

R. eutropha HoxF              KRGTPRVKPPFPVQQGYLGKPTSVNNVETFAAVSRIMEEGADWFRAMGTP 400
T. thermophilus Nqo1          LRANPRLKPPFPAQSGLWGKPTTINNVETLASVVPIMERGADWFAQMGTE 244
```

Figure 20. Part of amino acid sequence comparison between subunits HoxF from *R. eutropha* SH and Nqo1 from *T. thermophilus* Complex I generated using ClustalW software (available online at www.ebi.ac.uk/clustalw/#). The amino acid sequences were obtained from www.uniprot.org. Red letters indicates the residues reported to be involved in NADH binding. Letters highlighted in yellow represent residues involved in the binding of NADH in Complex I but not conserved in SH.

Figure 21 illustrates the favourable binding position of NADH close to the FMN catalytic centre of Complex I Nqo1 subunit, with amino acid residues postulated to help accommodate NADH.[29, 34] Upon binding, the adenine of NADH is stabilised by three phenylalanine residues: Phe-205, Phe-78 and Phe-70 which form stacking interactions

with the ring. Other hydrophobic interactions are formed between the nicotinamide ring of NADH and the isoalloxazine ring of the FMN, making the nicotinamide ring stacked in the position suitable for a direct hydride transfer. Hydrogen bonds are formed between the bound NADH and amino acid residues such as Lys-202 with O-2A of the pyrophosphate. Glutamic acid conserved at position 185 also forms hydrogen bonds with the adenosine ribose of the NADH. A further hydrogen bond is formed between Gly-67 from the glycine rich loop and the diol of the nicotinamide ribose and according to Sazanov and coworkers, there are approximately 10 hydrogen bonds formed between NADH and the protein.[34] Binding of NADH induces movement of Glu-97 residue from the FMN thus allowing nicotinamide to occupy its position. Glutamic acid at position 97 is involved in van der Waals interaction with the C-4 atom of the NADH nicotinamide, while pushing it closer to the N-5 atom of FMN thus promoting hydride transfer as shown in Figure 21 (dotted red line).

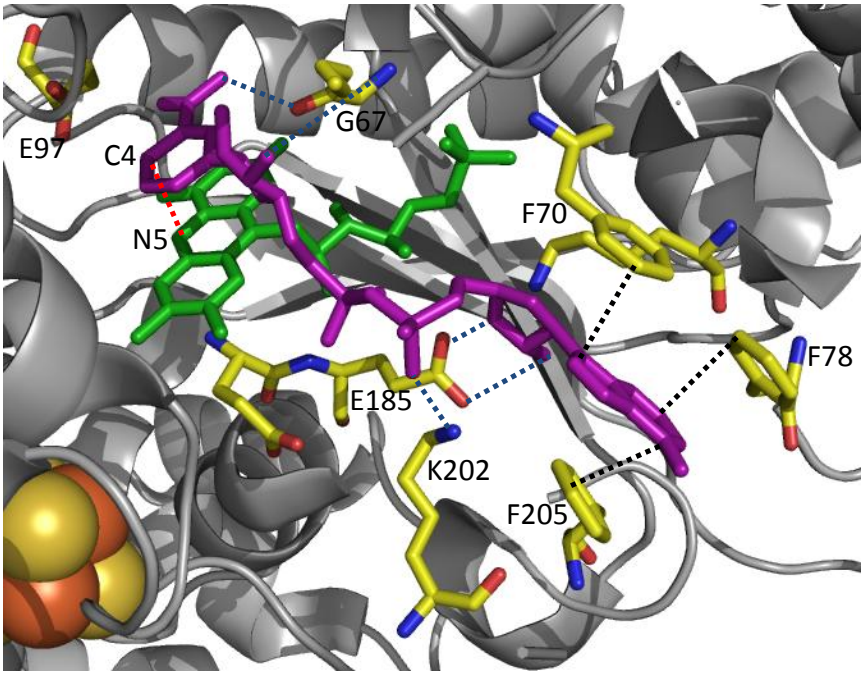

Figure 21. A close-up view of the NADH binding site of *T. thermophilus* Complex I resolved by Sazanov *et al*. Nicotinamide adenine dinucleotide (NADH) is shown as purple sticks, while flavin mononucleotide (FMN) is in green. Amino acid residues involved in interactions with

NADH and FMN molecules are shown as sticks and labelled. Hydrogen bonds are shown as dotted blue lines, stacking interactions are in black and the hydride transfer path is shown as a red dotted line. This picture was developed using Pymol, PDB code 3IAM.

1.6.3 FeS clusters composition in the SH

There are five FeS clusters in the SH, predicted by analogy with Complex I and detected using spectroscopic methods.[71, 77, 93, 94] One 4Fe4S cluster is present in HoxY together with FMN-a. The existence of this 4Fe4S cluster is confirmed by metal determination using total reflection X-ray fluorescence (TXRF) which showed a ratio of 6.2 Fe in the hydrogenase moiety, HoxHY.[20, 77] The ratio agrees well with the presence of a 4Fe4S cluster in HoxY alongside the Fe at the active site. The UV-Vis spectrum of HoxHY also shows a broad absorption peak between 350 nm and 500 nm, with a shoulder at 415 nm, characteristic of proteins containing FeS clusters.[77] Further experiments using extended X-ray absorption fine structure (EXAFS) confirmed the presence of one 4Fe4S cluster in the HoxY subunit.[20, 77]

UV-Vis spectrum of HoxFU diaphorase moiety shows broad shoulders at 322/380 nm and 421/480 nm, characteristic of 2Fe2S and 4Fe4S clusters, respectively. Based on the spectroscopic findings on the HoxFU diaphorase moiety and Complex I, three 4Fe4S clusters (two residing in HoxU and another in HoxF) and one 2Fe2S cluster (residing in HoxU) are predicted. Figure 22 shows a comparison between the C-terminal part of HoxF with part of the Nqo1 subunit showing the cysteine residues that are involved in binding of a 4Fe4S cluster in Complex I. The sequence alignment supports spectroscopic evidence that HoxF of the SH contains one 4Fe4S cluster.

```
T.thermophilus Nqo1              VILIPERVSMVDAMWNLTRFYAHESCGKCTPCREGVAGFMVNLFAKIGTG 377
R.eutropha HoxF                 FTIFNCKRDLLEIVRDHMQFFVEESCGICVPCRAG-NVDLHRKVEWVIAG 522
                                              *   **** * *** *

T.thermophilus Nqo1              QGEEKDVENLEALLPLIEGRSFCPLADAAVWPVKGSLRHFKDQYLALARE 427
R.eutropha HoxF                 KACQKDLDDMVSWGALVRRTSRCGLGATSPKPILTTLEKFPEIYQNKLVR 572
                                                      *

T.thermophilus Nqo1              KRPVPRPSLWR------------------------------ 438
R.eutropha HoxF                  HEG-PLLPSFDLDTALGGYEKALKDLEEVTR---------- 602
```

Figure 22. Sequence alignment of the C-terminal part of HoxF from *R. eutropha* SH with part of subunit Nqo1 from *T. thermophilus* Complex I. Cysteine residues involved in coordination of 4Fe4S cluster (N3) in Nqo1 subunit are highlighted. Amino acids residues conserved in both proteins are marked with a *.

The resolved crystal structure of Complex I shows that subunit Nqo3 contains four FeS clusters labelled as N3, N1b, N4 and N7. Three of these FeS clusters are suggested to be directly involved in transporting electrons from NADH oxidation, while one FeS cluster, the N7 due to its distance (20.5 Å edge to edge to N4, Figure 18C) is thought not to participate in tunnelling electrons to the quinone binding site. This subunit has also been shown to be similar to HoxU of the SH. As discussed earlier, spectroscopic experiments predicted that HoxF harbour three FeS clusters. Figure 23 shows a comparison between the amino acid residues of HoxU and Nqo3 subunits to illustrate the cysteine residues involved in coordinating FeS clusters in Complex I. From 16 cysteine residues involved in coordinating FeS clusters in Nqo3, 12 are conserved in HoxU suggesting the presence of three FeS clusters. The sequence alignment thus supports the spectroscopic evidence that HoxU harbours three FeS clusters.

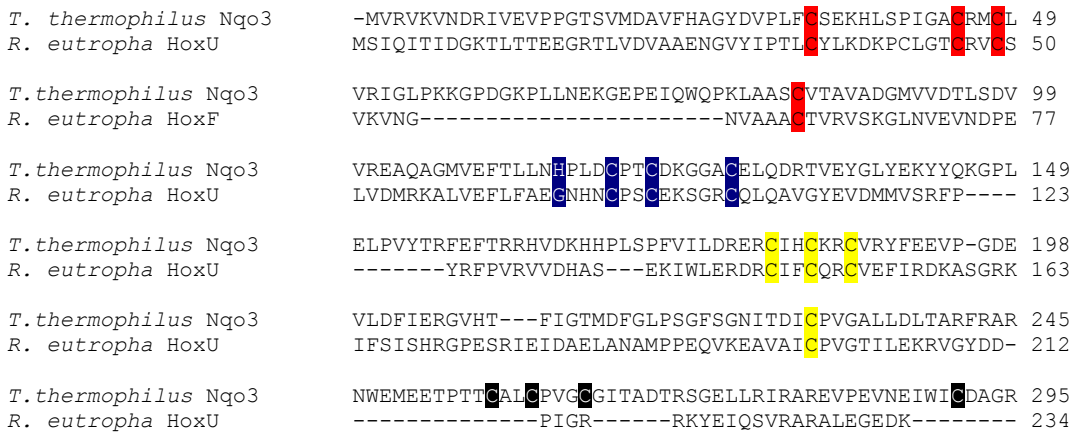

Figure 23. Part of sequence alignment of *R. eutropha* SH HoxU subunit with *T. thermophilus* Complex I Nqo3 subunit. Cysteine residues involved in coordination of FeS clusters in the Nqo3 subunit are highlighted (N1b in red, N4 in blue, N5 in yellow and N7 in black).

As mentioned earlier in this Section, Complex I oxidises NADH (to regenerate NAD^+ for the tricarboxylic acid cycle and fatty acid oxidation) and couples this reaction to quinone reduction while the main role of the SH is in H_2 oxidation coupled to NAD^+ reduction. The similarities between these two proteins indicate that they are phylogenetically related to each other.

1.6.4 Other Soluble Hydrogenases

The SH was the first bidirectional NiFe hydrogenase to be isolated and characterised in detail. It is closely related biochemically and genetically to the NiFe hydrogenase from the actinomycete, *Rhodococcus opacus*.[95-97] These two hydrogenases are so similar that the SH from *Rh. opacus* can be actively expressed in *R. eutropha*. The hydrogenase of *Rh. opacus* consists of four subunits, HoxHYFU and unlike the *R. eutropha* SH, it does not contain HoxI subunits. Furthermore, the SH from *Rh. opacus* is easily dissociated into HoxHY and HoxFU, while the *R. eutropha* SH remains stable as HoxHYFU.[95] Another important difference between these two hydrogenases is the apparent absence of the FMN-a in the HoxY subunit of *Rh. opacus* SH.

Other soluble hydrogenases have also been isolated from cyanobacteria such as *Synechocystis sp*. PCC 6803 and photosynthetic bacteria such as *Thiocapsa roseopersicina* and *Allochromatium vinosum*.[72, 98-100] These bidirectional hydrogenases are pentameric enzymes, consisting of a hydrogenase moiety (HoxHY) and a diaphorase moiety (HoxFUE). They harbour one extra subunit, HoxE which is homologous to subunit Nqo2 of Complex I, containing one FeS cluster but do not harbour HoxI that is present in *R. eutropha* SH. Although these hydrogenases have been isolated, thorough characterisations are yet to be performed. The schematic structure of the Soluble Hydrogenase from *Synechocystis sp*. PCC 6803 is shown in Figure 24.

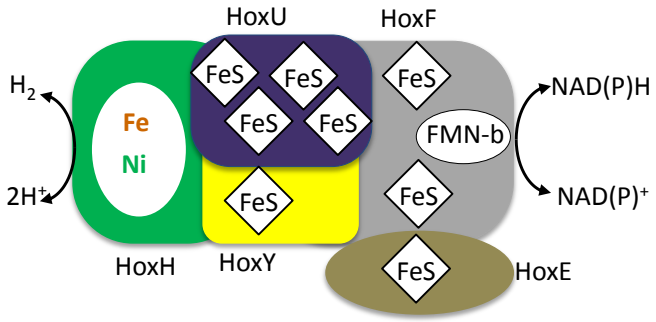

Figure 24. Bidirectional hydrogenase from *Synecocystis sp*. PCC 6803.

1.7 Applications of Soluble Hydrogenases in cofactor recycling

Selective oxidations of alcohols to carbonyl compounds or reduction of carbonyl compounds are important for industrially relevant applications. In biocatalysis, these reactions are catalysed by dehydrogenases and they normally require the presence of a cofactor, either NAD^+/$NADP^+$ or NADH/NADPH at stoichiometric levels. As these cofactors are expensive, efficient ways of recycling them are necessary. The *R. eutropha* SH has been tested as a potential catalyst for NADH regeneration. In an

early study, Monsan and coworkers showed that continuous NADH regeneration (equivalent to 111 NADH regeneration cycles over 45 hours of experiments) was obtained when the SH was covalently grafted onto corn stover particles.[101] In 1987, Okura and coworkers reported hydrogenation of ketones to alcohols in a system utilising H_2 gas as a reducing agent for NAD^+ reduction, using SH as the NADH recycling enzyme. They observed a total turnover number of 64 for a 65 hour reaction.[102] Later, Bergel and coworkers utilised the SH to regenerate NADH for transformation of α-ketoglutarate to L-glutamate by L-glutamate dehydrogenase with a turnover number of 450 per hour.[103] In a recent attempt to use the SH as catalyst for NADH regeneration, Ansorge-Schumacher and coworkers demonstrated that the SH, when coupled to *Candida parapsilosis* carbonyl reductase, gives a total turnover number of 143 666. This turnover number is higher than the common system utilising *Candida boidinii* formate dehydrogenase for NADH recycling coupled to formate oxidation to CO_2. Attempts to use the HoxFU diaphorase for NADH recycling are presented in Chapter 6 of this Thesis.

1.8 NAD(H) cycling on electrode

Elving and co-workers showed that NADH oxidation does not start until approximately 0.4 V on a pre-treated and NAD^+ covered pyrolytic graphite electrode.[104, 105] Electrochemical experiments utilising Platinum (Pt) and Gold (Au) as electrodes also show a huge overpotential requirement for NADH oxidation *i.e.* 1.3 V and 1 V on Pt and Au electrodes respectively.[106, 107]

Figure 25 illustrates the proposed pathways for NADH oxidation on an electrode.[108] The NADH oxidation on bare untreated electrodes has been reported to be

irreversible, accompanied by side reactions such as formation of an $(NAD)_2$-dimer complex and often poisoning of electrode surfaces.[105, 109, 110] It has been suggested that the high overpotential results from the very positive potential of the $NADH^{\cdot+}$/NADH couple ($E^{o'}$ of 1.12 V). Similarly, it is difficult to reduce NAD^+ by one electron alone, with the $NAD^+/NAD^{\cdot}$ potential having $E^{o'}$ of -0.92 V.

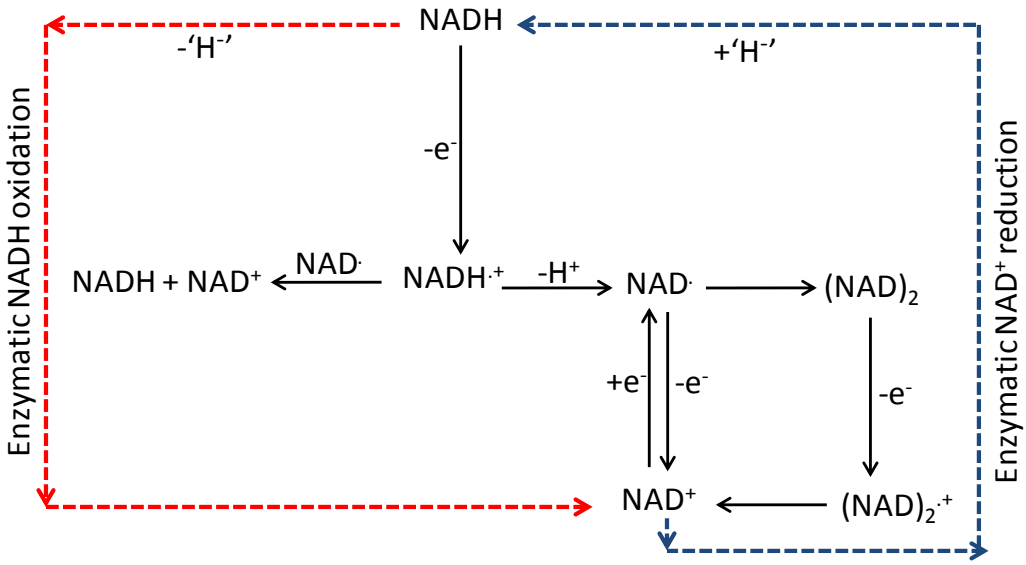

Figure 25. Some of the proposed reactions and side reactions in NADH oxidation at an electrode. NADH oxidation and NAD^+ reduction in enzymatic catalysed reactions are shown as dashed red and blue lines. Adapted with permission from ref[108].

Careful experimental procedures involving electrode pre-treatment and conditioning were employed by several research groups to obtain a reproducible results.[105-107] The pre-treatment procedure has been claimed to reduce the overpotential of NADH oxidation on a bare glassy carbon electrode by 0.1 V as reported by Blaedel and Jenkins.[107] They suggested that poising the glassy carbon electrode at potentials of 1.69 V and -1.69 V for two minutes helps to produce oxygen-containing functionalities groups such as hydroxyls and carbonyls that participate in NADH oxidation thus lowering the overpotential. These procedures, however, did not decrease the overpotential for NADH oxidation dramatically, thus hindering the possibility of

utilising these electrodes in an NADH regeneration system. In the case of NAD^+ reduction, it has been reported by Elving and coworkers that this reaction starts at approximately -1.2 V at pH 7.0 on a Mercury (Hg) electrode.[111] The reaction has been described as proceeding via the transfer of an electron to the pyridinium ring of NAD^+, followed by a fast NAD radical dimerization to form the catalytically inactive NAD dimer. The NAD dimer could be partially protonated and reduced to mixtures of 1,4-NADH and 1,6-NADH by polarising the Hg electrode at a much lower potential (around -1.6 V). Other electrode materials such as Au have been used for reducing NAD^+, albeit at a high potential of -1.1 V in phosphate pH 8.3.[112]

Considerable efforts have been put forward to reduce the overpotential requirements for either NADH oxidation or NAD^+ reduction on electrodes. For example, Kuwana and Tse reported the first chemically modified electrode to study NADH oxidation by covalently attaching 3-hydroxytyramine or 3,4-dihydroxybenzylamine onto a glassy carbon electrode thus forming a monolayer that has been activated with cyanuric chloride.[113] Both redox compounds attached onto the electrode revealed a reversible peak at around 0.16 V at pH 7.0 and in the presence of 1.0 mM NADH, an increase in the anodic current was recorded at approximately 0.2 V corresponding to mediated NADH oxidation. Thus the overpotential of NADH oxidation on a glassy carbon electrode could be reduced by 0.2 V by this method. Further improvements on chemically modified electrodes have been made by using dyes or polymers such as 3-amino-7-(diethylamino)-1,2-benzophenoxazin also known as Nile Blue A that was pretreated with aromatic acid chloride or aldehyde.[114] Again the pre-treatment procedure has been reported to increase the rate of reaction between adsorbed Nile Blue A and NADH in solution from 10 M^{-1} s^{-1} to 10^4 – 10^5 M^{-1} s^{-1}. A catalytic peak corresponding to NADH oxidation was observed at approximately 0 V

using this chemically modified electrode, indicating a decrease of 0.6 V in overpotential. Other techniques to reduce the NADH oxidation overpotential such as utilising polymeric mediators and immobilising NAD(P)H-dependent enzymes with mediators have also been explored.[115] In 2003, Karyakin and coworkers reported a reversible NADH oxidation and NAD^+ reduction on a glassy carbon electrode modified with poly(Neutral Red). The catalysis occurred close to the predicted $E(NAD^+/NADH)$, with negligible overpotential *i.e.* in an equal ratios of NAD^+:NADH, at pH 6, the theoretical $E(NAD^+/NADH)$ is -0.29 V and Karyakin and coworkers recorded a $E(NAD^+/NADH)$ of approximately -0.31 V. So far, this has been the first reversible NADH oxidation and NAD^+ reduction on a modified standard electrode.[116]

Nature, however, has evolved to produce an efficient group of enzymes that catalyse NADP(H) interconversion such as the bidirectional NAD^+/NADH NiFe-hydrogenases found in soil bacteria such as *Rh. opacus* MR11 and *R. eutropha* H16.[21, 95] These hydrogenases share amino acid sequence identity with Complex I that is important for oxidative phosphorylation in mitochondria. The most promising example of reversible NAD(H) cycling on a graphite electrode was reported by Hirst and co-workers, with an NAD-dehydrogenase subcomplex, purified from the Complex I of bovine heart mitochondria. The catalysis proceeds with no overpotential for 1 mM NAD^+: 1 mM NADH at pH 7.82.[117] Since the first reversible electrocatalytic NAD(H) interconversion reported by Hirst and coworkers, there has been no other literature report of efficient NADH catalysis by any other diaphorase enzymes and this Thesis will look at the ability of a diaphorase subcomplex from the *R. eutropha* SH to oxidise NADH and reduce NAD^+ on a graphite electrode.

1.9 Protein Film Electrochemistry for studying redox enzymes

Protein film electrochemistry (PFE) has been used to study a wide variety of proteins, ranging from simple cytochromes to complex hydrogenases.[118-129] In this technique, an aliquot of redox protein is adsorbed on to an electrode and the modified electrode is subjected to potential control. Provided that catalysis is not limited by intramolecular electron transfer, interfacial electron transfer or mass transport of substrate or product, the recorded current in PFE experiments on an enzyme is directly proportional to the catalytic activity: a higher current indicates that the redox enzyme is highly active, and exhibits a high turnover rate. Studying redox enzymes using PFE has made it possible to further understand their catalytic properties by revealing important thermodynamic information such as the affinity for substrates/inhibitors at specific potentials, and the occurrence of potential dependent inactivation/reactivation. A typical example of cyclic voltammograms for a subcomplex of bovine Complex I is shown in Figure 26. Upon sweeping the electrode potential towards higher values, positive current corresponding to a catalytic oxidation process (in this case NADH oxidation) is recorded and at low potential values, a negative current corresponding to a catalytic reduction (NAD^+ reduction) is observed. Other than that, information on the operating catalytic potential can also be extracted from cyclic voltammetry experiments. By comparing the experimental value with theoretical value, a measurement of catalyst overpotential can be obtained. A minimal overpotential requirement means that a reaction is catalysed efficiently by the redox protein. In the case of subcomplex of bovine Complex I as shown in Figure 26, catalytic current cuts sharply through the zero-current value indicating no detectable overpotential.

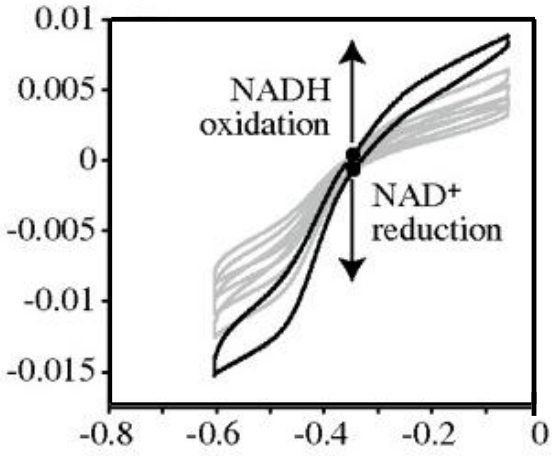

Figure 26. Reversible interconversion of NADH and NAD^+ by a sub-complex of hydrophilic domain of bovine Complex I reported by Hirst and co-workers. Adapted with permission from reference[117]

Quantitative information of an enzyme's affinity for its substrates and inhibitors can also be obtained through PFE experiments by holding the electrode potential at a constant value within the region of interest while changing the concentration of substrates/inhibitors. Since the catalytic current is proportional to the enzyme catalytic activity, current recorded at different substrate/inhibitor concentrations can then be analysed according to Michaelis-Menten kinetics to obtain the affinity constants. Further details of PFE are discussed in Chapter 2 of this Thesis.

1.10 Applications of enzymes on electrodes

1.10.1 Enzyme electrodes for H_2/O_2 fuel cells

Fuel cells convert energy derived from chemical reactions into electrical power. The performance of a fuel cell depends on the choice of electrocatalysts at the anode and cathode. Conventional fuel cells utilise precious metals such as platinum as a catalyst for the oxidation-reduction reactions. Platinum, apart from being rare and expensive, is also sensitive to CO and H_2S poisoning and this represents a significant

barrier to its application for future energy production. On the other hand, hydrogenases have been shown to adsorb on to an electrode surface and exhibit excellent catalytic activity: a turnover as high as 10 000 s^{-1} was achieved for *A. vinosum* NiFe hydrogenase on a graphite electrode.[130] Furthermore, at ambient temperatures and pressures, hydrogenases have been recognised to match Pt in their rates of catalysis. Several hydrogenases have also been shown to be O_2-tolerant,[119, 131-133] meaning that the catalysis is sustained in the presence of O_2, and essentially insensitive to CO. The high rate of H_2 oxidation exhibited by hydrogenases can be coupled to redox enzymes that catalyse reduction reactions, such as bilirubin oxidase, which in nature reduces O_2 to H_2O. An illustration of how these enzymes can be utilised to produce power in a fuel cell is shown in Figure 27.

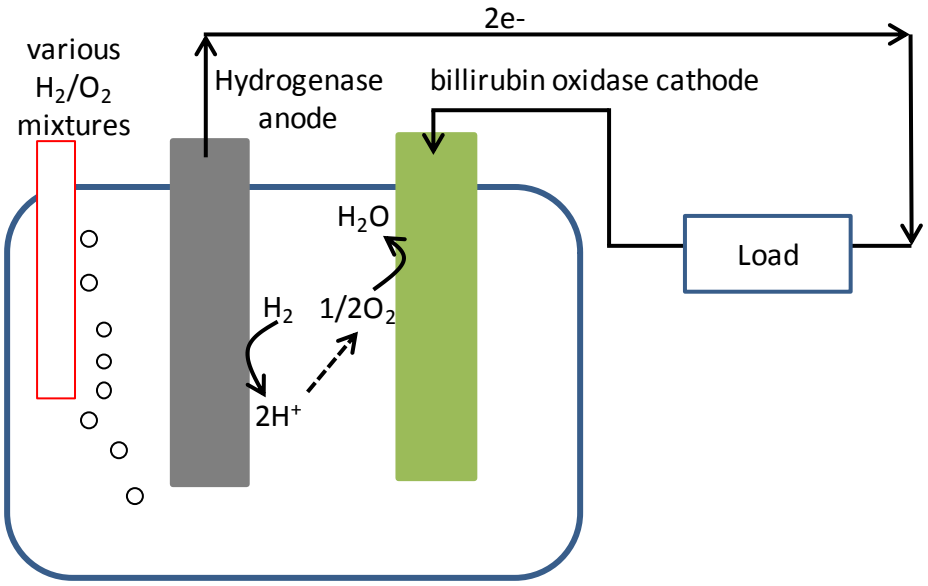

Figure 27. Schematic diagram of a enzyme fuel cell, utilising hydrogenase at the anode and bilirubin oxidase at the cathode, as demonstrated in reference [134].

The enzyme fuel cell illustrated in Figure 27 exhibits several advantages, for example it is non-toxic to the environment as it does not utilise heavy metals. In an enzyme fuel cell, a membrane separating the anode and cathode compartments is not necessary

because an enzyme is substrate specific, thus further reducing the cost. Very recently, Krishnan and Armstrong demonstrated an enzyme fuel cell comprised of covalently modified bilirubin oxidase (cathode) and *E. coli* Hyd1 (anode) with functionalised multi-walled carbon nanotubes which showed significant catalytic activity enhancement and stability.[135] Potentially, enzyme fuel cells open up possibilities for use of a broader choice of fuels by using different redox enzymes such as glucose oxidase for glucose oxidation, or fructose dehydrogenase for fructose oxidation, providing that these enzymes can be effectively 'wired' to electrodes.[136]

1.10.2 Biosensors

A chemical sensor is a device that converts chemical information into an analytically useful signal.[137] It consists of two components connected in a series: a chemical recognition system and a physico-chemical transducer. A biosensor is a chemical sensor that utilises a biochemical mechanism for its recognition system.[138] An example of commercially available biosensor is the blood glucose biosensor, which uses glucose oxidase to break down blood glucose into gluconic acid.[139] As glucose oxidase uses one molecule of O_2 to oxidise D-glucose, detection is often accomplished by monitoring the quantity of O_2 consumed during the reaction.

The vast range of NAD(P)(H) dependent dehydrogenases available offer a wide range of substrates specificities, and this makes it attractive for researchers to develop electrochemical biosensors based on the NAD(P)(H) cofactor.[140] However, one major drawback of utilising these dehydrogenases in electrochemical sensors is the high overpotential required for NADH oxidation or NAD^+ reduction on standard electrodes. Researchers have thus investigated the possibilities of minimising the overpotential requirements by using different types of mediators or electrode modifiers in the

systems. Enzymes capable of reversibly catalysing NAD^+/NADH have been used at electrodes with mediators for coupling with sensing systems and offer some improvements.[140] However, NAD^+/NADH cycling enzymes with suitable redox centres for direct electrons exchange with electrodes are rare.

1.11 Aims and structure of this Thesis

1.11.1 Understanding NAD^+/NADH cycling

In this Thesis, the ability of the SH from *R. eutropha* to catalyse NAD^+ reduction and NADH oxidation on a graphite electrode will be explored using PFE. Using protein engineering techniques implemented in the laboratory of Dr Oliver Lenz, the six subunits SH have been separated into two different catalytic moieties; electrochemical investigation into NAD^+/NADH cycling by the HoxFU moiety of the SH is described in Chapters 3 and 4, and characterisation of HoxHYFU is described in Chapter 5.

1.11.2 Exploring $NADP^+$/NADPH cycling

In Chapter 5, results are described for an electrochemical characterisation of a set of variants designed by our collaborators, Drs. Oliver Lenz and Lars Lauterbach to increase the affinity of the SH towards NADP(H). Up to now, there has been no demonstration of reversible $NADP^+$ reduction and NADPH oxidation at negligible overpotential on a graphite electrode, and Chapter 5 provides the first example of such an electrode, using graphite modified with these variants of the SH.

1.11.3 Developing a cofactor regeneration system

Protein Film Electrochemistry is used in this Thesis, to characterise the electrocatalytic behaviour of HoxFU and related enzyme constructs. This has provided insight into possible mechanistic features of the SH, and confirmed the success of mutations introduced to increase affinity for $NADP^+$. These results should underpin future applications, and methods of exploiting the diaphorase moiety, HoxFU for regeneration of NADH are explored in Chapter 6. The diaphorase is coupled with *R. eutropha* MBH for *in situ* regeneration of NADH by using H_2 oxidation as the electron source with no applied potential. The possibility of coupling a HoxFU electrode with an NADH-dependent oxidoreductase is also explored in Chapter 6. Both enzymes are co-immobilised on an electrode surface and the ability of HoxFU to recycle NADH for pyruvate reduction by lactate dehydrogenase is demonstrated.

Chapter 2: Electrochemical Theory and Experimental Methods

2.1 Introduction

This Thesis makes use of a technique called Protein Film Electrochemistry, in which the protein of interest is directly adsorbed onto the electrode surface, allowing a fast electron transfer between the electrode and the protein. Early studies of protein voltammetry involved protein solutions with small molecule redox mediators also in solution to assist with electron transfer. The usefulness of this technique was, however, limited by slow diffusion of protein and mediator to the electrode. Other than that, often a large amount of protein would be required and this is less useful if the enzyme of interest is not available commercially. In 1977, Kuwana[141] and Hill[142] both reported efficient electron transfer from a small redox protein, cytochrome *c* by utilising chemically modified electrodes that probably allowed transient association of the protein with the electrode surface. Kuwana and Yeh showed that cytochrome *c* solution shows a reversible electron transfer characteristics at a tin-doped indium oxide electrode with peak separation potentials of around 0.060 V, very close to the predicted value of 0.058 V for a one electron reaction of solution species. Hill and Eddowes illustrated that by using a planar gold disk electrode modified with 4,4'-bipyridyl or 1,2-bis-(4-pyridyl)ethylene, reversible cyclic voltammograms of horse heart ferricytochrome *c* were obtained.

It is now well established that redox proteins can be 'wired' onto electrode materials such as carbon and exhibit high rates of protein-electrode electron transfer.[57, 121, 143-146] Experiments described in this Thesis utilise the ability of redox proteins to exchange electrons with a pyrolytic graphite edge electrode which results in a diagnostic current as a measure of the enzyme catalytic turnover in response to variations in potential. Figure 28 is a schematic diagram of protein adsorption onto an electrode.

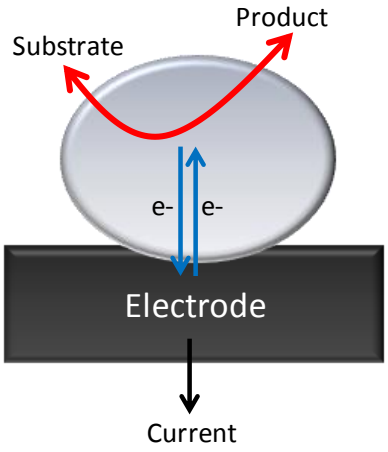

Figure 28. Cartoon showing direct electron transfer to an enzyme adsorbed on to an electrode.

The effective wiring of an enzyme on an electrode enables efficient control of the catalyst, thus allowing thorough characterisation of enzyme redox behaviour using a variety of electrochemical techniques. As the current corresponds directly to the enzyme catalytic rate, the enzyme may be probed with considerable precision. For example, the adsorbed enzyme can be transferred into different solutions containing different pH values while at the same time, substrates and inhibitors can also be introduced or removed. Non-turnover signals arising from electron exchange between redox-centres in the protein and the electrode can sometimes also be measured by PFE (depending on enzyme coverage on the electrode), and this will be explained in Section 2.3.4.3 of this Chapter.

2.2 Electrode surfaces and protein binding

It is important that electrodes used for electrochemical techniques have a good conductivity, however, extra factors also need to be taken into account for successful protein electrochemistry. It is essential that an enzyme, upon adsorption onto an electrode retains its natural folding. An electrode that could mimic the enzyme

interactions with its natural redox partners *in vivo* is a good choice, exploiting, for example, complementary hydrogen bonding or interactions between charged or hydrophobic regions thus allowing a kind of 'macromolecular recognition' between the surface and protein[147]. Commonly used electrodes for studying enzyme catalysis have been noble metals such as Au and Ag that been chemically modified with various surface functionalities,[148] since bare metal electrodes are thought to lead to denaturation and/or irreversible adsorption of an inactive protein. For example, irreversible adsorption of denatured cytochrome *c* on Ag was reported by Cotton and Hawkridge.[149, 150] Prior modification of a Ag surface was shown to facilitate electron transfer between the cytochrome *c* and the electrode, however, the voltammetric response was short-lived.[149-151] Many electrode materials such as Ni, Fe and Sn are found to be electroactive in the same potential window as the redox protein of interest and therefore utilising these electrodes would complicate the data interpretation due to interference from signals from the electrodes.[152]

Throughout this Thesis, a pyrolytic graphite edge (PGE) electrode has been employed due to its chemical inertness over a wide potential range (approximately -1 to +1 V vs SHE). The simple act of polishing the graphite surface with abrasives such as alumina generates an electrode with high levels of hydrophilic groups.[56, 153] Figure 29 shows a schematic diagram of pyrolytic graphite, which consists of a series of fairly ordered layered graphene sheets. Electrons flow parallel to the graphene sheets *via* delocalised (non-hybridised) p-orbitals. Theoretical calculations predict that graphite is a semi-metal in the direction parallel to graphene sheets, with zero band gap energy.[154]

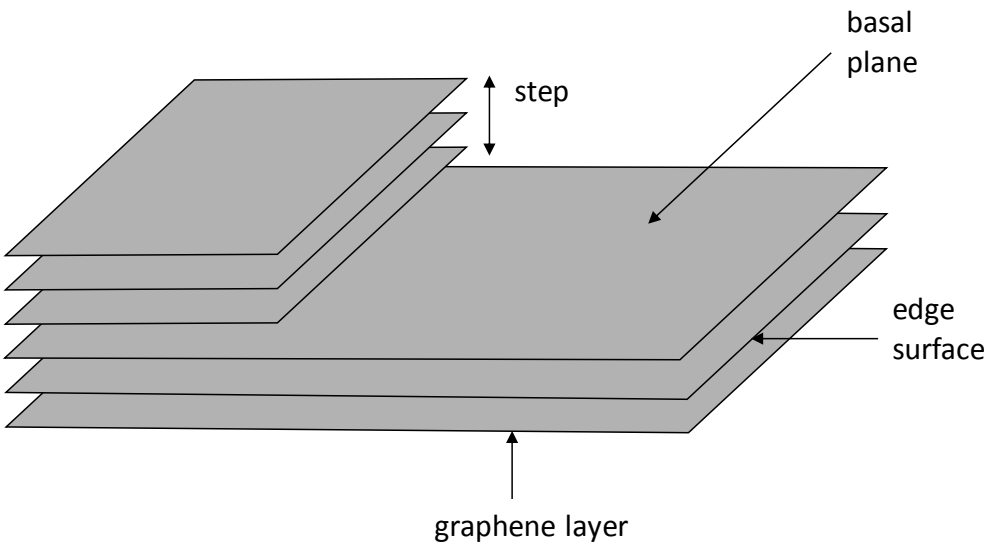

Figure 29. A cartoon representation of pyrolytic graphite showing directions of the edge (PGE) and basal (PGB) planes.

Compton and coworkers reported that the basal plane of the graphite is voltammetrically inert and that the efficient electron transfer occurs at the graphite edge plane sites.[155] Evidence for this was provided in a study in which they first 'protected' the edge plane of a graphite electrode by MoO_2 nanowires. Electrochemical reduction of 4-nitrobenzenediazonium cations that have been proved to produce radicals that chemisorb on graphite was then used to selectively block the basal plane terraces of graphite. Since the edge plane was 'protected' with MoO_2 nanowires, nitrophenyl radicals should chemisorb only on the basal plane terraces. The MoO_2-nanowires that protected the edge plane were then removed by placing the electrode into a solution of HCl. Theoretically by protecting the basal plane, the reversible cyclic voltammograms of $[Ru(NH_3)_6]^{3+}$ should be affected if electron transfer occurred at the basal plane terraces. However, they found out that blocking the basal plane terraces did not change the shape of voltammograms and reversible electron transfer was still observed. These findings thus confirmed their proposal that the basal plane terraces of graphite are inert,

and measurable electron transfer on an unblocked electrode was due to edge plane step defects.

Armstrong and coworkers have carried out an extensive series of direct electrochemical study of various redox proteins on pyrolytic graphite.[156] They showed that most proteins studied, except for blue copper azurin had a preference for hydrophilic edge than hydrophobic basal plane of the graphite surface. The presence of various oxidised C-O functionalities such as carbonyls, phenolic and carboxylic groups on the polished pyrolytic graphite edge surface was suggested to constitute reversible and productive binding domains for the proteins. In the case of blue copper azurin, the protein has been shown to also exhibit reversible signals on a basal plane graphite electrode. Armstrong and coworkers explained this difference by the fact that azurin contains a high proportion of non-polar side chains, and spatially distributed acidic and basic residues on its surface making azurin more suitable for interaction with the basal plane graphite that is more hydrophobic. Since then, many electrochemical studies have been performed on redox proteins directly adsorbed on to electrode surfaces, leading to a technique called protein film electrochemistry (PFE).[56, 57, 121, 123, 148, 157, 158]

In contrast to idealised adsorption of a protein molecule on a flat electrode surface as depicted in Figure 28, the reality is very different. Enzymes are normally large (HoxFU diaphorase studied in this Thesis is approximately 90 kDa) with complex and irregular surface shape and irregular electrostatic charge. Armstrong and Blanford showed that the surface of polished PGE is rugged and contains deep pores into which enzymes can access and bind: which in turn explains the observation that catalytic activity of hydrogenase on an electrode is retained even after an extensive polishing procedure.[153] Success in PFE depends on the choice of electrode used for measurement

and how the electrode surface is prepared and modified prior to protein adsorption or attachment.[123, 148]

Current measured in electrochemistry may stem from protein in the solution diffusing to the electrode surface and also from adsorbed protein on the electrode. To avoid the possibility of enzyme in solution contributing to the current, experiments in this Thesis were designed such that the enzyme-modified electrode was dipped into a clean buffer solution before the start of an experiment to remove unadsorbed protein. The electrochemical cell volume was typically 2 mL, so any desorbing protein would be extremely dilute and is therefore unlikely to contribute to the current response.

2.2.1 Film loss and selected film stabilisation strategies

One drawback of PFE is the gradual decrease in the catalytic current observed over time: a phenomenon often called 'film loss'.[159] The extent of this effect has been found to vary between enzymes and on the way the electrode was prepared prior to experiments. Several factors may contribute to film loss, including enzyme desorption from the electrode, denaturation or inactivation, and re-positioning of the enzyme from an active into an electro-inactive orientation.

Efforts have been employed to help minimise the film loss phenomenon, thus obtaining more stabilised enzymes on an electrode. For example, polycations such as polymyxin-B-sulphate are often effective in stabilising negatively surface charged proteins by forming cross linkages between the protein, electrode surface and adjacent protein molecules.[158]

There have also been attempts to adsorb proteins onto the surface of modified electrodes *e.g.* chemical modification of metal electrodes by formation of

self-assembled monolayers (SAM) to help enzyme stabilisation on electrodes. For example, de Lacey and coworkers developed a strategy for covalently attached *Desulfovibrio vulgaris* Hildenborough NiFeSe hydrogenase and *D. gigas* NiFe hydrogenase in a controlled orientation using a gold electrode modified with monolayers of 4-aminothiophenol.[160] Since the distal FeS cluster in *D. gigas* and *D. vulgaris* hydrogenases are surrounded by carboxylic groups, they suggested that amide bonds are formed between carboxylic and the amino groups of 4-aminothiophenol monolayer. Distinctive H_2 oxidation and H^+ reduction were observed after the SAM formation. Recently, the same group showed that the *D. vulgaris* Hildenborough NiFeSe hydrogenase in its native conformation (with the hydrogenase lipidic tail) can be attached onto modified gold electrode in a controlled orientation and exhibits clear H_2 oxidation.[161] Other redox proteins such as laccase from *Trametes hirsuta* and hydrogenase from *Aquifex aeolicus* have also been successfully immobilised onto modified gold electrodes.[162, 163] In the case of *A. aeolicus* hydrogenase, the recorded catalytic activity was only sustained for a short period of time (1 hour).

In 2005, de Lacey and coworkers reported a controlled immobilisation of *D. gigas* NiFe hydrogenase onto the surface of carbon electrodes.[164] They utilised the presence of several glutamic acid residues, close to the distal 4Fe4S cluster of the hydrogenase to electrostatically link the hydrogenase with electrodes modified with amine functionalities. At pH 6.0, most amine groups are protonated, making the electrode surface highly positive and the enzyme due to its surface charge, was postulated to orientate selectively to the modified electrodes through negatively charge glutamic residues, thus enabling direct electron transfer. A clear H_2 oxidation observed in the

absence of soluble mediator at pH 6.0 indicated direct electron transfer between the enzyme and electrode.

There have also been attempts to modify carbon electrodes in similar ways to that of metal electrodes. For example, Armstrong and Blanford illustrated with laccases from *Trametes versicolor* and *Pycnoporus cinnabarinus* that attachment of anthracene based units, which mimic the substrate, to the surface of PGE electrode not only enhanced the stability of protein film, but in fact also increased the current magnitude.[165]

Although there are efforts towards modifying the electrode surface for improved and stabilised adsorption of redox proteins, these techniques are normally specific for certain types of protein *e.g.* attachment of anthracene to the surface of PGE worked well for laccases as shown by Armstrong and coworkers because they possess a binding fold for organic substrates, but would not work for hydrogenases. Similarly the attachment strategies used for hydrogenases that rely on a surface patch of negative charge are not generalisable to all redox enzymes. For many studies of redox proteins by PFE, it is more straightforward to rely on direct adsorption onto graphite, although more robust ways of attaching the proteins may be necessary for development of applications of biocatalysis.

2.3 Methods of potential control

In PFE, provided that catalysis is not limited by mass transport or interfacial electron transfer, the current recorded is proportional to the catalytic turnover rate of the enzyme on an electrode. Experiments described in this Thesis mainly concern two types of techniques employed to study enzyme catalysis: cyclic voltammetry and chronoamperometry. This Section will briefly discuss these two techniques.

2.3.1 Chronoamperometry

In a chronoamperometry experiment, the working electrode is poised at a fixed potential or stepped through a series of different potentials, and a plot of current against time is recorded. Figure 30 illustrates that decreasing the substrate concentration (in this case H_2) while maintaining the electrode potential at a certain value, results in a current drop thus allowing a precise measure of enzyme catalytic activity at different substrate concentrations at a fixed potential value. This technique is applied in this Thesis for determining enzyme affinity for its substrate. PFE has been utilised to determine the enzyme affinity constants for many redox enzymes that obey Michaelis-Menten kinetics, such as [NiFe] hydrogenases of *D. gigas, D. fructosovarans, R. eutropha, E. coli, Salmonella* and *R. metallidurans*.[132, 133, 166-170]

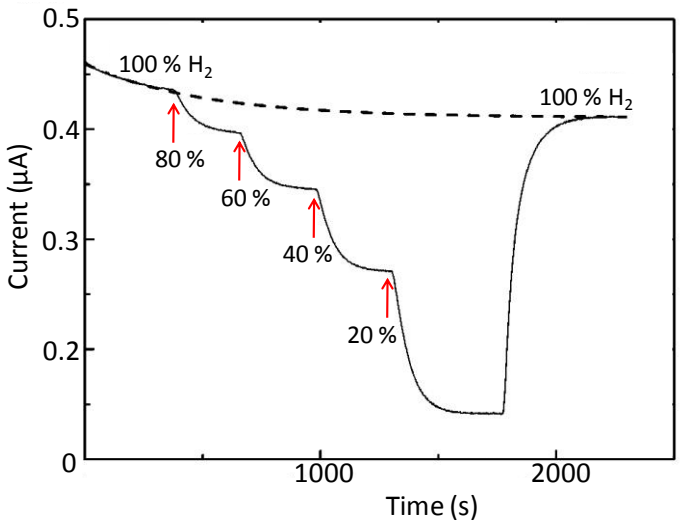

Figure 30. A plot of current against time showing decreasing the H2 concentration in the electrochemical cell decreases the catalytic current. Adapted with permission from reference[171].

Chronoamperometry can also be used to check for an inhibitor's effect on the catalytic activity of an enzyme, as shown in Figure 31. The working electrode in this case was poised at a value in which the enzyme is catalytically active and at the beginning of the experiment, a distinctive catalytic current was observed. When an

inhibitor is introduced into the cell solution (indicated by a grey box in Figure 31), a significant drop in current was recorded as the enzyme loses activity. Depending on the nature of the reaction, once the inhibitor is removed from the cell either by exchange of cell solution, or by flushing out a gaseous inhibitor with an inert gas, the catalytic activity may recover quickly or slowly. There is, however, the possibility that the current may not increase at all, indicating that the inhibition is irreversible or potential dependent *i.e*. the enzyme may need a different potential for reactivation.

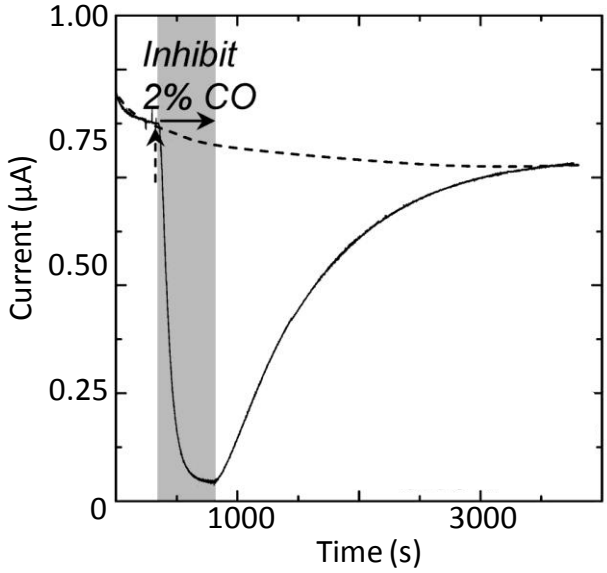

Figure 31. Hydrogen oxidation by a hydrogenase is inhibited by CO. A plot of current against time showing inhibitor (CO) injection (dashed black arrow), resulting in a decrease in current and as inhibitor being flushed out from the electrochemical cell (after the grey area), an increase in current is observed corresponding to activity recovery. Adapted with permission from ref[171].

2.3.2 Cyclic Voltammetry

In a cyclic voltammetry experiment, the working electrode potential is swept between two potentials at a specific scan rate (Figure 32A), whilst the current is recorded against applied potential, resulting in a cyclic voltammogram as shown in Panel B.

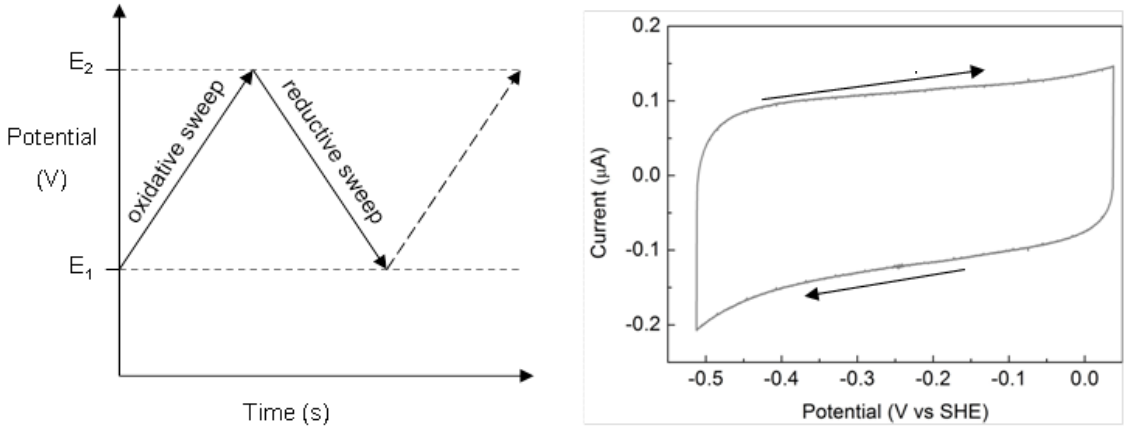

Figure 32. Panel A: the linear sweep potential waveform used in a cyclic voltammetry experiment. Panel B: a typical current against potential plot showing a response on an unmodified PGE rotating electrode. Arrows show the direction of scan. Experiment was performed in a Tris-HCl buffer solution at pH 8.0, at 30 ^{o}C with a rotation rate of 2500 rpm.

Current recorded from a cyclic voltammogram arises from two processes: Faradaic and non-Faradaic. Faradaic current will be discussed in the following sub-section. Non-Faradaic current is observed as the electrode potential is changed, giving rise to background currents observed in an unmodified electrode as shown in Figure 32B.

2.3.3 Non-Faradaic current contributions

When the electrode potential is swept between two values, the electrode surface is charged. To compensate for charge building up on the electrode surface, ions in the solution rearrange, and this results in formation of an electrical double layer which acts as a capacitor. The magnitude of this capacitive current depends on several factors such as electrode surface area, scan rate, temperature and solution composition.

Although non-Faradaic current results from non-redox electrochemistry (it is not caused by electrons flowing across the electrode-solution interface), its contributions

must be considered and in cyclic voltammetry experiments, a background scan is used in comparison with voltammograms which show a redox process.

2.3.4 Faradaic current contributions from adsorbed species

Experiments performed in this Thesis are mainly concerned with adsorbed redox-active species. In a cyclic voltammetry experiment for example, when the electrode potential is swept back and forth, a redox active species on the electrode surface will be oxidised and reduced. These processes occur because of electrons being rapidly exchanged between the electrode surface and the redox species, forming the Faradaic component of the current recorded. This gives a peak-like response for a simple electron transfer event, but for an enzyme in the presence of substrate, a catalytic wave is observed as the enzyme undergoes many cycles of electron transfer and catalysis.

During catalysis by a multi-redox centre enzyme adsorbed on an electrode, the overall rate of reaction will depend on the slowest component of the chain, as illustrated in Figure 33. Armstrong has defined the electrochemical control centre as the redox site that controls the catalysis, by becoming the limiting step in which the rate of electron transfer between the electrode and enzyme's redox centres before reaching this particular redox site is fast.[157, 172] Assuming that the intramolecular electron transfer is efficient, three factors that could be rate limiting during catalysis are the mass transport, the enzyme catalysis at the active site and the interfacial electron transfer between the electrode surface and enzyme.

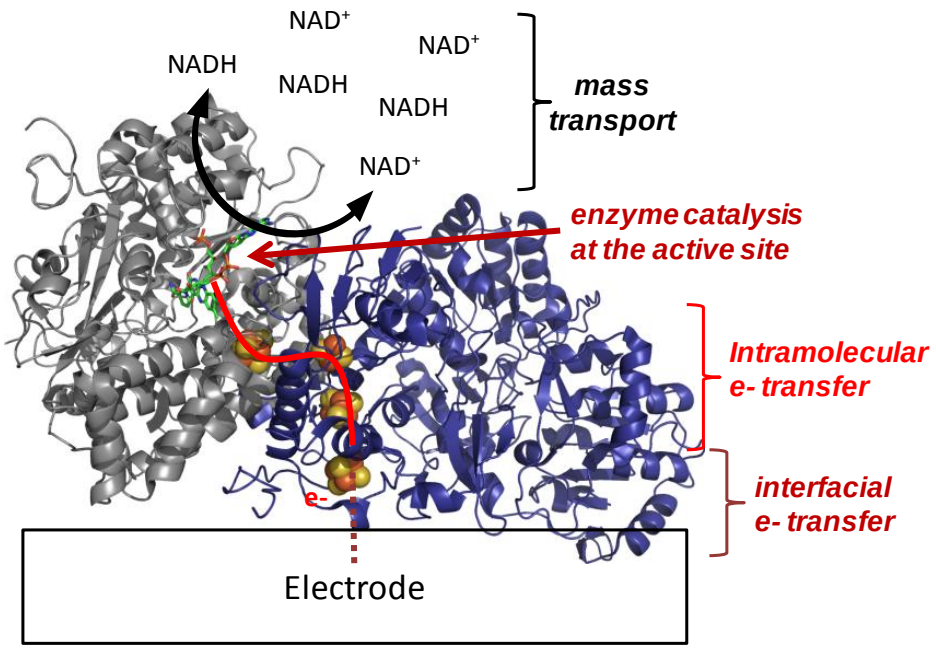

Figure 33. Possible rate determining steps during enzyme electrocatalysis of NAD^+ reduction and NADH oxidation by an immobilised enzyme.

Experiments in this Thesis have been carefully designed so that catalysis recorded is under enzymatic control and not limited by mass transport.

2.3.4.1 Mass Transport Effects

It is important that during catalysis, the substrate is constantly supplied to the electrode and the product is constantly removed to keep the surface concentration at the electrode close to the levels in the bulk solution. For this purpose, all experiments in this Thesis (unless described otherwise) were performed using a rotating disk PGE electrode. These homemade electrodes consist of a 2 mm diameter rod of pyrolytic graphite with the edge surface positioned to face the electrochemical cell solution, entrapped in insulating epoxy resin. The electrode is fitted to the shaft of a motor which rotates the electrode rapidly. Upon rotation, product in solution close to the electrode surface is spun away, and fresh solution is thus drawn close to the electrode surface

ensuring a constant supply of substrate at the electrode surface in addition to removal of product (Figure 34).

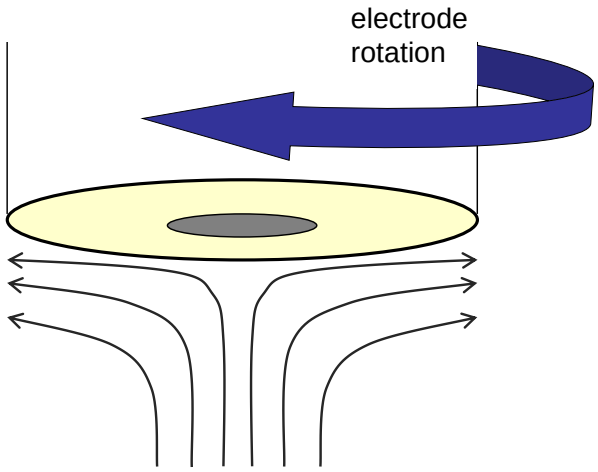

Figure 34. Schematic diagram of laminar flow at a rotating PGE electrode.[173]

The recorded current is dependent on the rate of electrode rotation, ω and the relationship between the rate and current, *i* is given by equation [3];

$$i = 0.62\, n\mathrm{F}A\mathrm{D}^{2/3}v^{-1/6}\omega^{1/2}[\mathrm{S}] \qquad [3]$$

in which in which D is the diffusion coefficient of the substrate, F is Faraday's constant, *A* is the electrode surface area, *v* is the kinematic viscosity of the solution and [S] is the concentration of the substrate. Equation [3] is also known as the Levich equation, and indicates that the current increases as the square root of the electrode rotation rate.

For a sparsely dispersed catalyst on the electrode surface (*e.g.* a large enzyme molecule), it may be possible to achieve a high rotation rate at which the catalytic current is no longer limited by the rotation rate i_{lim}, thus giving limiting current the relationship with electrode rotation rate as ω continues to increase and the enzyme takes

control of the catalytic rate. The relationship is now defined by the Koutecky-Levich equation (equation [4])

$$\frac{1}{i_{\mathrm{lim}}} = \frac{1}{i_{\mathrm{lim}}} + \frac{1}{0.62nFAD^{2/3}\omega^{1/2}\nu^{-1/6}[S]} \qquad [4]$$

where i is the current at rotation rate ω, and i_{lim} is the maximum limiting current achieved (or extrapolated) at infinite rotation rate. Based on equation [4], i_{lim} could be obtained by a plot of $1/i$ against $1/\omega^{1/2}$, however, it is impractical to carry out every experiment over a range of rotation rates, so an approximation of i_{lim} is obtained by using a rotation rate at which no significant increase in current is recorded when ω is increased. For experiments in this Thesis, a rotation rate of 2500 rpm was used (unless otherwise stated) which was sufficient to ensure the catalysis is controlled by the enzymatic reaction rather than mass transport. As the rotation rate was increased above 2500 rpm, no distinct increase in the current value was observed (data not shown) confirming that at 2500 rpm, catalysis by a typical film of the SH is not under mass transport control.

2.3.4.2 Interfacial Electron Transfer considerations

When a redox enzyme undergoes catalysis, interfacial electron transfer plays an important part for efficient product formation. Interfacial electron transfer is related to the location of the electron relay centres to the active site of the enzyme, and how efficiently at least one of these centres is able to make a good electronic contact with the electrode surface. It can be described using the Butler-Volmer equation, which is derived below (as set out in references[173, 174]):

Equation [5] shows a general equation for a redox reaction, in which n is the number of electrons involved in the reaction, F is the Faraday constant, k_{ox} and k_{red} are rate constants.

$$\mathrm{ox} + n\mathrm{e}^- \underset{k_{ox}}{\overset{k_{red}}{\rightleftharpoons}} \mathrm{red} \qquad [5]$$

The net current, i is given by the flow of charge as shown in equation [6],

$$i = i_{ox} - i_{red} = n\mathrm{F}Ak_{ox}\Gamma_{red} - n\mathrm{F}Ak_{red}\Gamma_{ox} \qquad [6]$$

in which Γ is the surface coverage of oxidised and reduced species, A is the electrode surface area.

Transition State Theory predicts that the rate of a reaction, k_r is given by equation [7]:

$$k_r = A\exp\left(\frac{-\Delta G_r^{\ddagger}}{\mathrm{RT}}\right) \qquad [7]$$

in which $G_r^{\ddagger}$ is the Gibbs energy of activation, R is the gas constant and T is the temperature.

In a reversible electron transfer process, the rates of oxidation and reduction increase exponentially with overpotential (E - E^0). In this theory, α is the transfer coefficient ($0 \leq \alpha \leq 1$): characteristic of the transition state (the closer α to zero, the transition state is more reactant like, and if the α is closer to 1, the transition state is more product like).[175] Expressing equations [6] and [7] in terms of α results in equation [8]

$$i = nFAk_{\mathrm{o}}\left(\Gamma_{\mathrm{red}}\exp\left(\frac{(1-\alpha)n\mathrm{F}}{\mathrm{RT}}\right)(E-E^{0}) - \Gamma_{\mathrm{ox}}\exp\left(\frac{-\alpha n\mathrm{F}}{\mathrm{RT}}\right)(E-E^{0})\right) \quad [8]$$

Equation [8] is known as the Butler-Volmer equation and it describes how the current recorded varies as a function of applied potential.[152, 176] A more precise relationship between the electron transfer rate and the applied potential can be derived from Marcus theory but this is significantly more complex and is unnecessary for experiments described in this Thesis.

2.3.4.3 Non-turnover process

Theoretically in the absence of substrate, when no catalysis takes place, any enzymatic redox sites that are capable of reversible electron transfer should give rise to reversible electrochemical signals centred on the redox potential of the redox sites.

The possibility to observe non-turnover signals depends on several factors such as the protein size and coverage. Small proteins such as ferredoxins, give high electroactive coverage on an electrode thus the non-turnover signal can be easy to detect. In comparison, a much larger protein such as hydrogenase will have a low electroactive coverage making the any non-turnover signal difficult to detect. Even so, a number of non-turnover signals for larger proteins such as cytochrome *c* peroxidase, fumarate reductase and NiFe hydrogenase from *A. vinosum* have been detected using PFE.[177-180]

2.3.4.4 Electrocatalysis

Experiments described in this Thesis are focussed on enzyme electrocatalytic current in the presence of substrates. When a substrate is present, the reversible electron

transfer is coupled to catalytic turnover which, in an ideal case, gives rise to a sigmoidal current response as shown in Figure 35.

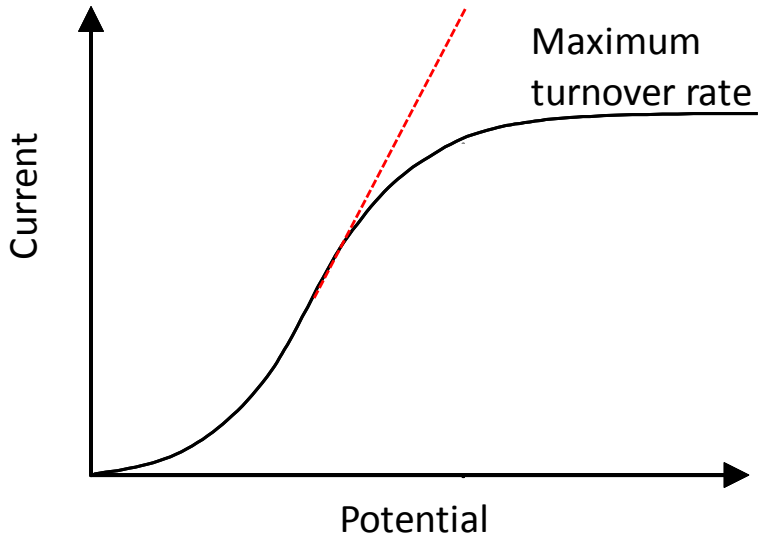

Figure 35. An ideal catalytic waveshape in which the current plateaus when the enzyme active site reaches its maximum rate of catalysis, limited by a chemical step rather than by the rate of interfacial or intramolecular electron transfer. The dashed red line reflects the residual slope, in which the catalytic current continues to rise with potentials.

From the voltammogram in Figure 35, some useful information can be extracted such as the current, i_{cat} which is a direct measure of the rate of catalytic electron flow through the enzyme active site to/from the electrode surface. If the enzyme electroactive coverage on the electrode is known, the enzyme catalytic turnover rate, k_{cat} can be calculated by using equation [9]:

$$i_{cat} = n\mathrm{F}A\Gamma k_{cat} \qquad [9]$$

Secondly, a voltammogram can also tell the potential at which catalysis starts, which in turn reflects the identity of the electrochemical control centre.[157, 172] In a normal electrochemical experiment with an enzyme, the intramolecular and interfacial electron transfer is fast, so the rate determining step during catalysis is the rate of reaction at the active site (control centre).

Thirdly, at high potentials, in an ideal case, the catalytic current will reach a plateau when the enzyme is said to have reached its maximum catalytic activity. This limit is reached because the rate of electron transfer at the active site is no longer the rate determining step that limits the rate of the catalytic reaction. However, it has been observed that the catalytic current for an immobilised enzyme often does not reach a plateau at high potentials. Instead the current displays a residual slope, continuing to rise with potentials (dotted red line in Figure 35). This phenomenon has been described thoroughly by Lèger and coworkers who attributed this effect to a dispersion of orientations of enzyme on the electrode.[121] In an ideal enzyme adsorption onto an electrode surface, the electron relay centres to the active site would be aligned with identical orientation, however, in reality the enzyme molecules are likely to adsorb in a variety of orientations. This thus gives rise to a range of distances between the enzyme electron relays and the electrode surface, creating a necessity for different magnitudes of overpotential to enable fast electron transfer.[157, 176, 178, 179, 181, 182]

2.4 Electrochemical apparatus

2.4.1 Electrochemical cell setup

Experiments described in this Thesis have been carried out using a three electrode cell system as shown in Figure 36 and Figure 37. During each experiment, a potential is applied between the working electrode and the reference electrode. The current generated due to redox reactions at the working electrode is passed mostly between the working electrode and the counter electrode instead of the reference electrode so that the reference electrode potential remains constant throughout experimental period.

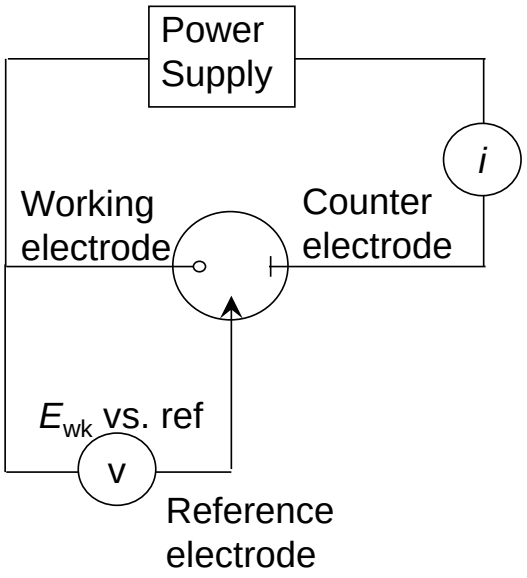

Figure 36. A schematic circuit diagram of a three electrode system used in this Thesis.

A schematic diagram of a homemade glass electrochemical cell is shown in Figure 37. A water jacket connected to a water circulator (Grant) was fitted into the electrochemical cell to allow the cell temperature to be controlled during all experiments. Platinum wire (Alfa Aesar) was used as a counter electrode, while a saturated calomel electrode (SCE, BACS) was used as a reference electrode. During experiments, the working electrode was connected to the electrode rotator (EG&G model 636) for efficient substrate supply and product removal. A specially designed sidearm, below the counter electrode compartment was used in experiments involving inhibitors/substrates injections. Experiments were performed using a potentiostat (Autolab PGstat128N, EcoChemie, The Netherlands) controlled by GPES software (EcoChemie) running on a computer.

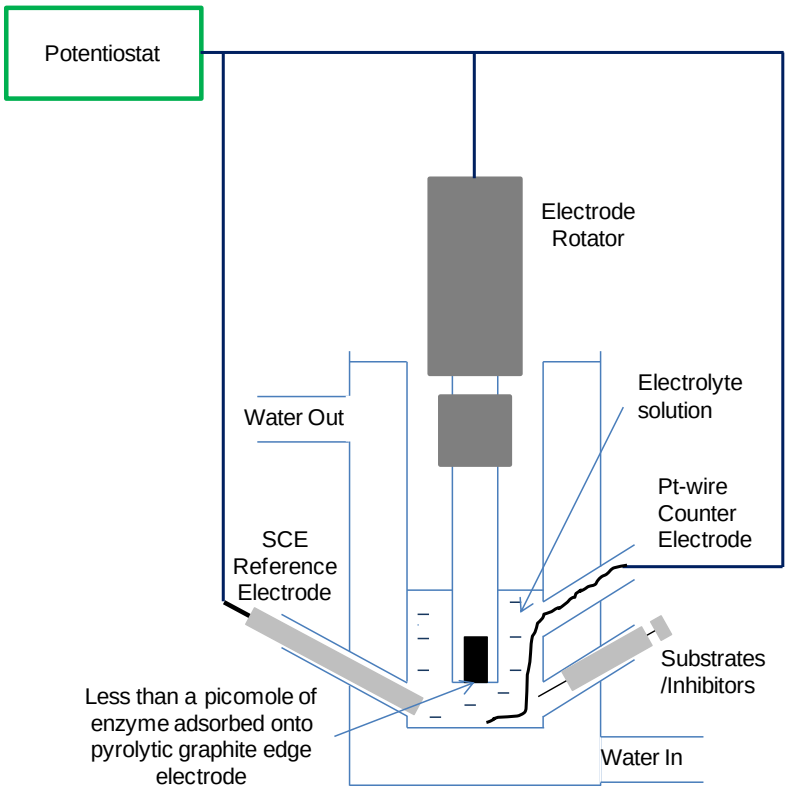

Figure 37. A schematic diagram of the homemade glass electrochemical cell used for experiments described in this Thesis.

The working electrode used throughout this Thesis was made using a pyrolytic graphite rod (Momentive Performance Materials) with an edge surface area of 0.03 cm^2, incorporated into a Delrin rotating disk electrode case (Figure 38).

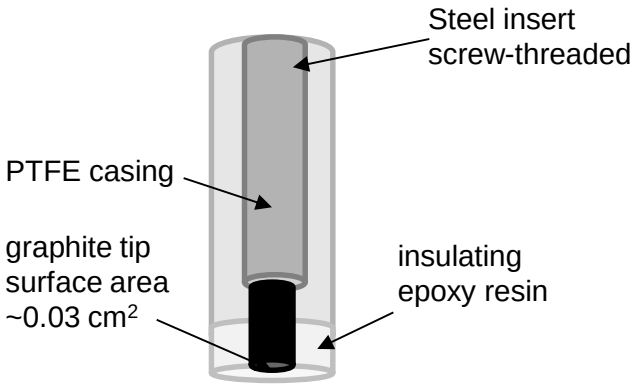

Figure 38. Schematic diagram of the pyrolytic graphite edge (PGE) rotating disk electrode used for experiments in the Thesis.

2.4.2 Glove box

All experiments described in this Thesis were performed or set up in an anaerobic glovebox (MBraun) which operates under N_2 to prevent enzyme exposure to O_2, or O_2 reduction at graphite complicating the voltammetric response.

2.5 Enzymes and preparation of enzyme films

2.5.1 Purification of *Ralstonia eutropha* SH HoxFU moiety

*I spent two one-week visits in Berlin at the Humboldt University learning protein purification with Lars Lauterbach.

Purification of HoxFU diaphorase dimer was performed by homologous overproduction of *hox*FU genes in a plasmid containing the SH-related *hox*FUYHWI operon. The *hox*YH genes encoding the hydrogenase module were deleted and a *Strep*-tagII-encoding sequence was placed at the 5' end of the *hox*F gene.

The plasmid was then transferred into a mutant derivative of *R. eutropha* that is inactive in producing the energy generating membrane bound and soluble hydrogenase. The cells were then grown in a liquid fructose glycerol minimal medium. The soluble cell extract was then subjected to a *Strep*-tactin affinity and size exclusion chromatography. As shown in Figure 39, the second purification step was effective in purifying HoxFU.

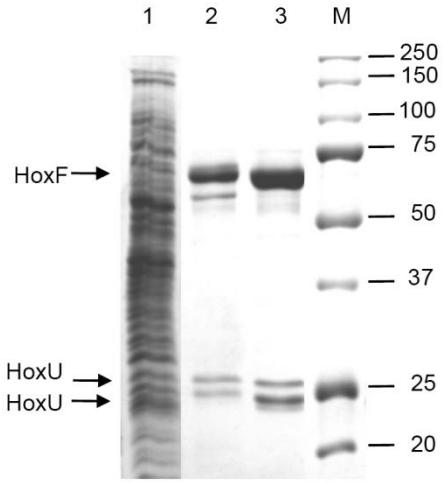

Figure 39. Analysis of HoxFU purity, before and after purification using sodium dodecyl sulphate polyacrylamide gel electrophoresis (SDS-PAGE). Soluble extract (20 µg, lane 1) and purified protein after *Strep*-Tactin affinity chromatography (3 µg, lane 2) and subsequent size exclusion chromatography (3 µg, lane 3) were separated by SDS-PAGE and stained with Coomassie blue. A standard protein ladder and the corresponding sizes in kDa are shown in lane M. Arrows indicate the HoxF protein at 67 kDa and two subforms of HoxU at approximately 27 and 23 kDa.

Two protein bands on the SDS-PAGE gel at approximately 23 and 27 kDa were assigned to HoxU by mass fingerprinting.[94] The purified HoxFU diaphorase moiety was then subjected to specific activity measurements by monitoring the changes in NADH absorbance in a UV assay using benzyl viologen (BV) as an electron acceptor. Table 2-1 shows that about 0.5 mg of high activity HoxFU was purified from 32 g (wet weight) of cells. Purification of $HoxFUI_2$ was performed as explained for HoxFU, but at low salt concentration to avoid dissociation of the HoxI subunits.

Table 2-1. Purification of HoxFU diaphorase.

Sample	Volume (ml)	Total protein (mg)	Specific NADH:BV oxidoreductase activity (Units mg^{-1})
Solubilised extract	40.0	1100.0	1.5
HoxFU after affinity chromatography	3.0	2.1	159.5
HoxFU after size exclusion chromatography	2.0	0.5	349.4

2.5.2 Membrane Bound Hydrogenase (MBH)

Samples of *Ralstonia eutropha* MBH used for experiments in Chapter 6 were kindly supplied by Dr Oliver Lenz of Humboldt University.[18]

2.5.3 Lactate dehydrogenase

A sample of L-lactate dehydrogenase from rabbit muscle was purchased from Sigma Aldrich and used without further purification. The sample comes as a lyophilised white powder and is stored at 4 ^{o}C. For experiments described in Chapter 6, the enzyme powder was dissolved in BisTris-HCl pH 6.0 at a concentration of 10 mg/mL, and used without further purification.

2.6 Solutions and gases

2.6.1 Electrochemical buffers

Most experiments described in this Thesis utilised Tris-HCl buffer made by dissolving 0.6057 g of Trizma base (Sigma Aldrich) into water in a 100 mL volumetric flask. When preparing buffer solution, the Milli-Q water (resistivity 18.2 MΩ cm) was added so that the solution volume was just below the calibrated 100 mL line. This procedure ensures that upon titration with HCl, an accurate final volume of 100 mL can be obtained. The prepared buffer was then titrated to the desired pH value with concentrated hydrochloric acid (Fisher Scientific) using a calomel pH electrode (Fisher Scientific), calibrated each time before use at the appropriate temperature using standard pH solutions.

Schneider and Schlegel have shown that the SH is sensitive to the concentration of Na^+ ions: the presence of 0.2 M Na^+ inhibits 70 % of its hydrogenase activity.[21]

Therefore, in Chapter 3 of this Thesis, where buffer solutions at different pH values were required, a mixed buffer system was used. The mixed buffer consists of several buffer species (at 15 mM; plus KCl at 100 mM), and was prepared using the following recipe (Table 2-2), for a 100 mL solution:

Table 2-2. Recipe used for making 100 mL of mixed buffer.

Chemical (supplier)	Molecular weight (g/mol)	Quantity needed (gram)
CHES (Sigma Aldrich)	207.29	0.3109
TAPS (Sigma Aldrich)	243.28	0.3649
HEPES (Sigma Aldrich)	238.31	0.3575
MES (Acros Organics)	195.23	0.3198
Sodium Acetate (Sigma Aldrich)	82.04	0.1230
KCl (Fisher Scientific)	74.56	0.7456

A BisTris-HCl buffer was employed for experiments described in Chapter 6 of this Thesis, prepared by mixing 1.0462 g of BisTris (Fluka) into a 100 mL volumetric flask and titrating to pH 6.0 with HCl.

When necessary, phosphate buffer was used by titrating 50 mM K_2HPO_4 (Fisher) and 50 mM KH_2PO_4 (Fisher) to the required pH. Most experiments in which phosphate buffer was utilised were performed at pH 7.0.

2.6.2 Substrate purification

Commercially available NAD^+, NADH, $NADP^+$ and NADPH often contain impurities such as adenosine diphosphate ribose (ADP-Ribose) and adenosine triphosphate (ATP) which have been shown to inhibit NADH catalysis by

Complex I.[117, 183-185] The reduced NAD-cofactor is also often contaminated with its oxidised form (see Chapter 3 Section 3.3.1) and this would cause considerable problems for quantitative data analysis. For example, since NADH is contaminated with NAD^+, it will cause a problem to determine the actual starting concentration of the NADH solution in a chronoamperometry experiment which would give a wrong interpretation of the substrate affinity constant for HoxFU. Furthermore, contamination also causes particular problems for studying HoxFU which is product inhibited. Thus it is necessary that these impurities are separated from the required cofactors before being used in electrochemical experiments.

A method was reported by Orr and Blanchard to effectively purify the oxidised and reduced forms of NAD and NADP cofactors by using a high performance anion exchange chromatography on a Pharmacia Mono Q anion exchange column.[183] They reported that at pH 7.7, each of the four nucleotides is cleanly separated by application of a 0.2 to 1.0 M NaCl gradient. An adapted version of this method was used in this Thesis project. A 1 mL AcroSep™ Q Ceramic HyperD F anion exchange chromatography column (Pall Corporation) was used to purify all nicotinamide solutions. The column was first cleaned by washing with 10 mL of 50 mM Tris-HCl buffer, before 1 mL of an unpurified solution of NAD(P)(H) was loaded into the column. An equal amount of washing buffer to that of the unpurified nucleotide solutions was added into the column so that all unbound impurities would be eluted from the column while nicotinamides are retained. A salt concentration gradient bringing the total concentration from 0 to 0.4 M KCl was applied to elute the bound nicotinamides. At pH 8.0, each of the four nucleotides are cleanly separated, with NAD^+ being eluted from the column first, followed by NADH, $NADP^+$ and NADPH (Figure 40).

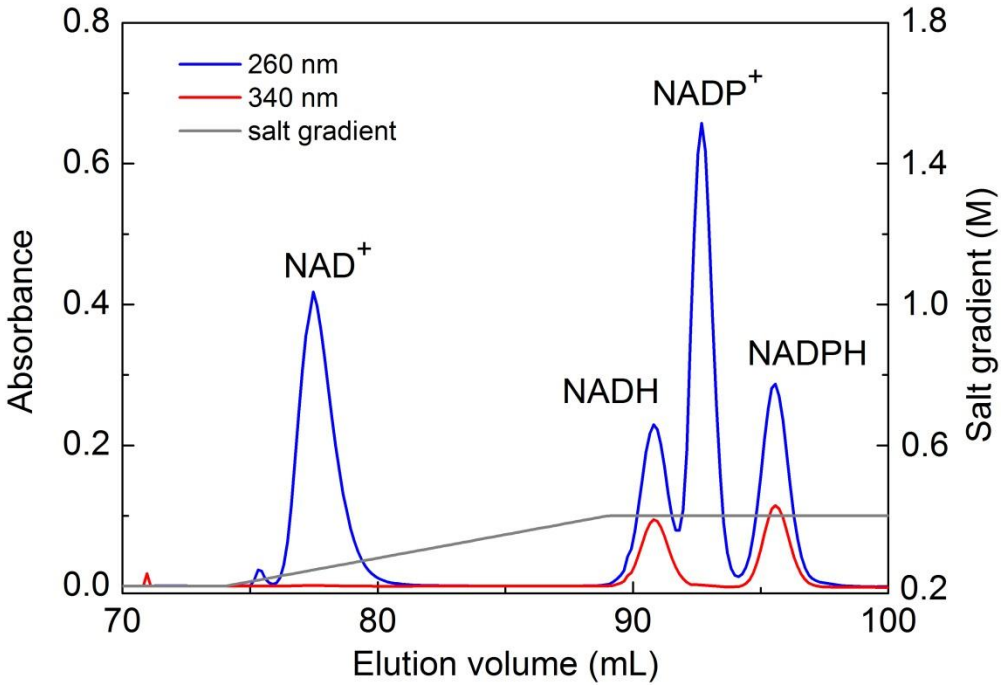

Figure 40. FPLC chromatogram of a mixture of nicotinamides. At *t* = 0 min, 1 mL solution containing 100 µM NAD^+, 100 µM NADH, 200 µM $NADP^+$ and 200 µM NADPH (all unpurified solution) was injected into the column. The flow rate used throughout purification procedure was 1.0 mL/min. The buffer used was pH 8.0 50 mM Tris-HCl. The salt gradient consisted of pH 8.0 50 mM Tris-HCl buffer containing 0 to 0.4 M KCl. This experiment was performed with assistance from Mr Daniel Grabarczyk (DPhil student in the group).

FPLC was not normally used for daily purification as the purification was performed inside the glovebox. A salt concentration gradient was performed manually by controlling the dripping of KCl solution into no-salt buffer using a syringe. The eluant was collected in 0.5 mL fractions, and UV-Vis spectroscopy (Nanovue, GE Healthcare, 0.2 mm pathlength) was used to identify fractions containing nicotinamides. To determine the concentration of the eluant, a standard curve based on known NAD(P)(H) concentrations was first constructed to obtained the extinction coefficient, ξ. The Beer-Lambert Law states a linear relationship between absorbance and the concentration of the absorbing species as shown in equation [10];

$$A = \xi c l \qquad [10]$$

where A, ξ, l and c refer to measured absorbance, extinction coefficient, path length and the analyte concentration respectively. According to this equation, a plot of absorbance against concentration will result in a straight line, crossing the axis at A = 0 and with the gradient equal to the extinction coefficient for a particular pathlength.

All nicotinamides (NAD^+, NADH, $NADP^+$ and NADPH) are known to show a UV absorbance peak at 260 nm, while the reduced forms show an extra peak at 340 nm (Figure 41 lane (i)). The extinction coefficient, ξ can then calculated by plotting a standard calibration curve at known nucleotide concentrations against the absorbance (Figure 41 lane (ii)).

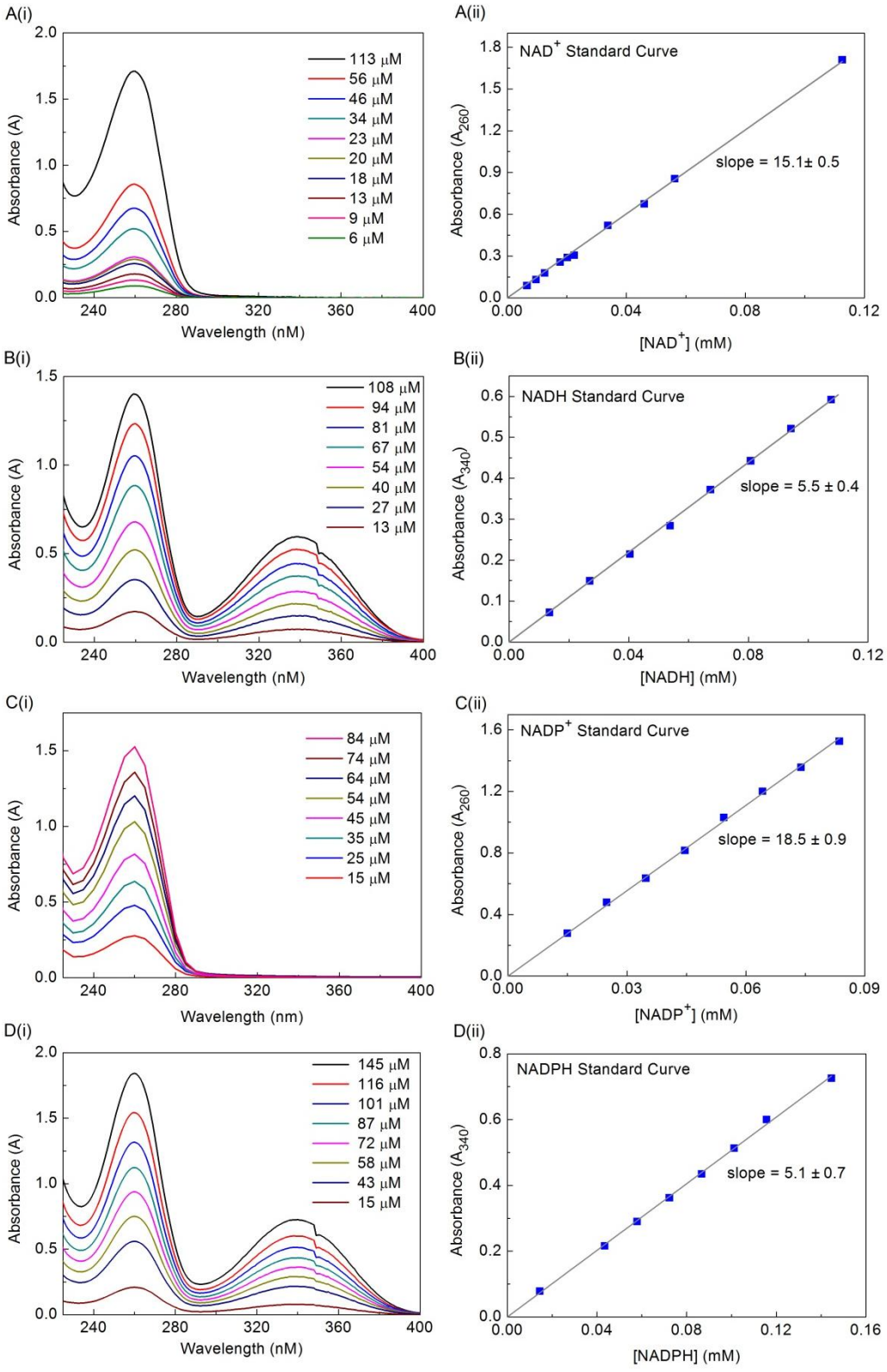

Figure 41. UV-Vis spectra of nicotinamides (lanes i) and the standard calibration plots (lanes ii) of NAD^+ (A), NADH (B), $NADP^+$ (C) and NADPH (D), recorded in 50 mM Tris-HCl buffer at pH 8. In lane (ii), A and c represent absorbance and concentration.

2.6.3 Gases

The gases used in experiments described in Chapter 6 were of high purity: H_2 Premier Plus grade (Air Products) and O_2 (BOC).

2.7 Graphite particles

The platinised graphite particles used in Chapter 6 were prepared by sanding a graphite rod that had first been cycled between -0.5 V and 0.5 V at 50 mV/s in a solution of *hydrogen hexachloroplatinate*(IV) hydrate (Sigma) in 100 mM, pH 7 phosphate buffer.

To analyse NADH molecules generated by enzyme modified particles, a plot of absorbance ratio against concentration ratio was designed for each NAD^+/NADH ratio taking advantage of the prominent peaks at 260 nm and 340 nm for NAD^+ and NADH respectively.

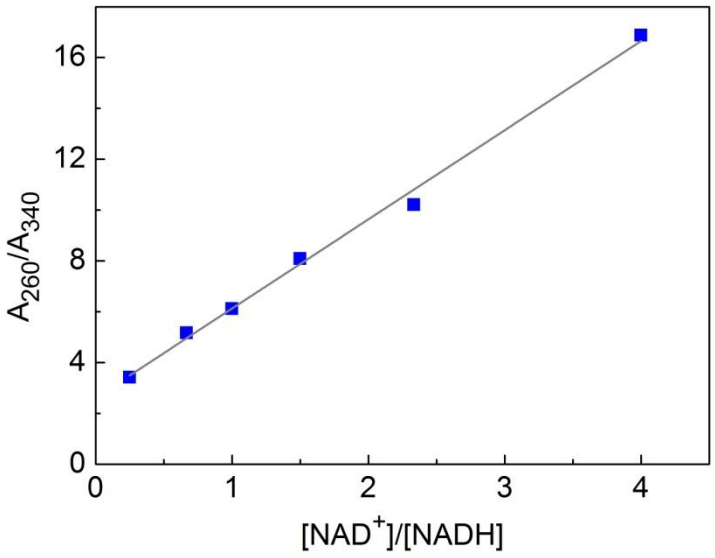

Figure 42. Plot of absorbance at 260/340 nm against the concentration of NAD^+/NADH at different ratios, while keeping the total NAD^+/NADH concentration at 0.1 mM.

2.8 Michaelis-Menten kinetics

(As discussed in references[27, 186])

One of the important indications of enzyme kinetics is the specific way an enzyme behaves in the presence of substrate. A kinetic model proposed by Leonor Michaelis and Maud Leonora Menten (shown in equation [11]) has been widely used to illustrate the reaction occurring between an enzyme and its substrate.

$$E + S \underset{k_{-1}}{\overset{k_1}{\rightleftharpoons}} ES \xrightarrow{k_2} E + P \qquad [11]$$

In the proposed model, when an enzyme, [E] reacts with a substrate [S], it will form an enzyme-substrate complex [ES] with a rate constant of k_1. The formed [ES] complex can either proceed to form the product, with a rate constant of k_2 or undergoes dissociation to [E] and [S] with a rate constant of k_{-1}. Assuming product formation is the slow step, from equation [11], the catalytic rate is dependent on the [ES] and k_2 which can be written as:

$$v = k_2[ES] \qquad [12]$$

Meanwhile, the rate of formation and breakdown of [ES] are given by:

$$rate\ of\ formation = k_1[E].[S] \qquad [13]$$

$$rate\ of\ breakdown = (k_{-1} + k_2)[ES] \qquad [14]$$

Applying the steady state assumption suggested by George Briggs and John Haldane: the concentrations of the intermediate, [ES] will be the same throughout the reaction even if the concentrations of the substrate and product are changing. The steady state

assumption is true when the rates of formation and breakdown of the [ES] complex are equal. Thus, equations [13] and [14] can be combined to give equation [15].

$$k_1[\mathrm{E}].[\mathrm{S}] = (k_{-1} + k_2)[\mathrm{ES}] \qquad [15]$$

By rearranging equation [15], equation [16] is obtained.

$$\frac{[\mathrm{E}][\mathrm{S}]}{[\mathrm{ES}]} = \frac{(k_{-1} + k_2)}{k_1} \qquad [16]$$

A new constant, called the Michaelis constant, K_M (equation [17])

$$K_\mathrm{M} = \frac{k_{-1} + k_2}{k_1} \qquad [17]$$

has been defined to help simplify equation [16]. Inserting equation [17] into equation [16] gives equation [18].

$$[\mathrm{ES}] = \frac{[\mathrm{E}][\mathrm{S}]}{K_\mathrm{M}} \qquad [18]$$

Throughout the reaction, the total enzyme concentration is equal to the concentration of unbound enzyme, [E] plus the concentration of the enzyme-substrate complex, [ES].

$$[\mathrm{E_T}] = [\mathrm{E}] + [\mathrm{ES}] \qquad [19]$$

The expression in equation [19] can be substituted into equation [18] which will give:

$$[\mathrm{ES}] = \frac{([\mathrm{E_T}] - [\mathrm{ES}])[\mathrm{S}]}{K_\mathrm{M}} \qquad [20]$$

By substituting equation [20] into equation [12], equation [21] is obtained.

$$v = k_2[\mathrm{E_T}]\frac{[\mathrm{S}]}{[\mathrm{S}] + K_\mathrm{M}} \quad [21]$$

A maximal rate, V_{max} is obtained when the catalytic site of the enzyme is saturated with the substrate.

$$V_{\max} = k_2[\mathrm{E_T}] \quad [22]$$

Substituting equations [22] into [21] yields the Michaelis-Menten equation:

$$v = \frac{V_{\max}[\mathrm{S}]}{[\mathrm{S}] + K_\mathrm{M}} \quad [23]$$

A plot of *v* against [S] will generate a hyperbolic curve passing through the origin as shown in Figure 43.

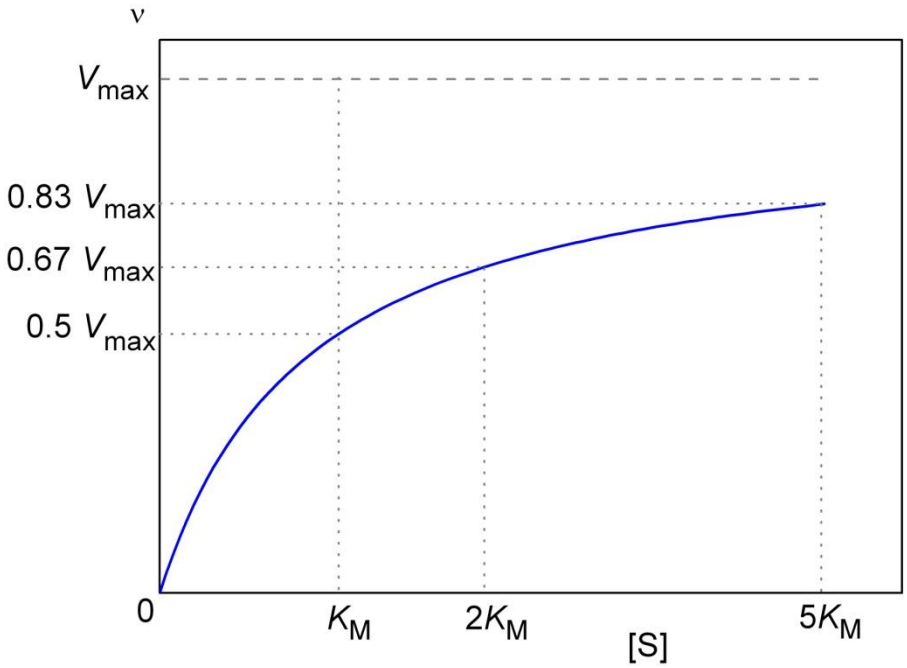

Figure 43. A plot of enzyme reaction rate, *v* against substrate concentration, [S] based on the Michaelis-Menten equation.

Based on equation [23], when the substrate concentration is equal to K_M, the equation can be simplified into equation [24]:

$$v = 0.5V_{max} \quad [24]$$

This thus indicates that K_M is the substrate concentration at which the enzyme is said to have half of its maximal catalytic activity. At a very large substrate concentration value, the denominator of equation [23] is governed by [S], so K_M is negligible in comparison with [S], thus $v \approx V_{max}$. At this substrate concentration, all of the enzyme active sites are occupied by substrate and the enzyme is saturated.

The affinity for substrates, K_M therefore can be understood in two ways; first it represents the concentration of substrate at which the enzyme active site is half filled. Therefore, one can expect that at the K_M value, a significant level of catalysis should takes place. Secondly, K_M is also a measure of the strength of the enzyme-substrate complex. If an enzyme has a high K_M value, the enzyme is said to have a weakly bound enzyme-substrate complex as it needs a high substrate concentration to be able to form products and thus reach half of its maximal catalytic activity.

It is, however, not easy to estimate the K_M value just by plotting v against [S] as shown in Figure 43, since the catalytic rate, v never reaches its maximal activity, V_{max} at a finite value of [S] and as noted by Cornish-Bowden, even at substrate concentration of ten times the K_M value, a difference of at least 10 % is still expected between v and V_{max}.[186]

2.8.1 Ways of analysing enzyme affinity constants

Plotting a graph of v against [S] is the easiest way to estimate a K_M value for an enzyme catalysed reaction, however, there are several drawbacks to use of this plot in quantitative analysis such as the difficulty to fit a hyperbolic plot accurately due to inability to detect deviations from the expected curve. Furthermore, as discussed before, it is also not easy to estimate and locate the asymptotes correctly.

In most cases it is preferable to rewrite the Michaelis-Menten equation so that a straight line plot is obtained. By taking reciprocals of both sides of the Michaelis-Menten equation (equation [23]), a new equation first introduced by Lineweaver and Burk [187] is obtained:

$$\frac{1}{v} = \frac{1}{V_{\max}} + \frac{K_M}{V_{\max}} \cdot \frac{1}{[S]} \qquad [25]$$

Based on equation [25], a plot of $1/v$ against $1/[S]$ will generate a straight line as shown in Figure 44 with a slope of K_M/V_{max} and y-intercept of $1/V_{max}$.

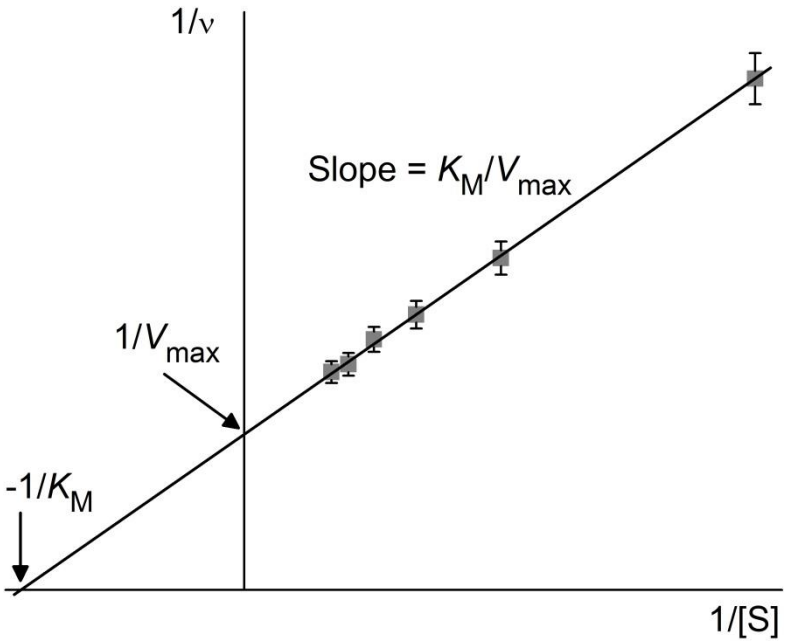

Figure 44. A typical example of a Lineweaver-Burk plot.

The Lineweaver-Burk plot is commonly used by researchers, however, it is prone to experimental data error as pointed out by Cornish-Bowden;[186] for a small value of *v*, a small error will lead to enormous error in 1/*v* whilst for a large value of *v*, the same error leads to negligible error in 1/*v*. This is particularly a problem when few data points are available for small values of [S]. Error bars shown in Figure 44 represent a noticeable unsymmetrical pattern although they were calculated from the same symmetrical error range. Thus the most unreliable data points can have a major effect on the slope and therefore on the calculated K_M value.

By multiplying both sides of equation [25] with [S], an equation for a plot called a Hanes-Woolf plot is obtained:

$$\frac{[S]}{v} = \frac{K_M}{V_{max}} + \frac{1}{V_{max}}[S] \qquad [26]$$

Equation [26] shows that a plot of [S]/v against [S] will also be a straight line, with slope of $1/V_{max}$ and y-intercept of K_M/V_{max}. A typical example of a Hanes-Woolf plot is shown in Figure 45.

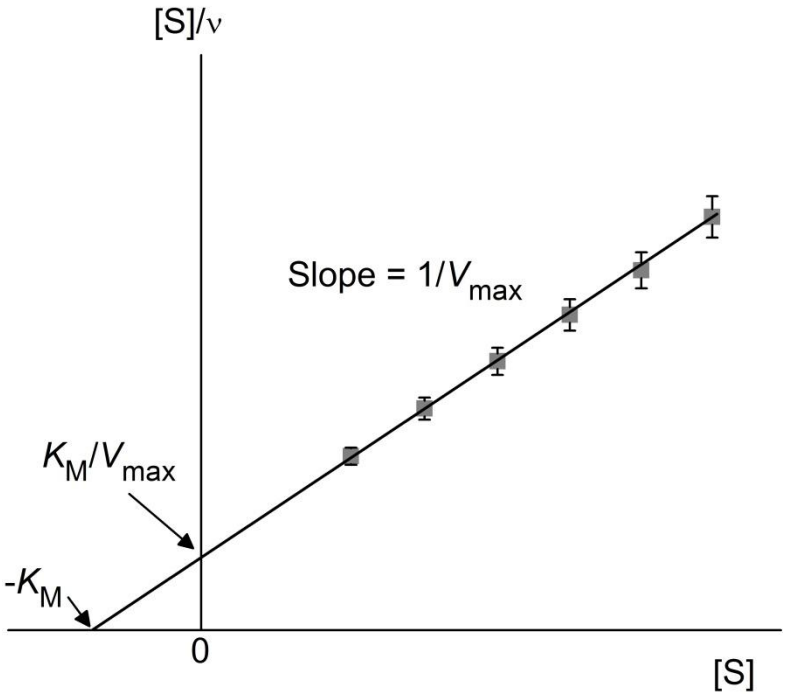

Figure 45. A typical Hanes-Woolf plot

As can be seen from the figure, over a wide [S] values, the deviation in errors in [S]/*v* is minimal and therefore this plot should be used over the Lineweaver-Burk plot particularly when few values of *v* are available for small [S]. In this Thesis, three different plots to determine the K_M values will be used and discussed.

2.9 Enzyme inhibition

(The discussion in this Section is based around references[186, 188])

A substance that decreases the enzymatic reaction rate is called an inhibitor and there are several types of inhibition such as competitive, mixed and uncompetitive. Competitive inhibition can occur via several means, a typical example is shown in Figure 46.

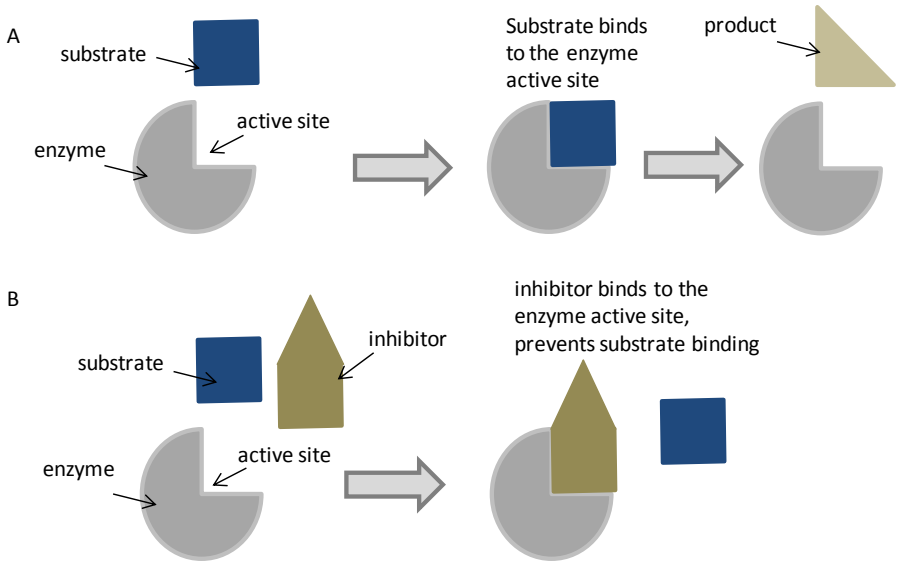

Figure 46. Panel A shows typical enzyme catalysis without the presence of inhibitor. Panel B shows one way a competitive inhibitor could bind to the active site and preventing catalysis.

Figure 46A illustrates the binding of a substrate onto the enzyme active site, forming an enzyme-substrate complex. This process as described in Section 2.8 is reversible and the complex then undergoes a catalytic step forming product and an active enzyme, ready for accepting more substrate. In the presence of an inhibitor (Panel B), if the enzyme affinity towards inhibitor is higher than towards substrate, the inhibitor will bind to the active site instead of substrate and form an enzyme-inhibitor complex. This process is also reversible, however, the complex is unable to undergo the catalytic step while inhibitor is bound. One good example of competitive inhibition is the inhibition by malonate of oxidation of succinate to fumarate in Complex II: succinate dehydrogenase.[189] Oxidation of succinate to fumarate involves formation of a double bond from a dimethylene group and since malonate does not have a dimethylene group it is unable to undergo the reaction. On the other hand, malonate is structurally very similar to succinate and therefore is able to bind to the Complex II binding site, thus blocking the binding of succinate.

In the case of uncompetitive inhibition, the inhibitor will only bind to the enzyme-substrate complex. On the other hand, a substance that acts as a mixed inhibitor

can bind to the free enzyme and to the enzyme-substrate complex. In both cases, the presence of inhibitor will decrease the apparent value of the enzyme maximal catalytic activity. Table 2-3 summarises the effect of inhibitor on enzyme apparent maximal activity V_{max}^{app}, apparent Michaelis-Menten constant K_M^{app} and V_{max}^{app}/K_M^{app}.[186]

Table 2-3. Characteristics of enzyme inhibitions.[186] K_{IC} and K_{IU} represent the inhibition constants for competitive and uncompetitive respectively.

Type of inhibition	V_{max}^{app}	K_M^{app}	V_{max}^{app}/K_M^{app}
Competitive	V_{max}	$K_M(1+[i]/K_{IC})$	$\frac{V_{max}/K_M}{1+[i]/K_{IC}}$
Uncompetitive	$\frac{V_{max}}{1+[i]/K_{IU}}$	$\frac{K_M}{1+[i]/K_{IU}}$	$\frac{V_{max}}{K_M}$
Mixed	$\frac{V_{max}}{1+[i]/K_{IU}}$	$\frac{K_M(1+[i]/K_{IC})}{1+[i]/K_{IU}}$	$\frac{V_{max}/K_M}{1+[i]/K_{IC}}$

In 1953, Dixon proposed a quantitative technique for determining the value of inhibition constants by utilising the modified Michaelis-Menten equation for competitive inhibition (equation [27]).

$$v = \frac{V_{max}[S]}{K_M\,(1+\frac{[i]}{K_{IC}}) + [S]} \quad [27]$$

Taking reciprocals of both sides of equation [27] will generate equation [28]:

$$\frac{1}{v} = \frac{K_M[i]}{V_{max}[S]K_{IC}} + \frac{1}{V_{max}}\left(1+\frac{K_M}{[S]}\right) \quad [28]$$

Dixon pointed out that, a plot of 1/v against inhibitor concentration, [i] at a constant substrate concentration, [S] will generate a straight line. At several different substrate

concentrations, a point of intersection can be found when $1/v$, [i] and V_{max} are the same for both lines (equation [29]):

$$\frac{K_M}{[S]_1} + 1 + \frac{K_M[i]}{[S]_1 K_{IC}} = \frac{K_M}{[S]_2} + 1 + \frac{K_M[i]}{[S]_2 K_{IC}} \quad [29]$$

and the point of intersection according to Dixon plot is equal to $-K_I$ (Figure 47 lanes (i)).

A Dixon plot can also be used to determine the K_I value for mixed inhibition. Cornish-Bowden shows that the terms containing K_{IU} are cancelled: meaning that a Dixon plot provides the value of the inhibition constant regardless of the inhibition type. If uncompetitive inhibition is present, the Dixon plot generates a set of parallel lines when K_{IC} is infinite. To differentiate between types of inhibition, a Cornish-Bowden plot can be used. This plot is generated by re-arranging equation [28] by multiplying with substrate concentration, [S] to give equation [30].

$$\frac{[S]}{v} = \frac{K_M}{V_{max}.K_{IC}}[i] + \frac{1}{V_{max}}([S] + K_M) \quad [30]$$

A plot of $[S]/v$ against [i] as proposed by Cornish-Bowden, and termed a Cornish-Bowden plot, is shown in lanes (ii) of Figure 47, and makes it possible to differentiate between mixed and competitive inhibition while at the same time giving the inhibition constant in the case of uncompetitive inhibition. Experiments described in Chapter 4 are concerned with inhibition of HoxFU by its reaction products and by molecules known to inhibit the related catalytic site in Complex I.

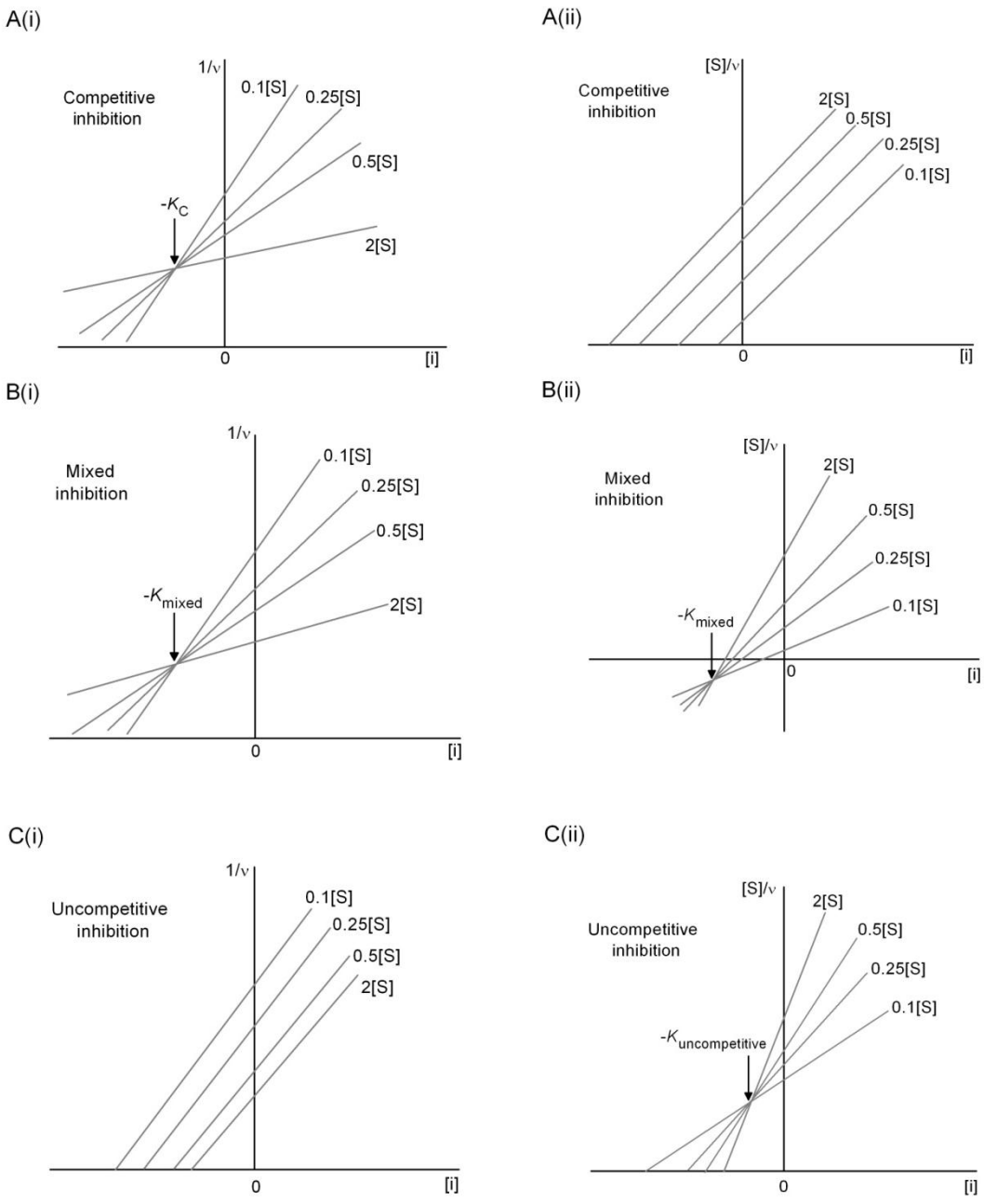

Figure 47. Lane (i) graphs show different Dixon plots for determination of the inhibition constant. Lane (ii) shows the Cornish-Bowden plots to differentiate the types of inhibition.[186, 188]

2.10 Relation of this Chapter to other Chapters

This Chapter introduced the concept of Protein Film Electrochemistry (PFE) and details of the experimental methods used throughout this Thesis. In the following Chapters, electrochemical techniques *i.e.* cyclic voltammetry and chronoamperometry

are used to investigate catalytic NAD^+ reduction and NADH oxidation by the SH and its variants. The theories underlying enzyme kinetics such as the affinity constant, K_M and inhibition constant, K_I have been discussed in this Chapter, and in Chapters 3, 4 and 5 are applied in conjunction with PFE to determine affinity/inhibition constants for the SH. In the final Chapter, the possibility of using electrochemistry to drive NADH regeneration by the diaphorase moiety is presented in detail.

Chapter 3: Electrochemical Characterisation of Diaphorase Moiety of Soluble Hydrogenase *Ralstonia eutropha* H16

3.1 Introduction

As discussed in Chapter 1, the Soluble Hydrogenase (SH) from *R. eutropha* H16 contains six different subunits, one $2H^+/H_2$ cycling [NiFe] centre, two flavin mononucleotides and five Fe-S clusters (Figure 48A).[13, 21, 73, 78, 190, 191] It resides in the cytoplasm and is able to reduce NAD^+ at the expense of H_2, generating NADH which provides reducing equivalents for biosynthesis of organic molecules from CO_2. Genetic engineering techniques applied in the laboratories of Dr Oliver Lenz at Humboldt University, Berlin have made it possible to separate this complex enzyme into several different modules thus making it easier to study by Protein Film Electrochemistry (PFE).

In PFE, the enzyme of interest is immobilised onto the surface of an electrode and the enzyme's behaviour is studied by precisely controlling the electrode potential.[56, 57, 121, 131, 157, 192-194] Figure 48B shows an ideal enzyme conformation upon adsorption onto the electrode, in an orientation favourable for electron exchange between the electrode and the catalytic centre via the electron relay FeS clusters. This Chapter will discuss the first electrochemical characterisation of the diaphorase (NAD^+/NADH cycling) subcomplex, HoxFU of the SH.

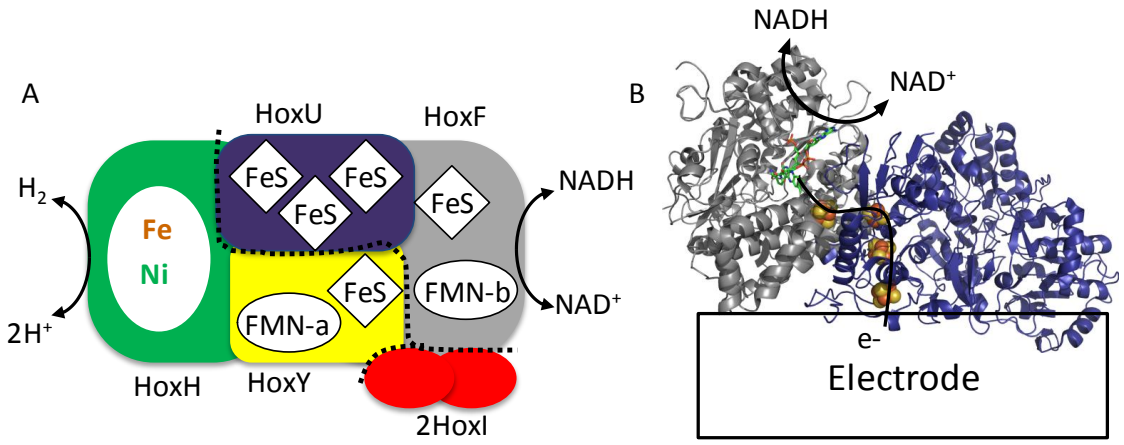

Figure 48. Panel A shows a schematic structure of the SH, comprising of six subunits $HoxHYFUI_2$. FeS refers to Fe-S cluster while FMN refers to flavin mononucleotide cofactor. Ni

and Fe refer to Nickel and Iron metals residing in HoxH. The SH can be purified into different moieties as indicated by the dotted line. Panel B shows the relevant subunits of Complex I present in the SH to indicate an ideal attachment of the enzyme onto a pyrolytic graphite electrode. The picture was constructed using the crystal structure of Complex I, to represent HoxFU in the SH. PDB code: 3IAM.[34]

3.2 Electrocatalytic NAD^+/NADH cycling on a bare graphite electrode

Figure 49 shows cyclic voltammograms of NADH oxidation (Panel A) and NAD^+ reduction (Panel B) on a bare pyrolytic graphite edge (PGE). No Faradaic current was observed when the electrode was placed in buffer solution containing no NAD^+ or NADH (grey line).

In Panel A, the electrode was placed in a solution of 1 mM NADH and the electrode potential was swept between -0.6 V and 1 V. In the presence of NADH, no catalytic current was recorded at potentials below 0.4 V. Above this potential, an increase in the current corresponding to NADH oxidation on the bare graphite electrode was observed (red and blue lines indicate the first and second cycle respectively).

The unmodified graphite electrode was then placed in a solution of 1 mM NAD^+ and the electrode potential was swept between 1 V and -0.9 V (Panel B). At the beginning of the scan, no catalytic reduction current was observed, but a negative current was recorded below -0.8 V due to NAD^+ reduction on the bare electrode.

From voltammograms in Figure 49 it is clear that pyrolytic graphite alone is able to oxidise NADH and reduce NAD^+. This, however, only occurs at very high overpotentials, well away from the theoretical value for $E(NAD^+/NADH)$. For example, at pH 8.0, 30 ^oC the expected onset potential at a relatively high $NADH/NAD^+$ is around -0.45 V. However, NADH oxidation on the graphite electrode did not start until

about +0.4 V. This indicates the requirement for an overpotential of approximately 0.85 V before NADH starts being oxidised on a graphite electrode. Similarly, a large overpotential is required for NAD^+ reduction on a bare graphite electrode. This is consistent with earlier reports of overpotential requirement on bare carbon or metal electrodes as discussed in Chapter 1.

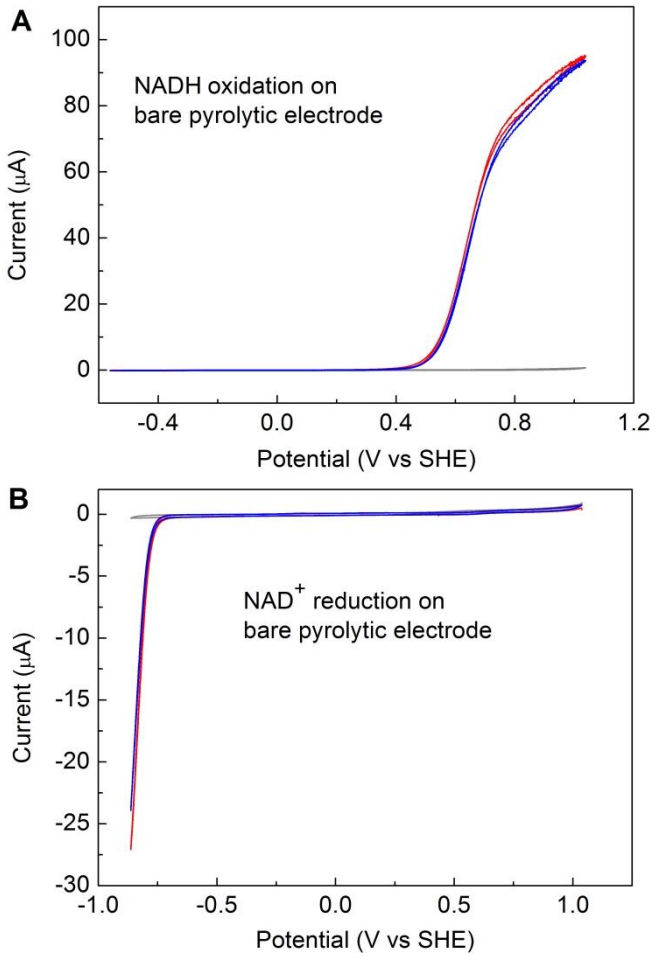

Figure 49. Cyclic voltammograms of NADH oxidation at 1 mM NADH (Panel A) and NAD^+ reduction at 1 mM NAD^+ (Panel B) on unmodified graphite electrode. Scans were recorded in Tris-HCl buffer, 50 mM at pH 8.0 at 30 ^oC with electrode rotation of 2500 rpm and scan rate of 10 mV/s. In both panels, the thick grey line represents a scan of unmodified electrode with no NADH nor NAD^+, while red and blue lines show the first and second cycles of either NADH oxidation or NAD^+ reduction.

3.3 Investigation of electrocatalytic NAD^+/NADH cycling by HoxFU

As shown in the previous Section, NADH oxidation and NAD^+ reduction on bare PGE electrode require a huge overpotential, which leaves a clear potential window on either side of the NAD^+/NADH potential to examine enzyme activity on the electrode. Experiments with HoxFU are usually performed in the potential range of -0.6 V to +0.1 V, and over this potential range, no Faradaic current is observed for an unmodified electrode in the cell solution containing NADH and/or NAD^+. Thus any contributions in this region from an enzyme modified electrode can be assumed to arise from the enzyme.

3.3.1 Interpreting an electrocatalytic cyclic voltammogram for HoxFU

Typical cyclic voltammograms of an electrode modified with HoxFU in the presence of different ratios of substrates, NAD^+ and NADH are shown in Figures 50-52. All experiments were performed at pH 8.0 at 30 ^oC using 50 mM Tris HCl buffer in order to compare the electrocatalytic activity of HoxFU with activity determined for the native enzyme in solution assays. The working electrode used for all experiments in this chapter was rotated at a high rotation rate (2500 – 3000 rpm) to make sure that the enzyme is continuously supplied with substrate thus eliminating mass transport effects on the catalytic current. The PGE rotating electrode was first polished with an aqueous alumina slurry, sonicated for 10 seconds and rinsed with milliQ water before an aliquot of 0.5 µL protein (concentration 0.4 mg/mL) was spotted onto the surface and left to adsorb over 30 seconds. In most experiments described in this and subsequent Chapters, a pipette was used to withdraw excess protein solution from the enzyme modified

electrode and the electrode was then washed with fresh buffer solution before being placed into the electrochemical cell. This avoids contributions from unadsorbed enzyme.

For the experiment shown in Figure 50, the HoxFU modified electrode was placed in a solution of 2 mM NAD^+. The presence of NAD^+ reduction at the beginning of the scan could be attributed to the fact that the starting potential was lower than that of $E(NAD^+/NADH)$ at this concentration. As the potentials were swept towards more positive values, the negative current decreased in magnitude as the driving force for NAD^+ reduction diminished. At high potentials, the enzyme electrode behaviour resembles that of the blank electrode and on the reverse cycle, NAD^+ reduction commences again at potentials below about -0.25 V.

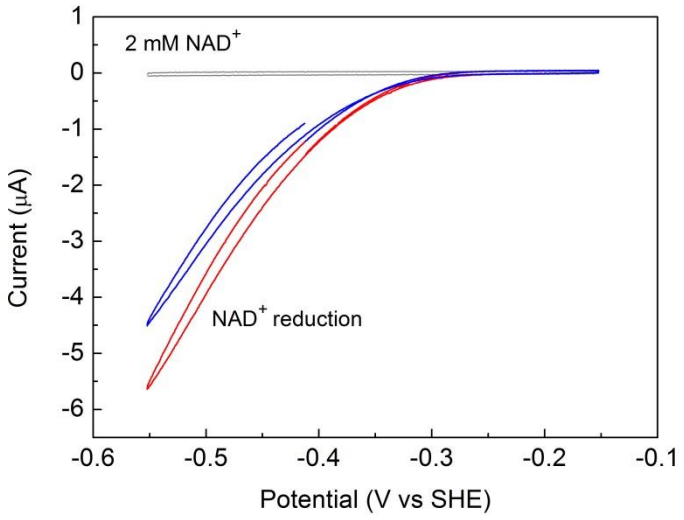

Figure 50. Cyclic voltammograms for a PGE rotating disk electrode modified with HoxFU recorded at 2 mM NAD^+. The red and blue lines represent the first and second cycles recorded after spotting the enzyme onto the electrode, while the grey line represent the respond for an unmodified electrode. Voltammograms were commenced at -0.44 V, with potential swept first towards positive values. Other conditions: All scans were performed in pH 8.0 Tris-HCl, 50 mM at 10 mV/s at 30 ^oC. The working electrode was rotated at 2500 rpm.

In the preliminary experiments utilising NADH, it was found that the commercially available NADH was contaminated with NAD^+. This caused significant

NAD^+ reduction during experiments as shown in Figure 51A. Therefore, when it is necessary, the NADH was purified according to the technique proposed by Blanchard and coworkers as described in Section 2.6.2.[183] The HoxFU modified electrode was then placed in a 2 mM solution of purified NADH (panel B). At the beginning of the scan, no catalytic current was observed and the current resembles that at a blank electrode. However, as the potentials were swept towards more positive values, an increase in positive current was observed commencing at approximately -0.45 V, indicating that the enzyme starts to oxidise NADH. On the second cycle, a distinctive catalytic activity of NADH oxidation was still recorded.

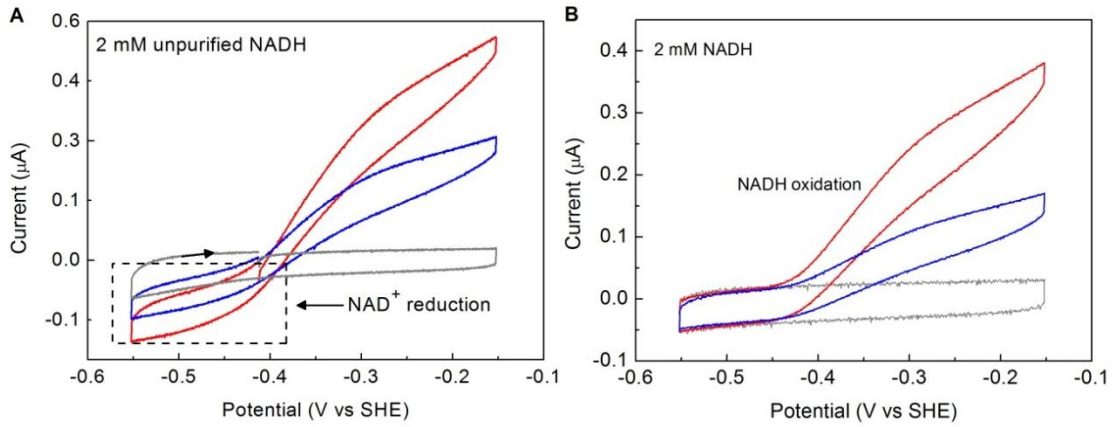

Figure 51. Cyclic voltammograms for a PGE rotating disk electrode modified with HoxFU recorded at 2 mM unpurified (panel A) and purified (panel B) NADH. The presence of negative current at low potential in panel A is due to NAD^+ reduction. In both panels, the first and second cycles are shown as red and blue lines respectively. The grey line shows voltammogram in the absence of HoxFU diaphorase on the electrode. Experiments were performed in Tris-HCl buffer 50 mM, pH 8.0 at 30 ^oC. Conditions: 2500 rpm, scan rate 10 mV/s. The electrode rotation would spin away any enzyme-generated NAD^+, so the observation of NAD^+ reduction in panel A confirms that the NADH is contaminated.

In Figure 50 and Figure 51, the decrease in catalytic current on the second cycle (both shown as a blue line) could be attributed to a phenomenon called 'film loss'. Since the enzyme is not covalently attached onto the electrode, it may easily dissociate from the electrode. However, it is not easy to distinguish by using cyclic voltammetry

whether the characteristic decrease in current observed was due to dissociation of the enzyme or from denaturation or damage.

The cyclic voltammograms in Figure 52 show the catalytic activity for NADH oxidation and NAD^+ reduction by a HoxFU modified electrode at different ratios of NADH:NAD^+, while the total concentration is kept at 2 mM. The total concentration of 2 mM is likely to cover the range found in the cytoplasm under physiological conditions.[195] The catalytic current crosses the potential axis fairly sharply, very close to $E(NAD^+/NADH)$ for each set of conditions indicating that HoxFU requires a very minimal overpotential for either reaction. For instance, at pH 8.0, 30 ^oC, and 1:1 ratio of NAD^+:NADH, the theoretical $E(NAD^+/NADH)$ calculated is -0.353 V compared to -0.341 V determined from experiment. The difference between these values could be attributed to uncertainty in concentrations of NAD^+ and NADH due to the purification procedure. The small overpotential in $E(NAD^+/NADH)$ is very significant because in the cell, the SH couples H_2 oxidation to the reduction of NAD^+ and these reactions are closely spaced in potential. The variation in $E(2H^+/H_2)$ over the likely physiological H_2 concentration range (100 nM to 10 μM) is shown as a shaded grey box in Figure 52. Thus the ability for the SH to catalyse NAD^+ reduction and NADH oxidation efficiently will maximise the driving force for coupling these reactions to H_2 oxidation and H^+ reduction. Electrochemical experiments on the hydrogenase moiety of the SH performed by Juan Liu in the Vincent group revealed that the hydrogenase moiety also catalyses $2H^+/H_2$ cycling with minimal overpotential.[77] The minimal overpotential requirement by the SH is important to minimise loss of energy during catalysis, making it an efficient catalyst for NADH production in the cell.

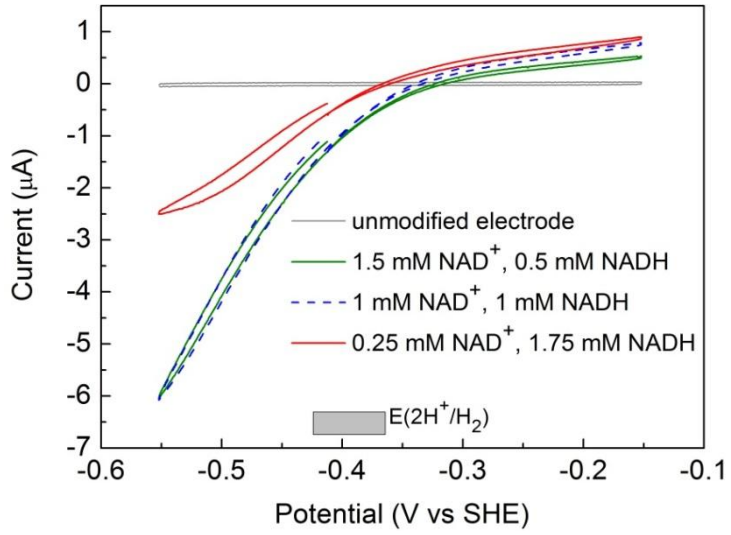

Figure 52. Cyclic voltammograms for a PGE rotating disk electrode modified with HoxFU recorded at different ratios of NAD^+/NADH as indicated. Only the first cycle is shown for each ratio of NAD^+/NADH. Grey line represents a voltammogram of an unmodified electrode. The shaded box indicates the range of potentials for $E(2H^+/H_2)$ at 30 ^oC, pH 8.0 between 100 nM and 10 μM H_2. Voltammograms in C were commenced at -0.44 Vwith the potential swept first towards positive values in each case. Other conditions: All scans were performed in pH 8.0 Tris-HCl, 50 mM at 10 mV/s at 30 ^oC. The working electrode was rotated at 2500 rpm.

Another useful piece of information that can be extracted from cyclic voltammograms is the enzyme catalytic bias at a particular set of conditions. Figure 53A shows a typical cyclic voltammogram recorded in the presence of NAD^+ and NADH. By taking an average current at 0.14 V above and below the thermodynamic potential, a plot of NAD^+:NADH current vs concentration ratio can be constructed (Panel B). From the plot we can see HoxFU is biased towards NAD^+ reduction at all NAD^+:NADH ratios sampled. This finding is as expected since in the cell, the main function of the SH is to oxidise H_2 for regeneration of reducing equivalents in the form of NADH.

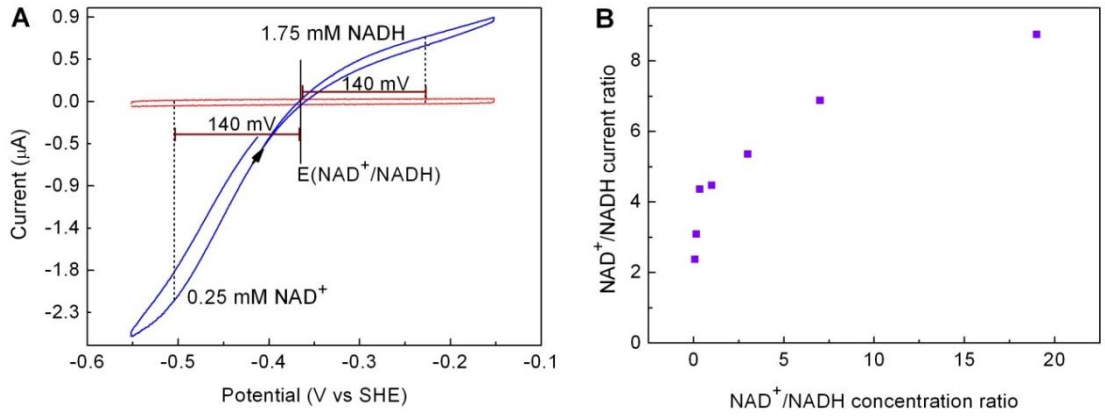

Figure 53. Panel A: Method of determination of enzyme catalytic bias from a cyclic voltammogram. Panel B: Plot of NAD^+:NADH current ratios against concentration ratios to illustrate the HoxFU catalytic bias.

The reversible electrocatalytic NADH oxidation and NAD^+ reduction exhibited by HoxFU, coupled with the ability of the enzyme to work with a minimal overpotential requirement opens up the possibility of utilising this catalytic domain for relevant biotechnological applications, which will be discussed further in Chapter 6. In the next section of this Chapter, further investigations on the effect of pH values and temperatures will be explored, for a better understanding of HoxFU catalysis.

3.3.2 The Effect of pH and temperature on catalytic activity

It is well known that the catalytic activity of enzymes is very dependent on the reaction conditions. Changes in pH, for example, will affect the state of ionisation of charged amino acid residues and such changes may have a large effect on the enzyme conformation. This may disrupt the enzyme substrate recognition and the enzyme may become inactive. Not only will extremes of pH affect the enzyme, but it may also disturb substrate binding to the active site thus preventing catalysis. Kaplan and coworkers reported a purification of a diaphorase enzyme from *Clostridium kluyverii* in 1969 that exhibits a pH optimum of 8.5 for its NADH oxidation reaction.[196] Their experiments were performed by utilising the colour changes of

2,6-dichlorophenolindophenol (DCPIP) from blue (oxidised form) to colourless (reduced form) upon receiving electrons from NADH oxidation.[196] They also showed that the diaphorase catalytic activity was significantly reduced at pH values higher than 8.5 in biochemical experiments.

Figure 54A shows NAD^+/NADH interconversion by a HoxFU modified electrode recorded at different pH values at equal concentrations of NADH and NAD^+. The experiments were performed over a broad range of pH values of 4.58 to 10.05 using a mixed buffer system. One obvious observation from the voltammograms in Panel A is the ability of HoxFU to sustain its catalytic activity over a wide pH range. Although it may be seen from the voltammograms that NADH oxidation is more favourable at high pH; one should not be confused with the fact that the thermodynamic potential of the reaction has shifted towards more negative values at high pH. Since the experiments were performed in a fixed potential window, a more negative $E(NAD^+/NADH)$ gives a wider window needed for NADH oxidation, while leaving NAD^+ reduction a limited window thus a smaller catalytic current is reached at the lower current vertex.

Each experiment in panel A was performed using a fresh enzyme film, therefore an exact measurement of enzyme activity with pH was not possible due to the different enzyme coverages obtained for each experiment. It is worth noting here that although HoxFU can function over a wide range of pH values, the enzyme film is very unstable at high pH (over 10.0) and the catalytic activity is vastly diminished on the second cycle (not shown). A similar observation was reported by Lauterbach on the basis of biochemical solution assays: HoxFU-mediated NADH oxidation was severely diminished at pH 10.0 after 30 seconds. This thus indicates the protein instability at this high, non-physiological pH.

The cyclic voltammograms in Figure 54A show that as the potential is swept up towards 0 V, there is a sudden change in slope; increasing catalytic activity was observed at about -0.2 V. The origin of this effect is still unknown, however, similar behaviour has been observed before electrochemically for the fumarate reductase from *E. coli*.[192] In fumarate reductase, the increase in current observed was postulated to be due to the interaction between one of the 4Fe4S clusters involved in the electron relay with the FAD active site; Armstrong and coworkers suggested that this enhancement may be because the 4Fe4S cluster provides a second relay system to mediate electrons to the FAD catalytic centre.

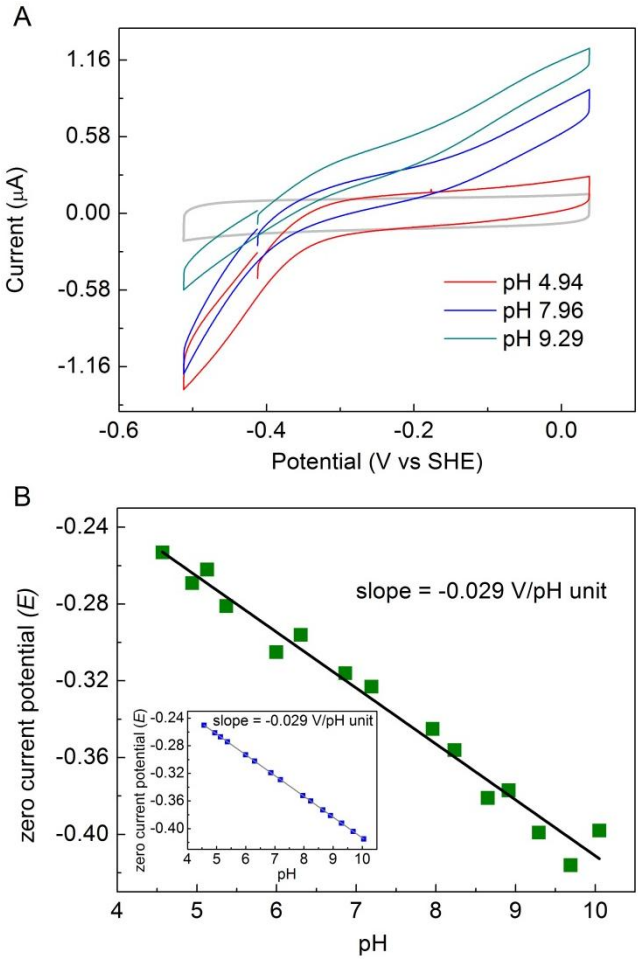

Figure 54. A. Cyclic voltammograms showing NAD^+/NADH cycling by HoxFU at different pH values. Experiments were performed in mixed buffer system at 10 mV/s, 30 ^oC. B. A plot of zero current potential as a function of pH. A fitted straight line in panel B has a slope of -0.029 V/decade (R^2 = 0.98), as predicted for a $2e^-/1H^+$ reaction.

Panel B shows a plot of $E(NAD^+/NADH)$ as a function of pH. Because NADH oxidation and NAD^+ reduction require proton transfer, the $E(NAD^+/NADH)$ should be dependent on the pH values as shown by equation [31]:

$$E = E^o - 29.939 \left(\log\left(\frac{[NADH]}{[NAD^+]}\right) + pH \right) \quad [31]$$

Based on equation [31], a change in the pH will shift the $E(NAD^+/NADH)$ by approximately -0.029 V. As can be seen from Panel B, there is a linear relationship between the thermodynamic potentials and pH in a range of pH 4.6 to 10.0. The $E(NAD^+/NADH)$ decreases linearly with increasing pH and this gives a best fit straight line with a gradient of -0.029 V per pH unit. This finding indicates that NAD(H) catalysis is reversible over a wide range of pH and the pH dependence on the thermodynamic potential is as expected since the interconversion of NAD(H) involves transfer of 1 proton and 2 electrons. Bovine heart Complex I was also reported to show a reversible catalysis of electrocatalytic NAD(H) interconversion over a pH range of 5.5 to 10.7 with a linear fit gradient of -0.029 V per pH unit.[117, 184]

Earlier biochemical studies on the whole SH performed by Schneider and Schlegel found that pH 8.0 was the optimum pH for H_2 oxidation coupled to the NAD^+ reduction reaction.[21] The most biochemical data is available for the SH at pH 8 and therefore, to be able to compare the electrochemical behaviour of HoxFU with previous studies, all subsequent experiments were performed at pH 8.0 unless otherwise stated.

In general, enzyme activity is also dependent on temperature. Normally, high temperatures will cause enzyme denaturation as it alters the enzyme conformation resulting in loss of catalytic activity. A condition at which the enzyme has maximum catalytic activity is called its optimum temperature and this is different for each

particular enzyme. For example, a FAD-containing NADH diaphorase purified from *Archaeoglobus fulgidus* has been shown to be catalytically active in a wide range of temperature (up to 90 ^{o}C) with the maximum catalytic activity at approximately 80 ^{o}C. This finding is not surprising as in nature, sulphate reducing *A. fulgidus* is found in a hyperthermophilic environment and cells were grown at a temperature of about 80 ^{o}C.[197]

Figure 55 illustrates the effect of temperature on NAD^+/NADH interconversion by HoxFU. Experiments were performed at different temperatures while maintaining an equal ratio of NAD^+/NADH during the course of experiments. Due to the enzyme stability on the electrode, each set of experiments was performed on a fresh HoxFU modified electrode. The voltammograms in Panel A show that HoxFU is able to catalyse both reactions in the experimental frame of 5 to 40 ^{o}C. At 40 ^{o}C, however, the enzyme film was very unstable on the electrode and on the second cycle of the experiment, only negligible catalytic activity was observed. Figure 55 also proves that NAD^+/NADH interconversion by HoxFU at all tested temperatures occurs with minimal overpotential. For example at an equal ratio of NAD^+:NADH, pH 8.0 at 20 ^{o}C the theoretical $E(NAD^+/NADH)$ is -0.345 V while the $E(NAD^+/NADH)$ from experiment was found to be -0.335 V. The difference in these $E(NAD^+/NADH)$ values could be attributed to the uncertainty in NADH and NAD^+ concentrations as explained earlier. At all temperatures explored, the catalysis is bidirectional and HoxFU is more active towards NAD^+ reduction.

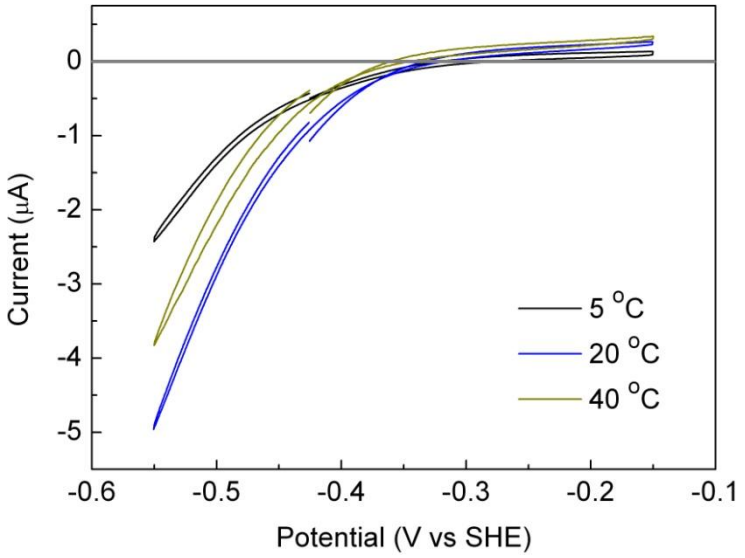

Figure 55. Bidirectional NAD(H) catalysis by HoxFU recorded at different temperatures. Experiments were performed at an equal ratio of 1 mM NAD^+: 1 mM NADH in 50 mM Tris-HCl buffer pH 8.0 at scan rate of 10 mV/s and electrode rotation rate of 2500 rpm.

Earlier research by Schneider and coworkers found that the SH has an optimal temperature of 30 ^oC; thus all experiments were performed at 30 ^oC unless otherwise stated, to enable direct comparisons with biochemical data on the whole SH.[21]

3.3.3 Potential-dependent inactivation

Bovine Complex I studied using PFE by Hirst and coworkers was shown to undergo reversible reductive inactivation at low potentials.[184] The switch off potential occurred at -0.41 V (pH 8.3), which is close to the potential of FMN in the enzyme (-0.40 V), and the nearest 2Fe2S cluster (-0.42 V to -0.49 V) resides in the 24 kDa subunit (analogous to Nqo2 of *T. thermophilus*). Cyclic voltammetry experiments performed across a wide pH range (6.5 to 9.5) showed that the switching in potential is also pH dependent (shifting approximately 0.06 V per decade) suggesting that the inactivation may result from a one proton, one electron process or result from two different forms of the enzyme with different affinities: as they discovered that at high NAD^+ concentration, the inactivation is less pronounced. Hirst and coworkers then

proposed two computational models designed to investigate the origin of the inactivation.[184] The first model suggested that the switch was due to the 2Fe2S cluster, which upon reduction changes the electrostatic environment close to the active site resulting in a decrease in NAD^+ reduction activity. The simulated data gave consistent values to the reduction potential values predicted for FMN and the 2Fe2S cluster. The second model proposed a second reaction pathway due to the substrate binding to the semi-reduced flavin, which also gave similar voltammograms to the experimental data. They, however, suggested that the second model may not be valid due to over-estimated in parameters during derivation of the model. This low potential inactivation was also suggested to help Complex I minimise reverse electron transport when the quinone pool is too reduced.

Cyclic voltammetry experiments were designed to check the presence of low potential inactivation in the region of NAD^+ reduction for HoxFU and typical voltammograms are shown in Figure 56. Experiments were performed at a slower scan rate of 1 mV/s to give a clear picture of the reactions happening at low potentials.

In Panel A, the electrode was placed into a solution of 2 mM NAD^+ and the electrode potential was swept between -0.2 V and -0.6 V. At the beginning of the scan, no catalytic current was observed as the electrochemical driving force was not enough to drive NAD^+ reduction. As the potential was driven towards more negative values, reduction current was observed as HoxFU started reducing NAD^+. At this high substrate concentration no distinctive low potential inactivation was observed, although the current dropped somewhat during the scan and between first and second cycles. If the enzyme modified electrode was placed in a solution of 25 μM NAD^+ (Panel B), a much clearer switch off in the catalytic activity was observed at low potentials. The catalytic activity, however, did not recover on the return scan and on the second cycle, a

substantial loss of activity was evident. This low potential inactivation effect is therefore reliant on the substrate concentration experienced by the enzyme.

In the case of Complex I, the inactivation at low potential is reversible: upon sweeping the potentials to positive values, the enzyme reactivates and a substantial catalytic activity remains on the second cycle. These experiments were recorded at a slightly higher scan rate (10 mV/s) than the experimental conditions for HoxFU (1 mV/s), and it should be pointed out that at 10 mV/s, low potential inactivation was not observed for HoxFU (see Figure 50).[117, 184]

Most NiFe hydrogenases such as *R. eutopha* MBH[131] and *E. coli* Hyd1[132] show reversible oxidative inactivation at high potentials. In the case of the MBH for example, inactivation at high potentials is assigned to oxidation of Ni at the active site of the hydrogenase from Ni-(II) to a catalytically inactive Ni-(III) state with a hydroxide being trapped in the active site. Upon sweeping the potentials to a low potential region, hydrogenases reactivate indicating that this inactivation is fully reversible. Recent literature on the heterodimeric (HoxHY) subunit of the SH from *R. eutropha* showed that HoxHY experienced catalytic activity loss at high potentials, however, no reductive reactivation peak was observed on the return scan.[77] Lauterbach *et al.* therefore concluded that the SH does not form the Ni-(III) inactive state and the loss of activity at high potentials could instead be due to potential dependent film loss and enzyme damage.[77]

Panel A and B of Figure 56 show considerably different catalytic shapes between the first and second scans. In both cases, the onset potential for NAD^+ reduction is shifted towards a slightly more negative value on the second cycle. This phenomenon is reproducible, but in comparison, upon scanning within a narrower

potential window (Panel C), minimum shift in onset was observed. Further analysis using an electrochemistry software developed by Lèger and Heering, SOAS[198] was performed to investigate this observation. The raw data were subjected to smoothing and differentiation to generate plots of d*i*/d*E* against *E* of the first and second scans in the reduction direction (panel D). The resulting plots of d*i*/d*E* show that the catalytic shape between first and second cycles overlay much better if the enzyme experienced a narrow potential window during the course of experiments.

Experiments performed in the presence of both substrates while keeping the total concentration at 2 mM as shown in Figure 56E revealed that inactivation at low potentials is still observed even in the presence of both substrates. This behaviour is distinct from 'film loss' since it is clearly dependent on electrode potential. The forward and return traces as shown in Figure 56 overlay well when the potential is taken down to -0.4 V but overlay poorly when more negative switch potentials are accessed.

The cause for low potential inactivation could be due to dissociation of the bound FMN from the enzyme subunit. It may also be possible that upon accessing such low potentials, the flavin in HoxF has changed position but has not been lost completely thus requiring extra driving force for catalysis. This could explain the difference in shape on the second cycle (panel A). It has been previously reported that the FMN-a residing in HoxY easily detaches from the enzyme subunit and that has caused a loss in the H_2:NAD^+ catalytic activity of the whole SH.[79] Earlier research has also shown that the second FMN (residing in HoxF), is involved in the hydride transfer with NADH and and would be retained in the subunit. However, in biochemical experiments performed by Lauterbach, it has been shown that pre-incubation of HoxFU with NADH at concentrations higher than the K_M value for 15 minutes leads to a significant decrease in NADH oxidation activity. Further analysis using fluorescence spectroscopy confirmed

that this decrease is due to FMN dissociation from the HoxFU subunit into the solution.[94]

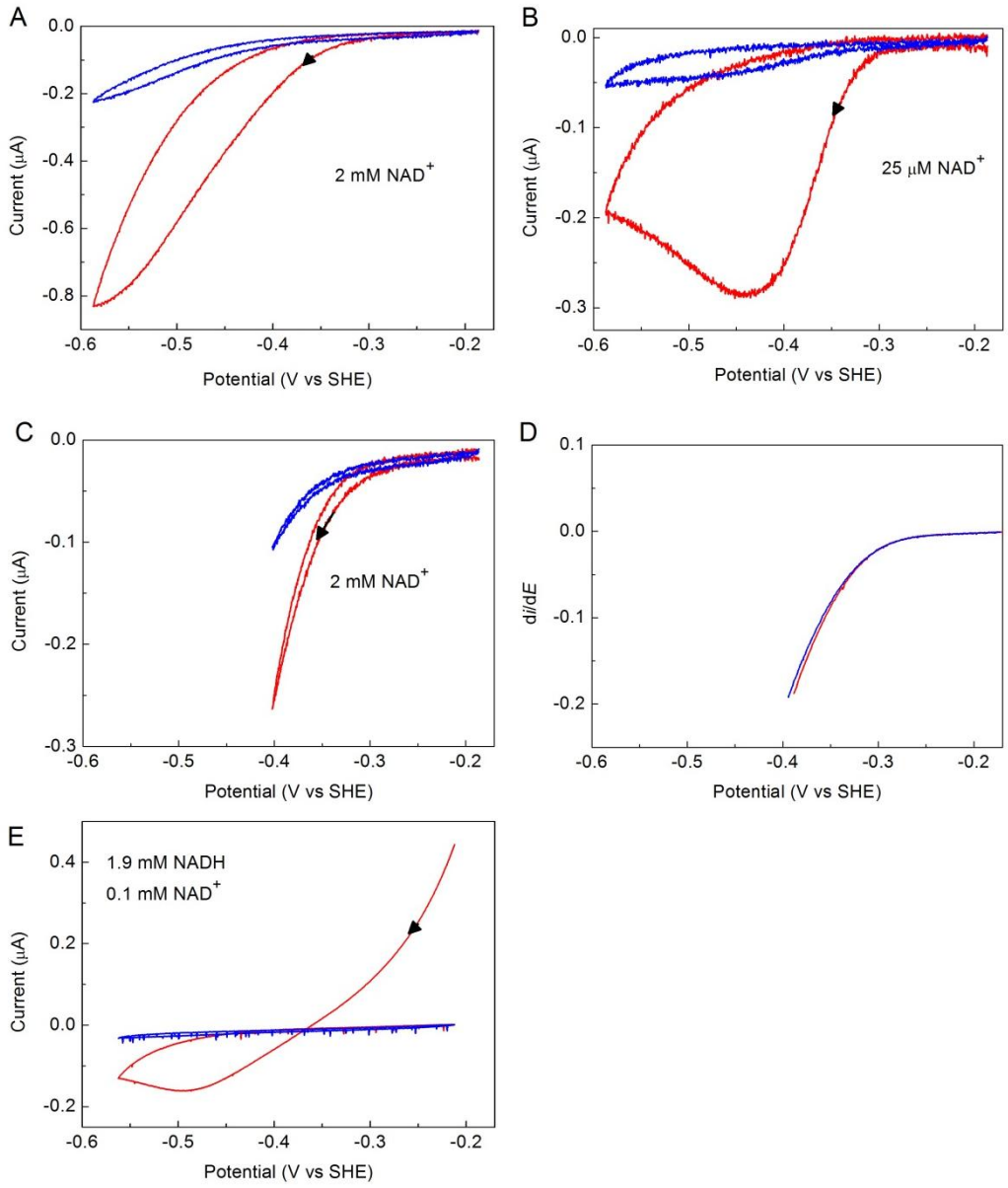

Figure 56. Cyclic voltammograms showing irreversible inactivation of HoxFU at low potentials at different substrates concentrations; (A) 2 mM NAD^+, (B) 25 μM NAD^+, (C) 2 mM NAD^+ at a narrow potentials window and (E) 0.1 mM NAD^+ and 1.9 mM NADH. Panel D shows the derivatives of forward scans of the first and second cycles at 2 mM NAD^+ analysed using SOAS software. In each case the scan rate was 1 mV/s, the electrode was rotated at 2500 rpm and other conditions were: 50 mM Tris-HCl buffer, pH 8.0 at 30 ^oC. The first cycle is shown as a red line and second cycle is shown as a blue line. Arrows indicated the direction of scan.

In electrochemical experiments, in the absence of substrates, cyclic voltammograms show clear peaks characteristic of surface adsorbed species at

approximately -0.28 V (Figure 57). An experiment with free FMN gave rise to peaks at a similar potential confirming that the signal observed in the absence of substrates was likely to be from dissociated FMN. The absence of this peak in the presence of substrates thus suggests that FMN is held more strongly in the protein when substrate is bound, although the small reversible signal of FMN would also be harder to detect against a clear and distinctive catalytic wave.

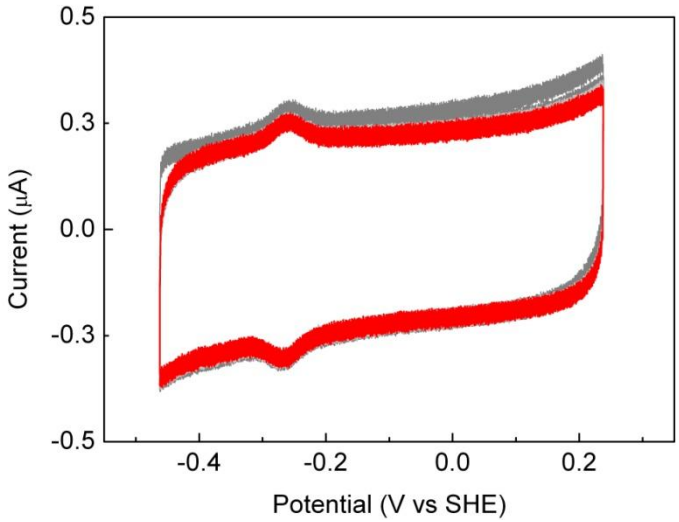

Figure 57. Cyclic voltammograms for a pyrolytic graphite edge electrode modified with 2 μM FMN (grey lines) and HoxFU (red line). All scans were performed in pH 8.0 Tris-HCl, 50 mM at 100 mV/s at 1 ^{o}C.

It is also worth mentioning here that experiments in Figure 57 were performed at a low temperature of 1 ^{o}C and even at this temperature, where the FMN is likely to be more stably bound, a clear FMN signal was observed suggesting that FMN is very unstable in the absence of substrate. In biochemical experiments, addition of excess FMN has been shown to restore and enhanced NADH oxidation activity of HoxFU, however, it is not possible to obtain electrochemical data to support this. Cyclic voltammetry performed in the presence of excess FMN on a HoxFU modified electrode did not show any recovery from the inactivation or increase in the reductive current (data not shown). The presence of excess FMN in the solution instead gave rise to

reversible peaks due to FMN adsorbed onto the electrode alongside an FMN signal from the dissolved species thus making data analysis more complicated.

3.4 The effect of substrate on catalytic activity

One important indicator of enzyme catalytic activity is the Michaelis-Menten constant, K_M. This constant (equation [32]) tells us about the binding between the enzyme and its substrate; a high K_M value indicates poor binding, which means that at low substrate levels, a small change in the substrate concentration will have a big effect on the catalytic activity.

$$v = \frac{V_{max}[S]}{K_M + [S]} \quad [32]$$

where v, [S] and K_M refer to the enzyme catalytic rate at a particular substrate concentration, the substrate concentration and the Michaelis-Menten constant, respectively. V_{max} represents the enzyme maximal catalytic activity. When [S] = K_M equation [33] is obtained:

$$v = \frac{V_{max}K_M}{2K_M} = 0.5V_{max} \quad [33]$$

At the K_M value, an enzyme obeying Michaelis-Menten kinetics will have half of its maximal activity. Therefore, one can expect that at the K_M value, significant catalysis should take place.

Conventional biochemical assays for redox enzymes utilise redox mediators such as benzyl viologen (BV) which will either supply or receive electrons for the reaction. The K_M value is obtained by monitoring the absorbance changes in BV

spectrophotometrically due to change in oxidation state. In the case of HoxFU, biochemical analyses are performed by monitoring the formation or consumption of a typical NADH absorbance at 340 nm. However, the drawback of this technique is the difficulty of finding the best slope to determine the initial rate of the reaction. Catalysis is often appears biphasic, starting with a 'linear' phase followed by a tailing off phase due to substrate consumption. This often causes the initial rate of catalysis to be underestimated thus overestimating the K_M.

Protein film electrochemistry therefore has been used to determine the K_M values of HoxFU. Since the enzyme is directly adsorbed onto the electrode, no mediator is needed and rotation is introduced during the experiment time frame so that a constant substrate supply and product removal is achieved. In PFE, the catalytic response, in this case the current recorded at each substrate level, represents the rate of the reaction at that substrate concentration and should remain stable at each substrate concentration since substrate in the bulk solution is not consumed significantly.

3.4.1 K_M for NADH oxidation

Figure 58 shows a typical experiment performed to determine the K_M for NADH oxidation by HoxFU. The electrode was poised at -0.062 V in order to drive NADH oxidation, and the experiment was initiated with no substrate presence in the cell thus only a small resistive current resulting from the electrode offset was observed. The electrode was only poised without substrate for a few seconds at the beginning of the experiment to prevent significant enzyme inactivation. The pyridine nucleotides were purified according to procedures established in Chapter 2 of this thesis. Purified NADH solution was then injected into the electrochemical cell solution and a positive catalytic

current due to NADH oxidation was observed. The catalytic current increases as more substrate is introduced.

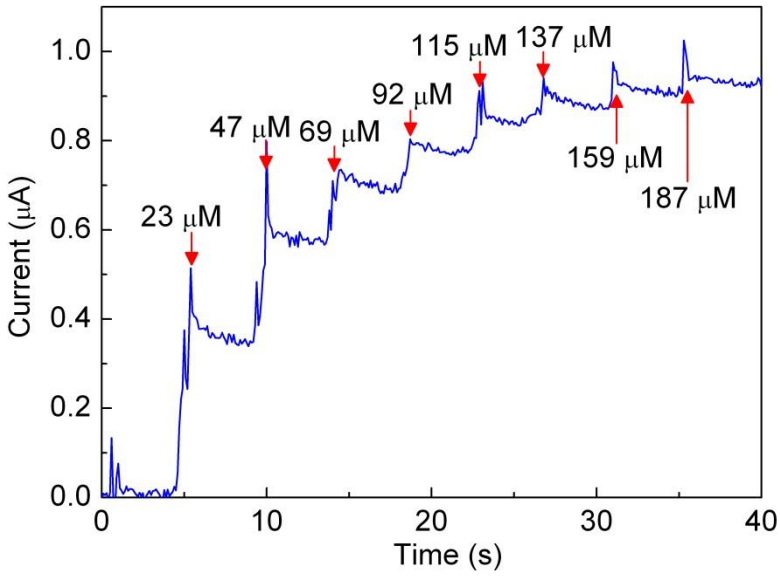

Figure 58. Chronoamperometry experiment designed to measure the value of the Michaelis-Menten constant, K_M for NADH oxidation. The potential was held at -0.062 V, NADH concentrations as indicated. The electrode was rotated at 2500 rpm in 50 mM Tris-HCl buffer at pH 8.0, 30 ^{o}C.

Figure 59 shows a plot of the current at each concentration against the substrate concentration, which resulted in a hyperbolic graph. This type of plot is typical of an enzyme obeying Michaelis-Menten kinetics. Based on the plot, the enzyme is predicted to have the maximum catalytic activity, V_{max} at a high substrate concentration. Since the K_M value is the substrate concentration at half of the maximum enzyme activity, the value can be determined by extrapolating the plot. Plotting the data this way gives a mean $K_M^{\text{NADH oxidation}}$ of 59 μM from six experiments. However, this plot has a few disadvantages such as the difficulty to draw an accurate rectangular hyperbola thus the predicted asymptotes can be underestimated.

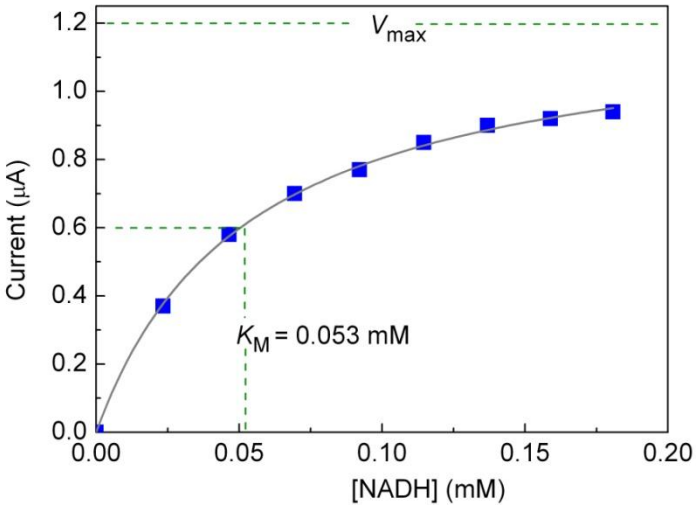

Figure 59. A plot of current against [NADH] to determine the K_M value for NADH oxidation. V_{max} is the approximate optimum catalytic current may be observed when the enzyme is fully saturated with substrate.

Figure 60 shows the data re-plotted as a Lineweaver-Burk plot (see Section 2.8.1).

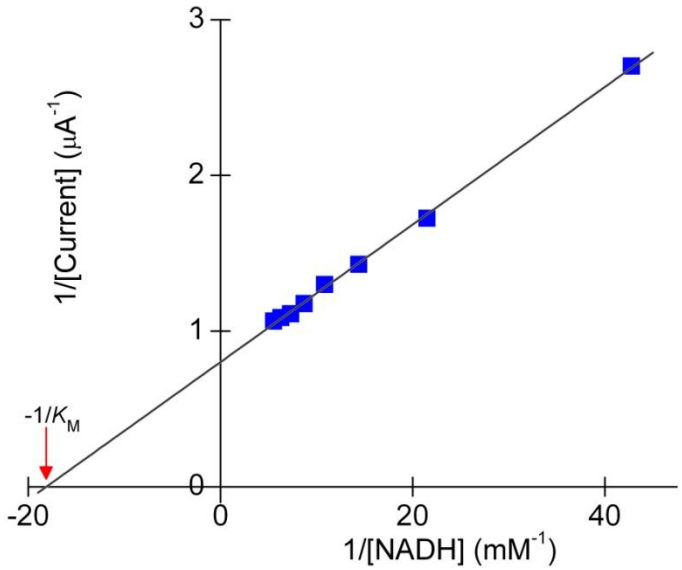

Figure 60. A typical Lineweaver-Burk plot obtained from chronoamperometry experiments to determine the K_M value for NADH oxidation.

Based on the Lineweaver-Burk plot, the $K_M^{\text{NADH oxidation}}$ can be extrapolated from the *x*-intercept of the graph. An average $K_M^{\text{NADH oxidation}}$ value of 64 ± 29 μM was

obtained from 6 experiments by this method. Although this plot has been widely used by enzymologists and biochemists, this plot is not recommended as it gives a misleading impression of the experimental error. For example, for small values of the enzyme activity *v*, small errors will give an enormous error in 1/*v* and cause the slope of the line of best fit to vary substantially. Since activity values at low substrate are typically the least reliable, this is likely to lead to errors in K_M.

Another technique that can be applied to determine the K_M value is shown in Figure 61, a Hanes-Woolf plot (see Section 2.8.1).

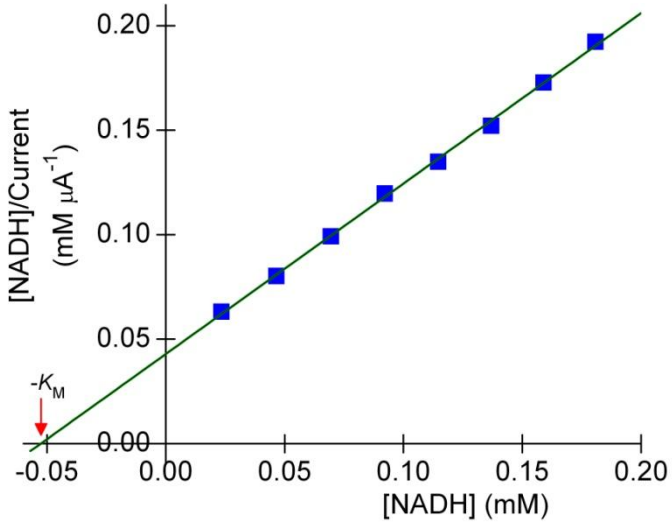

Figure 61. A typical Hanes-Woolf plot for determining the K_M value of HoxFU for NADH oxidation.

Plotting the data this way gives an average $K_M^{\text{NADH oxidation}}$ of 58 ± 18 μM from 6 experiments. This plot should give a more reliable value of K_M since the data can be more evenly distributed across a range of [NADH].

A summary of the $K_M^{\text{NADH oxidation}}$ value calculated from three different plots is shown in Table 3-1.

Table 3-1 summarises the K_M value for NADH oxidation by HoxFU calculated from three different plots.

Methods	$K_M^{\text{NADH oxidation}}$ (μM)	Standard deviation
v against [S]	59	19
Lineweaver-Burk	64	29
Hanes-Woolf	58	18

Based on Table 3-1, all three techniques gave a similar $K_M^{\text{NADH oxidation}}$ value. Comparing these three techniques, the smallest standard deviation was obtained using the Hanes-Woolf method. The Hanes-Woolf method was therefore used for all subsequent K_M analyses. Subsequent values are quoted ± one standard deviation.

A K_M value of 56 μM for NADH oxidation was determined in the biochemical assay performed by Lauterbach and this value is very close to the one calculated using these electrochemical techniques. This indicates that HoxFU does not suffer any damage to its catalytic properties upon adsorption onto the electrode. The value obtained is also of a similar magnitude to the one determined for bovine Complex I (90 μM).[199] Considering that the main function of Complex I is to oxidise NADH, this indicates that the SH is also equipped to function in oxidising NADH under certain physiological conditions despite its main role being for NADH formation.

3.4.2 K_M for NAD^+ reduction

The electrochemical technique was also used to determine the K_M value for NAD^+ reduction. The electrode was poised at -0.412 V to drive NAD^+ reduction by HoxFU and Figure 62A shows a set of typical data collected for this experiment. The HoxFU-modified electrode was first placed in a substrate-free solution so only the

background current arising from electrode offset was observed. Purified NAD^+ was then introduced into the cell solution and an increase in current was observed. Further injections increase the current respectively as shown in Figure 62A. Electrode current offset was taken into consideration upon analysing the data by subtracting the current value at the beginning of the experiment from all other current values. This is likely to arise from a resistive contribution from the electrode.

The data were then analysed using a Hanes-Woolf plot. The *x*-intersect of this plot gives the value of $-K_M$ and an average K_M value of 197 ± 28 μM for NAD^+ reduction was obtained from 9 experiments.

In solution, it has not been possible to drive NAD^+ reduction by common donors such as dithionite or methyl viologen, making it impossible to determine the K_M value for NAD^+ reduction using biochemical assays. However, by poising the potential of a HoxFU electrode at the region where NAD^+ reduction is observed, determination of the K_M value for NAD^+ reduction electrochemically is possible. This proves another advantage of electrochemistry in studying enzyme catalysis.

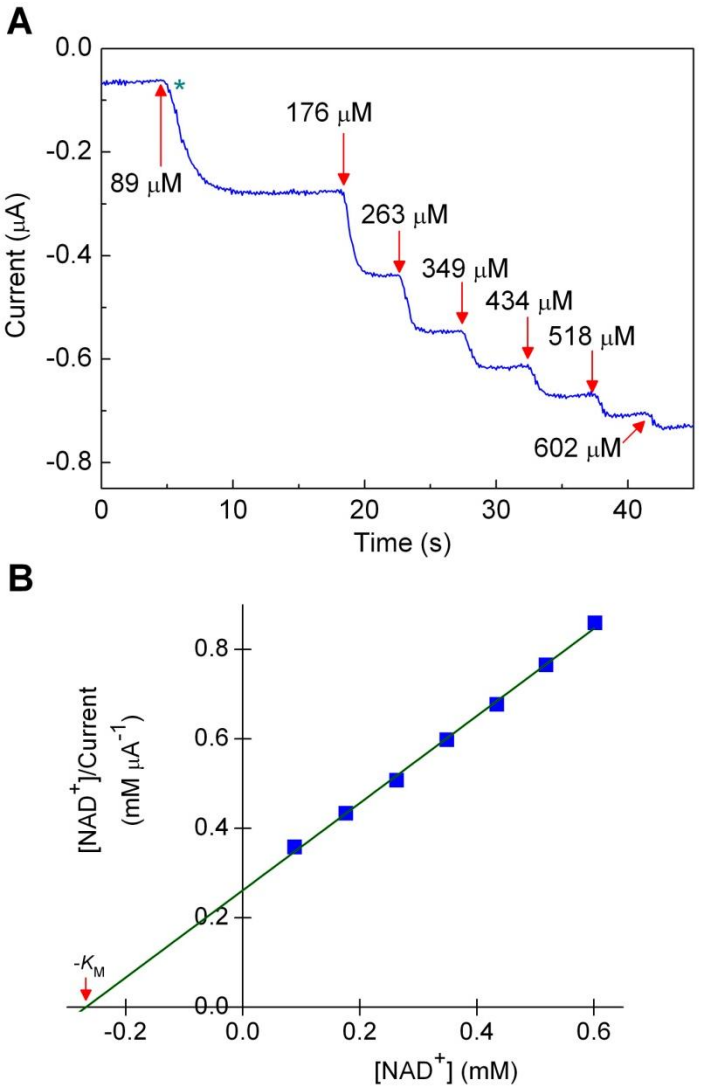

Figure 62. A. Chronoamperometry experiment designed to determine the K_M value for NAD^+ reduction by HoxFU. The electrode potential was hold at -0.412 V. No substrate was present at the beginning of the experiment and NAD^+ from stock solution was introduced into the electrochemical cell at concentrations as indicated in the figure. Electrode was rotated at 2500 rpm, and temperature was controlled using a thermostat waterbath at 30 ^oC. Panel B shows a typical Hanes-Woolf plot obtained.

3.4.3 Enzyme activation

From Figure 62, a slow increase in the current response was observed when HoxFU first encountered NAD^+. This effect is, however, not observed when the enzyme is first exposed to NADH, as shown in Figure 58 (the response to NADH is fast). Experiments were performed (Figure 63) to investigate this effect further by holding the

electrode potential at -0.412 V to drive NAD^+ reduction and adding different concentrations of substrate.

In panel A, the experiment was initiated with no substrate present so only the background current was observed first. At around 10 s, an aliquot of NAD^+ solution giving a cell concentration of 11 μM NAD^+ was injected into the electrochemical cell and an increase in current magnitude was observed. Upon NAD^+ injection, approximately 10 seconds was needed for the current to stabilise before film loss becomes evident.

Panel B shows an experiment on a fresh film of HoxFU, again starting from no substrate. With the first injection of NAD^+ (1.03 mM), a much faster time for activation was observed, with the current taking approximately 4 seconds to stabilise.

In panel C, the same enzyme modified electrode from Panel B was rinsed with a clean buffer solution before being placed in the electrochemical cell containing no substrate. An aliquot of 11 μM NAD^+ was injected into the cell at approximately 5 seconds after the scan started and surprisingly, a fast increase in catalytic response was observed.

Panel D shows an experiment on a fresh film of HoxFU and this time the enzyme was placed in a solution containing NADH before NAD^+ containing NADH at 107 μM NAD^+ was injected into the cell and this also gives a fast increase in catalytic response.

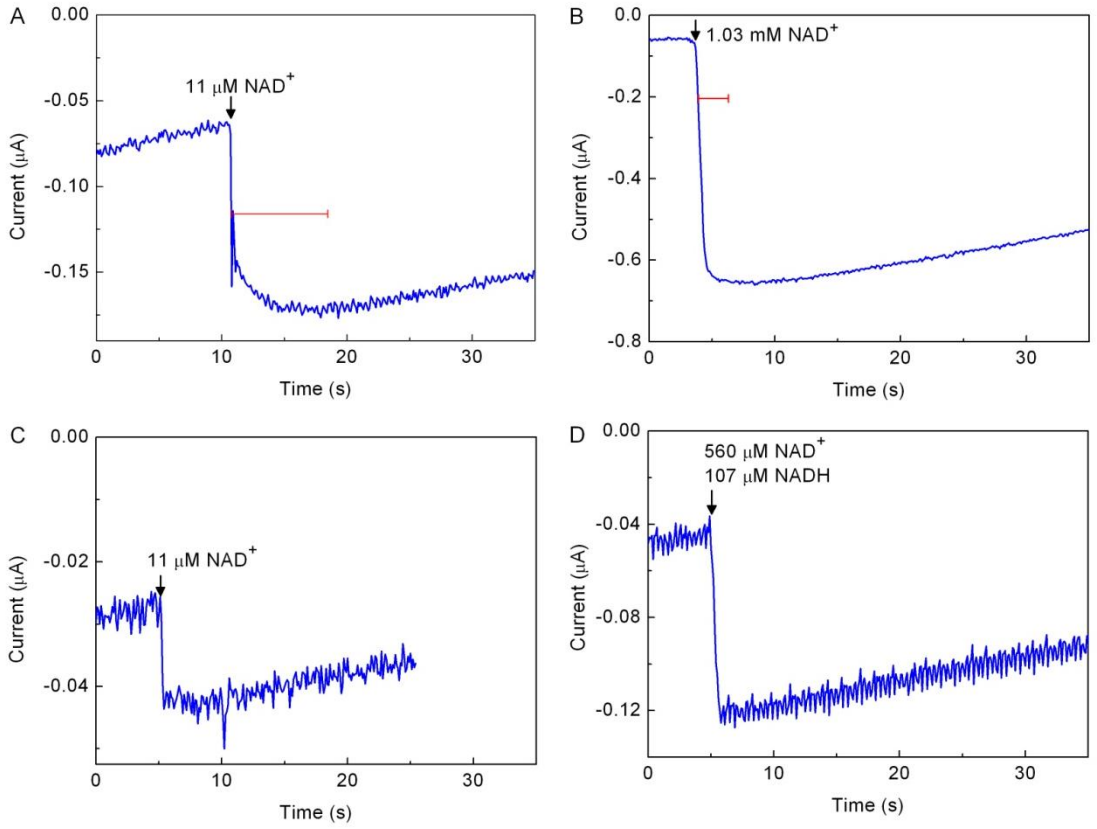

Figure 63. Experiments to investigate HoxFU substrate dependent activation were performed at -0.412 V to drive NAD^+ reduction. In Panels A and B, no NAD^+ was present at the beginning of the experiment, and an aliquot of NAD^+ was injected into the electrochemical cell to a final concentration of 11 µM and 1.03 mM at approximately 10 s and 5 s respectively. In Panel C, the same enzyme film from B was washed and put into a fresh buffer solution. An aliquot of 11 µM NAD^+ was injected at 5 s. Panel D shows results from experiment in which a fresh enzyme modified electrode was placed in a solution containing 107 µM NADH at the start of experiment. At 5 s, solution was injected to give 560 µM NAD^+ and 107 µM NADH in the cell solution.

These results can possibly be explained by examining a homology model of HoxFU constructed using the resolved crystal structure of Complex I as shown in Figure 64. According to the model an empty space is present close to the FMN catalytic centre in the absent of substrate. It can thus be postulated that the FMN is able to move freely in the absence of substrate, meaning a conformational change into a favourable position for catalysis is required when the enzyme first encounters its substrate.

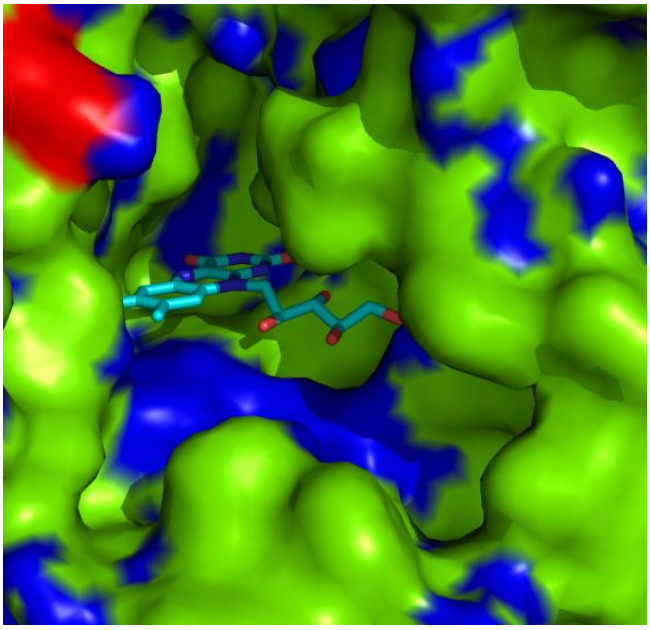

Figure 64. Surface representation model of HoxFU to show the space around FMN constructed using a homology model developed by using the resolved crystal structure of *T. thermophilus* Complex I without bound NADH. Flavin mononucleotide (FMN) is shown in stick. The homology model was developed by Lars Lauterbach and used as supplied.

3.5 The effect of potentials on K_M values

There are reports that changing the electrode potential (energy) affects an enzyme's affinity towards its substrates. For example, electrochemical studies on the MBH of *R. eutropha* by Cracknell showed that the K_M for H_2 oxidation is potential dependent, and values of K_M obtained increased by more than one order of magnitude.[166] This could occur if the substrate binds more tightly to one particular redox state of the active site. Therefore the effect of potential on K_M of HoxFU will be examined further in this Section.

3.5.1 NADH oxidation

*Experiments in this section were performed by Miss Kate Simpson-Wells, a Part II student under my supervision.[200]

To determine the potential dependence of the K_M, experiments procedures as described in Section 3.4.1 were performed at four different potentials within the NADH oxidation range: -0.06 V, -0.11 V, 0.04 V and 0.14 V. Figure 65(i) shows typical raw data obtained whilst panels (ii) illustrate Hanes-Woolf plots at potentials investigated for these experiments.

Table 3-2 summarises the mean K_M value calculated from Hanes-Woolf plot at each electrode potential.

Table 3-2. Comparison of the K_M values for NADH oxidation at different potentials.

Electrode Potential (V vs SHE)	**K_M ± standard deviation (μM)**
-0.11	35 ± 8
-0.06	53 ± 15
0.04	41 ± 6
0.14	35 ± 8

Table 3-2 shows that across the four different potentials no significant variation in $K_M^{\text{NADH oxidation}}$ was observed, taking into account the error limits. The K_M values are consistent with those previously reported from biochemical experiments (56 μM) without precise potential control.[94]

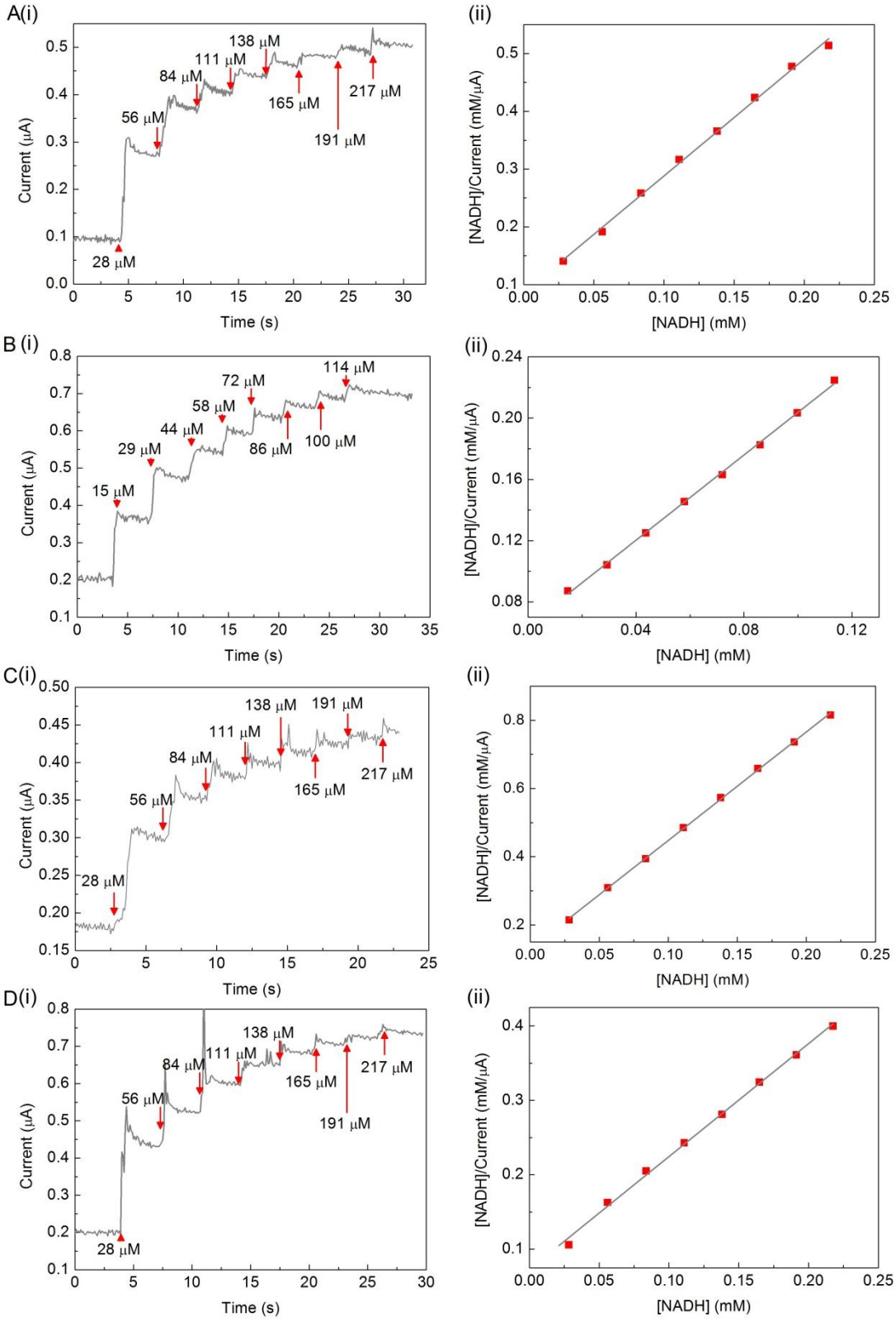

Figure 65. Lane (i) shows a typical chronoamperometry data obtained to determine the K_M for NADH oxidation at different potential values. The HoxFU modified electrode was poised at -0.11 V (Panel A), -0.06 V (Panel B), 0.04 V (Panel C) and 0.14 V (Panel D). Electrode in each experiment was rotated at 2500 rpm and temperature was set at 30 ^{o}C. Experiment was performed in Tris-HCl pH 8.0 buffer. The NADH stock solution was purified using column

chromatography before use electrochemically. Lane (ii) shows Hanes-Woolf plot for each set of data.

3.5.2 NAD^+ reduction

Experimental procedures as explained in Section 3.4.2 of this Chapter were also employed to explore the effect of potential changes in HoxFU affinity towards NAD^+. Four different potentials in the range of NAD^+ reduction were chosen (-0.392 V, -0.412 V, -0.462 V and -0.5 V) and Figure 66 lane (i) shows typical raw data obtained, with the respective Hanes-Woolf plots shown in lane (ii).

Table 3-3 summarises the mean K_M value calculated from Hanes-Woolf plot at each electrode potential.

Table 3-3. Comparison of the K_M values for NAD^+ reduction calculated at each potential and from style of plots.

Electrode Potential (V vs SHE)	**K_M ± standard deviation (μM)**
-0.39	160 ± 12
-0.41	199 ± 5
-0.46	168 ± 15
-0.50	182 ± 22

Table 3-3 shows that across four different potentials, no significant variation in $K_M^{NAD+\ reduction}$ was observed, taking into account the error limits. Data were collected over a relatively small potential range to avoid inactivation at low potentials (see Section 3.3.3).

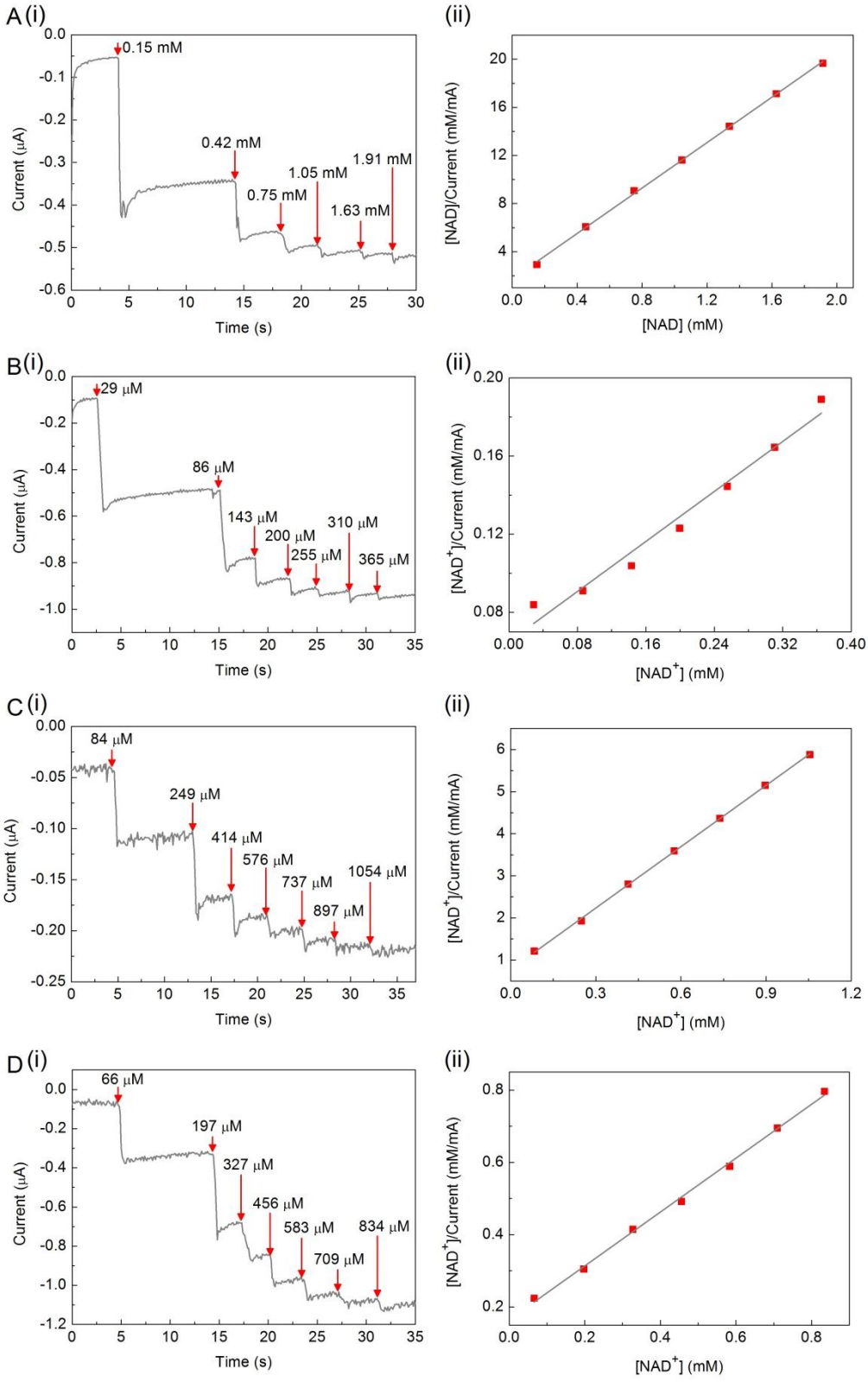

Figure 66. Lane (i) shows a typical chronoamperometry data obtained to determine the K_M for NAD^+ reduction at different potential values. The HoxFU modified electrode was poised at -0.39 V (Panel A), -0.41 V (Panel B), -0.46 V (Panel C) and -0.50 V (Panel D). The electrode in each experiment was rotated at 2500 rpm and temperature was set at 30 ^oC. Experiment was performed in Tris-HCl pH 8.0 buffer. The NAD^+ stock solution was purified using column

chromatography before use electrochemically. Lane (ii) shows Hanes-Woolf plot for each set of data.

3.6 Does HoxI have any effect on HoxFU activity?

The SH was first isolated, as a construct of four heterologous subunits, HoxHYFU. However, by utilising 50 mM Potassium Phosphate buffer at pH 7.0, low ionic strength and no affinity chromatography step throughout the purification procedures, an additional two subunits of the SH were purified in 2005 by Friedrich and coworkers.[78] These subunits, termed HoxI have a molecular weight of around 19 kDa.[13, 78] These adjacent HoxI subunits have been suggested to be associated with HoxF while sitting in close proximity for a direct electron transfer to FMN-a in HoxY, based on the finding that HoxI subunits do not copurify when the SH hydrogenase module was deleted during purification steps.

Friedrich and coworkers also suggested that each of the HoxI subunit conserved a mononucleotide binding site and together they formed a dinucleotide binding site that is suitable for NADPH binding. This assumption was supported by the ability of NADPH (25 μM) to reductively activate the hydrogenase activity of hexameric SH while the tetrameric SH requires a very high NADPH concentration (40 mM) for activation. In biochemical experiments, they also found that HoxI subunits dissociate upon prolonged incubation with Tris-HCl pH 8.0.

Electrochemical experiments in this Section will check the effect HoxI subunits may have on the electrocatalytic properties of the SH.

3.6.1 NADH catalysis

Electrochemical experiments involving HoxI were performed in 50 mM BisTris-HCl buffer pH 7.0 at 30 ^{o}C owing to the fact that HoxI easily dissociates from the subunit at high pH and salt concentration. Figure 67 shows cyclic voltammograms for a $HoxFUI_2$ modified electrode in a solution of equal ratios of NADH to NAD^+. At the beginning of the scan, negative current corresponding to NAD^+ reduction was observed. As the potentials were swept towards more positive values the negative current decreased and above the dotted black line which indicates $E(NAD^+/NADH)$ under these conditions, the catalytic current increases due to NADH oxidation by $HoxFUI_2$. At this substrate ratio, the current magnitude for NAD^+ reduction is bigger than NADH oxidation showing that the $HoxFUI_2$ is biased towards NAD^+ reduction.

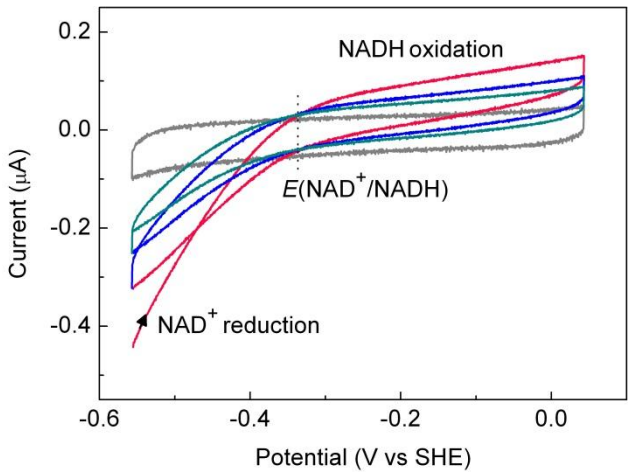

Figure 67. Cyclic voltammograms showing NADH oxidation and NAD^+ reduction catalysed by $HoxFUI_2$ in of 0.5 mM NADH: 0.5 mM NAD^+. Scans were recorded between -0.58 mV and 0.05 V and the black arrow indicates the direction of scans. Grey line represents the unmodified electrode scan. First, second and third cycles for the enzyme modified electrode are shown as red, blue and green lines respectively. A straight dotted black line shows the $E(NAD^+/NADH)$ at these conditions. Other conditions: scan rate 10 mV/s and electrode rotation rate 2500 rpm. Experiments were recorded using pH 7.0 BisTris-HCl buffer, 50 mM at 30 ^{o}C.

Cyclic voltammetry experiments performed on a HoxFU-modified electrode also revealed that HoxFU exhibits the same bias towards NAD^+ reduction bias under

identical experimental conditions. These findings indicate that $HoxFUI_2$ is catalytically active in NAD^+ reduction and NADH oxidation on electrode and the presence of the extra two HoxI subunits does not alter the enzyme preferences towards its substrate.

3.6.2 Inactivation at low potentials

Further experiments were performed to investigate whether HoxI may have an effect on low potential inactivation at different substrate concentrations. Figure 68A shows cyclic voltammograms recorded at NAD^+ concentrations well above the K_M value. At this concentration, no obvious inactivation was recorded. However, at low NAD^+ concentration as shown in panel B, the $HoxFUI_2$ shows irreversible low potential inactivation similar to that observed for the HoxFU.

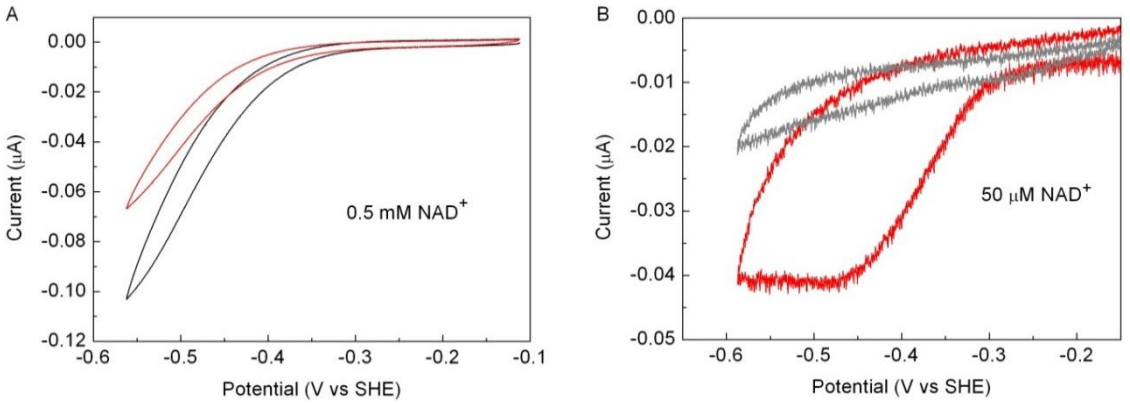

Figure 68. Cyclic voltammograms recorded at different NAD^+ concentrations; Panel A at 0.5 mM NAD^+ whilst Panel B at 50 µM NAD^+ to investigate $HoxFUI_2$ low potential inactivation. Experiments were performed in 50 mM BisTris-HCl buffer at pH 7.0, 30 ^oC at a slower scan rate of 1 mV/s. The enzyme modified electrode was rotated at high speed (2500 rpm) to ensure a constant substrate supply and product removal.

The cyclic voltammetry experiments on $HoxFUI_2$ revealed that the subcomplex experiences low potential inactivation and has no significantly different behaviour to that of HoxFU.

3.7 Summary

This Chapter presents the first electrochemical characterisation of the HoxFU diaphorase module of *R. eutropha* O_2-tolerant NAD^+-reducing soluble hydrogenase. The diaphorase module has been shown to display electrocatalytic NADH oxidation and NAD^+ reduction on a graphite electrode. The success of purification techniques to isolate HoxFU from the multi subunit $HoxHYFUI_2$ has allowed characterisation of this domain in isolation from its hydrogen cycling moiety, HoxHY and its full electron transfer chain. The electrochemical results are interpreted alongside biochemical experiments in the context of the physiological role of the SH in the cell and its relationship with Complex I. In the next Chapter, investigation of inhibition of the diaphorase activity will be studied.

Chapter 4: Inhibition

4.1 Product inhibition of HoxFU

Product inhibition is a type of inhibition experienced by enzymes when the product of the reaction binds to the enzyme active site thus preventing the substrate binding.[27] An example of product inhibition is shown by the NADH cytochrome *c* reductase isolated from spinach NADH-nitrate reductase complex,[201] which uses one molecule of NADH to reduce two of ferricytochrome c. In 1981, Palacian and Delarosa showed that NAD^+ competitively inhibits NADH oxidation of this diaphorase by binding to the enzyme active site.[201]

In the case of mitochondrial NADH-ubiquinone oxidoreductase (Complex I), NAD^+ was also found to inhibit NADH oxidation and an inhibition constant of 1 mM to 2 mM has been reported.[202, 203] In this section, product inhibition reactions experienced by HoxFU will be explored qualitatively and quantitatively.

4.1.1 NADH oxidation

In Protein Film Electrochemistry, the catalytic current is directly proportional to enzyme catalytic activity and changes in the catalytic current can be used to report on inhibition after injection of an inhibitor.[56, 57] Figure 69A shows a typical experiment designed to examine the inhibition of NADH oxidation by its product, NAD^+. The experiment was performed by holding the potential at -0.062 V to drive NADH oxidation by HoxFU. This potential was chosen to allow a fair comparison with other electrochemical data such as the K_M for NADH oxidation. At the beginning of the experiment, the enzyme modified electrode was placed in a substrate free buffer solution, thus only a background current was recorded. Once the background current stabilised, 50 μM NADH was introduced into the cell and an increase in current due to

NADH oxidation by HoxFU was observed. Throughout the experiment, the working electrode was rotated rapidly to bring fresh substrate to the enzyme film and spin away product from the electrode surface, so the substrate and product concentrations at the electrode surface were similar to the bulk solution. To check for product inhibition, aliquots of a NAD^+ stock solution, also containing 50 μM NADH were injected into the electrochemical cell to give concentrations as indicated on Figure 69A. These injections each resulted in a drop in positive current. The presence of NADH at 50 μM in the NAD^+ stock solution ensured that the decrease in catalytic current observed was not due to substrate dilution.

Panel B shows an experiment designed to confirm that the decrease in the current observed in panel A was not due to the dilution of substrate. Additions of buffer solution containing 50 μM NADH was performed as indicated (blue arrows), and as expected no drop in current was observed. This experiment thus confirms that the decrease in the NADH oxidation current upon injections of NAD^+ solution is due to NAD^+ inhibiting NADH oxidation by HoxFU.

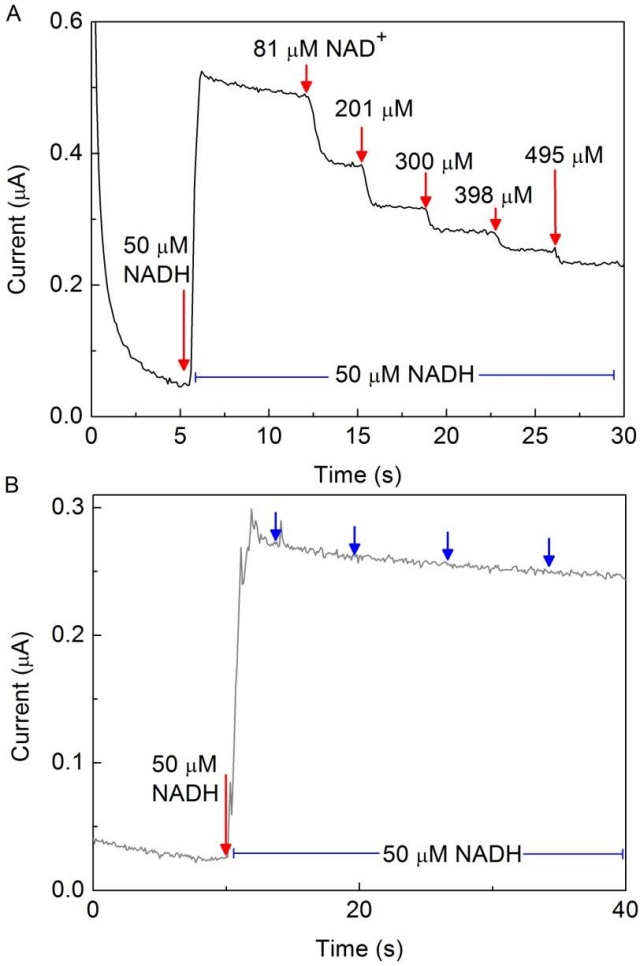

Figure 69. Panel A. Demonstration that NADH oxidation is product inhibited by NAD^+. The experiment was performed at -0.062 V with no substrate present at the beginning of the experiment. An injection to give 50 μM NADH was made at around 5 s and aliquots of NAD^+ containing 50 μM NADH were injected into the cell solution to give concentrations as indicated in the figure. Chronoamperometry experiment as shown in panel B was performed according to procedures described in panel A, with injections of buffer solution containing 50 μM NADH replacing the stock NAD^+. Conditions: pH 8.0 Tris-HCl buffer 50 mM, 30 ^oC and rotation rate of 2500 rpm.

Increasing the proportion of NAD^+ will change the thermodynamic potential of $E(NAD^+/NADH)$ according to the Nernst equation and is expected to lead to a small decrease in current due to diminished driving force for NADH oxidation (Figure 70). Based on Figure 70, the change in effective driving force relative to $E(NAD^+/NADH)$ throughout the experimental period, will lead to an approximately 4 % decrease in the catalytic current. However, the decrease in current upon injection of NAD^+ (Figure 69)

is too large just to be attributed to the change in driving force. This experiment thus confirms that NAD^+ inhibits NADH oxidation of HoxFU.

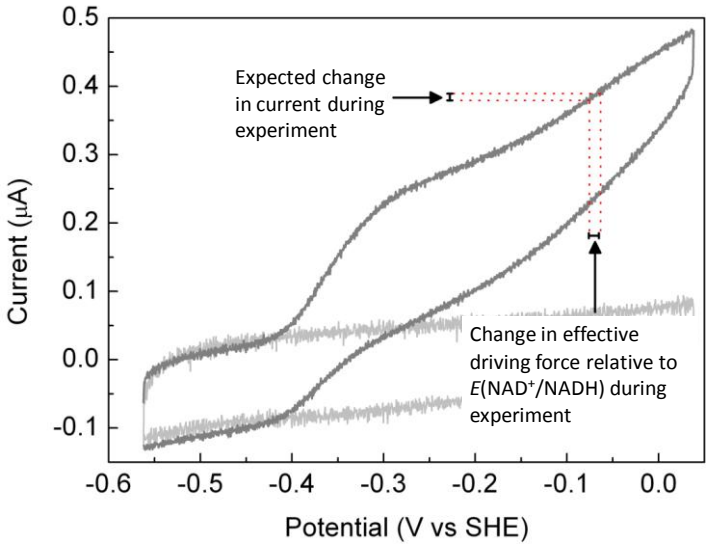

Figure 70. Cyclic voltammogram of a HoxFU modified electrode showing NADH oxidation. The region of change in effective driving force due to the addition of NAD^+ is marked on the figure and the expected current change is also shown. Experiments were performed in a solution of 0.5 mM purified NADH. Other conditions: pH 8.0, Tris-HCl buffer 50 mM, at 30 ^oC, electrode rotation of 2500 rpm, scan rate of 10 mV/s.

Further chronoamperometry experiments were designed to determine the product inhibition constant for NADH oxidation. For this, a set of inhibition data at different substrate concentrations is needed. The film to film variation in enzyme activity creates a problem here. Also, enzyme film stability on the electrode has to be taken into consideration and based on electrochemical experiments discussed in Chapter 3, the enzyme exhibits significant film loss during the course of an experiment. Therefore a strategy was developed for all the chronoamperometry data collected at different substrate concentrations to be combined into a single plot by normalising the current to the level recorded in a control step at 50 μM NADH. The total NADH concentration in the electrochemical cell was then either increased by injecting more NADH (panel A) or decreased (panel B) by introducing buffer after the control step. In Figure 71A the NADH concentration was increased to 100 μM and a further increase in

current was recorded, as expected. Aliquots of NAD^+ containing the same final NADH concentration (100 µM in this case) were then injected into the cell solution leading to a drop in current due to inhibition. Panel C shows an overlay set of chronoamperometry data after normalisation to the control step. The data show that inhibition was pronounced at all NADH concentrations investigated and inhibition is worst at low NADH concentration as expected, since product is expected to act as a competitive inhibitor (although note that the magnitude of the injections is different in each case).

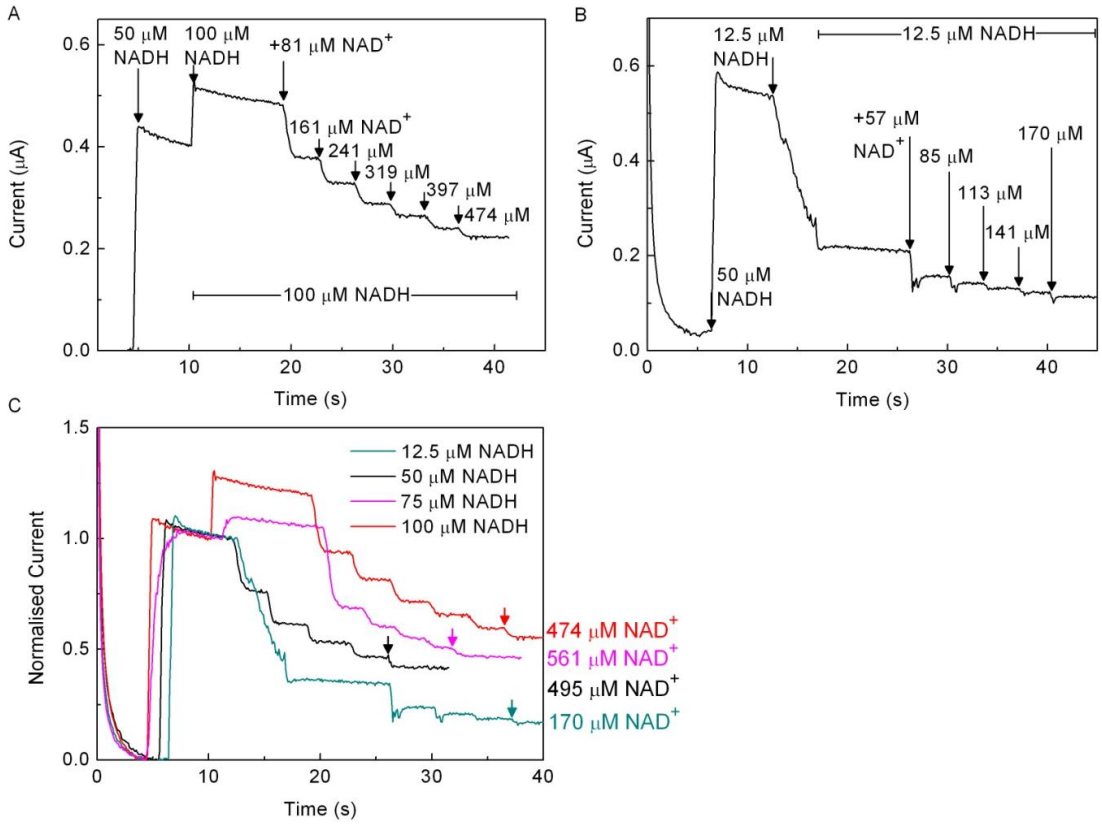

Figure 71. Current time plots from chronoamperometry experiments designed to determine the HoxFU product inhibition constant for NADH oxidation. Panels A and B: No NADH was present at the beginning of the experiment, then 50 µM NADH was introduced into the cell to give a 'control' current for normalising to other data sets. Further injection of NADH (or dilution by addition of buffer) was performed to a final concentration of 100 µM NADH (panel A) or 12.5 µM NADH (panel B). Inhibitor containing the same final concentration of NADH was then introduced into the electrochemical cell to give concentrations as indicated by black arrows. The electrode was poised at -0.062 V vs SHE, and rotated at 2500 rpm. Experiments were performed at 30 ^oC, in a 50 mM Tris-HCl pH 8 buffer solution. Panel C shows a set of chronoamperometry data at different final NADH concentrations, normalised to the control step. The final concentrations of inhibitor, NAD^+ are marked with coloured arrows and labelled accordingly.

The mechanism representing competitive inhibition is shown in Figure 72. Product inhibition is one example of inhibition in this way.

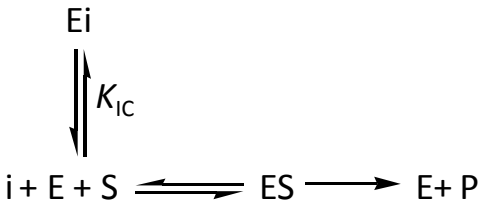

Figure 72. Mechanism that produces competitive inhibition. E, i, S and P represent enzyme, inhibitor, substrate and product respectively.

As discussed in Chapter 2, for a competitive inhibitor of a reaction obeying Michaelis-Menten kinetics, a plot of $1/v$ against [i] will give a straight line, with a gradient dependent on the reciprocal of the known substrate concentration. By overlaying data from different substrate concentrations, a set of straight line plots called a Dixon plot is generated and the point of intersection of these lines represents the negative of the inhibition constant.[204, 205] Since in PFE the catalytic current is proportional to the catalytic activity of the enzyme film *v*, an inhibition constant thus can be determined, without it being necessary to know the coverage of the film.

The raw data obtained from experiments such as that of Figure 71 were then analysed to determine the NADH inhibition constant, $K_I^{\text{NADH oxidation}}$ and the results are shown in Figure 73. Figure 73 shows a typical Dixon plot obtained from experiments to determine the K_I value for NADH oxidation. The lines intersect in the region of -0.1 to -0.3 suggesting that the K_I is in the range of 0.1 to 0.3 mM. Theoretically, if several lines are drawn at different substrate concentrations, a clean intersection at the point where [i] = $-K_I$ should be obtained but in practice, experimental error will give some variation as shown in Figure 73. The variation is typical for inhibition experiments as

shown by other researchers. For example, on the product inhibition of liver alcohol dehydrogenases, Wratten and Clalend showed that reduction of acetaldehyde is inhibited by ethanol and a plot of $1/v$ against 1/[i] at different inhibitor concentrations intersect in the region of -0.3 to -1.8 suggesting an inhibition constant in the range of 0.3 to 1.8 mM.[186, 206]

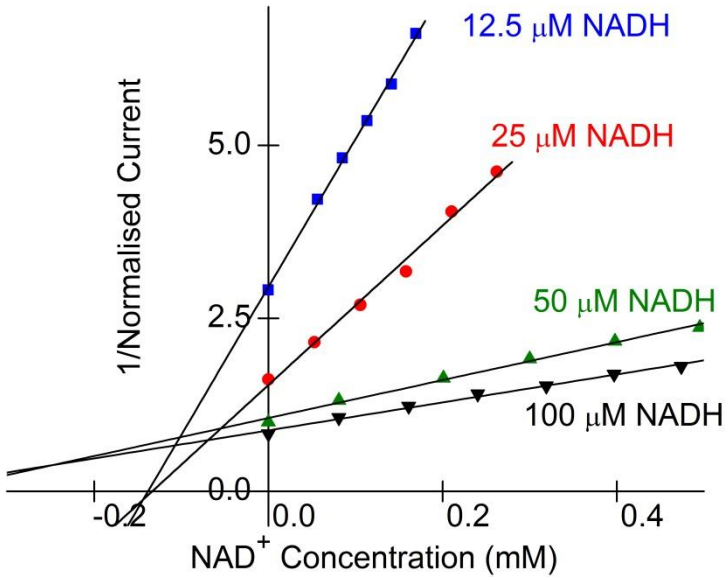

Figure 73. A typical Dixon plot for a set of data at different NADH concentrations recorded for HoxFU electrodes according to the conditions set out in Figure 71.

Although a value for the inhibition constant can be calculated from the Dixon plot, plotting data using this method, however, does not differentiate unambiguously between mixed and competitive inhibition. Therefore another method of analysing the inhibition data termed a Cornish-Bowden plot was employed.[188]

Figure 74 shows a plot of [NADH]/normalised current against NAD^+ concentration at different substrate concentrations. This plot resembles a plot of [S]/*v* against [i] as first proposed by Cornish-Bowden in 1974 [188] to help assign the type of inhibition. This plot can differentiate between mixed and competitive inhibition. Multiple straight lines for different substrate concentrations will generate a set of

parallel lines with different intercepts on the *y*-axis that increase with an increase in substrate concentration for the case of competitive inhibition.

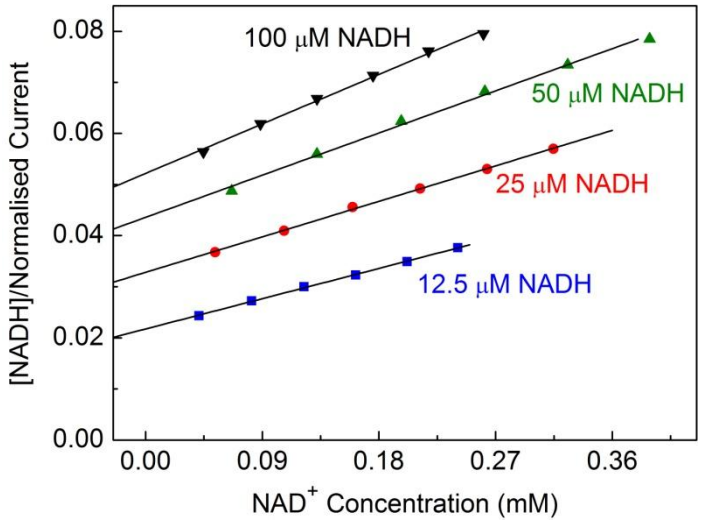

Figure 74. A plot of [NADH]/normalised current against [NAD^+] at different substrate concentrations to differentiate types of inhibition.

For mixed inhibition, the straight lines are expected to intersect cleanly on the negative region of the plot. The term mixed inhibition reflects ability of an inhibitor to bind both the free enzyme to form an enzyme-inhibitor (Ei) complex giving a dissociation constant of K_{IC} or to the enzyme-substrate complex to give an enzyme-substrate-inhibitor (ESi) complex with a dissociation constant of K_{IU}, as shown in Figure 75.

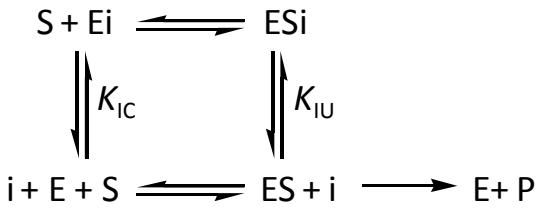

Figure 75. A mechanism produces mixed inhibition. E, i, S and P represent enzyme, inhibitor, substrate and product respectively.

If the enzyme undergoes mixed inhibition, its apparent affinity towards substrate will be decreased, $K_M < K_M^{app}$ and it will have a much lower maximal rate of reaction, $V_{max}^{app} < V_{max}$. According to Cornish-Bowden, mixed inhibition is an important case of product inhibition when a different form of enzyme than the one that binds substrate is generated upon product formation.[186, 188]

Plotting the data using the Cornish-Bowden technique revealed that competitive inhibition is the most likely to be the type of inhibition experienced by HoxFU. In summary NADH oxidation by HoxFU is competitively inhibited by the product NAD^+ with K_I in the range of 0.1 to 0.3 mM.

4.1.2 NAD^+ reduction

To check for inhibition of NAD^+ reduction by NADH a chronoamperometry experiment as shown in Figure 76A was designed. Experiments in this region are complicated due to contamination of NADH with NAD^+ (approximately 5 % NAD^+ is often apparently present in unpurified NADH as indicated by the NAD^+ reduction current in a cyclic voltammogram-see Section 2.6.2), therefore the NADH was purified using an anion exchange column as described in Chapter 2 before use and the final concentration of purified NADH was determined by UV-vis spectroscopy in comparison to a standard curve. During the course of the experiment, the enzyme modified electrode was poised at -0.412 V to drive NAD^+ reduction. No NAD^+ was present at the beginning of the scan hence only a small background current was observed. At approximately 5 seconds, an aliquot of NAD^+ was injected into the solution giving a total cell concentration of 50 µM and causing an increase in current due to NAD^+ reduction. Introduction of 32 µM NADH containing 50 µM NAD^+ at 10 seconds leads to a decrease in the catalytic current confirming that NADH inhibits

NAD^+ reduction. The catalytic current decreases as more NADH is introduced into the cell.

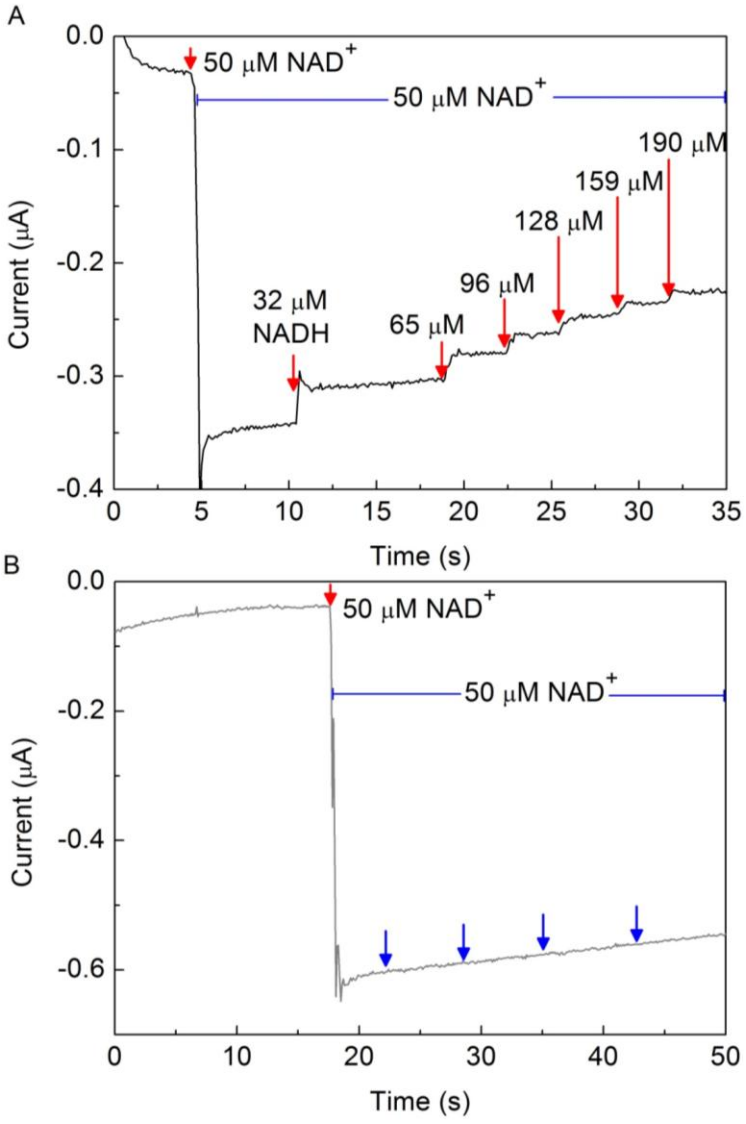

Figure 76. Panel A. Demonstration of NAD^+ reduction being product inhibited by NADH. The experiment was performed at -0.412 V with no substrate present at the beginning of the experiment. An injection of 50 μM NAD^+ was made at 5 seconds and aliquots of NADH containing 50 μM NAD^+ were injected into the cell solution at concentrations as indicated in the figure. The chronoamperometry experiment shown in panel B was performed according to procedures described for panel A, with injections of buffer solution containing 50 μM NAD^+ replacing the stock NADH. Conditions: pH 8.0 Tris-HCl buffer 50 mM, 30 ^oC and rotation rate of 2500 rpm.

Figure 76B shows an experiment designed to confirm that the decrease in the current observed in panel A was not due to any perturbation of the system upon

injection of solutions into the electrochemical cell. Additions of buffer solution containing 50 μM NAD^+ were introduced as indicated (blue arrows), and as expected no drop in current was observed. This experiment thus confirms that the decrease in the NAD^+ reduction current upon injections of NADH solution is due to NADH inhibiting NAD^+ reduction of HoxFU.

Further experiments were performed to determine the inhibition constant for this reaction utilising a similar strategy to that explained in Section 4.1.1. Figure 77A shows an experiment performed with a control step at 50 μM NAD^+. The total NAD^+ concentration was then increased by addition of more NAD^+ or decreased by injection of buffer solution into the cell. In Panel A, more NAD^+ was introduced into the cell to a final concentration of 100 μM NAD^+. The raw data was analysed to determine the inhibition constant and type of inhibition. Panel B shows a set of chronoamperometry data overlaid after normalisation to the control step.

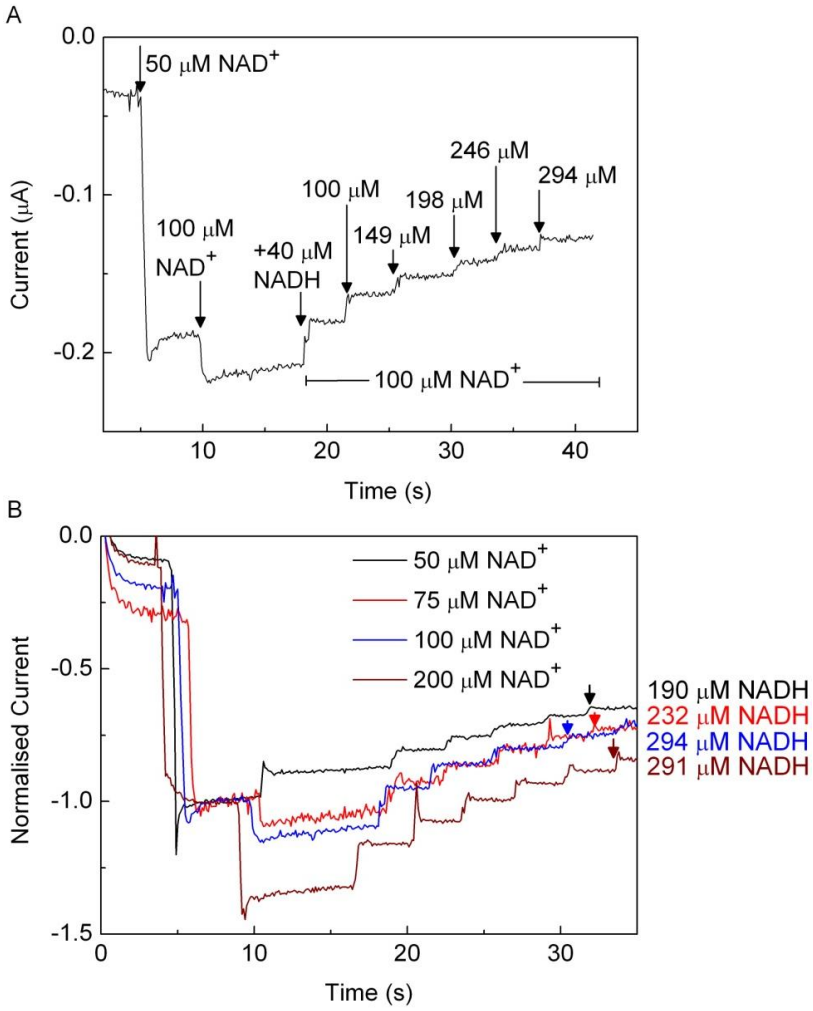

Figure 77. Panel A: Typical chronoamperometry result showing that NAD^+ reduction is inhibited by its product, NADH. The experiment was initiated with no substrate present; hence no catalytic current was recorded. At approximately 5 seconds, 50 µM NAD^+ was injected into the cell solution and a further injection of NAD^+ was performed to give a final concentration of 100 µM NAD^+. Aliquots of inhibitor containing the same final NAD^+ concentration were injected into the cell solution to give concentrations indicated by black arrows. Conditions: 50 mM Tris-HCl buffer, pH 8.0 at 30 ^oC, the electrode potential was poised at -0.412 V. Panel B: Set of chronoamperometry data normalised to the control step. The final concentrations of inhibitor, NADH are marked with coloured arrows and labelled accordingly.

A typical Dixon plot was constructed from several sets of experiments performed at different substrate concentrations as shown in Figure 78A. In contrast to Figure 73, the lines intersect more clearly in the region of -0.2 to -0.3 suggesting that the K_I is around 0.2 to 0.3 mM.

In Panel B, a Cornish-Bowden plot suggests that the inhibition is competitive, similar to the NAD^+ inhibition of NADH oxidation described earlier.

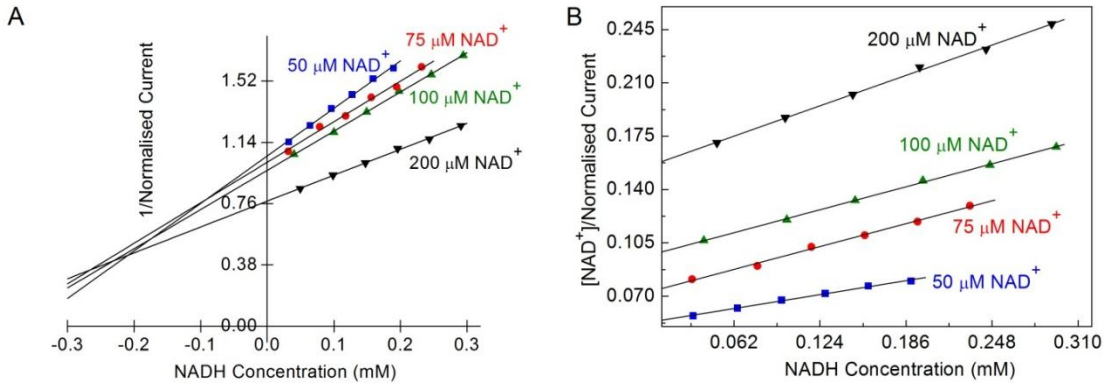

Figure 78. Panel A: Analysis of the raw data for NADH inhibition of NAD^+ reduction. Panel A shows a plot of 1/normalised current against [NADH]. Panel B: A Cornish-Bowden plot.

The data in Figures 69, 71, 76 and 77 were analysed by assuming film loss has a negligible effect on the catalytic current of a HoxFU film during the course of one experiment. This, however, is not completely accurate for either case of HoxFU product inhibition. For example in the case of NADH oxidation, Figure 69 reveals that the enzyme film experiences a substantial 'film loss' at the beginning of the experiment, seen by the decreasing current, however, the current stabilised as NAD^+ was injected into the electrochemical cell solution. This phenomenon is interesting as it suggests that the presence of both substrates helps to minimise the loss of enzyme electrocatalytic activity. It does, however, complicate quantitative analysis of the product inhibition constant, K_I for the reaction. The following section examines the effect on K_I of assuming film loss continues at its initial rate throughout the experiments: a worst case scenario analysis.

4.1.3 Analysing HoxFU product inhibition assuming worst case scenario film loss

As can be seen from Figure 69 and Figure 76, the initial catalytic current for a HoxFU electrode before introduction of the inhibitors decays quickly. Although it is clear that both reactions are inhibited by the products, the enzyme instability does complicate the quantitative analysis of the K_I values as the expected current magnitude may be under-estimated due to the rate of enzyme film loss as inhibitor is introduced into the cell. Unfortunately, there is no simple way to model the background decay in current since the current stability is affected (throughout the experiment) by the availability of NAD^+ and NADH. For example, in Figure 69 introduction of NAD^+ stabilises the NADH oxidation current.

To compensate for the film loss, a 'worst case scenario' analysis has been performed in which an exponential decay function is fitted to the data at 0 mM inhibitor and extrapolated over the remaining current data. Panels A and B of Figure 79 show the corrected raw data after subtraction of the exponential film loss function while Panels C and D show Dixon plots generated from the corrected data.

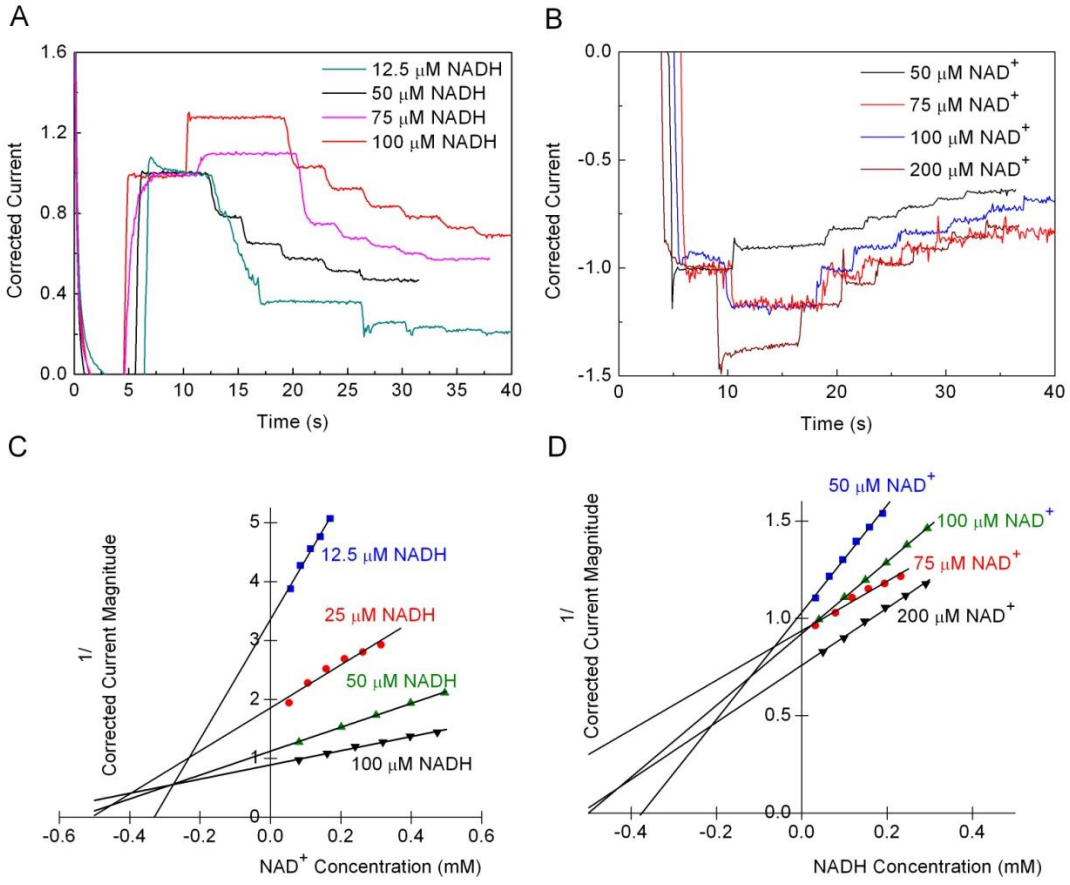

Figure 79. Panels A and B show the corrected sets of raw data after correction for an exponential fit as described in the text. Dixon plots of the corrected data for NAD^+ inhibition of NADH oxidation (C) and NADH inhibition of NAD^+ reduction (D).

For NADH oxidation inhibited by NAD^+ (shown in Panel C), the lines intersect in the region of -0.2 to -0.5 indicating that the inhibition constant is in the range of 0.2 to 0.5 mM. For NAD^+ reduction inhibited by NADH, the lines intersect in the range of -0.1 to -0.5 suggesting that the inhibition constant is in the range of 0.1 to 0.5 mM, Panel D. The values obtained after correcting for the film loss were found to be very close to the uncorrected data, although spanning a slightly wider range.

In the case of product inhibition of NAD^+ reduction, the 'worst case scenario' analysis is likely to overcompensate for the decay in current since the recorded current during the inhibition experiment was not particularly unstable and stabilises during the experiment (Figure 77B). This could explain the unexpected position of the straight line

for 75 µM NAD^+ data in the plot; this line should be in between 50 µM and 100 µM NAD^+ in an actual Dixon plot. Due to the problems of overcompensation for film loss, and its fairly minor effect on the K_I range, film loss has been ignored in subsequent data analysis.

4.1.4 Discussion of product inhibition results

Chronoamperometry experiments performed on HoxFU confirm that NADH formation and the reverse reaction are product inhibited. However, for both cases, the presence of inhibitors did not fully inhibit the enzyme over a range of physiologically relevant NAD^+/NADH concentrations. For example, at 474 µM NAD^+ concentration (two times the K_M for NAD^+) approximately 45 % NADH oxidation current was sustained. Based on examination of the data, the K_I values for HoxFU have been reported in a range rather than as a discrete value. Film loss has a fairly minor effect on the K_I range obtained, and has therefore been ignored because it is not possible to accurately assess film loss due to variations in film stability during experiments. For NADH oxidation, a range of 0.1 to 0.3 mM was calculated while a range of 0.2 to 0.3 mM was determined for NAD^+ reduction. The K_I value for NADH oxidation by HoxFU is an order of magnitude smaller than that has been reported for mitochondrial Complex I by Vinogradov and coworkers.[202] It has been suggested that the positive charge in the nicotinamide moiety of NAD^+ plays a major influence on Complex I affinities towards NADH and NAD^+. Vinogradov note that the product inhibition of NADH oxidation in Complex I by NAD^+ is weak, and since the overall nicotinamide cofactor concentration is high and the NADH/NAD^+ pool is predicted to be in a reduced condition, Complex I is unlikely to be product inhibited under physiological conditions.[207] The reverse reaction (NAD^+ reduction coupled to quinone oxidation) was

also found to be product inhibited in Complex I, however, with a much smaller inhibition constant (μM range) than that of NADH oxidation (mM range). Since the SH is thought to be bidirectional in its physiological role, the low K_I values could acts as a control mechanism in balancing the rates of reaction in order to balance the ratios of NADH and NAD^+ in the cell. For example, if the NAD^+/NADH pool has become too reduced, NADH inhibition of NAD^+ reduction would help to favour NADH oxidation to restore the redox balance.

4.2 Investigating the effect of Complex I inhibitors on HoxFU

(Experiments in this Section were performed by Miss Kate Simpson-Wells (2011 MChem Part II) under my supervision.)

The close similarity of HoxFU and Complex I raises a question of whether the inhibitors for Complex I will have the same effect on HoxFU catalytic activity. In Complex I, alongside other inhibitors, it has been shown that Adenosine Diphosphate (ADP), Adenosine Diphospho Ribose (ADP-Ribose), Adenosine Monophosphate (AMP), Adenosine Triphosphate (ATP) and 5,5'-dithiobis-(2-nitrobenzoic acid) (DTNB) inhibit NADH oxidation.[208-210] There is, however, no reported data on inhibition of Complex I by nicotinamide mononucleotide and adenosine, although these molecules have structural similarity to NAD(H).

The study of Complex I inhibitors on HoxFU is important not only for a better understanding of HoxFU and the SH but also due to the fact that any consideration of the possibility of utilising the diaphorase moiety in biotechnological applications will have to take into account all factors that would affect HoxFU catalytic performance. Furthermore it has been shown that commercially available nicotinamides often

contains impurities.[183, 185] This Section will explore the possibility of inhibition of HoxFU by Complex I inhibitors.

4.2.1 Adenosine Diphosphate (ADP)

Adenosine Diphosphate (ADP) is a nucleoside diphosphate that consists of a dipyrophosphate, a ribose and an adenine unit. In the cell, ADP is generated from dephosphorylation of ATP by an enzyme called ATPase.[27] A comparison between the structure of an NADH molecule and ADP is shown in Figure 80 and it can be seen that these two molecules are closely related. An earlier study on Complex I inhibition showed that ADP inhibits its NADH-fericyanide reductase activity with a K_I value in the range of 10^{-2} M.[209, 210]

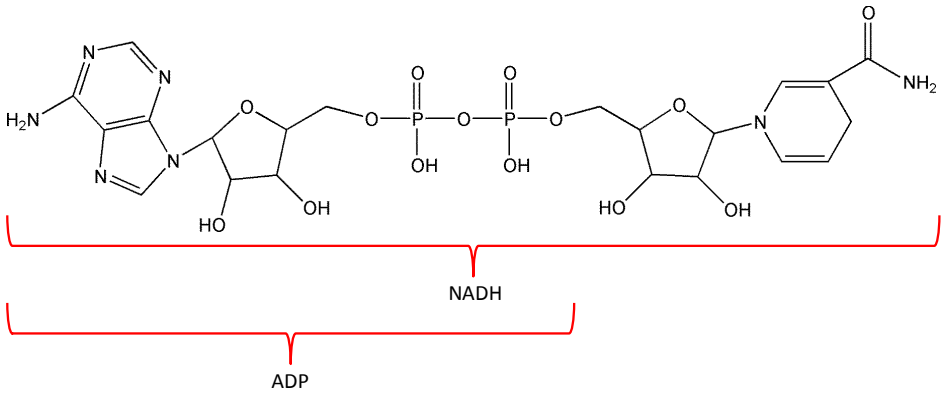

Figure 80. A structural comparison between a molecule of NADH and ADP.

Experimental techniques as discussed in Section 4.1 have been employed to examine the effect of ADP on the NADH oxidation activity of HoxFU. Figure 81 shows data from a typical chronoamperometry experiment used to check for ADP inhibition. As can be seen, a substantial decrease in HoxFU catalytic current is recorded when 2.5 mM ADP containing 100 µM NADH was added into the electrochemical cell solution at approximately 26 seconds.

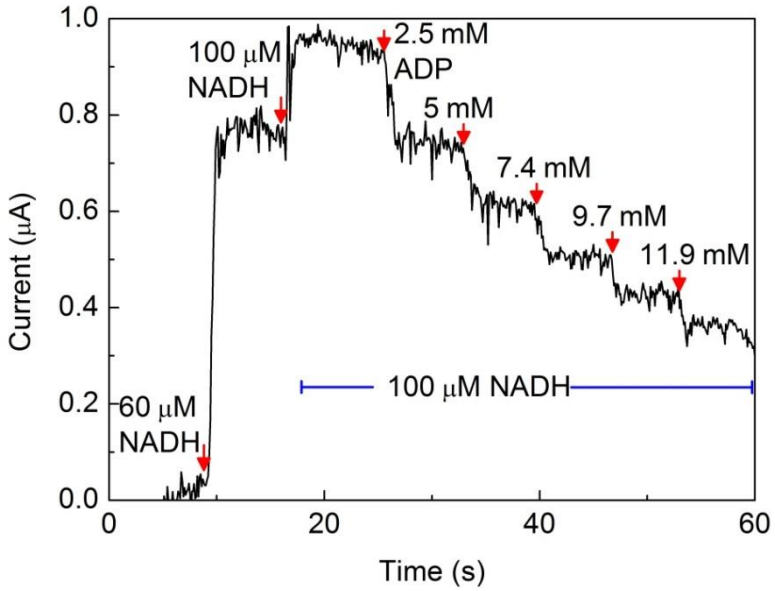

Figure 81. Chronoamperometry experiment used to check for NADH oxidation inhibition by ADP. The experiment was performed at -0.062 V with no substrate present at the beginning of the experiment. An injection of 60 µM NADH was made at around 9 seconds and used as a control step for comparison with subsequent experiments. A further injection of NADH to bring the total cell concentration to 100 µM was performed at 18 seconds and aliquots of ADP containing 100 µM NADH were injected into the cell solution to give concentrations as indicated. Conditions: pH 8.0, Tris-HCl buffer 50 mM, 30 ^{o}C and rotation rate of 2500 rpm.

Further chronoamperometry experiments were performed at several NADH concentrations and these data were combined and analysed using the techniques described in Section 4.1.1. Figure 82 illustrates Dixon (panel A) and Cornish-Bowden (panel B) plots used to determine the inhibition constant and type of inhibition by ADP. The lines in the Dixon plot in Panel A intersect in the range of -1 to -3 suggesting a K_I value of around 1 to 3 mM. The Cornish-Bowden plot (panel B) indicates that the most likely mode of inhibition observed for ADP is competitive inhibition.

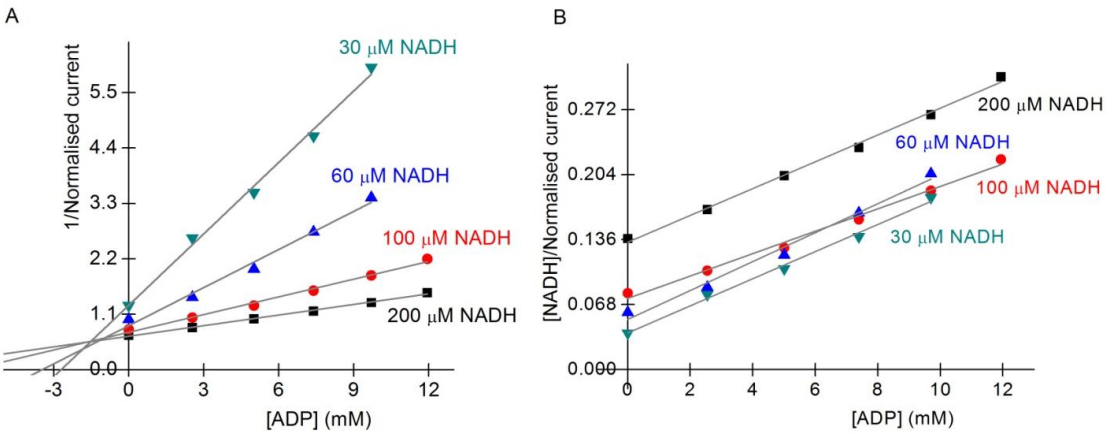

Figure 82. Typical plots of 1/normalised current against ADP concentration (Panel A) and [NADH]/normalised current against ADP concentration (Panel B) at different NADH concentrations.

The inhibition by ADP of Complex I has been reported to be more effective at low NADH and high ADP (12 mM) concentrations by Hanstein and coworkers, suggesting an inhibition constant in the range of 10^{-2} M.[210] The K_I value obtained for HoxFU is ten times smaller than the K_I value for Complex I inhibition by ADP. The K_I value for ADP inhibition of NADH oxidation by HoxFU is larger than the K_I value for inhibition by NAD^+, indicating that HoxFU has a higher affinity for NAD^+ than ADP. This is expected because NAD^+ is the native substrate of the SH.

4.2.2 Adenosine Monophosphate (AMP)

Figure 83 shows a structural comparison between a molecule of NADH and AMP. Both molecules are relatively similar; with the NADH molecule containing an extra phosphate, ribose and nicotinamide group. AMP is used as a monomer for RNA, which is essential for living organisms, and it can be produced by an enzyme called adenylate kinase during ATP synthesis.[27] AMP differs from ADP only in the presence of one phosphate group.

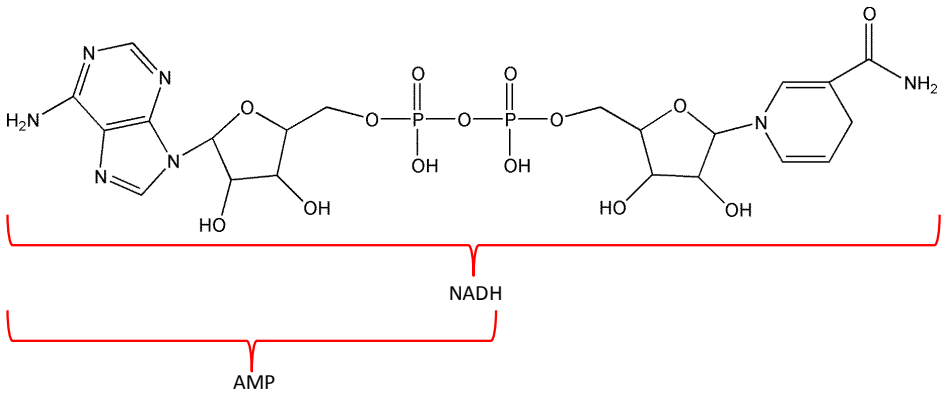

Figure 83. Structural comparison between NADH and AMP.

Experimental procedures as described in Section 4.1.1 were employed for determination of the K_I value for AMP and a typical current against time plot is shown in Figure 84. The initial NADH oxidation current observed at 100 µM NADH for this experiment was quite low, so the low signal-to-noise level complicates the experiment. However, a clear decrease in the NADH oxidation current was observed upon injection of 2.12 mM AMP containing 100 µM NADH into the electrochemical cell confirming that AMP inhibits HoxFU NADH oxidation reaction.

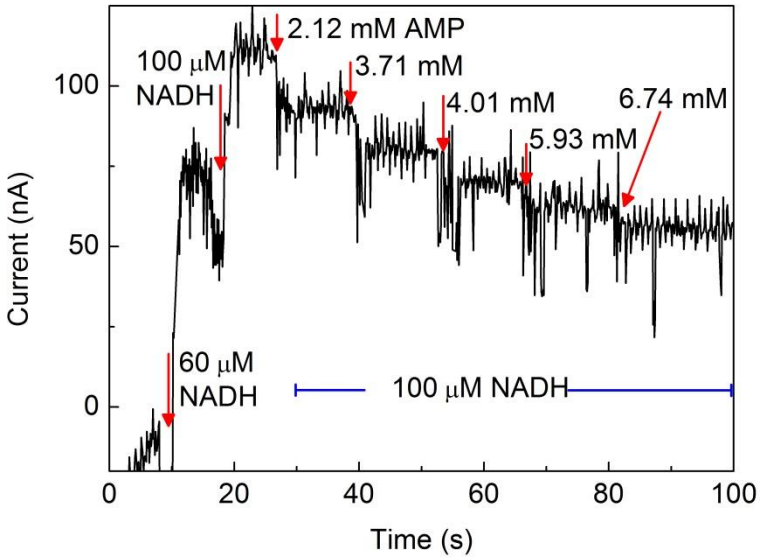

Figure 84. Chronoamperometry experiment designed to determine the inhibition constant for AMP. The experiment was performed at -0.062 V with no substrate present at the beginning of the experiment. Injection of 60 µM NADH was made at around 9 seconds and used as a control step for subsequent experiments. A further injection of NADH, bringing the total cell concentration to 100 µM, was performed at 18 seconds and aliquots of AMP containing 100 µM

NADH were injected into the cell solution at concentrations indicated. Conditions: Tris-HCl buffer 50 mM, 30 ^{o}C and rotation rate 2500 rpm.

Raw data from a set of similar experiments were analysed using the established method as described in Section 4.1.1. Figure 85 shows Dixon (panel A) and Cornish-Bowden (panel B) plots constructed at different NADH concentrations.

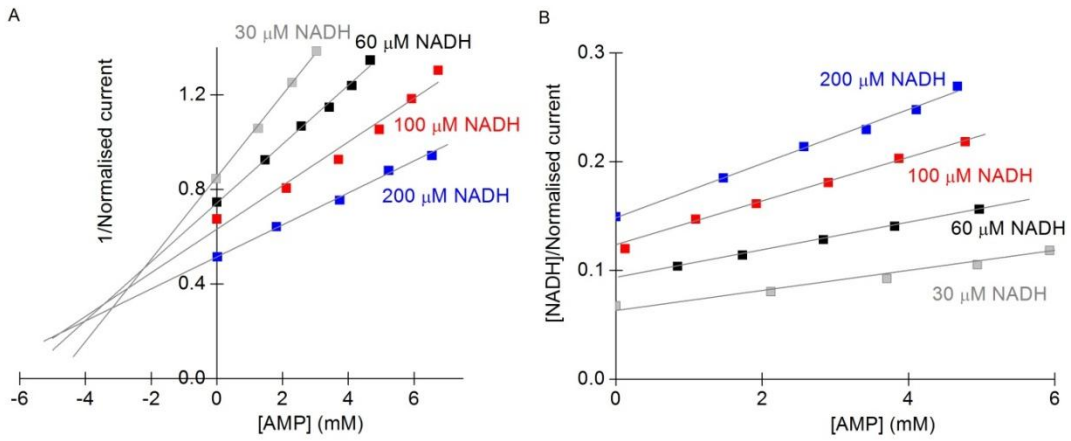

Figure 85. Typical plots of 1/normalised current against AMP (Panel A) and [NADH]/normalised current against AMP (Panel B); both were constructed at different NADH concentrations.

The Dixon plot intersects in the range of -1 to -5 suggesting a K_I value in the range of 1 to 5 mM AMP. This value is two times smaller than the value obtained for AMP inhibition of Complex I. The inhibition is also likely to be a competitive as shown by the Cornish-Bowden plot.

4.2.3 Adenosine Triphosphate (ATP)

Adenosine triphosphate (ATP) is an important high energy molecule, and its hydrolysis is used to release energy necessary for cellular functions. ATP is recycled from the energy generated during food oxidation and according to Karp, more than 2 x 10^{26} molecules of ATP (equivalent to 16 kg) are formed in the human body daily.[211] A Nobel Prize in Chemistry was awarded to three scientists in 1997 for their discovery

of ATPase and elucidation of the enzymatic mechanism underlying the synthesis of ATP. An ATP molecule consists of three components: a ribose in the middle, with adenine and a string of phosphate groups attached to opposite sides. Figure 86 shows a comparison between the structure of NADH and ATP.

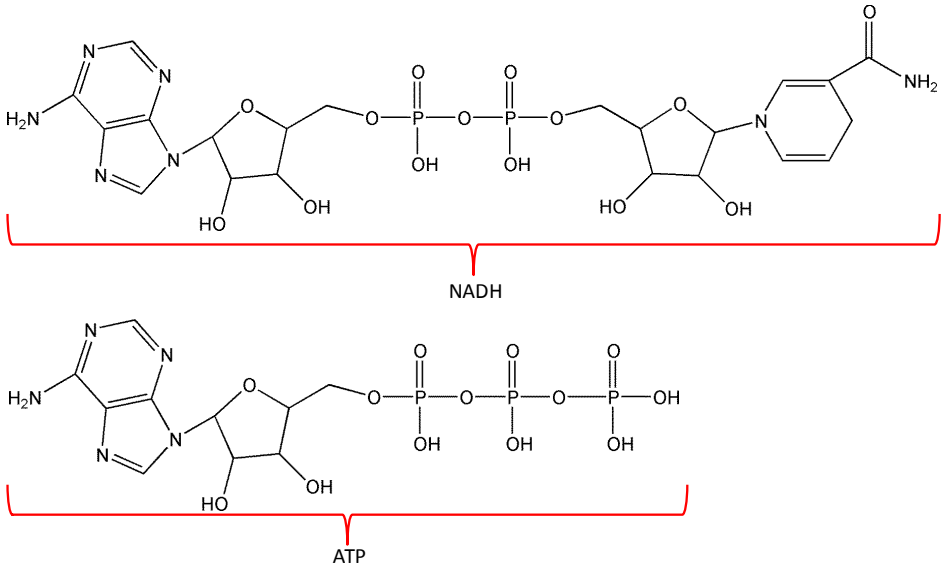

Figure 86. Comparison between the structures of NADH and ATP.

An electrochemical technique explained in Section 4.1.1 was employed to check for ATP inhibition of HoxFU and a typical current against time plot is shown in Figure 87. Upon injection of 4.41 mM ATP containing 200 µM NADH at 28 seconds, a clear decrease in the catalytic current due to ATP inhibition was recorded.

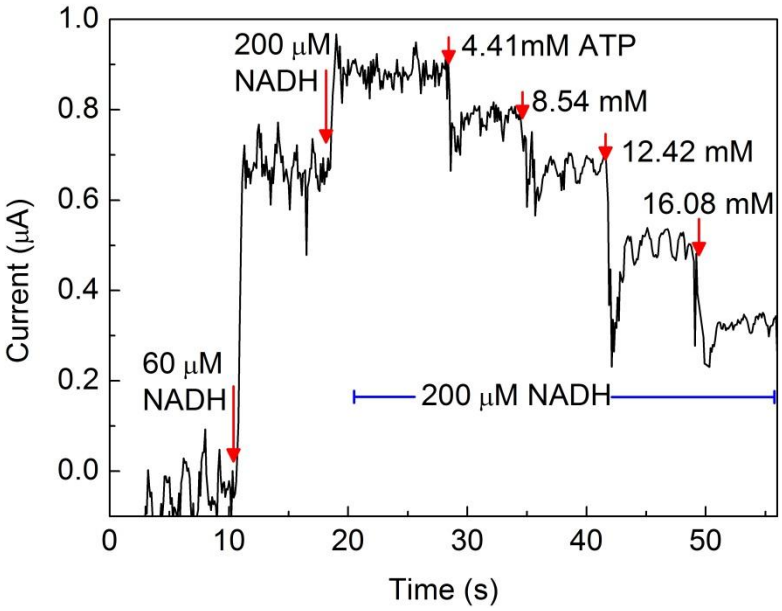

Figure 87. A typical result from an experiment designed to determine the K_I for the inhibition of NADH oxidation by ATP. The experiment was performed at -0.062 V with no substrate present at the beginning of the experiment. Injection of 60 μM NADH was made at around 10 seconds and used as a control step for subsequent experiments. A further injection of NADH bringing the total cell concentration to 200 μM was performed at 18 seconds and aliquots of ATP containing 200 μM NADH were injected into the cell solution at concentrations as indicated. Conditions: Tris-HCl buffer 50 mM, 30 ^{o}C and rotation rate 2500 rpm.

The experiment shown in Figure 87 was repeated at several different NADH concentrations and the data were analysed according to methods described in Section 4.1.1. Figure 88 shows Dixon and Cornish-Bowden plots obtained from several experiments.

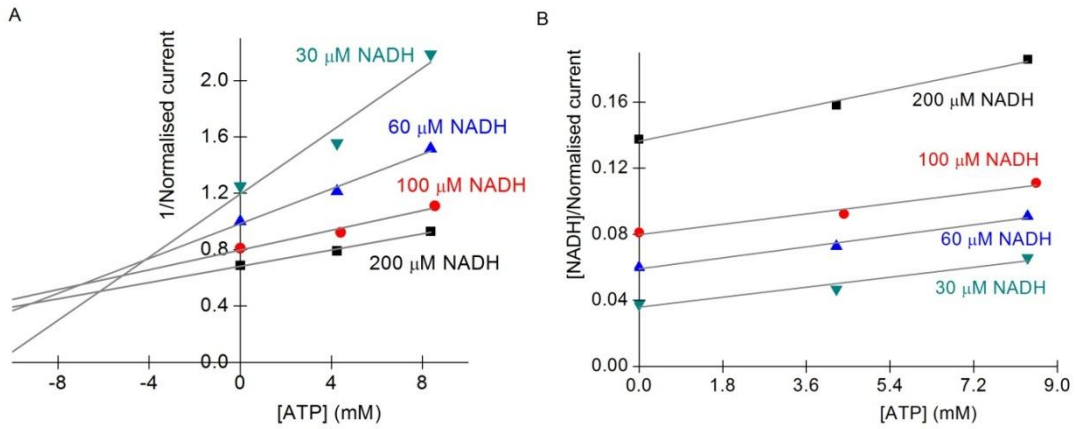

Figure 88. Typical plots of 1/normalised current against [ATP] (Panel A) and [NADH]/normalised current against [ATP] (Panel B); both were constructed at different NADH concentrations.

The lines in panel A intersect in the region of -4 to -9, suggesting a K_I value in the range of 4 to 9 mM, and inhibition is again competitive. This value is almost comparable to the inhibition constant calculated for Complex I (10^{-2} M range).[210]

4.2.4 Adenosine Diphospho-Ribose (ADP-Ribose)

Figure 89 shows a structural comparison between a molecule of NADH and ADP-Ribose indicating that these two pyridine nucleotides are very similar to each other: differing only by the presence of a nicotinamide group replacing the hydroxyl group of ADP-Ribose. Competitive inhibition of Complex I NADH oxidation by ADP-Ribose was reported by Vinogradov and coworkers in 1997.[209] They reported K_I values of 26 μM, 30 μM and 180 μM for bovine heart submitochondrial particles (SMP), purified Complex I and three-subunit NADH dehydrogenase (FP), respectively. The low K_I values indicate that ADP-Ribose is a strong inhibitor for NADH oxidation and ADP-Ribose may be competing at the same binding site as NADH.

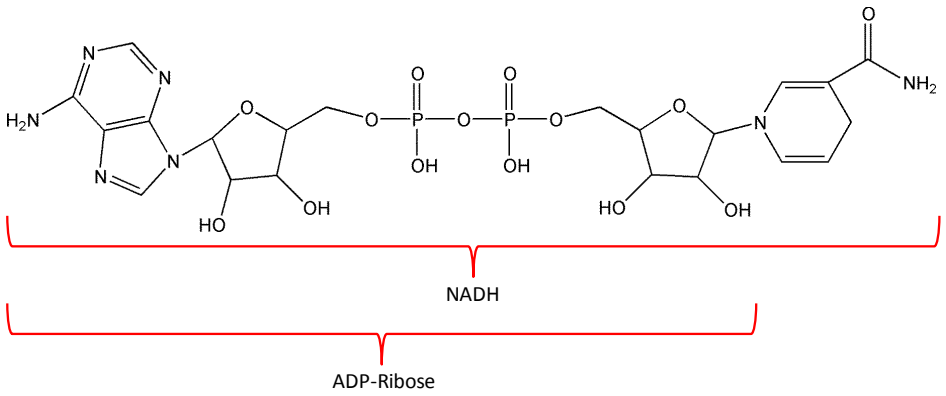

Figure 89. A structure of NADH and its comparison to the ADP-Ribose structure.

Chronoamperometry experiments based on the strategy discussed in Section 4.1.1 were employed to check for inhibition of NADH oxidation by HoxFU by ADP-Ribose and a typical current against time plot is shown in Figure 90.

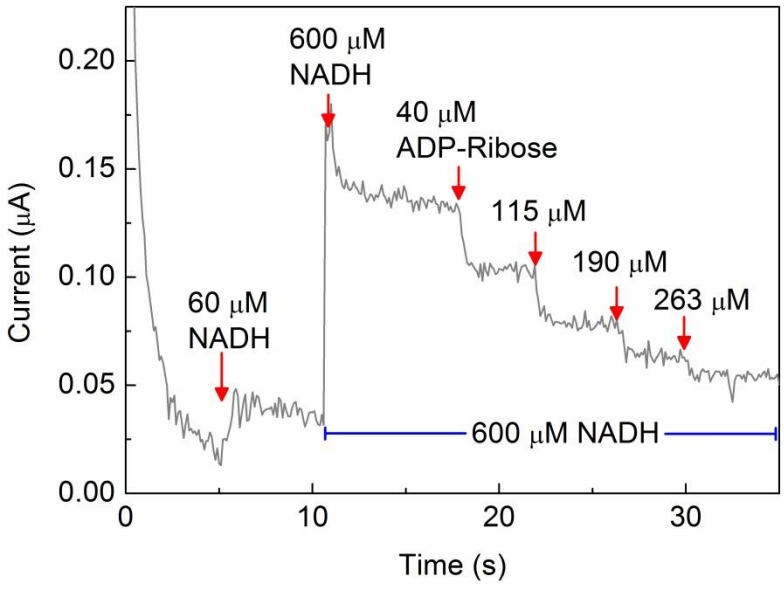

Figure 90. A typical result from an experiment designed to determine the K_I for the inhibition of NADH oxidation by ADP-Ribose. The experiment was performed at -0.062 V with no substrate present at the beginning of the experiment. Injection of 60 μM NADH was made at around 5 seconds and used as a control step for subsequent experiments. A further injection of NADH bringing the total cell concentration to 600 μM was performed at 11 seconds and aliquots of ADP-Ribose containing 600 μM NADH were injected into the cell solution at concentrations as indicated. Conditions: Tris-HCl buffer 50 mM, 30 ^{o}C and rotation rate 2500 rpm.

The data were then analysed in the form of Dixon plot according to the procedures described in Section 4.1.1.

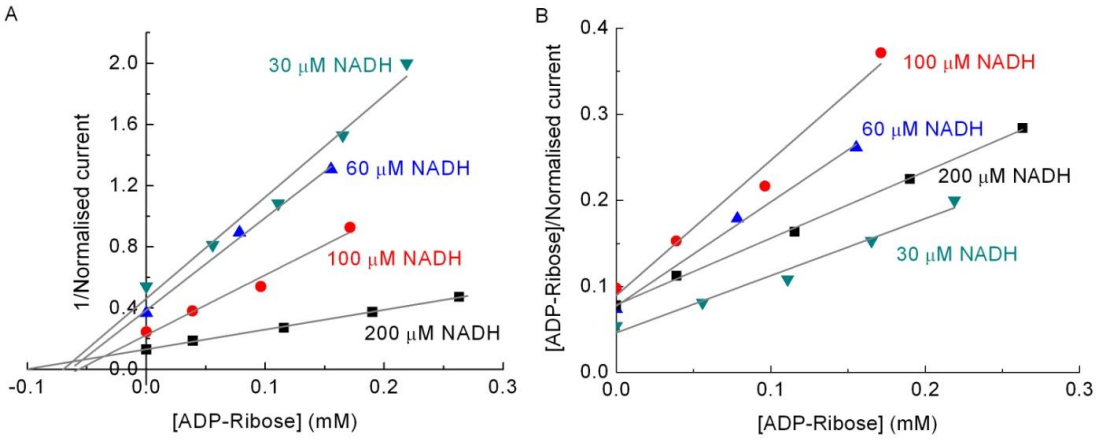

Figure 91. Typical plots of 1/normalised current against [ADP-Ribose] (Panel A) and [NADH]/normalised current against [ADP-Ribose] (Panel B); both were constructed at different NADH concentrations.

These experiments clearly show that ADP-Ribose inhibits HoxFU NADH oxidation with a low K_I value (0.02 to 0.1 mM) that is comparable to NADH oxidation inhibition in Complex I (0.03 to 0.18 mM).[209] The low K_I also indicates that the HoxFU binding site has a high affinity for ADP-Ribose. Kinetic data for Complex I was interpreted in terms of purely competitive inhibition of NADH oxidation by ADP-Ribose consistent with the structural similarity between NADH and ADP-Ribose. The Cornish-Bowden plot for HoxFU does not give a clear set of parallel lines suggesting the mechanism could be more complex, although the low catalytic activity of the HoxFU samples used for this set of experiment makes confident interpreting the results difficult.

In Complex I, there is no evidence for inhibition of NAD^+ reduction by ADP-Ribose, and it has been reported that ADP-Ribose in fact stimulates NAD^+ reduction.[209] This has prompted a hypothesis as to the presence of another binding site in Complex I and that only the NADH-specific binding site is sensitive towards ADP-Ribose. However, as argued by Ulrich Brandt, the resolved crystal structure of *T. thermophilus* Complex I shows a linear arrangement of the FeS clusters and the FMN

catalytic centre making it unlikely that there is a need for a second NADH binding site.[81] In the case of HoxFU, preliminary experiments have shown that ADP-Ribose inhibits NAD^+ reduction and this type of inhibition will be used as a test system in confirming the ability of HoxFU to sustain its catalytic activity in the presence of O_2 later in this Chapter.

4.2.5 5,5'-dithiobis-(2-nitrobenzoic acid) (DTNB)

Complex I acts as an entry point for reducing equivalents to the respiratory chain and as an energy transducing device. Its position in the metabolic network requires the enzyme activity to be finely regulated according to its surroundings. Under physiological conditions, it has been shown that Complex I undergoes slow reversible interconversion between inactive and active states.[208] The inactive form of Complex I has been reported to be susceptible to alkylation, and DTNB has been shown to inhibit Complex I.[208] Figure 92 shows the structure of a molecule of DTNB, which can add to sulfhydryl groups present in cysteine residues surrounding the active site, thus blocking substrate access to the enzyme catalytic centre. The equation for the reaction between DTNB and free sulfhydryl groups provided by cysteine residues in or surrounding the active site is shown in Figure 92.

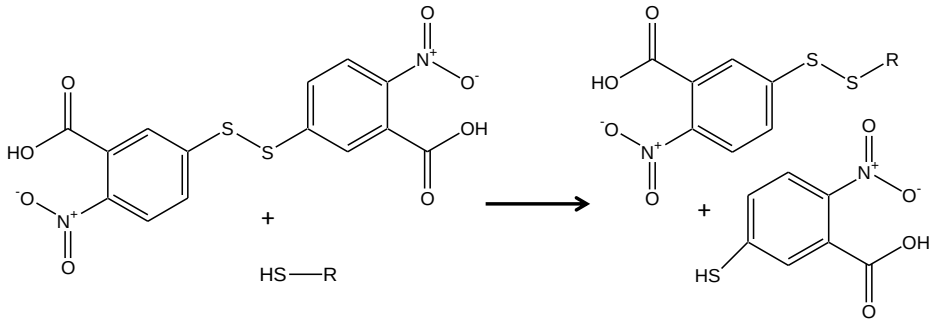

Figure 92. DTNB reaction with sulfhydryl group.

Experimental procedures as described in Section 4.1.1 were employed to check for DTNB inhibition of HoxFU NADH oxidation. A typical current against time plot is shown in Figure 93. No catalytic current was recorded at the beginning of the experiment as there was no NADH present. More NADH was introduced into the cell and at approximately 30 seconds, 0.85 mM DTNB containing 200 µM NADH was injected into the cell, bringing a decrease in the NADH oxidation current. This confirms that DTNB inhibits HoxFU NADH oxidation reaction.

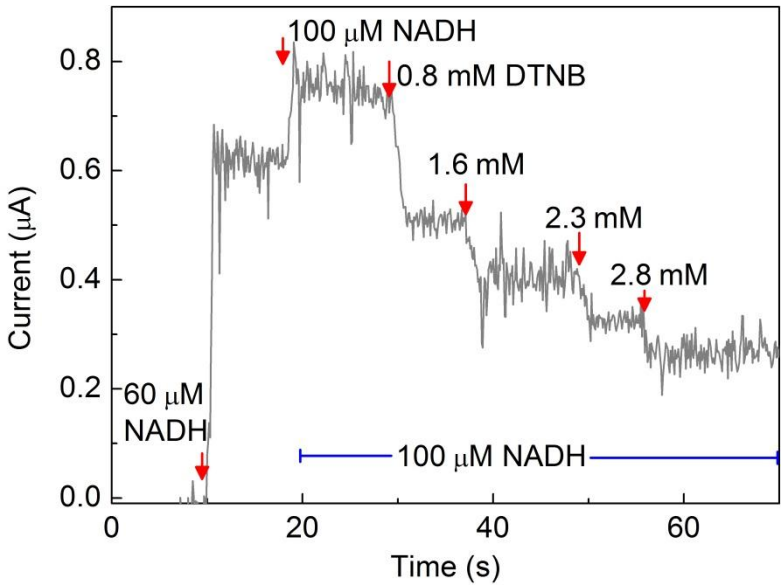

Figure 93. Chronoamperometry experiment designed to check for inhibition by DTNB. The stepwise increase in NADH concentration is labelled in blue, whilst the stepwise increase in DTNB concentration is labelled in purple, the concentration of substrate/inhibitor is given at each step. The modified working electrode was held at -0.062 V vs SHE and the experiment was performed at pH 8 in Tris buffer at 30 °C. The working electrode was rotated at 2500 rpm.

Inhibition by DTNB has also been reported for several other redox enzymes such as NADH-glutamate and lecithin-cholesterol acyltransferase.[212, 213] A variant of lecithin-cholesterol acyltransferase, which had its cysteine residues mutated out, was shown not to be significantly inhibited by DTNB. Inhibition by DTNB in the SH, by modification of sulfhydryl groups, should be irreversible, as reported in the case of Complex I.

4.2.6 General discussion on the inhibition of HoxFU by Complex I inhibitors

This Section discusses the inhibition results obtained for inhibition of HoxFU NADH oxidation by several Complex I inhibitors. Electrochemical results shown in this Chapter indicate that ADP, AMP, ATP and ADP-Ribose are able to inhibit NADH oxidation by HoxFU. The electrochemical inhibition constants calculated for ADP, AMP, ATP and ADP-Ribose are all comparable to those for Complex I (Table 4-1). In particular, the K_I value for ADP-Ribose of HoxFU is in the range of μM, very close to the K_M value for NADH, suggesting a strong competition between the inhibitor and substrate (in this case NADH) to the same binding site, as for Complex I. These results confirm the functional as well as structural similarity between HoxFU and Complex I diaphorase domain.

Table 4-1. Inhibition constants for the HoxFU diaphorase and Complex I.

Inhibitor	K_I (mM)		Ref
	HoxFU	Complex I	
ADP	1 to 3	~10	[210]
AMP	1 to 5	~10	[210]
ATP	4 to 9	~10	[210]
ADP-ribose	0.02 to 0.1	0.03 to 0.18	[209]

The much higher K_I values found for ADP, AMP and ATP compared with ADP-ribose indicate that at low concentrations of these species, a minimal inhibition for HoxFU NADH oxidation reaction would be observed. In contrast, a small concentration of ADP-Ribose would give a significant effect on HoxFU catalytic activity.

DTNB was also found to inhibit NADH oxidation by HoxFU. Figure 94 shows the position of cysteine residues in the HoxFU moiety. As discussed before, a DTNB

molecule may add to one of the free cysteine residues positioned close to the NADH binding site and block the substrate access to the active site, thus irreversibly inhibiting NADH oxidation. Alternatively, the ability of DTNB to add to the cysteine residues (Figure 94) may also change the enzyme surface charge thus making the enzyme undergo a conformational change and become catalytically inactive.

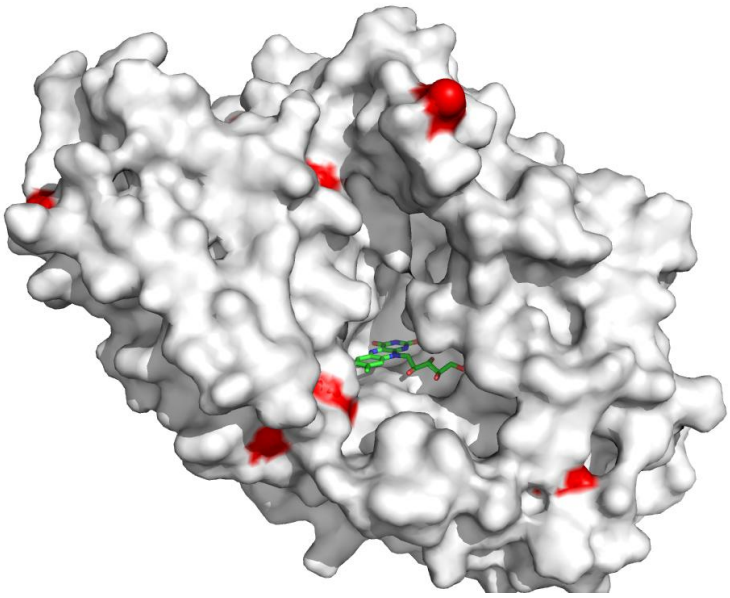

Figure 94. Surface representation of HoxFU moiety showing FMN catalytic centre in stick form and free cysteine residues in red. The picture was produced based on a homology model of HoxFU constructed using amino acid residues of HoxFU subunits by Lars Lauterbach.

Nucleotide triphosphate species like ATP are used extensively as cofactors in many enzyme-catalysed phosphoryl transfer reactions, *i.e.* involving the formation or cleavage of P-O bonds. These enzyme catalysed reactions are exploited in organic synthesis as an alternative to multi-step chemical phosphorylations.[214] The ability to investigate inhibition properties of these species for the HoxFU diaphorase moiety is thus significant in order to evaluate HoxFU's versatility as a redox component of industrial biosynthetic processes. Based on the electrochemical results, it is unlikely that Complex I inhibitors would cause problems should HoxFU is to be used in industrial processes, as the K_I values are quite high.

4.3 HoxFU turnover in the presence of O_2

Ralstonia eutropha is one of the facultative chemolithoautotrophic microbes (Knallgas bacteria) which have adapted such that their H_2-oxidising systems can survive continuous exposure to O_2.[13] The SH of *R. eutropha* for example couples H_2 oxidation to NAD^+ reduction in aerobic conditions.[215] The enzyme, under standard lithoautotrophic conditions, was grown in a mixture of 80 % H_2, 10 % O_2 and 10 % CO_2. Friedrich and coworkers showed that increasing the O_2 concentration to 15 % did not affect the growth of the SH.[215] An earlier report by Hall and coworkers also indicated that at an O_2 concentration of 0.7 mM (equivalent to 60 % O_2 partial pressure), only 17-19 % of the SH H_2:NAD^+ activity was diminished.[216]

The SH has therefore attracted interest for its ability to sustain cofactor regeneration[101, 103, 217-219] driven by H_2 in the presence of O_2 and this Section will investigate the effect of O_2 on HoxFU catalytic activity. Electrochemical experiments performed by Juan Liu have shown that the hydrogenase moiety of the SH, HoxHY is not completely tolerant to O_2, but is sufficiently tolerant at low potentials to be able to oxidise H_2 at redox potentials imposed by NAD^+/NADH pool.[77]

4.3.1 NADH oxidation

Figure 95 shows a typical experiment designed to examine the capability of HoxFU to oxidise NADH in the presence of O_2. A HoxFU modified electrode was placed in an electrochemical cell solution containing 2 mM purified NADH. The electrode was poised at +0.243 V to drive NADH oxidation while avoiding direct O_2 reduction at the graphite electrode. At the beginning of the experiment, positive current was recorded corresponding to NADH oxidation by HoxFU. At approximately

25 seconds, an aliquot of O_2 saturated buffer containing 2 mM purified NADH was injected into the cell solution. No decrease in current was observed upon the injection indicating that NADH oxidation is not affected by the presence of 0.33 mM O_2.

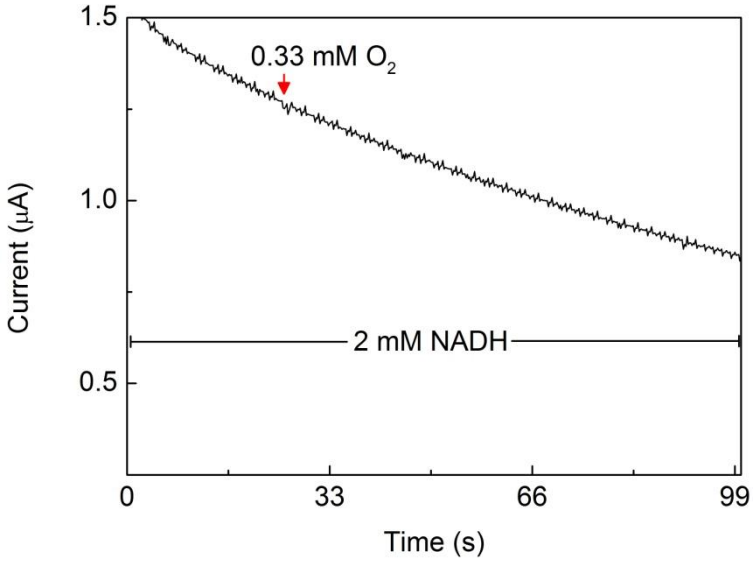

Figure 95. Does O_2 affect NADH oxidation? This experiment was performed in Tris-HCl buffer 50 mM, pH 8.0 at 30 ^{o}C. The HoxFU modified electrode was held at +0.243 V, rotated at 2500 rpm and placed in a solution of 2 mM NADH. At approximately 25 s, an aliquot of O_2 saturated buffer containing 2 mM NADH was injected into the electrochemical cell to give a final O_2 concentration of 0.33 mM.

4.3.2 NAD^+ reduction

Experiments were then designed to explore the ability of HoxFU to sustain NAD^+ reduction in the presence of O_2 by utilising substrate concentration and potential dependent inactivation as a marker for HoxFU electrocatalytic activity. Electrochemical experiments in this region are complicated as O_2 is directly reduced at the graphite electrode. The electrode was placed in solution containing 25 μM NAD^+ and rotated throughout the experimental period to help flush out O_2 from the electrochemical solution into the headgas stream of N_2, following an injection of O_2.

The black thick line in Figure 96 shows a cyclic voltammogram for a HoxFU modified electrode without any O_2 injection, with low potential inactivation observed at

this low NAD^+ concentration as expected. In the case of an unmodified electrode (blue line), injection of O_2 saturated buffer containing 25 µM NAD^+ to give a final concentration of 2 µM lead to an increase in current magnitude corresponding to direct O_2 reduction by graphite. However, the current diminished soon after the injection because O_2 is being removed from the solution by the rotating electrode and N_2 stream. The red line in Figure 96 shows a scan for a HoxFU modified electrode with an O_2 injection (to give the same O_2 concentration as for the control blue line). At the beginning of the scan, no catalytic current was recorded and the current resembles that of an unmodified electrode. At approximately -0.25 V, an increase in reduction current was observed as HoxFU starts reducing NAD^+, and at -0.3 V, an aliquot of O_2 saturated buffer containing 25 µM NAD^+ was injected into the cell solution (to a final O_2 concentration 2 µM) giving a substantial rise in the current magnitude. The current observed now arises from both NAD^+ reduction catalysed by HoxFU and from O_2 reduction at the graphite electrode. As the electrode was rotated during the course of experiment, O_2 is constantly removed from the cell solution therefore the catalytic wave shape slowly returns to the level expected for the enzyme film under anaerobic conditions. The presence of the inactivation feature in the voltammogram acts as a marker confirming that HoxFU must stay active in the presence of O_2. Furthermore, the subtracted grey trace is similar in shape to the black line, indicating that characteristic shape of the HoxFU electrocatalytic wave is retained in the presence of O_2.

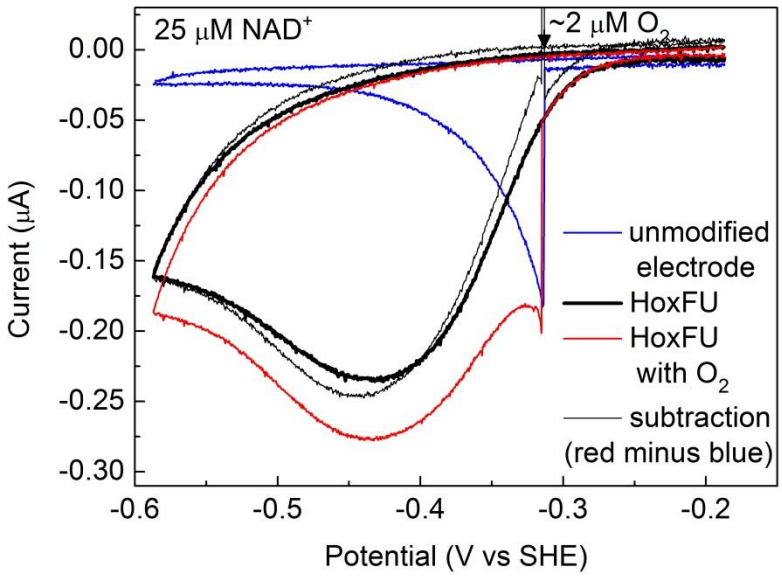

Figure 96. Experiments designed to probe the ability of HoxFU to reduce NAD^+ in the presence of O_2. A series of cyclic voltammetric experiments recorded at a scan rate of 1 mV/s with the electrode rotated at 2500 rpm in a solution of 50 mM Tris-HCl pH 8.0 containing 25 μM NAD^+. The solid black line shows the response for a HoxFU film as the potential is swept from -0.2 V to -0.6 V and back to -0.2 V. The blue line shows the response for an unmodified electrode, with O_2 introduced into the solution during the forward scan as indicated. The red line shows the response when the same amount of O_2 is introduced during a potential cycle for an electrode modified with a fresh film of HoxFU (normalised to the current magnitude of the black forward trace at -0.3 V).

Further experiments to confirm the ability of HoxFU to work in the presence of O_2 were carried out by employing an inhibitor for the enzyme in a similar technique to that previously reported by Armstrong and coworkers for experiments on MBH enzymes from *R. metallidurans* and *R. eutropha*.[167] They utilised the fact that H_2 acts as a potent product inhibitor to validate the H^+ reduction ability of both MBH enzymes in the presence of O_2. Their experiments were performed by holding the electrode potential at -0.45 V in a solution containing 100 % N_2 at which substantial H_2 formation by the MBH is observed. Hydrogen gas (5 %) was then introduced into the cell solution and a decrease in the catalytic current was recorded due to product inhibition. The inhibitor was flushed out from the electrochemical cell by flowing N_2 through the headspace and a recovery from the enzyme inhibition was observed. Introduction of 2 % O_2 gave rise to a significant reduction current due to non-enzymatic O_2 reduction on the

bare regions of the graphite electrode, but a rapid loss of catalytic current was still recorded upon introduction of 5 % H_2 while maintaining the 2 % O_2 in the system. The decrease in the current observed was found to be of the same magnitude as that of an experiment in which 5 % H_2 was introduced under anaerobic conditions. Removal of H_2 and O_2 gases from the headgas by replacing them with N_2 restored anaerobic conditions, and a clear H^+ reduction was observed. Further introduction of 5 % H_2 again led to a decrease in the reduction current confirming that during the whole process, *R. metallidurans* and *R. eutropha* MBH enzymes are able to sustain their catalytic activity in the presence of O_2.

In the case of HoxFU, it has been shown in Section 4.2.4 that the electrocatalytic activity is inhibited by ADP-Ribose. The ADP-Ribose shares structure similarity with NADH: differing only by the presence of a hydroxyl group, which replaces the nicotinamide of NADH. Therefore it has been chosen as a marker to confirm the ability of HoxFU to sustain its NAD^+ reduction activity in the presence of O_2.

A chronoamperometry experiment in which a HoxFU modified electrode was placed in an electrochemical cell containing 0.14 mM NAD^+ is shown in Figure 97. This concentration of NAD^+ is just below the reported K_M value of HoxFU and was chosen in order to get a distinctive reduction activity by HoxFU. The experiment was performed by holding the electrode potential at -0.412 V, chosen as it is sufficient to drive NAD^+ reduction but does not lead to significant low potential inactivation of HoxFU. At the beginning of the experiment, reductive current corresponding to NAD^+ reduction catalysed by HoxFU was observed. Two aliquots of ADP-Ribose were injected into the cell solution during the experiment and these led to a decrease in the current magnitude confirming that ADP-Ribose inhibits the NAD^+ reduction activity of HoxFU under these conditions. In Panel B, an unmodified electrode was placed in a solution of

0.14 mM NAD^+ and at approximately 10 seconds, O_2 saturated buffer containing a similar NAD^+ concentration was introduced to the cell solution (to give a final O_2 concentration of 0.33 mM). An increase in current magnitude was recorded due to direct O_2 reduction on the graphite electrode. No decrease in current was observed upon multiple injection of ADP-Ribose into the cell solution. However, in panel C, for a HoxFU modified electrode, after exposure to O_2, a decrease in current was recorded upon introduction of ADP-Ribose into the cell confirming that the negative current must, in part, be due to NAD^+ reduction by active HoxFU in the presence of O_2 *i.e.* HoxFU remains catalytically active in the presence of O_2.

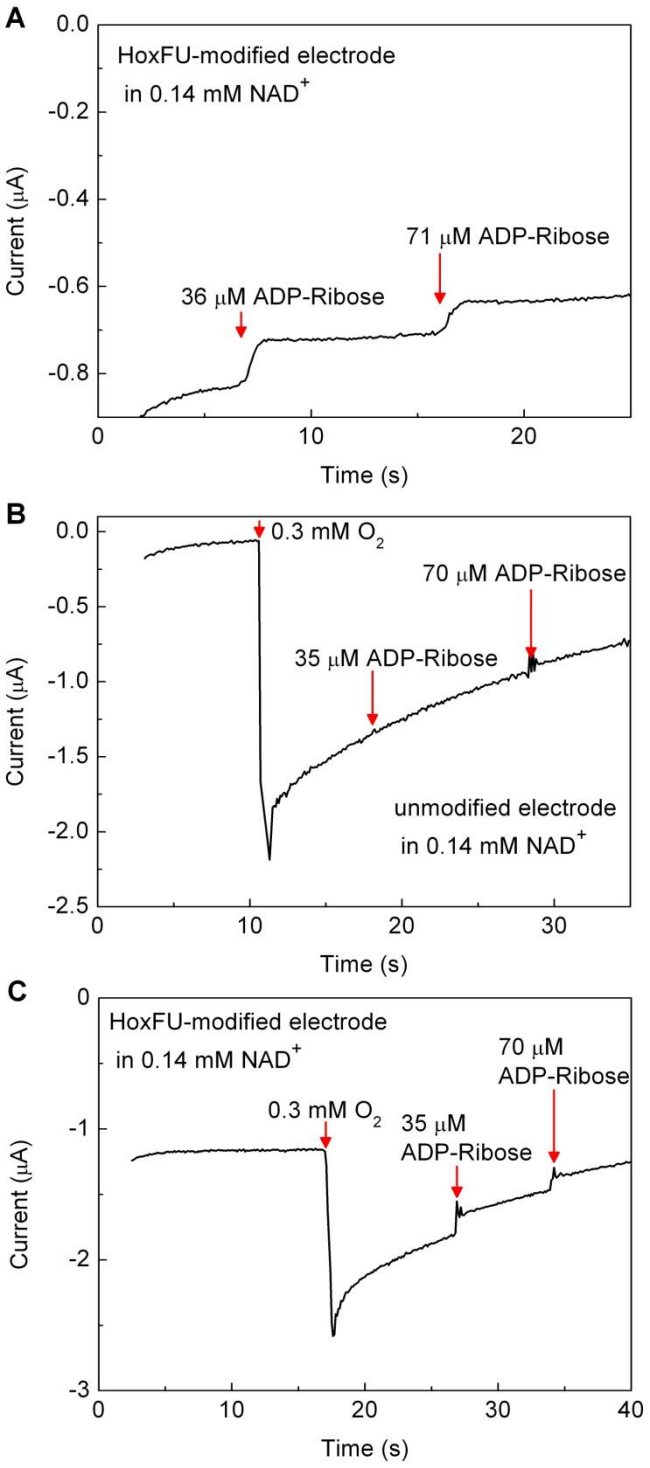

Figure 97. Experiments designed to confirm that HoxFU remains active in the presence of O_2 using an inhibition method established by Armstrong and coworkers. In all experiments the electrode was poised at -0.412 V in 0.14 mM NAD^+, pH 8.0 Tris-HCl buffer, 50 mM. ADP-Ribose was used without further purification. Panel A shows the effect of injections of ADP-Ribose on NAD^+ reduction by HoxFU, confirming that ADP-ribose is an inhibitor. Panel B shows O_2 reduction by an unmodified electrode following injection of O_2, and confirms that injections of ADP-Ribose do not affect the O_2 reduction current on the bare electrode. Panel C shows an analogous experiment on a film of HoxFU, showing that injections of ADP-Ribose now cause a drop in current magnitude, confirming that HoxFU must remain active in the

presence of O_2, with electrocatalytic NAD^+ reduction current contributing to the total negative current.

As discussed in Chapter 1, there are several hydrogenases that remain catalytically active in the presence of O_2 such as *R. eutropha* MBH, Hyd1 of *E. coli* and *A. aeolicus*, and very recently Hyd5 of *Salmonella* has been added to this list.[119, 132, 133, 166, 167] Electrochemical experiments performed on the hydrogenase moiety of the SH, HoxHY showed that it is susceptible for O_2 attack and inactivated in the presence of O_2.[77, 220] The diaphorase moiety of HoxFU is clearly able to sustain catalysis in either direction in the presence of O_2, which would support activity in air, and also reverse electron transfer to the HoxHY moiety under aerobic conditions to re-activate inactive hydrogenase.

4.3.3 Discussion: Observations of Superoxide ($O_2^{\cdot-}$) production in solution assays of HoxFU

Schneider and Schlegel have shown that the SH generates a substantial amount of superoxide free radical anion.[221] They utilised hydroxylamine as a trapping agent for the produced superoxide because it did not influence SH catalytic activity nor react with the SH. In the presence of superoxide, hydroxylamine is oxidised to nitrite and the product can then be detected spectroscopically by addition of α-naphthylamine and sulphanilic acid into the mixture, and measured the UV absorbance at 530 nm .[222]

Recent biochemical experiments performed by Lauterbach showed that HoxFU produces 53.5 nmol of superoxide per mg per min which corresponds to 5.9 per min turnover rate at 21 % O_2.[94] In a fully O_2-saturated solution, the superoxide production increased by eight to nine fold. The high turnover rate of superoxide by HoxFU,

compared to that of the whole SH (0.5 per min) thus indicates that the diaphorase moiety is the main source for superoxide production in the SH.

Superoxide production has also been reported for bovine Complex I with a turnover rate of 40 min^{-1}.[223] In Complex I, the presence of an extra 2Fe2S cluster (N1a) close to the FMN catalytic centre is believed to diminish the production of superoxide by accepting electrons from the reduced FMN.[224, 225] This extra cluster, however, is not conserved in the SH and may be the cause of the high superoxide production.

The high superoxide production by the HoxFU moiety compared to the whole SH can be explained as follows: in the intact SH, a full electron transfer chain and the ready availability of H^+ is likely to support rapid electron transfer from the flavin to the NiFe active site thus preventing rapid superoxide production. In PFE experiments, the electrode acts as a sink for rapid removal of electron from the reduced FMN, making superoxide reduction less likely. Furthermore, the rate of superoxide formation is much lower than that of NAD^+ reduction, meaning it is likely to be undetectable in PFE.

4.4 Final summary of HoxFU inhibition implications for SH catalysis

Chapters 3 and 4 of this Thesis show how electrochemistry can be utilised as a tool for studying part of a complex enzyme. The Soluble Hydrogenase, which comprises six subunits has been successfully isolated and purified by protein engineering techniques into two different functional catalytic moieties which make it easier for a comprehensive electrochemical characterisation. The diaphorase subcomplex, HoxFU subunits, exhibits reversible NADH oxidation and NAD^+ reduction on a pyrolytic graphite electrode. In biochemical experiments, the HoxFU subcomplex has also been shown to be catalytically active transferring electrons from NADH

oxidation to benzyl viologen. Chapters 3 and 4 of this Thesis examined the electrocatalytic properties of the diaphorase subcomplex alongside its substrate affinities, product inhibition, effects of other inhibitors and its ability to function in the presence of O_2. The electrochemical results are now interpreted alongside biochemical assays, the known physiological role of the SH and its relationship to Complex I.

4.4.1 Direction of catalysis and possible control mechanisms

No crystal structure is yet available for the SH but a high resolution crystal structure of hydrophilic domain of *T. thermophilus* Complex I shows that during catalysis, NADH is stacked very close to the FMN in subunit Nqo1 in a position favourable for a direct hydride transfer from NADH to FMN (the distance between FMN catalytic centre and the NADH is found to be approximately 3.2 Å).[29, 34] As mentioned earlier in this Thesis, HoxF of the SH shares 30 % sequence identity with Nqo1 of *T. thermophilus* Complex I while HoxU shares 23 % sequence identity with Nqo3. Based on amino acid sequence analysis and a homology model constructed between subunits Nqo1 and HoxF, it is very likely that NADH oxidation in the SH proceeds via hydride transfer to oxidised FMN. Thus, with its FeS clusters, HoxFU on an electrode is able to convert hydride transfer to electron transfer.

The normal direction of catalysis when the SH is expressed under aerobic conditions is NAD^+ reduction assisted by H_2 oxidation.[13] The majority of the NADH produced by *R. eutropha* will then be used by its Complex I to establish a proton motive force while some will be converted to NADPH by transhydrogenases for anabolic metabolism.[226] Schlegel and coworkers suggested that the SH may also act as an electron valve by working in the reverse direction (NADH oxidation coupled to H^+ reduction) when the NADH/NAD^+ pool has become too reduced.[191] This reaction is

probably important in balancing the NADH/NAD^+ pool especially when *R. eutropha* is shifted from aerobic to anaerobic growth conditions.[13, 191] Operation in the reverse direction (NAD^+ reduction coupled to quinol oxidation) has also been suggested in the case of Complex I under certain conditions.[80] Furthermore, electrochemical experiments performed by Juan Liu have shown that the NiFe active site of the SH requires low potential electrons for re-activation, making the ability of the SH to channel electrons from NADH oxidation to the NiFe active site important in re-activating the oxidised states of the NiFe centre.[77]

The affinity constant for NADH oxidation agrees closely with results from biochemical assays: a K_M of 58 ± 18 µM was calculated using electrochemistry compared to 56 µM calculated from assays utilising Benzyl Viologen (BV) as an electron acceptor. This suggests that HoxFU does not suffer any major structural change upon adsorption onto the electrode. The value of $K_M^{\text{NADH oxidation}}$ determined for HoxFU was also found to be of a similar magnitude to that of bovine Complex I.[199] This suggests that the SH would be capable of functioning in the NADH oxidation direction under certain physiological conditions. However, assuming that the ratio of NAD^+/NADH in *R. eutropha* under aerobic conditions is 10:1, as determined previously for *E. coli*,[195] and taking into account high product inhibition observed, significant NADH oxidation by the SH is rather unlikely.

The diaphorase moiety also shows a clear NAD^+ reduction catalytic activity with a calculated affinity constant (K_M) of 197 ± 28 µM. This value is approximately 2.5 times lower than the value obtained earlier for the intact SH (500 µM)[21] but significantly higher compared to the value calculated for bovine Complex I (7 µM).[227] The affinity constants calculated for NADH oxidation and NAD^+ reduction, together with product inhibitions observed may serve as control mechanisms to balance these

reactions. For example, the low affinity of the SH for NAD^+ and product inhibition observed for this reaction would slow the rate of H_2 oxidation coupled to NAD^+ reduction activity, perhaps assisting NADH oxidation under conditions when the NADH/NAD^+ pool has become too reduced by hindering the back reaction.

Electrochemical experiments also confirm that HoxFU catalyses NADH oxidation and NAD^+ reduction efficiently with a minimal overpotential *i.e.* close to the predicted $E(NAD^+/NADH)$. The ability of HoxFU to work efficiently is important because $E(H^+/H_2)$ is closely spaced to $E(NAD^+/NADH)$ thus leaving a minimal driving force for either reaction. Voltammetric experiments performed over a range of NAD^+/NADH ratios show that catalysis is most active in the NAD^+ direction despite the $K_M^{\text{NAD+ reduction}}$ being higher than $K_M^{\text{NADH oxidation}}$. Although the value of the catalytic constant, k_{cat} is unknown due to the inability to determine the enzyme electroactive coverage on the electrode, the catalytic constant must be higher for NAD^+ reduction relative to NADH oxidation in order for the observed current magnitude to be higher for NAD^+ reduction. Furthermore, continual consumption of NADH produced by SH by Complex I or transhydrogenases in *R. eutropha* will keep the NADH/NAD^+ pool relatively oxidised. These electrochemical results, alongside biochemical findings, suggest that the diaphorase moiety of the SH is finely tuned to balance the NADH/NAD^+ ratio within tight limits.

4.4.2 Potential-dependent effects on activity and FMN release

Hirst and coworkers showed that NAD^+ reduction by a subcomplex of Complex I from bovine heart mitochondria undergoes a reversible inactivation at low potentials.[184] The low potential inactivation occurs at potentials close to that of the FMN centre and as such Hirst proposed two models to explain the observations. The

first model described the effect of the reduced proximal 2Fe2S cluster, while the second model explored the effect of enhanced catalytic ability of the flavin centre. These two models both gave simulated voltammograms consistent with the experimental data. Based on the simulation and experimental data, they suggested that the reversible potential-dependent inactivation observed could have a physiological role in hindering the reverse electron transfer reaction (quinol oxidation coupled to NAD^+ reduction).

In the case of HoxFU, experiments performed at a slow scan rate of 1 mV/s did not show any obvious low potential inactivation at NAD^+ concentrations above the $K_M^{NAD+\ reduction}$ value. However, HoxFU shows irreversible low potential inactivation at NAD^+ concentrations below the K_M value. This observation is very likely due to reductive damage to the protein upon exposure to such low potentials. At NAD^+ concentrations well below the K_M value, the flavin site spends significant time unoccupied and when the electrode is driven to low potentials, the FMN will be readily reduced and could thus be lost. Early research on the SH suggested that loss of enzyme catalytic activity was due to dissociation of FMN-a upon enzyme exposure to reducing conditions, while FMN-b remained bound to the subunit. However, recent biochemical data on HoxFU subcomplex showed that incubation of HoxFU with NADH at a concentration higher than the K_M value results in a loss of catalytic activity and the activity can be restored upon addition of free FMN into the assay. Further analysis using fluorescence spectroscopy confirmed that the loss in catalytic activity was due to the dissociation of FMN-b from the HoxFU moiety. In cyclic voltammetry experiments shown in Chapter 3, a clear FMN signal was recorded for HoxFU modified electrode in the absence of substrate. This evidence indicates that FMN-b of HoxFU moiety dissociates from the subunit. No evidence of activity recovery was observed in electrochemical experiments upon addition of excess FMN into the test system, but

addition of excess FMN complicates the data interpretation due to extra redox signals from FMN in the solution and FMN adsorbed onto the electrode. Electrochemical experiments also show that the presence of both substrates does help stabilise the electrocatalytic current indicating that bound substrates improve enzyme stability to some extent.

4.4.3 Ability of the SH to function under aerobic conditions

Electrochemical experiments confirm that NADH oxidation and NAD^+ reduction by HoxFU are sustained in the presence of O_2. This is consistent with the requirement for the SH to work under aerobic conditions,[13] although some electrons may be consumed at the FMN catalytic centre for O_2 reduction. In biochemical experiments, it has also been shown that HoxFU may be the major contributor of superoxide production in the SH and the rate of HoxFU superoxide production is an order of magnitude higher than that of the whole SH. The hydrogenase moiety of the SH has also been shown to suffer from O_2 attack and requires low potential electrons for reactivation. In the SH, electrons for reactivation are most likely supplied from NADH oxidation at the FMN-b NAD^+/NADH catalytic centre. Figure 98 illustrates the current understanding of catalytic bias, O_2-tolerance, regulation and superoxide production of the SH.

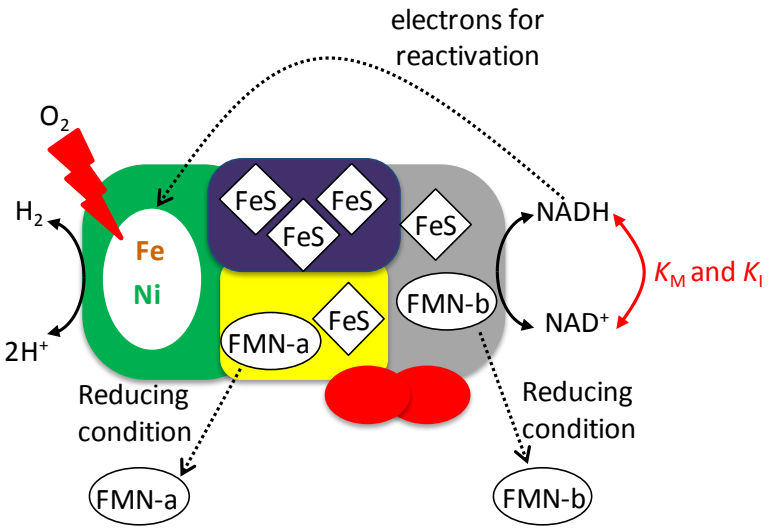

Figure 98. Schematic diagram of the SH showing the current understanding of its catalysis. The red arrows indicate inhibition reactions. The O_2-inactivated state of the SH requires low potential electrons and *in vivo*, these are supplied by NADH oxidation at the FMN-b catalytic centre. The electrons are transferred via a chain of FeS clusters to the NiFe active site. Under reducing conditions, FMN-a dissociates from the subunit, while FMN-b in the absence of NAD(H) also appears to dissociate from the subunit.

4.4.4 Towards applications in the supply of NADH to NADH-dependent dehydrogenases

Among the 3000 wild type classified enzymes known today, a third of these are oxidoreductases that require a non-proteinaceous redox cofactor for their reactions.[140] Some of these cofactors such as FMN, flavin adenosine dinucleotide (FAD) and heme groups are found bound to the redox enzymes structure. However, there are also cofactors required by these redox enzymes that exist as soluble components of the enzymes such as NAD^+ and NADH. These redox enzymes are attractive as biocatalysts because they may be applied to produce chiral compounds required for the pharmaceutical or chemical industries. One hindrance to utilising these redox enzymes in industrially important reactions is their requirement for stoichiometric amounts of the expensive soluble cofactors like NADH and NADPH. Efficient NAD^+ reduction and NADH oxidation in the presence of O_2, with the minimal overpotential requirement

exhibited by the HoxFU diaphorase moiety indicates that HoxFU may be a promising system for electrochemical regeneration of NAD(H) cofactors for biotechnological applications. Preliminary results to demonstrate this are provided in Chapter 6.

Chapter 5: Towards $NADP^+$/NADPH cycling

5.1 Introduction

As discussed earlier, NADP(H) is used by many dehydrogenases as a cofactor for their redox reactions. It has been reported that around 150 dehydrogenases utilise NADP(H) as a hydride ion donor/acceptor during a reaction.[140] The difference between a molecule of NADH and NADPH is the presence of an extra phosphate group on the ribose ring that carries the adenine moiety (Figure 99).

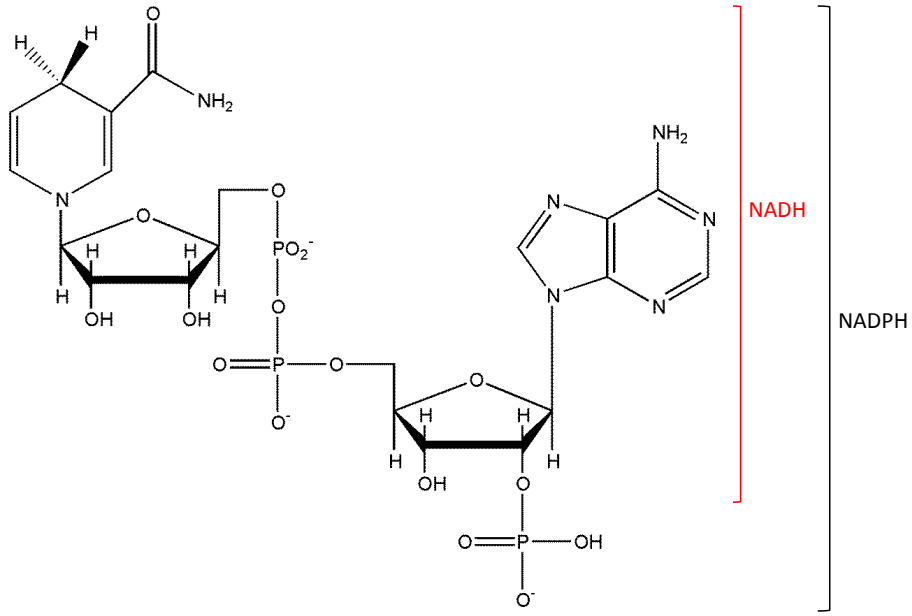

Figure 99. Comparison between the structures of NADH and NADPH.

An example of an NADPH dependent dehydrogenase is Gre2p, a γ-diketone reductase isolated from *Saccharomyces cerevisiae* which is used for reduction of 2,5-hexanedione to (2*S*,5*S*)-hexanediol.[228, 229] Bertau and coworkers have shown that the reaction will not proceed if NADPH is replaced with NADH.[228]

For dehydrogenases to be used in bioreductions, a source of NADPH is required and NADPH is less stable and far more expensive than NADH. According to Sigma Aldrich website, one gram of NADPH with up to 95 % purity costs £3136 as compared

to £310 for one gram of NADH. Therefore in an ideal enzyme based transformation, the cofactor used is recycled during the process, making the ability to regenerate the cofactor economically important.

Electrochemical experiments performed on the HoxFU diaphorase moiety in Chapters 3 and 4 of this Thesis confirm that the diaphorase moiety is an excellent electrocatalyst for NAD(H) cycling. The very close structures of NADPH and NADH raise the question of whether it would be possible to use HoxFU (or the whole SH) for $NADP^+$ reduction and NADPH oxidation. Early biochemical studies on the SH by Schneider and Schlegel reported that the SH exhibits NADPH oxidase activity with an affinity constant of 6.4 mM.[21] The experiments were performed by utilising ferricyanide, methylene blue, DCPIP, cytochrome *c* or molecular O_2 as oxidants, with NADPH acting as a hydride donor. Theoretically, the K_M value represents the substrate concentration at which an enzyme is at half of its maximal catalytic activity, thus a K_M in the mM range is considered high, especially when the K_M for NADH is in the μM range. Complex I from *E. coli* also exhibits NADPH oxidase activity although a very low activity was observed, about a fifth of the NADH activity at pH 6.[210, 230, 231] In 2011, Thorsten Friedrich and coworkers reported attempts to engineer the respiratory *E. coli* Complex I for better NADPH affinity.[232] They succeeded in decreasing the K_M value for NADPH, for example, a single mutation at the glutamic acid residue at position 183 to histidine enhances the catalytic activity for NADPH oxidation by 200-fold (K_M for WT was decreased from 1.87 mM to 25 μM).[232]

The success in changing the activity discrimination of Complex I has led to the possibility of engineering the SH for better NADP(H) activity. Site directed mutagenesis in the lab of Lenz and Lauterbach has led to variants designed for better affinity towards $NADP^+$. This Chapter will evaluate the electrochemical characterisation

of these variants for NADPH cycling, showing for the first time the possibility of efficient electrocatalytic $NADP^+$ reduction and NADPH oxidation. The variants purified by Lenz and Lauterbach are mostly in the HoxHYFU tetrameric forms *i.e.* with the hydrogenase moiety attached, thus this Chapter will begin by discussing the ability of wild type HoHYFU to function on an electrode and whether this big and complex enzyme is able to efficiently catalyse NAD^+ reduction and NADH oxidation as shown for the HoxFU dimer. After that, electrochemical experiments performed on the wild type HoxHYFU, HoxFU and $HoxFUI_2$ to check for $NADP^+$ reduction and NADPH oxidation activities will also be discussed. In the subsequent Sections, electrochemical characterisation of one of the variants will be discussed in terms of its ability to catalyse NAD(P)H cycling, the affinity constants, inactivation at low potentials and product inhibition. Data obtained from electrochemical experiments on a series of HoxHYFU and HoxFU variants will then be summarised and discussed.

Apart from being expensive and less stable, commercially available $NADP^+$ and NADPH cofactors are often contaminated with NADH and NAD^+. This contamination has previously been ignored by some researchers due to the assumption that the state of the art methods used by companies produce high quality nicotinamide cofactors. However, very recently Engel and coworkers discovered that a small NAD^+ contamination of 0.37 % in unpurified $NADP^+$ had resulted in an underestimation of *Clostridial* glutamate dehydrogenase substrate affinity by a factor of ten (*i.e.* the K_M values for $NADP^+$ determined before and after purification of the cofactor were 0.26 ± 0.01 mM and 3.2 ± 0.4 mM respectively).[185] Experiments described in this Chapter have therefore been carefully designed and all the nicotinamide cofactors used were freshly purified on the day of experiments as described in Chapter 2.

5.2 Electrocatalytic activity of wild type HoxHYFU

Figure 100 shows a schematic representation of a tetrameric moiety of the Soluble Hydrogenase that consists of four subunits, HoxHYFU: one NiFe H^+/H_2 cycling centre, two flavin mononucleotide groups and several FeS clusters. The tetrameric SH was purified by employing a high ionic strength and alkaline pH that caused the dissociation of HoxI from the intact enzyme.[13, 21, 73, 78, 79]

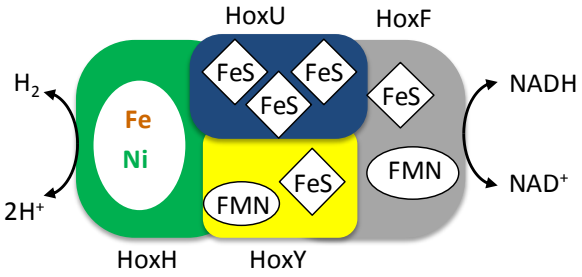

Figure 100. Cartoon illustrating the tetrameric structure, HoxHYFU of the SH.

Electrochemical experiments in this Section will begin by looking at the ability of HoxHYFU to catalyse NAD^+ reduction and NADH oxidation, followed by set of chronoamperometry experiments to determine quantitatively the HoxHYFU affinity constants towards its substrates. The inactivation at low potential of the HoxHYFU moiety will also be discussed in this Section.

5.2.1 Interpreting an electrocatalytic cyclic voltammogram for HoxHYFU

Experiments were designed to investigate the catalytic activity of HoxHYFU on a graphite electrode. In Figure 101A, the HoxHYFU modified electrode was placed in a solution containing 2 mM NAD^+. The electrode potential was swept between -0.15 V and -0.55 V and the electrode was rotated at 2500 rpm. At the beginning of the

experiment, no reduction current was recorded and the scan (red line) looks similar to the blank electrode (grey line). Upon scanning to more negative potentials, an increase in the current magnitude was recorded, attributed to NAD^+ reduction catalysed by HoxHYFU. On the reverse cycle, the current magnitude decreases as the potentials were swept towards more positive values and resembles the blank electrode at high potentials. The second cycle (blue line) shows some 'film loss' (see discussion in Chapter 3).

The HoxHYFU modified electrode was placed in a solution of 2 mM purified NADH for the experiment shown in panel B and the potential was swept between -0.56 V and 0.04 V. No catalytic current was observed at low potentials, however, at approximately -0.42 V an increase in the current due to NADH oxidation was noticed. A much lower NADH oxidation activity was recorded on the second cycle (blue), indicating 'film loss' again.

Experiments in panel C were performed by keeping the total NAD^+ and NADH concentration at 2 mM. As mentioned earlier in Chapter 3, the total concentration used for these experiments is sufficient to cover the expected NAD^+:NADH concentration range experienced by the SH in its native environment. At all substrate concentration ratios, the voltammograms crossed $E(NAD^+/NADH)$ sharply indicating that catalysis in both directions is efficient with minimal overpotential requirement. For example, the theoretical value of $E(NAD^+/NADH)$ at 1.5 mM NAD^+: 0.5 mM NADH at pH 8.0 30 ^oC is -0.339 V and a value of -0.320 V was attained from experimental data. Due to difficulty in calculating NAD(H) concentrations accurately after purification, the small deviation from the expected value is likely to result from incorrect determination of concentration. Panel C also discloses a similar point to that noted for HoxFU in Chapter 3; catalysis is biased towards NAD^+ reduction at all NAD^+:NADH ratios tested.

For instance, the current magnitude for NAD^+ reduction is eight times higher than NADH oxidation even at 0.5 mM NAD^+: 1.5 mM NADH, at 0.14 V above and below $E(NAD^+/NADH)$.

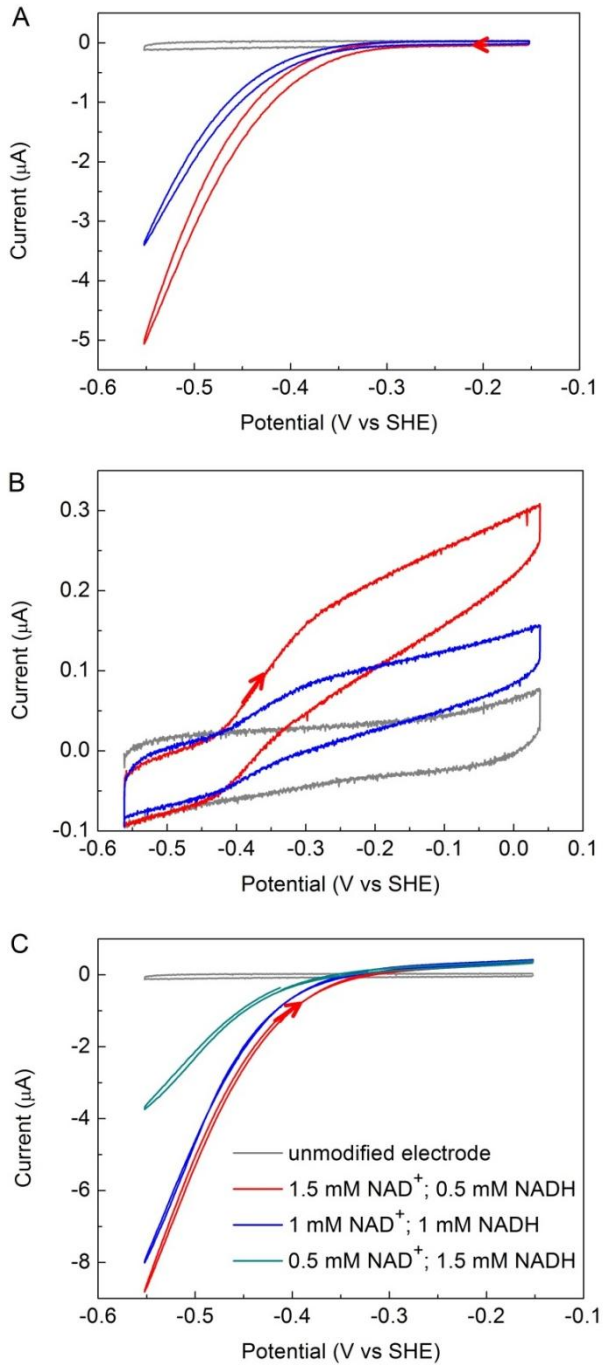

Figure 101. Electrocatalytic NAD^+ reduction and NADH oxidation by HoxHYFU. Experiments in panels A and B were performed in a solution of 2 mM NAD^+ and 2 mM NADH respectively. Panel C shows cyclic voltammograms of HoxHYFU in a mixture of NAD^+ and NADH; the concentrations used are as labelled in the figure. Other conditions: Tris-HCl buffer 50 mM, pH 8.0, 30 ^oC, electrode was rotated at 2500 rpm, scan rate 10 mV/s.

Figure 101 demonstrates that the tetrameric moiety of the SH is electrocatalytically active in NAD^+ reduction and NADH oxidation. The presence of hydrogen cycling moiety, HoxHY which is able to catalyse H^+ reduction may contribute to the total reduction current observed, and therefore must also be taken into account. When necessary, cyclic voltammetry experiments were performed in a fresh buffer solution to check for H^+ reduction activity of HoxHYFU as shown in Figure 102. Only negligible reductive current was recorded at low potentials that may correspond to H^+ reduction activity by HoxHYFU. In the absence of NAD^+ or NADH, a clear reversible peak at around -0.3 V is recorded. This peak probably corresponds to the dissociation and electrode-adsorption of one of the flavin groups in the SH.

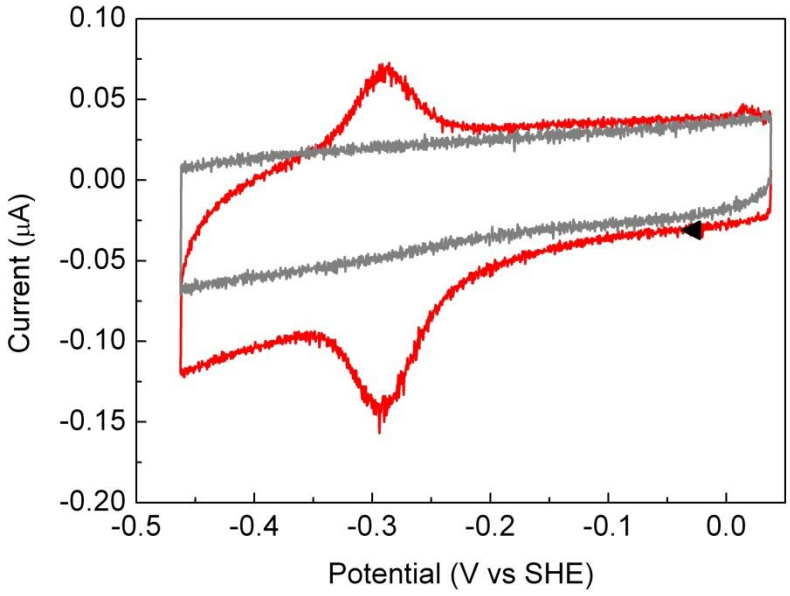

Figure 102. Cyclic voltammograms recorded in the absence of NAD^+ (red line). Experimental conditions: 50 mM Tris-HCl buffer, pH 8.0, at 30 ^oC with scan rate of 10 mV/s, the electrode was rotated at 2500 rpm. The grey line represents a voltammogram for an unmodified electrode.

Electrochemical experiments performed by Juan Liu at pH 7.0 showed that HoxHYFU is catalytically active in H^+ reduction.[220] However, in her experiments, no clear reversible peak at around -0.3 V was recorded. The fact that the experiment in

Figure 102 was performed on a rotating electrode may explain this difference, as a loosely held flavin may be spun away by the rotating electrode. In the rotating disk electrochemical experiments shown in this Chapter, H^+ reduction makes a very minor contribution to current at low potentials. Experiments were performed under a N_2 atmosphere, so H_2 oxidation at higher potentials can be discounted.

In 2011, Jones and coworkers reported an electrochemical investigation on the hydrogenase activity of a bidirectional hydrogenase from *Synecocystis sp*. PCC 6803. They showed that the pentameric enzyme is catalytically active in H_2 production and H_2 oxidation on a graphite electrode, with catalysis biased towards H_2 production. The high electrocatalytic current observed for H^+ reduction in *Synecocystis sp*. PCC 6803, however, means that it will be complicated to study this enzyme for NAD^+ reduction reaction: due to the difficulty in differentiating the current contributions, arising from NAD^+ reduction and H^+ reduction. In the case of the *R. eutropha* SH, the low activity for H^+ reduction is beneficial as it means the catalytic current observed in the presence of NAD^+, must mainly contribution of NAD^+ reduction by HoxHYFU.

5.2.2 Quantifying substrate affinity for NAD^+ and NADH

A similar procedure to determine the K_M value for NAD^+ reduction and NADH oxidation as discussed in Chapter 3 was applied to HoxHYFU and typical plots of current against time are shown in Figure 103 (panel A for NAD^+ reduction and B for NADH oxidation). The raw data were corrected by subtracting the background electrode contribution at zero substrate concentration and the corrected data obtained were then analysed using the Hanes-Woolf technique (panels C and D).[233, 234]

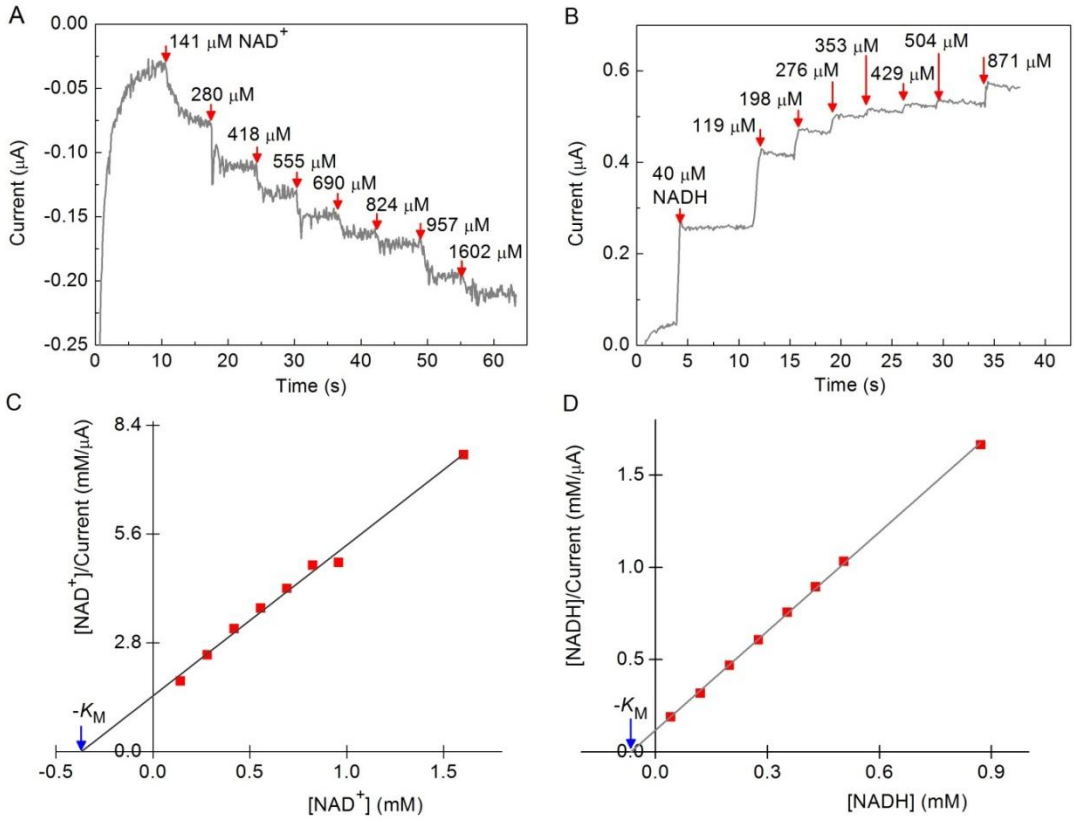

Figure 103. Chronoamperometry experiment designed to determine the affinity constant of HoxHYFU for NAD^+ (panel A) and NADH (panel B). The experiment was performed in a Tris-HCl 50 mM, pH 8.0 at 30 ^oC. The working electrode potential was set at -0.412 V (panel A) and -0.063 V (panel B) and NAD(H) stock solutions were injected into the electrochemical cell as indicated. The electrode was rotated at 2500 rpm during the course of the experiment. Typical Hanes-Woolf plots are shown in panels C and D for NAD^+ reduction and NADH oxidation respectively.

An average K_M value for NAD^+ reduction of 357 ± 45 μM was obtained from eight consecutive experiments while a K_M value of 63 ± 6 μM for NADH oxidation was calculated out of nine consecutive experiments. The K_M values acquired electrochemically for HoxHYFU are close to the value reported from biochemical assays (325 μM and 74 μM for NAD^+ and NADH respectively).[235] This implies that HoxHYFU does not suffer any structural damage upon attachment onto a graphite electrode. The K_M value for NADH oxidation of HoxHYFU also agrees with the value calculated for HoxFU (58 μM)[94] and is similar to that of bovine Complex I (90 μM).[199]

In the case of NAD^+ reduction, the value obtained for HoxHYFU (357 µM) is a bit higher than the value calculated for HoxFU (197 µM). The reason for this difference is unknown but may result from a slight structural change to the binding site on separation of the HoxFU fragment. A 50-fold lower K_M value was obtained for Complex I (7 µM).[227]

5.2.3 Potential dependent inactivation

Figure 104 demonstrates potential dependent inactivation experienced by HoxHYFU. In panel A the HoxHYFU modified electrode was placed in a solution of 50 µM NAD^+ and the electrode potential was swept between -0.22 V and -0.61 V. The shape of the voltammogram suggests that irreversible inactivation occurs, and on the second cycle (blue line) only a small fraction of the catalytic activity is retained. Panel B shows cyclic voltammograms recorded at 2 mM NAD^+ (6 times K_M). Here, inactivation is less pronounced and approximately 40 % of HoxHYFU initial catalytic activity is retained on the second cycle. Voltammograms in Panel C were executed in a solution of 1 mM NAD^+ and 1 mM NADH; with a total substrate concentration of 2 mM. Again, inactivation is less pronounced than in panel A, but similar to the situation in panel B. These experiments show that inactivation at low potentials is dependent on the concentration of NAD^+. At low NAD^+ concentration *i.e.* lower than the K_M value, a pronounced inactivation is observed.

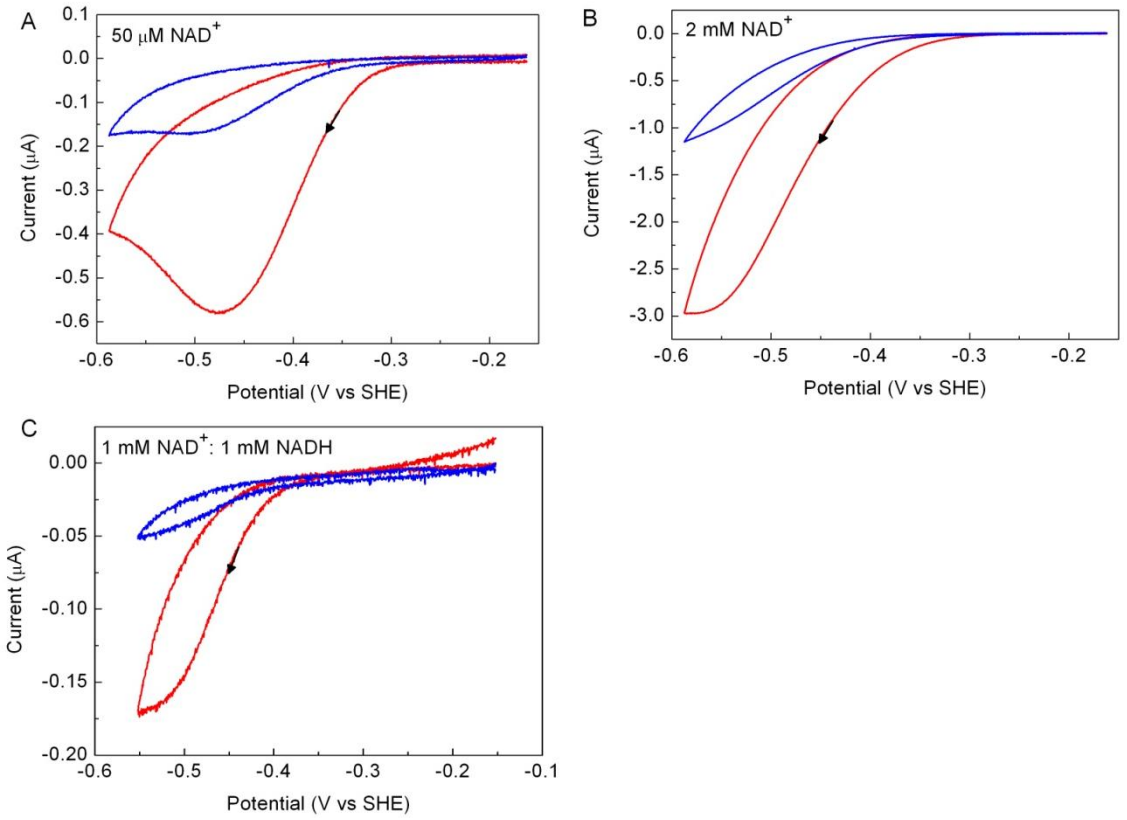

Figure 104. Cyclic voltammetry experiments to check for low potential inactivation by HoxHYFU at different NAD^+ and NADH concentrations: 50 μM NAD^+ (A), 2 mM NAD^+ (B) and 1 mM NAD^+: 1 mM NADH (C). Experimental conditions: Tris-HCl buffer 50 mM at pH 8.0, 30 ^oC. The experiments were performed at a slow scan rate of 1 mV/s while the electrode was rotated at 2500 rpm. The first cycle of each scan is shown as a red line and the second cycle is shown as a blue line. Arrows indicate the direction of scan.

Experiments on HoxHYFU described in this Section confirm that the electrocatalytic properties of the tetrameric moiety are similar to that of HoxFU diaphorase moiety. Thus examination of HoxHYFU site directed variants should give a good indication of how the same variants in HoxFU should behave. In the next section, the wild type HoxFU, HoxHYFU and $HoxFUI_2$ will be checked for activity in $NADP^+$ reduction and NADPH oxidation.

5.3 Are $NADP^+$ and NADPH substrates or inhibitors for HoxFU, $HoxFUI_2$ and HoxHYFU?

5.3.1 $NADP^+$ reduction and NADPH oxidation

As discussed earlier in this Chapter, the SH has been shown to exhibit NADPH oxidation activity in biochemical experiments.[13, 21] Thus it is interesting to check whether HoxFU, $HoxFUI_2$ and HoxHYFU moieties are capable of catalysing NADP(H) interconversion electrochemically.

Figure 105A shows a set of cyclic voltammograms to investigate $NADP^+$ reduction by HoxFU. No reduction current was recorded when the bare electrode was placed in a solution of 15 mM purified $NADP^+$, shown as a grey line. For the HoxFU modified electrode, no catalytic current was observed at the beginning of the scan and the current recorded resembles the blank scan. However, as the potential was swept towards more negative values, an increase in the current magnitude corresponding to $NADP^+$ reduction was observed.

Panel B shows an experiment designed to test whether HoxFU on an electrode can oxidise NADPH. The grey line shows a cyclic voltammogram recorded in the presence of 15 mM purified NADPH showing that there is no significant NADPH oxidation on a bare electrode. Only very faint current signals (red line) are observed that may indicate weak NADPH oxidation by HoxFU but by the second cycle, the current resembles the blank electrode.

In 2005, Friedrich and coworkers discovered that the SH harbours two additional closely related subunits; termed HoxI.[13, 78] They reported that while the hydrogenase activity of the tetrameric form of the SH (HoxHYFU) is instantly activated

by NADH (5 μM), it needs a much higher NADPH (40 mM) to activate while the hexameric SH ($HoxHYFUI_2$) can be activated by either NADH (5 μM) or NADPH (25 μM). These findings have prompted speculation that a specific binding site for NADPH may be formed by the HoxI subunits. Electrochemical experiments were therefore designed to check whether the presence of HoxI subunits would affect the enzyme affinity towards $NADP^+$ and NADPH. Electrochemical experiments involving $HoxFUI_2$ were performed in pH 7.0 BisTris-HCl buffer due to the fact that the HoxI subunits dissociate easily at high pH.[73, 78] Figure 105 (panels C and D) show cyclic voltammograms recorded to check for $NADP^+$ reduction and NADPH oxidation activities for $HoxFUI_2$. Similar catalytic behaviour as discussed for the HoxFU moiety was observed in electrochemical experiments on $HoxFUI_2$. The presence of two HoxI subunits in addition to HoxFU does not seem to help towards enzyme activity for NADP(H).

Panel E shows cyclic voltammograms to check for the ability of HoxHYFU to reduce $NADP^+$ at low potentials. The moiety is indeed able to reduce $NADP^+$, albeit giving a much lower current than for NAD^+ reduction. Experiments designed to check for NADPH oxidation by HoxHYFU, however, did not show any proof of activity in this direction (tested up to 15 mM purified NADPH).

To confirm that the enzyme films used for this set of experiments were active films, the electrochemical cell was washed after each experiment and the buffer solution was changed to a 2 mM NAD^+ solution. The same enzyme film was then rinsed using fresh buffer solution and placed into the electrochemical cell. Using the same enzyme film, a clear NAD^+ reduction was recorded in each case confirming that the enzyme on the electrode was active, and therefore should have given a current with NADPH if NADPH oxidation is able to occur.

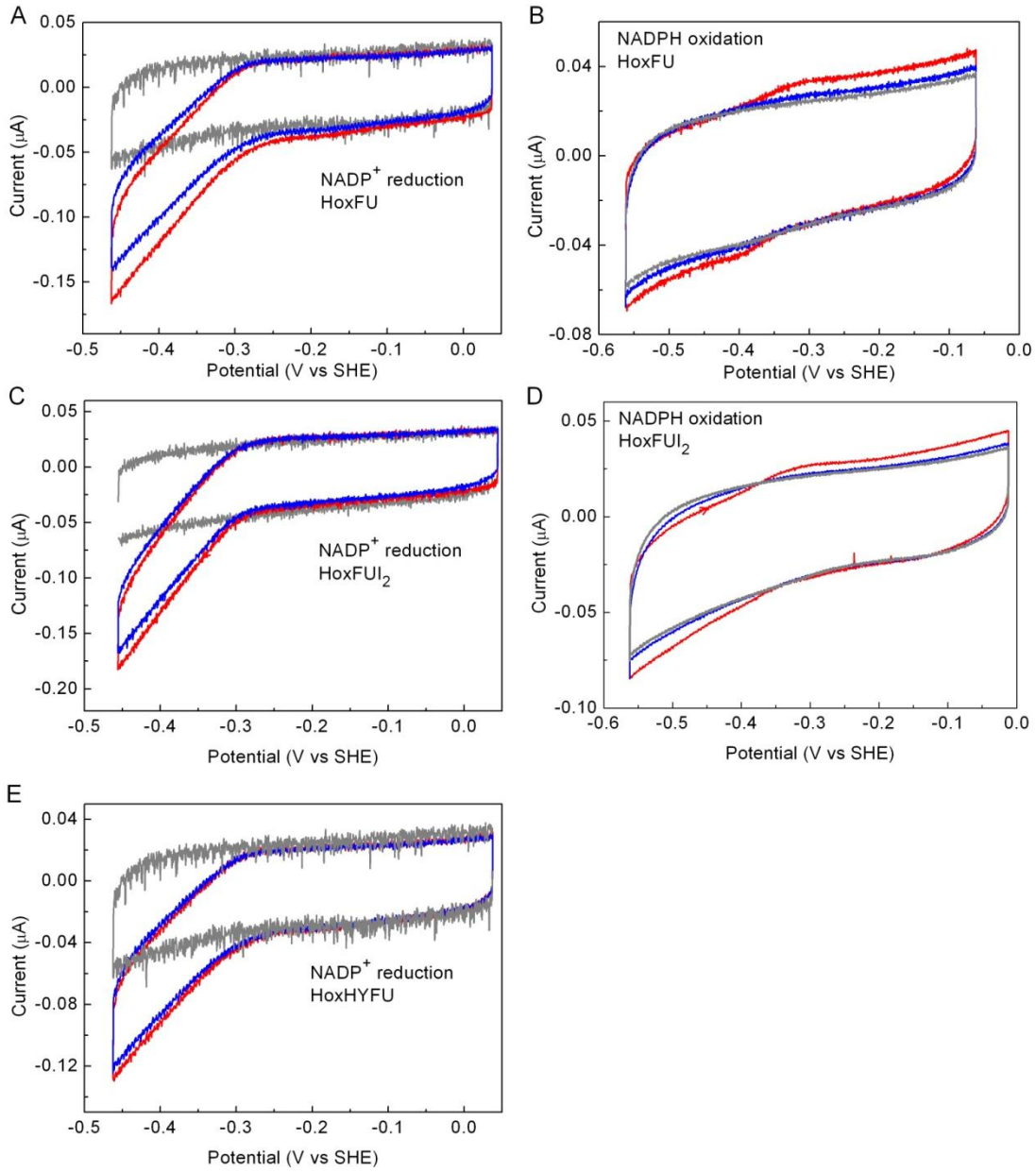

Figure 105. Ability of HoxFU (panels A and B), $HoxFUI_2$ (panels C and D) and HoxHYFU (panel E) to perform $NADP^+$ reduction and NADPH oxidation. Experiments were performed in Tris-HCl buffer pH 8.0 at 30 ^oC except for experiments involving $HoxFUI_2$ which were performed in BisTris-HCl pH 7.0. The electrode was rotated at 3000 rpm in a solution of either 15 mM purified $NADP^+$ (panels A, C and E) or 15 mM purified NADPH (panels B and D). In $NADP^+$ reduction experiments, the electrode potential was swept between 0.06 V and -0.46 V whilst for NADPH oxidation experiments the electrode potential was swept between -0.55 V and -0.05 V. A scan rate of 10 mV/s was used throughout the experiments.

Cyclic voltammetry experiments described above confirm that HoxFU and $HoxFUI_2$ moieties are able to catalyse $NADP^+$ reduction and possibly weak NADPH oxidation on an electrode. The tetrameric SH also shows $NADP^+$ reduction, however,

no evidence of NADPH oxidation was found. The catalytic current observed for all catalytic moieties, however, was very low compared to the current recorded for NAD^+ reduction and NADH oxidation, in line with the fact that the SH native substrates are NAD^+ and NADH. As the moieties exhibit some $NADP^+$ reduction electrocatalytic activity, it is interesting to investigate whether $NADP^+$ or NADPH would act as inhibitors of NADH oxidation and NAD^+ reduction.

5.3.2 Investigation of $NADP^+$ and NADPH as inhibitors

Figure 106A shows an experiment designed to check for NADPH inhibition for NAD^+ reduction by HoxFU. A HoxFU modified electrode was first placed in a fresh buffer solution and was poised at -0.412 V. No catalytic current was detected at the beginning of the experiment as no NAD^+ was present. An increase in reductive current due to NAD^+ reduction by HoxFU was observed upon injection of 0.1 mM NAD^+ into the electrochemical cell. At approximately 24 seconds, an aliquot of purified NADPH containing 0.1 mM NAD^+ was injected into the cell. Further NADPH injections were performed as indicated by red arrows in Panel A. No decrease in the current magnitude was recorded upon introduction of NADPH into the cell solution indicating that NADPH does not inhibit NAD^+ reduction over this concentration range.

In panel B, the HoxFU-modified electrode was placed in a fresh buffer solution and poised at -0.063 V. Then, at approximately 10 seconds, an aliquot of 50 µM of purified NADH was injected into the electrochemical cell thus resulting in an increase in the catalytic current corresponding to NADH oxidation by HoxFU. Injections of $NADP^+$ stock solution containing 50 µM NADH were performed as indicated by the red arrows in Panel B. No drop in catalytic current was observed upon injection of $NADP^+$

solutions indicating that $NADP^+$ does not inhibit NADH oxidation over this concentration range.

Chronoamperometry experiments as described above were performed on HoxHYFU modified electrode to check for NADPH inhibition of NAD^+ reduction and $NADP^+$ inhibition of NADH oxidation (panels C and D). Similar observations were recorded; NAD^+ reduction and NADH oxidation are not inhibited by NADPH or $NADP^+$, consistent with weak binding of NADP(H).

Although in the case of NAD^+ inhibition of NADH oxidation, additions of NAD^+ help to stabilise the catalytic current, as shown in Figure 106, additions of $NADP^+$ do not stabilise the enzyme film on electrode and a gradual decrease in the catalytic current was recorded. In all panels, slow decreases in catalytic current were recorded over time, attributed to 'film loss' as discussed in Chapter 3.

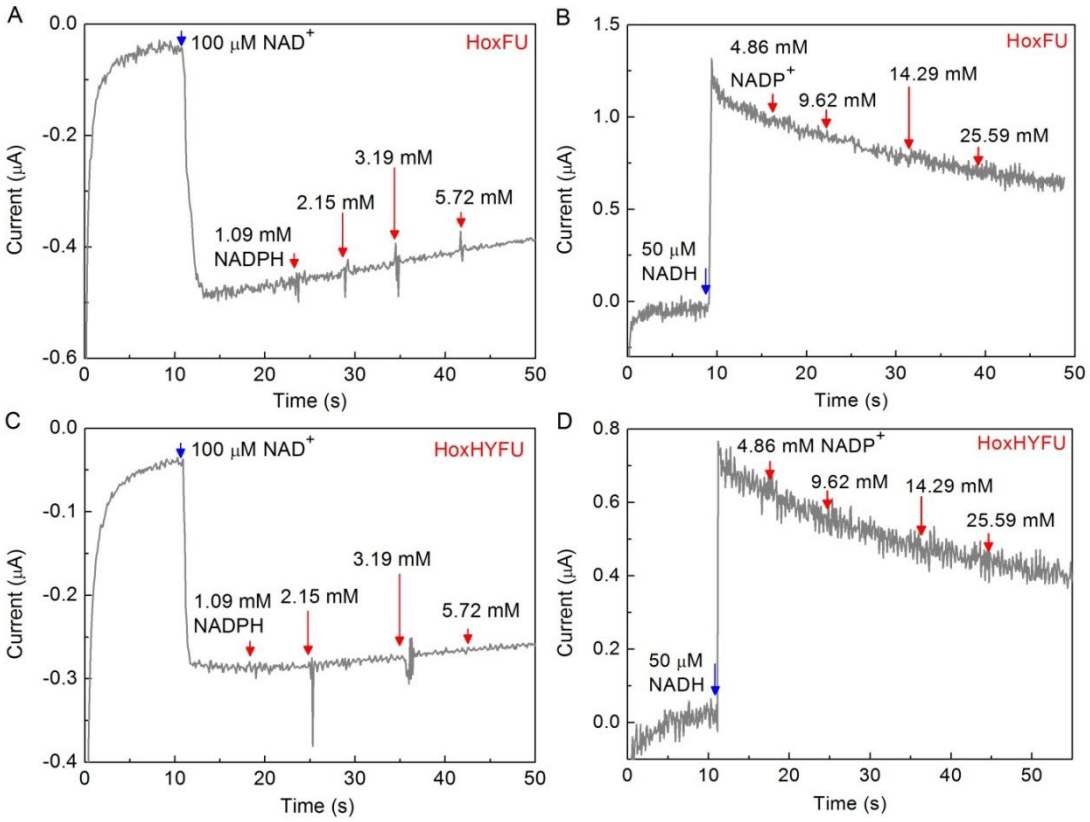

Figure 106. Ability of HoxFU (panels A and B) and HoxHYFU (panels C and D) to sustain NAD^+ reduction and NADH oxidation in the presence of NADPH (panels A and C) and $NADP^+$ (panels B and D). Experiments in A and C were performed by holding the working electrode potential at -0.412 V, while in panels B and D the electrode was poised at -0.063 V. Other conditions: Tris-HCl buffer 50 mM at pH 8.0, temperature control of 30 ^oC and electrode was rotated at 2500 rpm.

5.3.3 Quantifying substrate affinity for $NADP^+$ and NADPH

Figure 107A and B show typical chronoamperometry experiments performed to determine the K_M values for $NADP^+$ reduction by HoxFU and HoxHYFU at -0.412 V. Upon injections of purified $NADP^+$, increases in current magnitude due to $NADP^+$ reduction by HoxFU and HoxHYFU were observed. The chronoamperometry experiments were repeated five times and the data were then analysed using Hanes-Woolf technique, and an average value for K_M was determined.

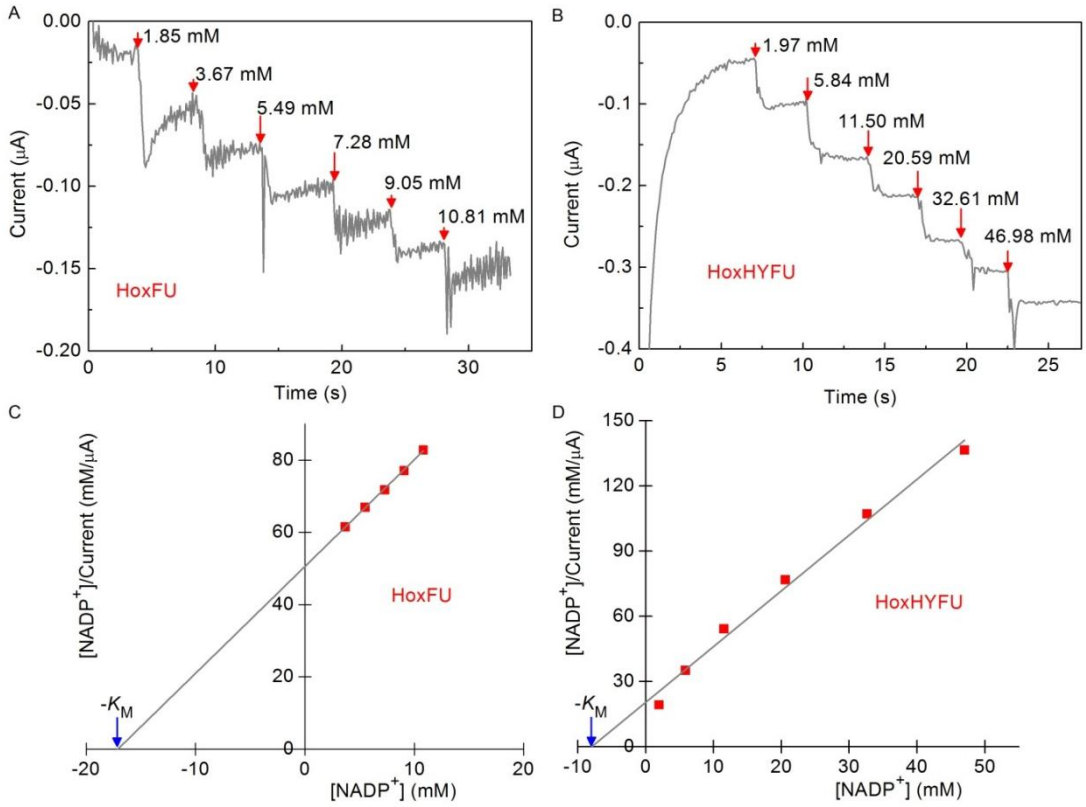

Figure 107. Determination of HoxFU and HoxHYFU affinity constants for $NADP^+$ reduction. Panels A and B show typical chronoamperometry experiments designed to investigate the K_M value. The electrode was poised at -0.412 V, with no $NADP^+$ present to begin with. Purified $NADP^+$ was then added as indicated in the figure. Panels C and D show typical Hanes-Woolf plots to calculate the K_M values. Other experimental conditions: Tris-HCl buffer 50 mM, pH 8.0, titrated to 30 ^oC and the electrode was rotated at 2500 rpm.

Typical Hanes-Woolf plots are presented in panels C and D. From five consecutive experiments, average K_M values of 8.3 ± 1 mM for HoxFU and 8.0 ± 1.2 mM for HoxHYFU were calculated using this method. The K_M values for HoxHYFU and HoxFU are very similar, but are 40-fold higher than the K_M values for NAD^+ reduction by HoxFU and HoxHYFU. This indicates that although $NADP^+$ reduction is possible, the binding of this cofactor within the enzyme is weak relative to NAD^+. This also agrees well with the actual function of the SH in the cell, to reduce NAD^+ thus providing the cell with NADH at the expense of H_2.

Experiments were also performed to determine the affinity constant of HoxFU for NADPH and a typical chronoamperometry data set is shown in Figure 108A. The electrode was positioned in an electrochemical cell containing no NADPH and was poised at -0.063 V. An increase in oxidative current magnitude was recorded following injections of purified NADPH into the electrochemical cell.

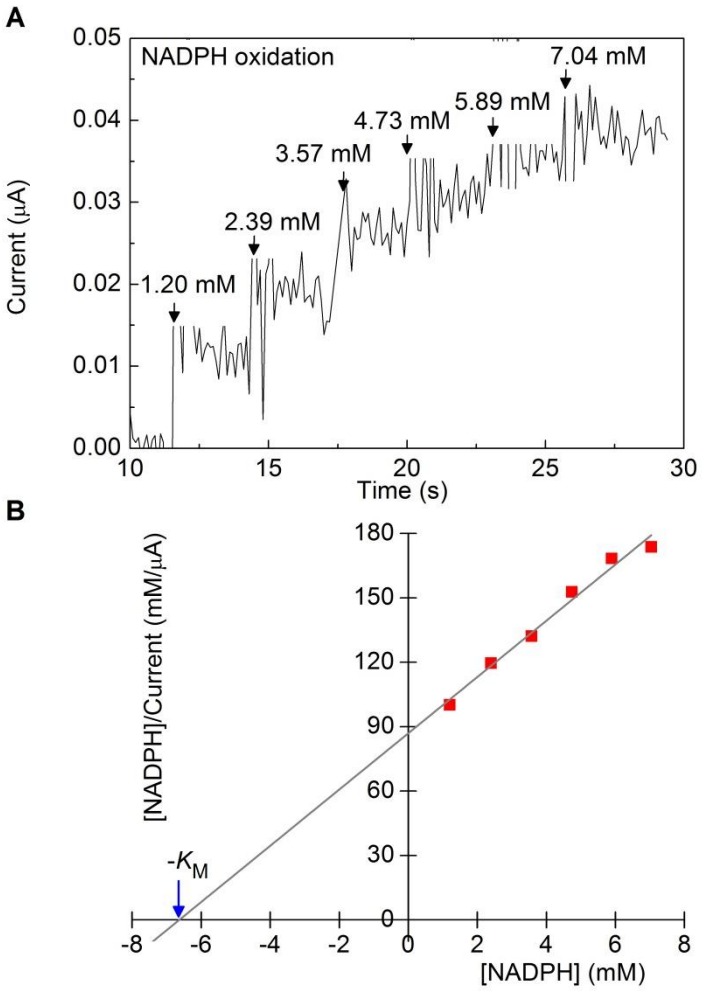

Figure 108. Panel A shows a typical chronoamperometry experiment designed to determine the HoxFU affinity constant for NADPH. The experiment was performed in a 50 mM Tris-HCl buffer, pH 8.0, titrated to 30 ^{o}C and the electrode was poised at -0.062 V and rotated at 2500 rpm. In panel B, a typical Hanes-Woolf plot is shown.

The raw data were then analysed by using the Hanes-Woolf technique[233] (Figure 108B) and a K_M value of 5.2 ± 1.7 mM for NADPH oxidation was calculated from six different experiments. This is close to the value determined from biochemical assays:

6.78 mM utilising benzyl viologen as an electron acceptor. A previous study on the whole SH by Schneider and Schlegel gave a K_M value of 6.4 mM for NADPH oxidation[21], also similar to the value determined here for HoxFU.

A summary of the substrate affinity constants determined electrochemically for HoxFU and HoxHYFU in comparison with Complex I is shown in Table 5-1. Generally, the K_M values for HoxFU and HoxHYFU are in agreement with each other. This may suggest that studying the genetic variants of HYFU is expected to give a good indication of the behaviour of HoxFU variants. The main difference between the K_M values for the SH and Complex I is the higher K_M value of the SH for NAD^+. Although the SH main function is to reduce NAD^+, its K_M value is nearly 50-fold higher than Complex I.

Table 5-1. The K_M values of HoxFU, HoxHYFU and Complex I. Values are from this study unless otherwise specified.

	K_M value			
	NAD^+ (μM)	NADH (μM)	$NADP^+$ (mM)	NADPH (mM)
HoxFU	197 ± 28	58 ± 18	8.3 ± 1	5.2 ± 1.7
HoxHYFU	357 ± 45	63 ± 6	8.0 ± 1.2	ND*
Complex I	7[227]	90[199]	ND*	1.9[232]

ND*: not determined

The low affinity of HoxFU towards NADP(H) could possibly be explained by examining the homology model constructed for HoxF of the SH using the subunit Nqo1 crystal structure for *T. thermophilus* Complex I as shown in Figure 109.

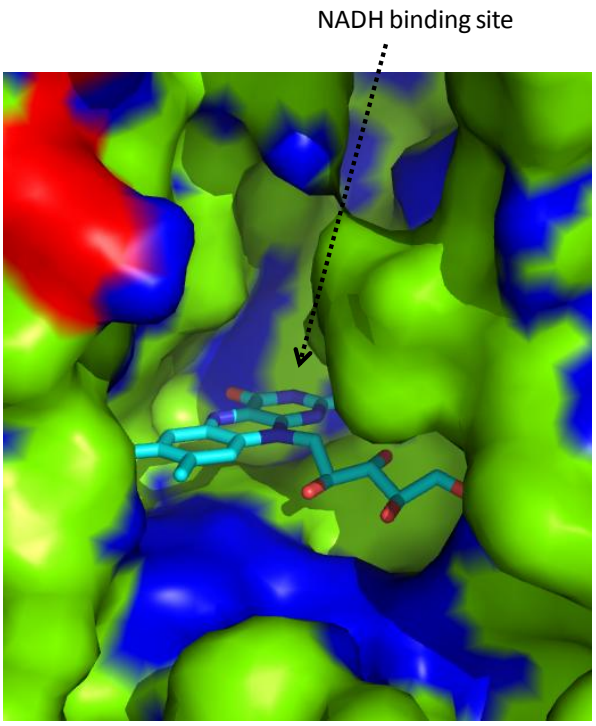

Figure 109. Surface representation of NADH-binding site showing conserved FMN (stick) in HoxF subunit of SH. Negatively charge amino acid residues are shown in blue, while positively charge is shown in red. The homology model was kindly provided by Lars Lauterbach.

The FMN catalytic centre where hydride transfer takes place is surrounded by negatively charge amino acid residues such as glutamic acid at position 340 and aspartic acid at position 341. These amino acid residues generate a negatively charged protein environment at the position where cofactor binding takes place. Thus it is likely to be less favourable to accommodate a molecule of NADP(H) which contains an extra negatively charged phosphate group. According to Carugo and Argos,[45, 46] the specificity of reactions catalysed by dehydrogenases is dependent on the residues surrounding the FMN catalytic centre; a negatively charge environment will favour NAD(H) reactions and a more positive environment will favour NADP(H) reactions. Complex I also showed NADPH oxidation catalysis, albeit at a much lower activity *i.e.* at 1-2 % in comparison to NADH oxidation, and Sazanov and co-workers suggested that the presence of limited unoccupied space close to the Oxygen atom of the

adenosine ribose of NADH may provide space to accommodate the extra phosphate of NADPH.[29, 34, 230]

For both Complex I and the SH, the K_M values for NADP(H) reactions are in the millimolar range, which indicates a low affinity for these substrates. In the next Section, several variants of HoxHYFU intended to increase the affinity for $NADP^+$ are subjected to electrochemical investigations.

5.4 Site-directed mutagenesis designed to increase affinity for $NADP^+$/NADPH

(Some experiments in this Section were performed by Kate Simpson-Wells and Thomas Lyle (Part II students) under my supervision.)

The Soluble Hydrogenase of *R. eutropha* has been demonstrated to exhibit good electrocatalytic NAD^+ reduction and NADH oxidation on a graphite electrode with a minimal overpotential requirement. The SH also showed $NADP^+$ reduction, however, the catalytic activity observed for this reaction was low. Furthermore, high substrate affinity constants were calculated from electrochemical experiments for HoxFU for $NADP^+$.

As mentioned earlier in this Chapter, a large number of dehydrogenases utilise NADP(H) as a cofactor for oxidation of alcohols and reduction of carbonyl groups. These enzyme catalysed reactions are important for synthetic applications as they yield chiral products. For example, a ketoreductase variant from *Lactobacillus kefir* produces (2*S*,3*R*)-2-(benzamidomethyl)-3-hydroxybutyrate, which is an important precursor for the synthesis of carbapenem derivatives at high conversion rates (approximately 99 %) with excellent selectivity.[236, 237] This dehydrogenase requires NADPH as a cofactor for the process necessitating for a constant supply of cofactor, and since NAD(P)H based

cofactors are expensive, diaphorase enzymes are attractive because they have the potential to produce and recycle catalytically active nicotinamide cofactors.

Most of the dehydrogenases used in industry require specific nicotinamide cofactors for their reactions. In the case of horse liver alcohol dehydrogenase, which is used in preparation of (1*S*,2*R*)-*cis*-2-carboxymethyl-3-cyclopenten-1-ol lactone (a starting compound for prostaglandin synthesis), a high yield of the enantiomer is obtained only with NAD^+.[103, 238, 239] For reduction of 2,5-hexanedione to (2*S*,5*S*)-hexanediol by the γ-diketone reductase Gre2p only NADPH is accepted as the co-substrate.[228, 229] Finding a catalytic system for regenerating the desired nicotinamide cofactor efficiently is essential.

Carugo and Argos suggested that the presence of negatively charged amino acid residues (aspartate or glutamate) in a position possible for forming a hydrogen bond with the 2'-diol group of NADH may contribute to the cause of NADH discrimination over NADPH.[45, 46] When a molecule of NADH binds to the active site, a negatively charged residue (normally aspartate) forms a hydrogen bond to the diol group of the ribose ring close to adenine and directs its side chain toward the plane of adenine. Amino acid residues close to aspartate form hydrogen bonds with the protein segment to ensure an attachment of the diphosphate group to the protein. In the case of NADPH, a similar systematic analysis of several crystal structures of NADP-dependent enzymes shows that the NADPH conformation upon its binding to the active site is more flexible than that of NADH. Carugo and Argos argued that in the NADP-dependent enzymes they studied, the only largely conserved structural feature is the presence of a positively charged amino acid residue (arginine for example) whose side chain stacks against adenine plane and interacts with the phosphomonoester of NADPH via hydrogen bonds.[45, 46] In *E. coli* Complex I, mutations performed at the glutamate residue at

position 183 (equivalent to Glu^{341} in HoxF of the SH) successfully enhanced the variants' affinity towards NADPH.[232] Thorsten Friedrich and coworkers reported that changing the negatively charged glutamate to positively charged histidine decreases the K_M for NADPH from 1870 μM to 25 μM.[232] The increase in the variant affinity for NADPH may be due to lowered steric hindrance and an electrostatic stabilisation of the negative charge of the phosphate group when glutamate is replaced with histidine.

Site directed mutagenesis has been employed by our collaborators at the Humboldt Universität of Berlin to engineer the SH binding site to have a greater affinity towards $NADP^+$ and NADPH. Several attempts to change the binding specificity for other NAD(P)-dependent enzymes have focussed on mutations of the negatively charged amino acid residues that bind the 2'-diol of NADH and some of these mutations have succeeded in shifting the enzyme's affinity.[47, 232, 240, 241] In the case of the SH, the protein environment of the HoxF subunit, where NAD(H) catalysis takes place, contains many negatively charged residues which may act to repel NADP(H) molecules (Figure 110).

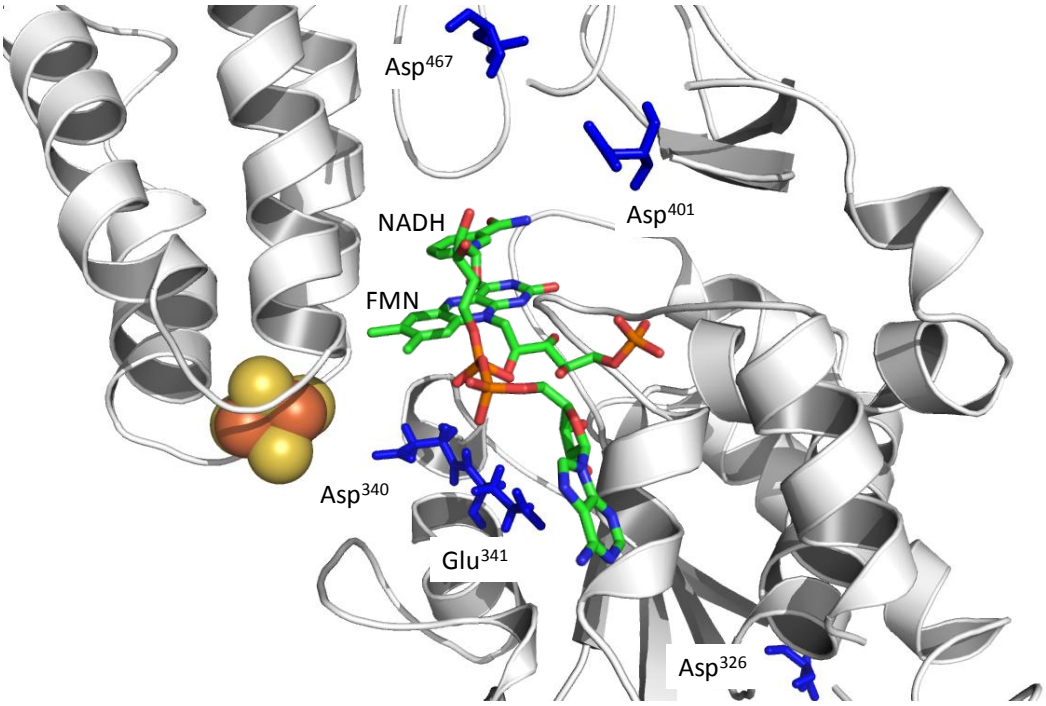

Figure 110. A cartoon of the homology model of HoxF subunit constructed using the resolved crystal structure of *Thermus thermophilus* showing the NADH binding site with FMN and the adjacent FeS cluster. Negatively charged amino acid residues mutated as part of this study are shown as blue sticks and labelled as appropriate. The homology model was prepared by Lars Lauterbach.[235]

These negatively charged amino acid residues are the subject for site directed mutagenesis and a total of nine variants of HoxHYFU and two of HoxFU (Table 5-2) have been successfully over-expressed and purified to homogeneity.[242]

Table 5-2. The variants investigated in this Thesis.

HoxHYFU tetrameric variants	HoxFU dimer variants
D340A	D340A
E341A	E341A
E341H	
D326K	
D401K	
D467S	
D401K D340A	
D467S E341A	
D401K D326K	

Protein film electrochemistry has been employed to investigate the catalytic activities of these variants. In this Section, only one will be discussed comprehensively in terms of its activity with each of nicotinamide cofactors. Results obtained for all variants will then be summarised in Section 5.4.2 and discussed.

5.4.1 HoxHYFU D401K

Figure 111A shows a line representation of HoxF modelled using Nqo1 of *T. thermophilus* showing the position of the mutations introduced: the negatively charged Aspartate residue has been mutated to a positively charged Lysine residue (panel B). Although the Aspartate residue is quite far from the FMN catalytic centre (22.6 Å), it is part of the Rossmann fold that is involved in NAD(H) binding during catalysis. Thus in theory, this residue would act as a gate for binding of the substrate, and since Aspartate is a negatively charged residue, it will repel the binding of NADP(H) which contains an extra negatively charged phosphate group. It is thus interesting to investigate how the variant catalytic activity is affected as compared to the wild type.

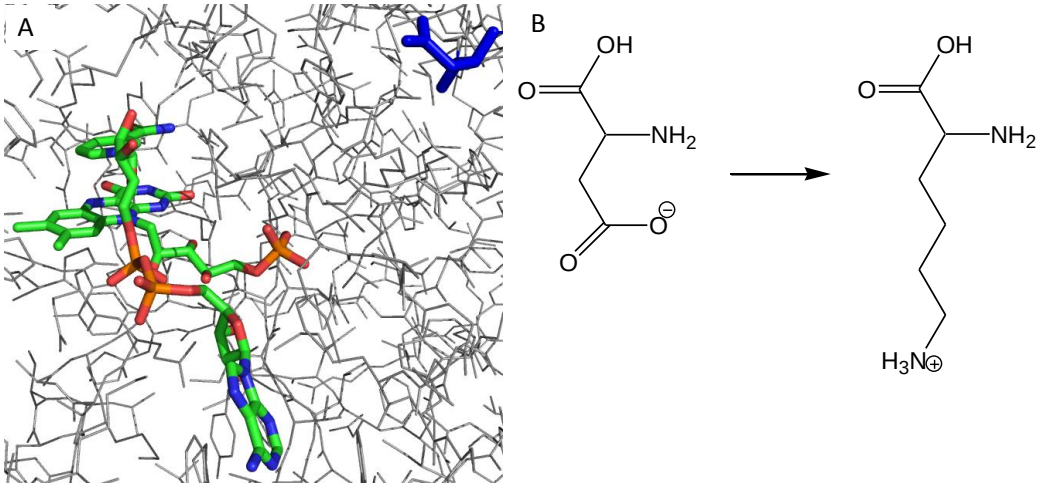

Figure 111. Panel A shows the NADH binding site in the HoxF subunit with the mutated amino acid residue shown as blue sticks. Panel B shows the mutation performed for this variant: a change from aspartic acid to lysine.

5.4.1.1 Investigating NAD(H) Catalysis

Figure 112 shows cyclic voltammograms for D401K HoxHYFU recorded at different NAD^+ and NADH ratios. In panel A, the enzyme modified electrode was placed in a solution of 2 mM NAD^+ while the electrode potential was swept between -0.05 V and -0.55 V. At the commencement of the experiment, no catalytic current was recorded and the scan (red line) resembles the unmodified electrode (grey line). At approximately -0.3 V the enzyme starts reducing NAD^+ resulting in an increase in the negative current. On the return scan, as the potential was swept towards more positive value the driving force for NAD^+ reduction decreases and at potentials higher than -0.3 V, the scan looks like the unmodified electrode.

In panel B the enzyme modified electrode was positioned in a solution of 2 mM purified NADH and the electrode potential was swept from -0.55 V and -0.05 V. No catalytic current was recorded at low potentials and the scan (red line) resembles the

unmodified electrode (grey line). The enzyme starts oxidising NADH at around -0.4 V and this result in an increase in the catalytic current.

Cyclic voltammograms in panel C were recorded on fresh enzyme films at different NAD^+:NADH concentrations, while keeping the total substrate concentration at 2 mM. At all concentrations investigated in panel C, the lines crossed the zero current potential sharply indicating efficient catalysis with a minimal overpotential requirement. For instance, at pH 8.0, 30 ^oC, and 0.25:1.75 ratio of NAD^+:NADH, the theoretical $E(NAD^+/NADH)$ calculated is -0.379 V compared to -0.365 V determined from experiment.

The voltammograms also show that the variant is strongly biased towards NAD^+ reduction rather than NADH oxidation at all NAD^+ and NADH concentrations investigated. For example, by taking an average current magnitude at 0.14 V above and below the thermodynamic potential at 1:1 ratio of NAD^+:NADH, the activity for NAD^+ reduction is 25-times higher than that of NADH oxidation. Under analogous conditions, the wild type HoxHYFU also shows a similar catalytic bias towards NAD^+ reduction: the current magnitude ratio was found to be 22-times higher for NAD^+ reduction than NADH oxidation.

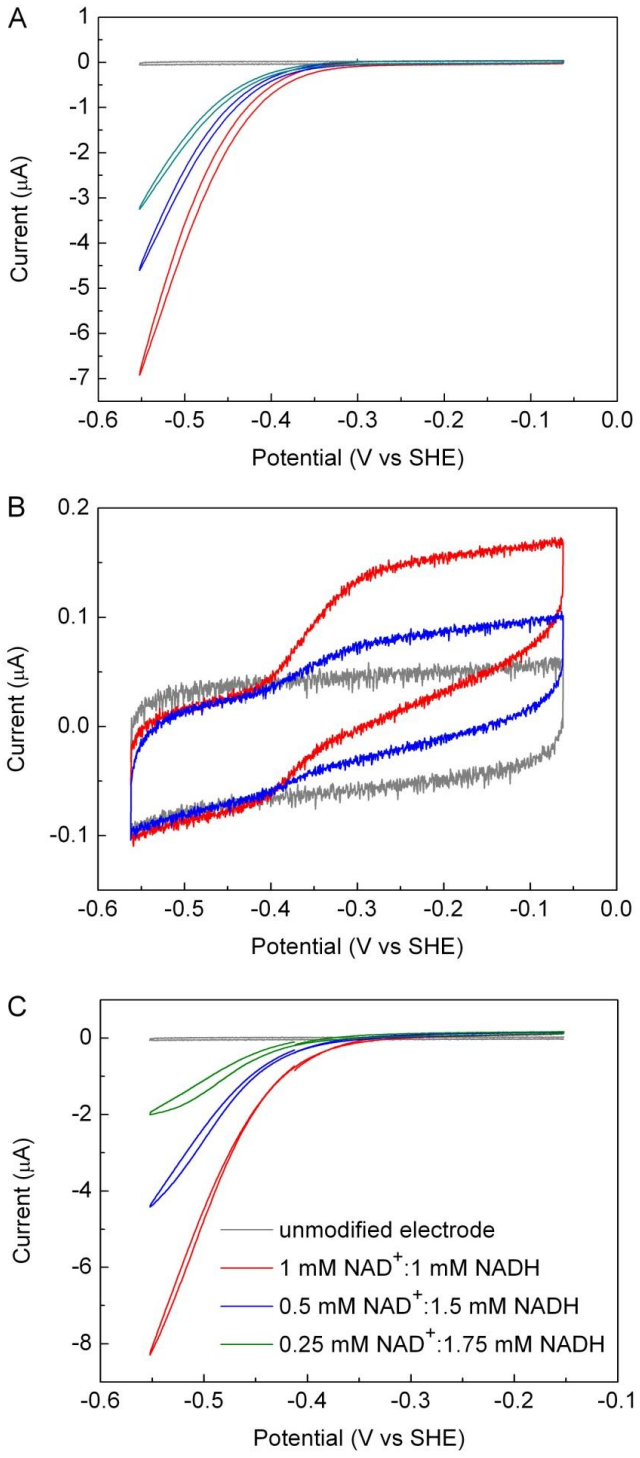

Figure 112. Typical cyclic voltammograms obtained with a PGE electrode modified with a D401K HoxHYFU moiety film. In panels A and B, the first (red), second (blue) and, where applicable third (green) scans are shown against a scan for an unmodified PGE electrode (grey). All scans were recorded at scan rate 10 mV/s in Tris-HCl 50 mM pH 8.0 at 30 ^{o}C with the working electrode rotated at 2500 rpm. Panel A shows the current response obtained in the presence of 2 mM NAD^{+}, whilst panel B shows the catalytic response at 2 mM NADH. In panel C, experiments were performed in a mixture of NAD^{+} and NADH at concentrations as labelled, while keeping the total concentration at 2 mM.

The voltammetric experiments described above indicate that the D401K HoxHYFU variant is electrocatalytically active in producing NAD^+ and oxidising NADH efficiently. The variant also shows a bias towards NAD^+ reduction, similar to the WT enzyme.

5.4.1.2 Investigating NADP Catalysis

The variant was designed to have a greater affinity towards $NADP^+$ and NADPH than the wild type HoxHYFU. The cyclic voltammetry experiment shown in Figure 113 executed in a solution of 1 mM $NADP^+$ shows a clear electrocatalytic wave for $NADP^+$ reduction. In contrast, at 1 mM $NADP^+$, no distinctive catalytic activity was recorded for the wild type HoxHYFU, suggesting that the variant may have a higher affinity towards $NADP^+$ than the wild type.

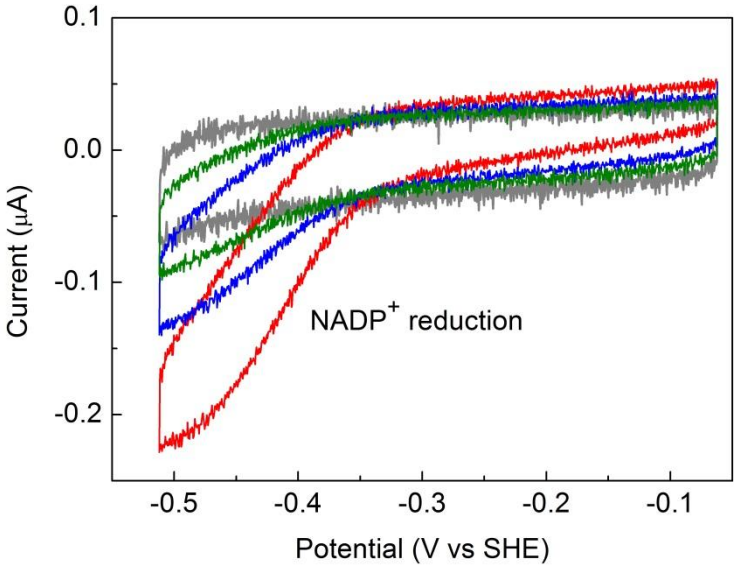

Figure 113. Typical cyclic voltammograms recorded for HoxHYFU D401K variant on a PGE electrode showing $NADP^+$ reduction. First, second and third cycles are shown as red, blue and green lines respectively. The grey line represents a cyclic voltammogram recorded on an unmodified electrode. Experiments were performed in 1 mM $NADP^+$, utilising Tris-HCl 50 mM, pH 8.0 at 30 ^oC. The working electrode was rotated at 2500 rpm. Scan rate used throughout experiment was 10 mV/s.

Experiments were also performed to check for NADPH oxidation, however, the results obtained were not convincing due to low activity. In the next section, the variant will be subjected to chronoamperometry experiments to determine the affinity constants for NAD^+, NADH and $NADP^+$.

5.4.1.3 Affinity towards NAD^+ and NADH

Determination of the K_M values for NAD^+ and NADH was performed according to procedures described in Section 3.4 and typical results are shown in Figure 114. From eleven consecutive experiments, a mean K_M value for NAD^+ of 544 ± 136 µM was calculated for this variant. The K_M value obtained is two times higher than the value reported for the wild type HoxHYFU suggesting that replacement of aspartic acid residue at position 401 in HoxF subunit has lowered the affinity of the enzyme for NAD^+. An average K_M value for NADH of 158 ± 22 µM was calculated from 13 separate experiments for this variant. The K_M value for NADH obtained electrochemically for this variant is almost three times higher than the value calculated for the wild type HoxHYFU (63 µM). This indicates that changing the negatively charged residue to positively charged residue has also lowered the enzyme affinity towards NADH.

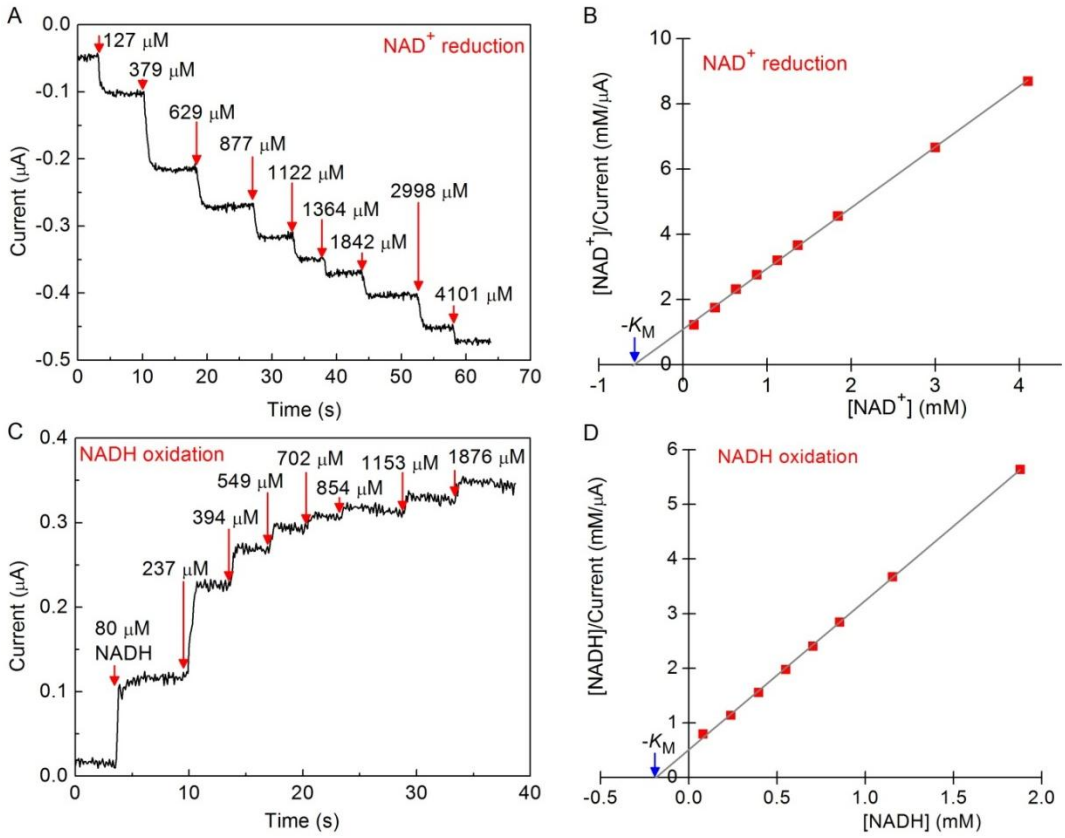

Figure 114. (A) A typical result of chronoamperometry experiment designed to determine the affinity constant for NAD^+ reduction by HoxHYFU D401K variant. The enzyme modified electrode was poised at -0.412 V and placed in a solution containing no NAD^+ at the beginning of the experiment. Aliquots of NAD^+ were injected into the electrochemical cell to give concentrations as indicated in panel A. (B) An example of $[NAD^+]$/Current against $[NAD^+]$ plot that resembles a Hanes-Woolf plot used to determine the K_M value for NAD^+ reduction. (C) A typical result of chronoamperometry experiment designed to determine the affinity constant for NADH oxidation by HoxHYFU D401K variant. The enzyme modified electrode was poised at -0.063 V and placed in a solution containing no NADH at the beginning of the experiment. Aliquots of purified NADH were injected into the electrochemical cell at concentrations as indicated in panel C. (D) An example of [NADH]/Current against [NADH] plot that resembles a Hanes-Woolf plot used to determine the K_M value for NADH oxidation. Other conditions: Tris-HCl buffer 50 mM, pH 8.0 at 30 ^oC. The working electrode was rotated at 2500 rpm.

5.4.1.4 Affinity towards $NADP^+$

A similar procedure was used to determine the D401K HoxHYFU affinity constant for $NADP^+$ (Figure 115A). From six different experiments, an average K_M value for $NADP^+$ of 1.69 ± 0.27 mM was calculated.

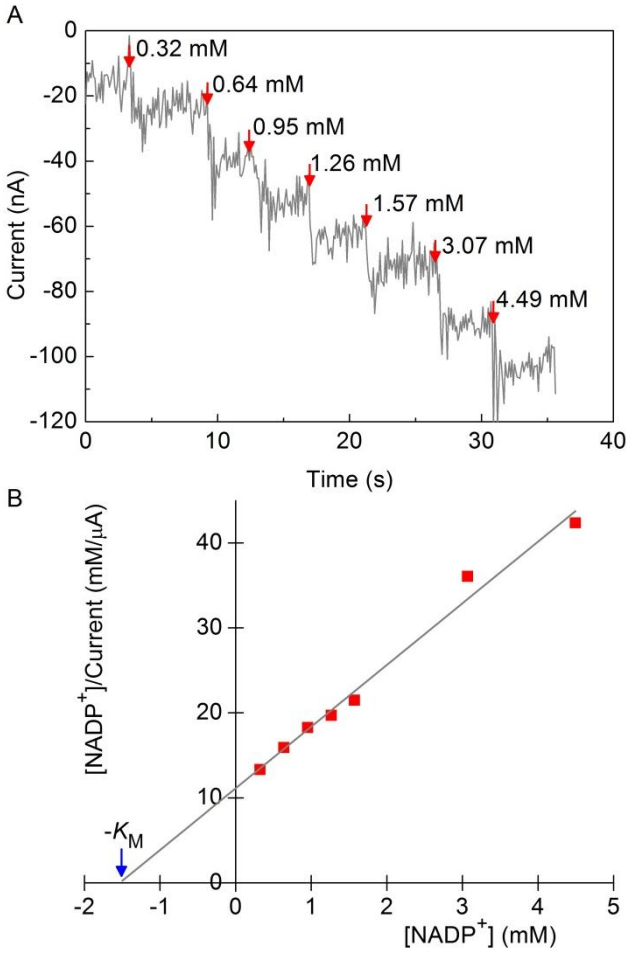

Figure 115. Chronoamperometry experiment designed to determine the affinity constant of D401K HoxHYFU for $NADP^+$ (panel A). Experiment was performed in a Tris-HCl 50 mM, pH 8.0 at 30 ^oC. The working electrode potential was set at -0.412 V and $NADP^+$ stock solutions were injected into the electrochemical cell as indicated. The electrode was rotated at 2500 rpm during the course of experiment. A typical Hanes-Woolf plot used to determine the K_M value is shown in panel B.

The value obtained is four times lower than the value calculated for the wild type HoxHYFU suggesting that mutation of the aspartate residue increases the variant affinity towards $NADP^+$.

5.4.1.5 Potential dependent Inactivation

It is also important to assess whether the variant is susceptible to low potential inactivation as found for the wild type HoxHYFU and HoxFU. Figure 116 shows cyclic voltammograms recorded at a slow scan rate of 1 mV/s at different NAD^+

concentrations. In Panel A, the enzyme film was placed in a solution of 50 μM NAD^+ and at around -0.44 V a decrease in the catalytic current magnitude was observed. There was, however, no sign of activity recovery on the return scan of the first cycle (red line) and on the second cycle, only a small fraction of the catalytic activity remained. This shows that the variant is still susceptible to low potential inactivation.

The variant was placed in a solution of 2 mM NAD^+ in the experiment shown in panel B. Inactivation is now less pronounced and on the second cycle approximately 50 % of the original catalytic activity was still observed. Experiments performed in the presence of both substrates (NAD^+ and NADH) while keeping the total concentration at 2 mM as shown in Figure 116C revealed no significant difference in catalytic behaviour compared with panel B; inactivation at low potentials was observed even in the presence of both substrates.

This set of experiments shows that changing the aspartate residue does not protect the variant from inactivation at low potential. There is, however, a small shift in the starting potential at which the catalytic activity begins switching off at low NAD^+ concentration. At 50 μM NAD^+, the catalytic activity of wild type HoxHYFU begins to switch off at around -0.5 V while in D401K HoxHYFU variant, at the same NAD^+ concentration, the decrease in catalytic current begins at -0.44 V. This observation may be related to the high K_M for NAD^+ of this variant compared to the wild type HoxHYFU.

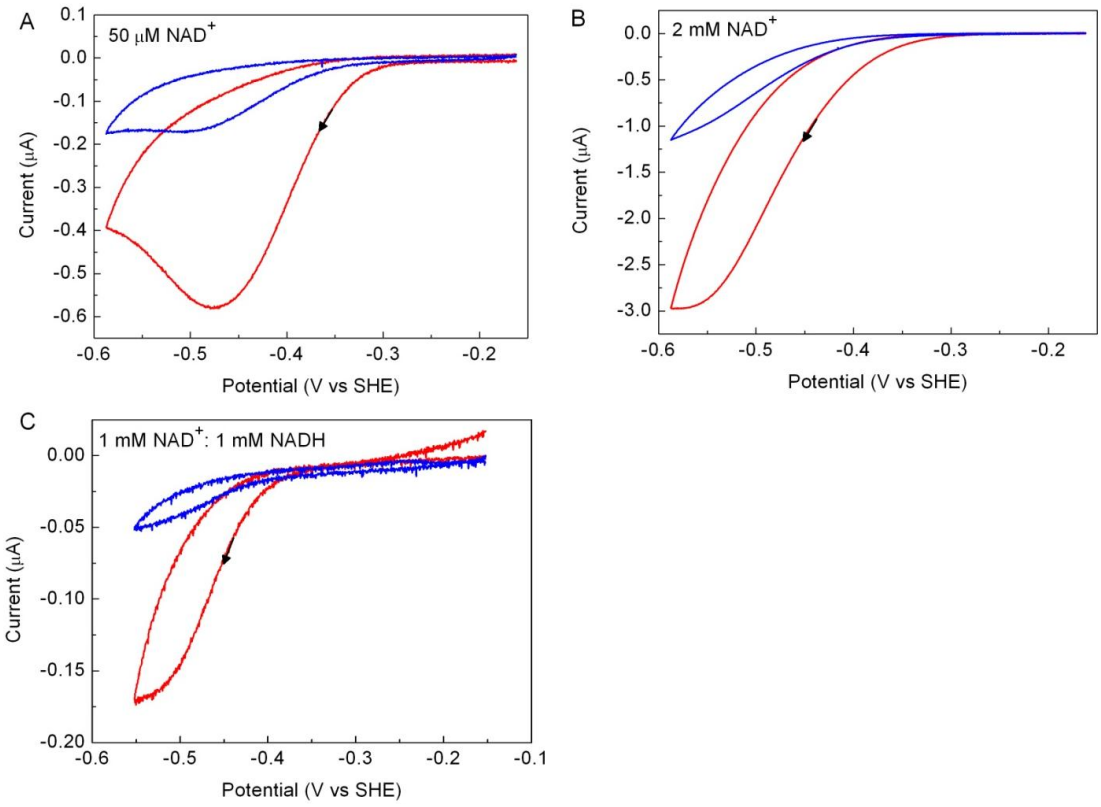

Figure 116. Cyclic voltammograms showing irreversible inactivation of D401K HoxHYFU at low potentials at different substrates concentrations; (A) 50 μM NAD^+, (B) 2 mM NAD^+ and (C) 0.25 mM NAD^+ and 1.75 mM NADH. In each case the scan rate was 1 mV/s, the electrode was rotated at 2500 rpm and other conditions were: 50 mM Tris-HCl buffer, pH 8.0 at 30 ^oC. The first cycle is shown as a red line and second cycle is shown as a blue line.

The variant was designed to increase the SH affinity towards NADP(H), and as shown in Figure 113, this D401K HoxHYFU variant is electrocatalytically active in $NADP^+$ reduction, with a K_M for $NADP^+$ found to be of 1.69 ± 0.27 mM. The low potential inactivation observed for this variant during NAD^+ reduction raises the question of whether this variant will also inactivate at low potential in the presence of $NADP^+$. Therefore, electrochemical experiments as shown in Figure 117 were performed to check for low potential inactivation.

The experiment shown in panel A was performed by placing the enzyme modified electrode in a solution containing 0.5 mM purified $NADP^+$, and the electrode potential was swept between -0.18 V and -0.52 V. The experiment was performed at

this concentration to check for the ability of the HoxHYFU D401K variant to reduce $NADP^+$ at concentrations lower than the K_M for $NADP^+$. At the commencement of the scan, there was no catalytic current observed and at approximately -0.3 V, an increase in the current magnitude was recorded indicating that the variant started to reduce $NADP^+$. The catalytic current magnitude is expected to increase upon scanning towards more negative potentials, as more driving force for $NADP^+$ reduction is made available, but as shown in panel A, no significance increase in the catalytic current was recorded. This suggests that low potential inactivation is overlaid on the normal waveshape. On the second cycle (blue line), only a small fraction of catalytic activity was observed.

Cyclic voltammograms shown in panels B and C were performed at much higher $NADP^+$ concentrations: 2 mM (panel B) and 5 mM (panel C). The variant shows clear $NADP^+$ reduction, with no pronounced low potential inactivation at these concentrations. On the second cycle, some catalytic activity was still recorded. These experiments show that the variant is susceptible to inactivation in $NADP^+$ solutions, but that the reaction is less pronounced at higher levels of $NADP^+$.

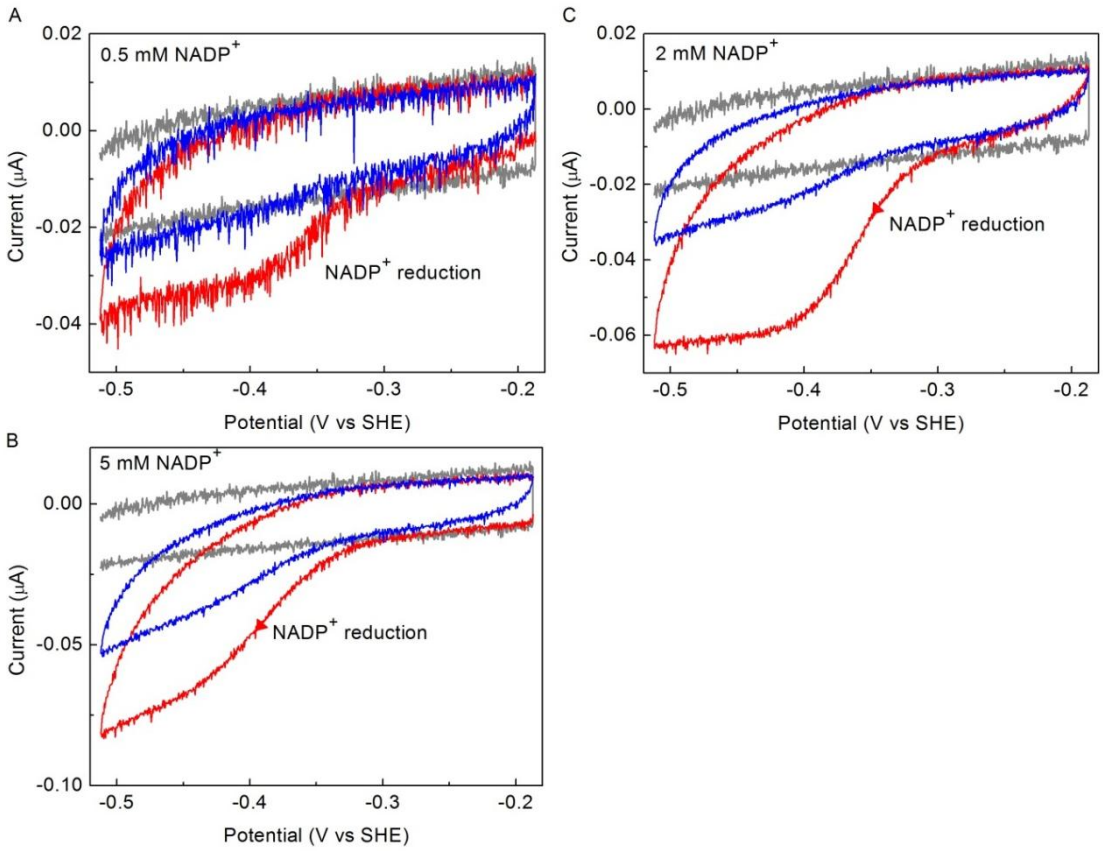

Figure 117. Cyclic voltammograms showing irreversible inactivation of HoxHYFU D401K at low potentials at different substrates concentrations; (A) 0.5 mM $NADP^+$, (B) 2 mM $NADP^+$ and (C) 5 mM $NADP^+$. In each case the scan rate was 1 mV/s, the electrode was rotated at 2500 rpm and other conditions were: 50 mM Tris-HCl buffer, pH 8.0 at 30 ^oC. The first cycle is shown as a red line and second cycle is shown as a blue line.

5.4.2 Overall electrochemical data for variants

Alongside the HoxHYFU D401K variant discussed in Section 5.4.1, electrochemical experiments were performed for other variants and a summary of the electrochemical data is shown in Table 5-3 (selected PFE data are shown in Appendices 2, 3 and 4):

Table 5-3. Summary of electrochemical data for variants investigated in this Thesis.

Variant	NAD(H) catalysis	$NADP^+$ reduction	K_M			K_I		Inactivation at low potential
			NAD^+ (μM)	NADH (μM)	$NADP^+$ (mM)	NAD^+ (μM)	NADH (μM)	
HoxHYFU Wild Type	active	active	357	63	8.0	ND[2]	ND[2]	Observed at low $[NAD^+]$
HoxHYFU D401K	active	active	544	158	1.70	300	250-400	Observed at low $[NAD^+]$
HoxHYFU D326K	active	active	603	494	4.15	300-400	400-500	Observed even at 2 mM $[NAD^+]$
HoxHYFU D467S	active	active	642	302	2.91	100	100-200	Observed even at 2 mM $[NAD^+]$
HoxHYFU D340A	active	active	ND[1]	ND[1]	ND[1]	ND[1]	ND[1]	ND[1]
HoxHYFU E341A	active	active	ND[1]	ND[1]	ND[1]	ND[1]	ND[1]	ND[1]
HoxHYFU E341H	active	active	ND[1]	ND[1]	ND[1]	ND[1]	ND[1]	Observed even at 2 mM $[NAD^+]$
HoxHYFU D401K D340A	active	active	932	360	2.3	100-500	400-700	Observed at low $[NAD^+]$
HoxHYFU D467S E341A	active	active	714	ND[2]	ND[2]	ND[2]	ND[2]	Observed even at 2 mM $[NAD^+]$
HoxHYFU D401K D326K	active	active	900	700	ND[2]	ND[2]	ND[2]	Observed at low $[NAD^+]$
HoxFU Wild Type	active	active	197	58	8.30	200-300	100-300	Observed at low $[NAD^+]$
HoxFU D340A	active	active	ND[1]	ND[1]	ND[1]	ND[1]	ND[1]	ND[1]
HoxFU E341A	active	active	ND[1]	ND[1]	ND[1]	ND[1]	ND[1]	ND[1]

ND[1]: not determined due to very low catalytic activity. ND[2]: not determined in this Thesis but experiments are still on-going.

All variants studied in this Thesis were found to be electrocatalytically active in reducing NAD^+, which indicates that the mutagenesis performed has not damaged the enzyme completely. Some of the variants, for example HoxHYFU D340A, HoxHYFU E341A and HoxHYFU E341H, however, showed relatively low catalytic activities and poor stability over time on the electrode and during low temperature storage of the protein samples and were therefore difficult to analyse electrochemically. The positions of the mutations in these variants are very close to the FMN catalytic centre, in fact Asp^{340} and Glu^{341} have been shown to be directly involved in binding of NADH in Complex I. Mutagenesis at these sites may have interrupted NAD^+ binding by changing the ideal position for direct hydride transfer between the FMN and NAD^+, thus resulting in a low catalytic activity. More comprehensive electrochemical investigations were performed on the variants with high catalytic activities such as HoxHYFU D467K and HoxHYFU D401K. Mutations in these variants, although a bit far from the FMN catalytic centre, are part of the Rossmann fold that contributes to binding the substrate. It is believed that these residues act as a gateway for NAD(H) binding during catalysis and they may prevent access of NADP(H) that contains an extra negatively charged phosphate to the catalytic centre. Site directed mutagenesis performed at these residues was shown to decrease the variants' affinities towards NAD^+ and NADH. For instance, HoxHYFU D467S variant (the negatively charged aspartate was changed to an uncharged but polar serine residue) exhibits a K_M value of 642 μM for NAD^+ reduction, which is two times higher than the value calculated for the wild type enzyme. Most variants studied also showed an increased affinity towards $NADP^+$. This finding indicates that site directed mutagenesis performed on the variants by changing the negatively charged residues has partially worked to lower the discrimination of the SH for NAD^+ over $NADP^+$. The electrochemically determined K_M values for $NADP^+$ of the

variants, however, are still in the millimolar range, and further improvements in affinity for $NADP^+$ are desirable. A millimolar K_M value may still be regarded as high if these variants are to be exploited in cofactor regeneration systems, as K_M corresponds to the substrate concentration at which the enzyme is at half of its maximal catalytic activity.

Cyclic voltammetry experiments performed on the highly active variants also show that catalysis for NAD^+ reduction and NADH oxidation is reversible and efficient in both directions with a minimal overpotential requirement. Most of the variants studied exhibit irreversible low potential inactivation that is dependent on the substrate concentration. However, a few variants such as D326K HoxHYFU and D467S/E341A HoxHYFU show low potential inactivation even at higher substrate concentrations (tested up to 5 mM NAD^+): this suggests that it may be possible to tune the extent of inactivation of the SH.

Further improvements of the purification and protein engineering are necessary prior to use of the variants in a practically applicable cofactor regeneration system for NADP(H). As an alternative strategy, it may be possible to isolate the diaphorase modules of NADP-dependent [NiFe]-hydrogenase enzymes such as Hydrogenase II of *Pyrococcus furiosus*[243] or *Synechocystis* sp. PCC 6803.[244] The Hydrogenase II of *Pyrococcus furiosus* for example has a K_M value for $NADP^+$ of 17 μM.[243] This value is 100-fold lower than the K_M value of D401K HoxHYFU and may be a good option for NADPH regeneration.

5.4.3 HoxHYFU D401K/D340A

The D401K/D340A HoxHYFU prepared by the Humboldt Universität shows the first reversible $NADP^+$ reduction and NADPH oxidation on an electrode (Figure 118).

The voltammograms cross the zero current potential efficiently suggesting that this variant catalyses these reactions efficiently *i.e.* the theoretical $E(NAD^+/NADH)$ at this concentration is -0.368 V compared to the experimental $E(NAD^+/NADH)$ value of -0.361 V.

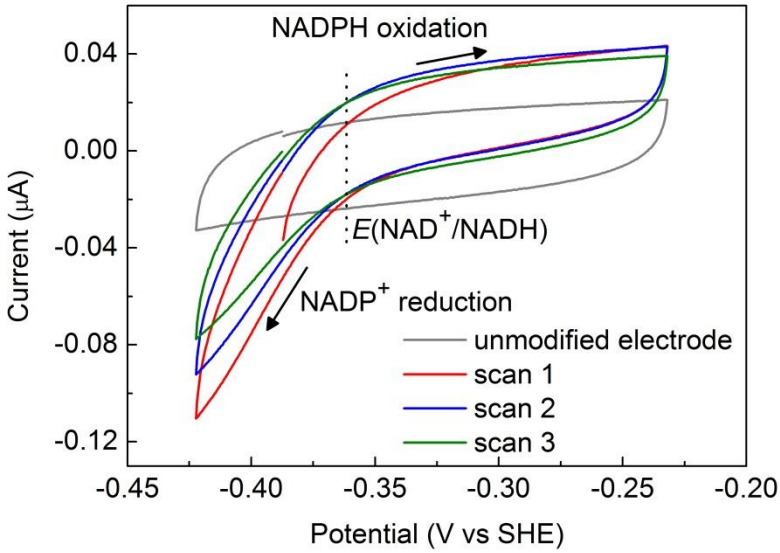

Figure 118. Cyclic voltammetry experiments on HoxHYFU D401K/D340A variant showing reversible $NADP^+$ reduction and NADPH oxidation catalysis on a PGE electrode. Experiments were executed in a solution of 3 mM purified NADPH and 1 mM purified $NADP^+$. Other conditions: Tris-HCl buffer 50 mM at pH 8.0, 30 ^oC. The working electrode was rotated at 2500 rpm with scan rate of 5 mV/s.

5.5 Summary

This Chapter discussed attempts made to increase the SH affinity towards $NADP^+$ and NADPH. In the first part of this Chapter, electrochemical experiments were performed to characterise HoxHYFU wild type. As shown in Section 5.2, the wild type HoxHYFU electrocatalytic properties are not so different to that of HoxFU diaphorase moiety. This suggests that both enzymes are fully functional on a graphite electrode and that separation of HoxHY (which carries the hydrogen cycling moiety in the SH) does not perturb the diaphorase activity. Electrochemical findings on the ability of HoxFU

and HoxHYFU moieties to catalyse $NADP^+$ reduction and NADPH oxidation were explored and discussed. Cyclic voltammetry experiments confirm that HoxFU is able to catalyse these reactions although the catalysis only occurs when the enzyme is exposed to a high concentration of $NADP^+$ or NADPH. Meanwhile HoxHYFU can catalyse $NADP^+$ reduction but no evidence for NADPH oxidation was observed in cyclic voltammetry. The electrocatalytic activity observed for these reactions for both moieties was found to be lower than that of NAD^+ reduction and NADH oxidation. In terms of HoxFU affinity towards $NADP^+$ and NADPH, chronoamperometry experiments show that the K_M values are in the range of millimolar for both reactions. These values indicate a low affinity for $NADP^+$ and NADPH, as the K_M values for NAD^+ and NADH are in the range of micro-molar. Chronoamperometry experiments also showed that NAD^+ reduction and NADH oxidation reactions catalysed by HoxFU are not inhibited by either $NADP^+$ or NADPH, probably because of the much higher affinity of the enzyme for its native substrate which competes effectively for the binding site.

Since its discovery in 2005, subunits HoxI have been proposed to harbour an extra binding site for NADPH. Electrochemical experiments performed under analogous conditions to that of HoxFU experiments, however, did not show any significance difference between these sub-complexes, suggesting that the $NADP^+$ reduction activity is associated with the normal catalytic FMN site, similar to NAD^+ reduction.

Most of the variants studied in this Thesis show an increase in the affinity towards $NADP^+$, which also suggests that site directed mutagenesis performed on these variants has been somewhat successful in favouring catalysis of $NADP^+$ reduction. This finding is important as it opens up the possibility of utilising these variants in many important enzyme based industrial reactions that require NADPH as a cofactor. Possible applications are discussed further in the next Chapter.

Chapter 6: Applications

6.1 Introduction

Chiral chemicals including alcohols, amino acids and esters are often required as starting materials in the industrial synthesis of chemicals and pharmaceuticals.[245, 246] One way of achieving a high enantiomeric excess ee, is by using redox enzymes, due to their high degree of chemo-, regio- and stereo-selectivity compared to conventional chemical synthesis processes. Redox enzymes can be applied not only to produce desired enantiomers from a prochiral starting material, but can also be utilised to purify a racemic mixture by selectively reacting with a single enantiomer.[103, 246-250] Specific enzymatic catalysis also lowers the number of by-products produced thus minimising the need to separate the desired product at the end of the reaction. Table 6-1 shows selected industrial reactions that utilise redox enzymes as catalysts. The high ee values indicate that the enzymes produce extremely stereochemically pure products.

Table 6-1. Examples of enzyme-catalysed reactions used in industry, [251] nd implicates 'not disclosed'. DH represents dehydrogenase.

Product	Enzyme used	Yield (%)	ee (%)	Scale	Company
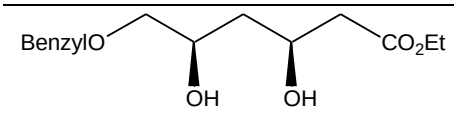	*Acinetobacter calcoaceticus* (cell extract)	92	99	nd	Bristol-Myers Squibb
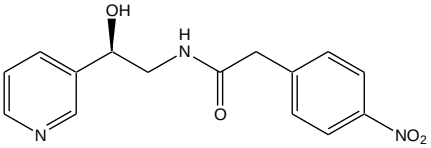	*Candida sorbophilia*	82.5	> 98	Multi kg	Merck
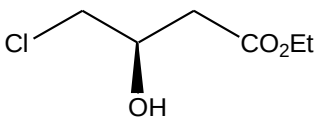	*Geotrichium candidum*	95	99	Multi kg	Bristol-Myers Squibb
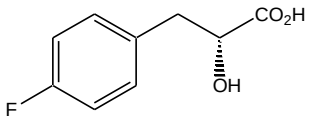	*Staphylococcus epidermidis* (isolated DHs)	99	99	Multi kg	Pfizer
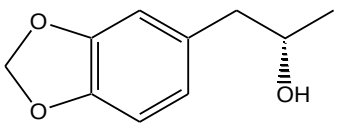	*Zygosaccharo-myces rouxii*	96	> 99.9	300 L	Eli Lilly

Redox enzymes employed in biosynthetic industrial reactions normally require the presence of cofactors in a stoichiometric amount to act as a source or sink of electrons.[252-254] The cofactors required can be found bound or attached to the enzyme structure, such as flavin adenine dinucleotide (FAD), flavin mononucleotide (FMN) and heme groups. However, the common cofactors needed such as NAD^+, NADH, $NADP^+$ and NADPH exist as soluble components which interact transiently with the enzymes and these cofactors are extremely expensive when needed in stoichiometric quantities in industrial reactors.[248, 252, 254]

There are several techniques employed to regenerate the cofactors during a reaction, with enzymatic approaches favoured over chemical methods.[247, 255, 256] For example, an enzyme that uses both the reduced and oxidised forms of the cofactor can be applied to catalyse the desired biotransformation using one substrate while at the same time, regenerating the cofactor using a sacrificial substrate.[246, 257] A second dehydrogenase which is highly specific for the sacrificial co-substrate can also be introduced. A well-established industrial enzymatic approach for regeneration of NADH is by using *Candida boidinii* formate dehydrogenase which oxidises formic acid to carbon dioxide.[258] This regeneration system is employed on a tonne scale by Degussa for the production of L-*tert.* leucine (Figure 119). As the by-product of this reaction is gaseous CO_2, it is easily separated from the desired product, L-*tert.* leucine and the reaction equilibrium is shifted towards producing NADH, making the desired reaction thermodynamically favourable.

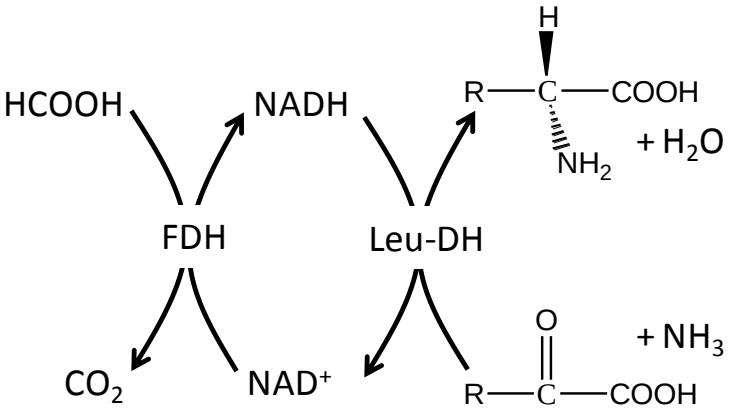

Figure 119. Production of L-*tert*. leucine. FDH and Leu-DH represent formate dehydrogenase and leucine dehydrogenase respectively.[258]

A selection of enzymatic based NAD(P)H regeneration systems is shown in Table 6-2. Regeneration of NAD(P)H using glucose dehydrogenase is increasingly popular due to the fact that glucose dehydrogenase has a higher specific activity than formate dehydrogenase. However, as can be seen from Table 6-2, this system produces a high amount of gluconic acid as a co-product giving lower atom efficiency than the system utilising formate dehydrogenase.

Table 6-2. Common co-substrates and catalysts used for regeneration of NAD(P)H.[251]

Co-substrate	Co-product	Catalyst	g (co-product) per mole of NAD(P)H	ref
Glucose	Gluconic acid	Glucose dehydrogenase	196	[259]
Isopropanol	Acetone	Alcohol dehydrogenase	58	[259]
Ethanol	Acetic acid	Aldehyde dehydrogenase/ alcohol dehydrogenase	30	[260]
Formic acid	CO_2	Formate dehydrogenase	44	[259]
H_2	H_2O	Hydrogenase	18	[261, 262]

Electrochemical steps as illustrated in Figure 120 have also been suggested for cofactor regeneration, however, this approach has not been applied in industrial scale

applications.[254] Some advantages of this technique are that no co-substrate is necessary and the process uses electricity, which is cheap compared to enzymes and sacrificial substrates.[247, 252] However, drawbacks of electrochemical cofactor regeneration are the large overpotential requirement for direct $NAD(P)^+$ reduction and NAD(P)H oxidation on most bare electrodes, and the formation of dimers and other biologically inactive cofactor forms which have no further use.[247, 263, 264] To counter these problems, several approaches have been developed. One example is the use of a mediator that will shuttle electrons between the electrode surface and the cofactor, so that the nicotinamide cofactors are reduced or oxidised in solution.[252, 257] Organic dyes such as *N*-methyl-phenazinium, 1-methoxy-*N*-methyl-phenazinium and Medola Blue have been used as potential mediators for minimising the overpotential requirement for NAD(P)H oxidation on bare electrodes. Gründig and coworkers reported that when *N*-methyl-phenazinium was immobilised onto a graphite-epoxy electrode, the overpotential for NADH oxidation was lowered by approximately 0.3 V and the electrode showed stability for over 15 days.[265] Although mediators may have managed to lower the overpotential, often the electron transfer between mediator and NAD(P)H is slow. The usage of a second enzyme that will regenerate the cofactor while at the same time, undergo redox reactions with a mediator has also been reported.[254, 263, 264] These approaches help in minimising the overpotential requirement and a substantial increase in the production of enzymatically active cofactors is observed.[264] The reliance on mediators, however, means that cofactor recycling is dependent on diffusion-controlled transfer of mediators to/from the electrode.[252] The mediator also needs to be chosen carefully so that a minimal overpotential (less extra energy) requirement for cofactor regeneration is achieved.

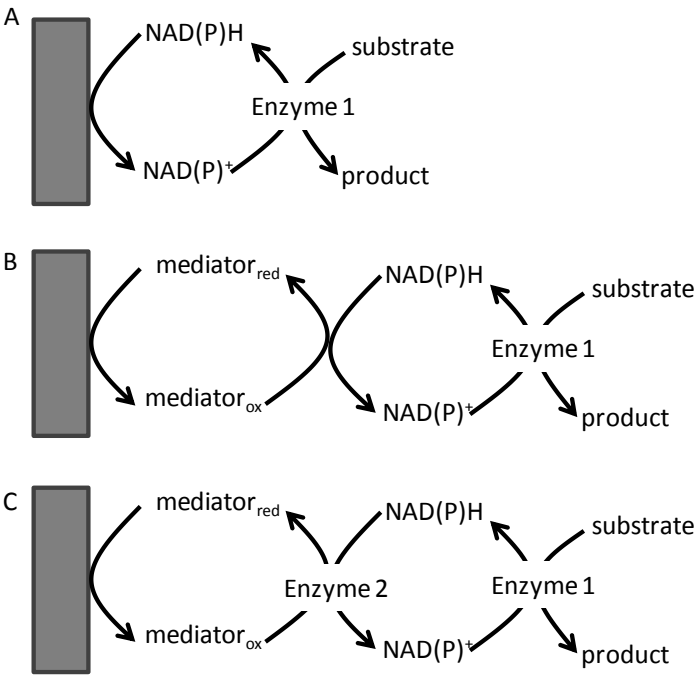

Figure 120. Schematic representation of the possible methods for regenerating oxidised cofactors via electrochemical reactions, for substrate transformation by Enzyme 1.

One way of achieving a high cofactor regeneration rate is by using diaphorase enzymes that have minimal overpotential. In Chapters 3, 4 and 5 of this Thesis, it is shown that the HoxFU diaphorase and HoxHYFU moieties of *R. eutropha* are electrocatalytically active and efficient catalysts for recycling of NAD(H). In this Chapter, the possibility of utilising the HoxFU moiety for NAD(H) regeneration will be explored.

6.2 Particles for H_2-driven cofactor recycling

6.2.1 The thermodynamics of the reaction

The ability of HoxFU moiety to catalyse NAD^+ reduction and NADH oxidation efficiently has opened up the possibility of utilising this subcomplex domain for cofactor regeneration. Early research on recycling NADH by exploiting the SH was performed by Schneider and coworkers; they covalently immobilised the SH onto corn

stover particles to support continuous lactate formation by NADH-dependent lactate dehydrogenase. In their experiments, over a period of 45 hours, a total of 1612 µmol lactate was collected which was equivalent to 111 NADH regeneration cycles.[101] Very recently, Ansorge-Schumacher and coworkers showed that the SH exhibits up to 143 666 turnovers when coupled to *Candida parapsilosis* carbonyl reductase.[217, 266] The high turnover number is superior to that of *Candida boidinii* formate dehydrogenase, which is commonly used for NADH recycling.[267, 268] The regeneration system presented by Ansorge-Schumacher, however, is subject to high sensitivity towards changes in temperature, pH and mechanical stress of the reactor system.[217] These findings confirm that specific conditions must be met before the SH (or HoxFU) is utilised in a cofactor regeneration system.

As discussed earlier in this Thesis, the NAD^+/NADH cycling of the HoxFU moiety is coupled to H_2/H^+ cycling in the SH, providing the cell with reducing equivalents in the form of NADH from H_2 oxidation.[13, 21] Electrochemical experiments performed on HoxHY hydrogenase and HoxFU diaphorase moieties show that these reactions proceed efficiently, with minimal overpotential requirement.[77, 94, 220] The potentials for these reactions are very close to each other and dependent on pH as predicted by the Nernst equation.

For the hydrogen production reaction

$$2\mathrm{H}^+ + 2\mathrm{e}^- \rightarrow \mathrm{H}_2 \qquad [34]$$

the Nernst equation is given by equation [35],

$$E = E^o - \frac{2.303\mathrm{RT}}{n\mathrm{F}} \log\left(\frac{[\mathrm{H}_2]}{[\mathrm{H}^+]^2}\right) \qquad [35]$$

where E^o is the formal potential for the couple, R, T and F are the gas constant, temperature and Faraday's constant respectively. The number of electrons involved in the reaction is termed *n*. At room temperature, RT/F is 26 mV. Solving equation [35] will now give an expression relating *E* with log [H_2] and log [H^+]: equation [36].

$$E = E^o - 29.939(\log[\mathrm{H_2}] - 2\log[\mathrm{H^+}]) \qquad [36]$$

(where the potential are in mV).

Since pH is equal to –log [H^+], equation [36] simplifies to become equation [37],

$$E = E^o - 29.939(\log[\mathrm{H_2}] + 2\mathrm{pH}) \qquad [37]$$

which now confirms that the potential of the hydrogen half reaction is lowered by 59 mV per pH unit.

Similarly, for NADH formation

$$\mathrm{NAD^+ + H^+ + 2e^- \rightarrow NADH} \qquad [38]$$

the Nernst equation is given by equation [39].

$$E = E^o - \frac{2.303\mathrm{RT}}{n\mathrm{F}} \log\left(\frac{[\mathrm{NADH}]}{[\mathrm{NAD^+}][\mathrm{H^+}]}\right) \qquad [39]$$

Solving equation [39] yields equation [40],

$$E = E^o - 29.939 \left(\log\left(\frac{[\mathrm{NADH}]}{[\mathrm{NAD^+}]}\right) + \mathrm{pH}\right) \qquad [40]$$

which confirms that NAD^+/NADH cycling is also pH dependent, and the potential of NAD^+/NADH couple is lowered by 30 mV for each factor of ten change in the

hydrogen ion concentration (pH unit). Thus the NAD^+/NADH couple changes less steeply with pH than the H_2 couple.

At pH 7.0, 25 ^oC, 1 bar H_2, the relationship between the NAD^+/NADH and $2H^+/H_2$ potentials at different ratios of NADH/NAD^+ can thus be illustrated by Figure 121.

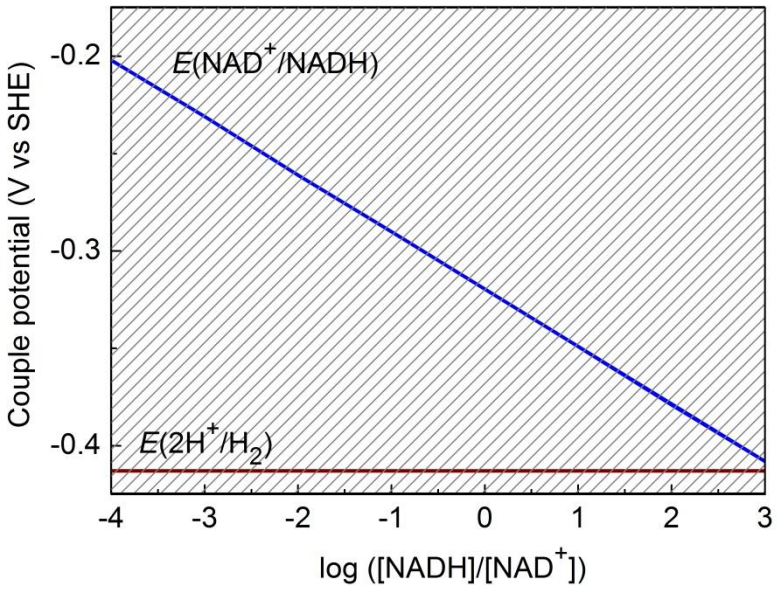

Figure 121. The relationship between $E(NAD^+/NADH)$ with that of $E(2H^+/H_2)$ at different NADH/NAD^+ ratios for conditions at pH 7.0, 1 bar H_2 and 25 ^oC.

Theoretically, regeneration of NADH coupled to H_2 oxidation is possible providing that the $E(NAD^+/NADH)$ potential is less negative than $E(2H^+/H_2)$ as shown for all ratios in Figure 121. The greater the difference in couple potentials, the higher the driving force. For this to be achieved, several factors such as a constant supply of H_2 and a higher concentration of NAD^+ than NADH in the system throughout experimental procedures must be taken into account. Apart from that, the enzymes that will be utilised must also be catalytically active under the experimental conditions required. Experiments described in this Section utilise platinised graphite particles and enzymes adsorbed onto graphite particles for the regeneration of NADH.

6.2.2 Using HoxFU and Platinised Particles

(Experiments described in this Section were performed by Miss Holly Reeve, former Part II student in the group under my supervision.)

As mentioned earlier, a vast number of oxidoreductases that may be useful in producing chiral compounds require NADH as a cofactor in a stoichiometric quantity, making the ability to develop a regeneration system highly desirable. Due to the close separation between $E(NAD^+/NADH)$ and $E(2H^+/H_2)$, these reactions will only proceed spontaneously if catalysts are available to facilitate the reactions at minimal overpotential. Chapter 3 showed that HoxFU is an excellent catalyst for NAD^+ reduction and NADH oxidation. Platinum on the other hand, is an excellent catalyst for H_2 oxidation and H^+ reduction because it operates close to the theoretical $E(2H^+/H_2)$ giving a greater driving force throughout the reactions. Platinum has also been shown to be able to oxidise NADH, however, this reaction only occurs at a very high overpotential, so is not expected to be significant under the experimental conditions described in this Section. This Section will investigate the ability of HoxFU to regenerate NADH using electrons provided by H_2 oxidation at Platinum.

Experimental procedures as described in Chapter 2 were employed for preparing the platinised graphite particles. The platinised particles were collected into a 1.5 mL vial and 50 µL Tris-HCl 50 mM pH 8.0 buffer was added and the mixture was sonicated for 10 seconds. The particle suspension was split into two samples, one being a control. To the control sample, 5 µL buffer was added while 5 µL HoxFU was added into the actual experimental sample. Both samples were left at *ca.* 4 ^oC for 30 minutes to allow better enzyme adsorption onto the platinised particles. An aliquot of 100 µL H_2 saturated solution (1 bar H_2) containing 1 mM NAD^+, prepared using the same buffer solution, was added into each vial. To compensate for H_2 escaping from the prepared

solutions, H_2 was bubbled into both vials for 5 minutes and the vials were then sealed with septa. At several time intervals, aliquots of 25 µL were taken from the vials and subjected to centrifugation to remove particles. The aliquots were then diluted with 750 µL buffer and UV-Vis spectra were taken (Figure 122). From the spectra, it is clear that this system is able to produce NADH as the typical peak for NADH at 340 nm increases over time. The decreases in absorbance at 260 nm are also consistent with NAD^+ conversion to NADH.

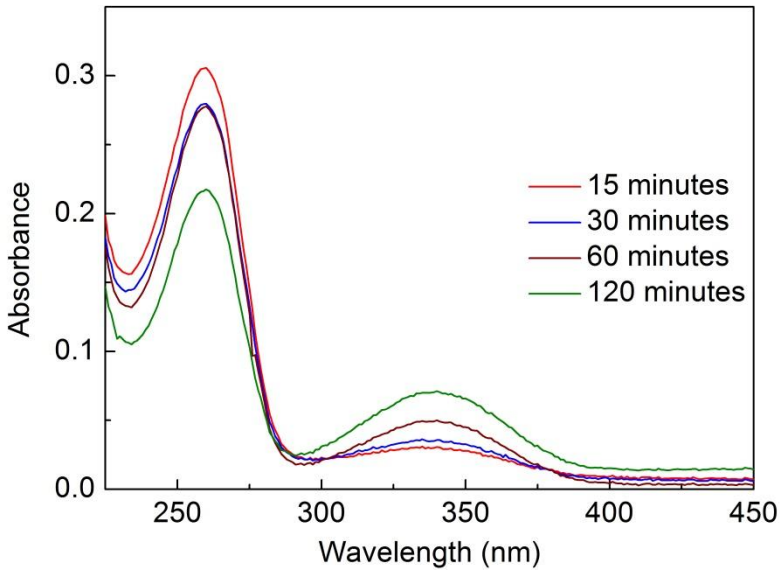

Figure 122. UV-Vis spectra of graphite particles modified with HoxFU and Pt, showing NAD^+ conversion to NADH over time.

Control experiments with no HoxFU present also showed some production of NADH (Figure 123). Comparison of the absorbance magnitude, however, shows that the absorbance at 340 nm for the control samples is much lower than the HoxFU modified platinised particles.

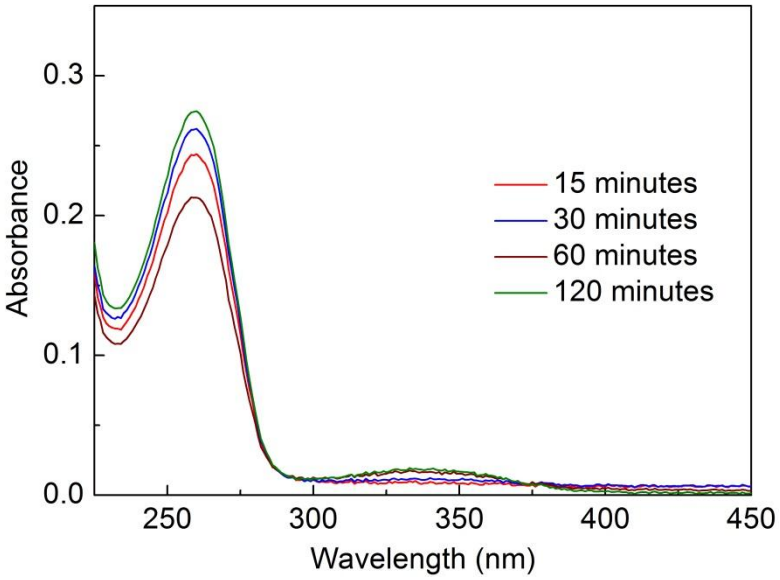

Figure 123. UV-Vis spectra of platinised particles with no HoxFU showing slight production of NADH over time.

To determine the percentage of NADH production in both systems, and to be able to compare the results more quantitatively, ratios of the peaks (at 260 nm and 340 nm) were taken and compared to values from known ratios of NAD^+ and NADH (see Section 2.7). Figure 124 shows a plot of the amount of NADH generated against time confirming that the HoxFU-modified platinised particles produced more NADH during the two hour reaction period than the platinised particles with no HoxFU (grey dots). With the HoxFU-modified platinised particles, approximately 90 % conversion of NAD^+ into NADH after 2 hours was achieved corresponding to a turnover frequency of 0.74 molecules of NADH per second per HoxFU molecule. The rate of NADH production in this system is low in comparison with the activity of HoxFU (approximately 1000 s^{-1})[235] suggesting that this system is far from optimised. For the platinised particles with no HoxFU, only around 1% NADH was produced.

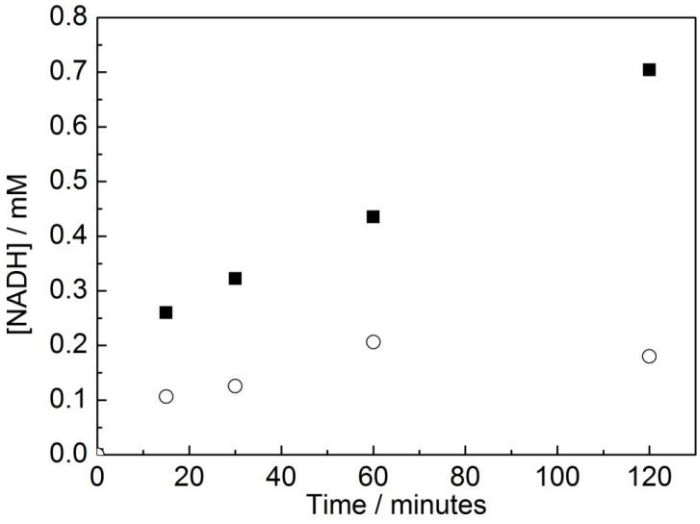

Figure 124. NADH regeneration from HoxFU platinised particles. (from data in Figure 122 and Figure 123). Black squares show the response obtained with HoxFU modified platinised particles while the white circles are the response for control experiments with only platinised particles. Conditions: Tris-HCl pH 8 50 mM, 1 mM NAD^+ at 1 bar H_2.

This set of experiments show that this system is able to function as a tool for generating NADH from NAD^+. The success of this system is most probably due to the fact that H_2 oxidation occurs efficiently at platinum (with negligible overpotential), thus giving a sufficient energetic force for driving NAD^+ reduction by HoxFU. Utilising platinum, however, means that this system cannot be used in the presence of O_2 since platinum is susceptible to O_2 reduction, even with a small quantity of O_2 present. Dioxygen reduction will consume electrons from H_2 oxidation, meaning they are unavailable for NAD^+ reduction by HoxFU.

This leads onto the possibility of using two enzymes, adsorbed onto graphite particles for NADH regeneration experiments: one acting as an electron donor and one as an electron acceptor on conducting particles was suggested by Armstrong and coworkers in 2007 when they coupled highly active *Allochromatium vinosum* NiFe hydrogenase to either *E. coli* nitrate reductase or fumarate reductase using graphite particles.[269] The products; nitrite when nitrate reductase was used and succinate if fumarate reductase was employed, were unambiguously assayed by a simple

colourimetric method for nitrite and NMR for succinate. The success of coupling complementary enzymes onto graphite particles opens the possibility of using any enzymes available for transferring electrons to HoxFU to be utilised for an NADH regeneration system. One particular group of enzymes that is of interest are the so-called 'O_2-tolerant' hydrogenases.[119, 131-133] This group of hydrogenases has been shown to sustain H_2 oxidation in the presence of O_2. In the next section, the membrane bound O_2-tolerant NiFe hydrogenase from *R. eutropha* is utilised as an electron donor for HoxFU. Description of experiments in the next section will begin with efforts to find the best conditions for both enzymes, followed by experiments to check for the ability of these enzymes to produce NADH from NAD^+ on particles.

6.2.3 Finding Suitable Enzymes and Conditions for NADH Regeneration

To utilise coupling complementary enzymes onto graphite particles, it is desirable that enzymes used are not limiting each other and both processes should occur efficiently under analogous conditions. Enzymes are also sensitive to the surrounding conditions, making it necessary to find the best possible conditions for experiments. The *R. eutropha* MBH has been shown to exhibit optimal H_2 oxidation activity at slightly acidic pH. Most electrochemical experiments on HoxFU described in Chapter 3 were performed at pH 8.0, however, HoxFU also exhibits efficient NAD^+ reduction and NADH oxidation over a wider pH range. To bring conditions into a range more suitable for MBH, HoxFU catalytic activity was tested at pH 7.0. Cyclic voltammograms shown in Figure 125 illustrates the ability of HoxFU to catalyse NAD^+ reduction and NADH oxidation at this pH. The voltammograms cross the zero current potential calculated for

this NAD^+/NADH ratio indicating an efficient catalysis with minimal overpotential requirement, particularly for NAD^+ reduction.

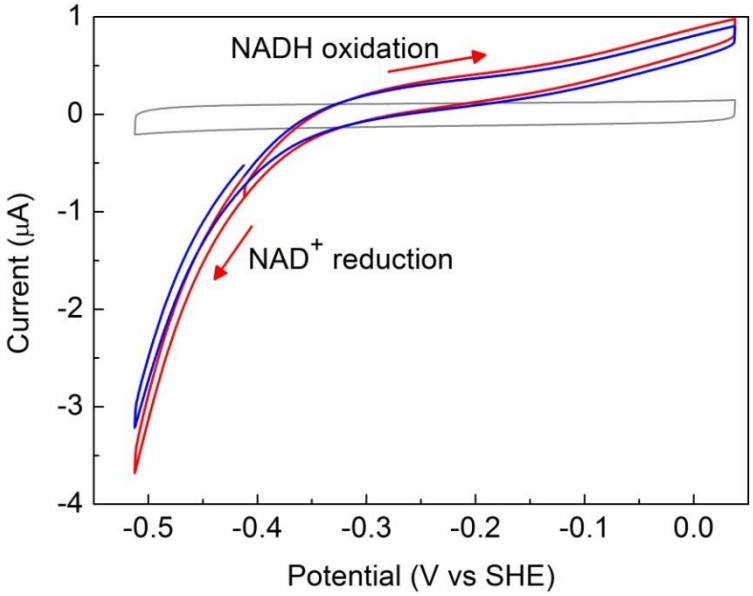

Figure 125. Cyclic voltammograms of a HoxFU modified electrode recorded at pH 7.0 showing NAD^+ reduction and NADH oxidation. Conditions: 1 mM NAD^+ and 1 mM NADH, mixed buffer system, scan rate of 10 mV/s, the working electrode was rotated at 2500 rpm in a temperature-controlled electrochemical cell at 30 ^oC.

Cyclic voltammetry experiments were also performed on the MBH at 1 bar H_2 at pH 7.0 and the corresponding cyclic voltammogram is shown in Figure 126. At pH 7.0, the MBH shows distinctive H_2 oxidation that starts around 0.08 V higher than the theoretical $E(2H^+/H_2)$ value as shown in the figure. This overpotential requirement observed has been reported to be a typical characteristic of the *R. eutropha* MBH and several O_2-tolerant hydrogenases.[56, 57, 119, 132, 133, 166, 167] Another distinctive catalytic property of the *R. eutropha* MBH and several other O_2-tolerant hydrogenases is the lack of H^+ reduction at low potentials under H_2 (the reaction is reported to be strongly inhibited by H_2). At pH 7.0, MBH does not significantly produce H_2 under 1 bar H_2.[166] The H_2 oxidation activity of MBH is switched off at high potentials in an anaerobic environment, and upon sweeping the potential towards more negative values the

enzyme reactivates. This reversible anaerobic inactivation is observed for most of the NiFe hydrogenases and has been assigned to be due to the formation of an inactive state, Ni-B.

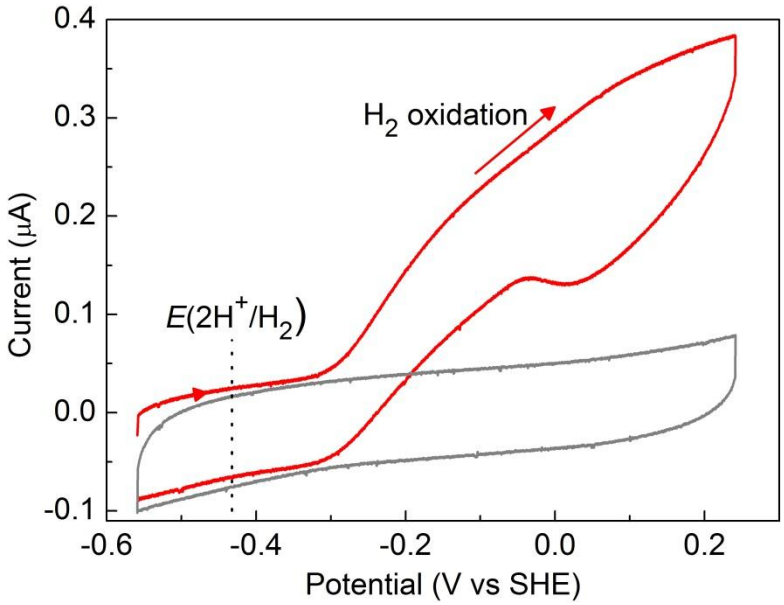

Figure 126. Cyclic voltammogram showing H_2 oxidation catalysed by the NiFe MBH of *R. eutropha*. Experiments were performed at pH 7.0 phosphate buffer (50 mM). Conditions: 1 bar H_2, scan rate of 10 mV/s, working electrode was rotated at 2500 rpm.

Experiments were also performed by mixing both enzymes together at different ratios and spotting the enzyme mixture onto an electrode to find the best conditions for operating both enzymes together. A typical result is shown in Figure 127. Since the MBH has been shown not to be really active in H^+ reduction, the observed negative current at low potentials can be attributed to NAD^+ reduction by HoxFU. Positive current recorded at high potentials is attributed to H_2 oxidation by MBH as no NADH was added to the electrochemical cell during the course of experiments. These experiments show that both enzymes are adsorbed onto the graphite electrode, and exhibit clear H_2 oxidation and NAD^+ reduction activities.

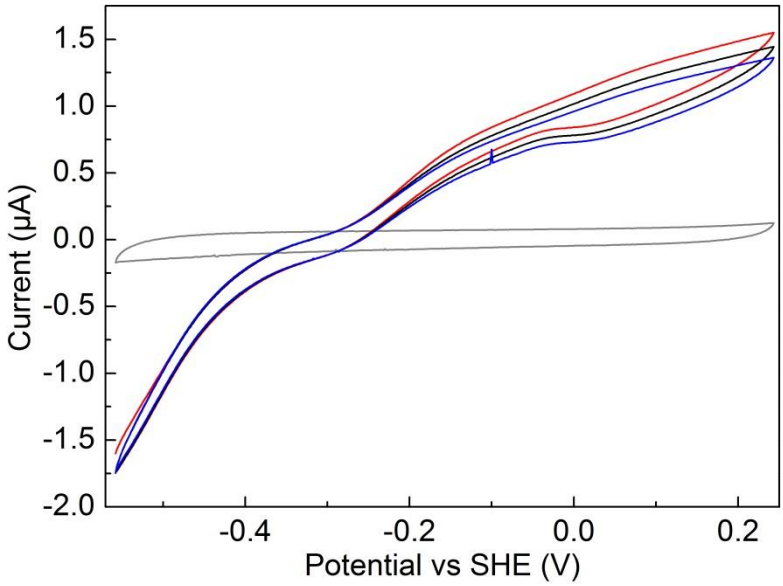

Figure 127. Hydrogen oxidation and NAD^+ reduction by *R. eutropha* MBH and HoxFU adsorbed onto a PGE electrode. A film prepared from equal amounts of HoxFU and MBH was placed in H_2 saturated buffer containing 1 mM NAD^+. The first three scans are shown in red, black and blue recorded overlaid on a voltammogram recorded for an unmodified electrode (grey line). Other conditions: phosphate buffer 50 mM, pH 7.0 at 25 ^oC. Scan rate: 10 mV/s. The working electrode was stationary during experiment.

As the H_2 oxidation by MBH requires an overpotential of around 0.08 V, the actual starting potential for catalysis, E^{onset} is approximately -0.33 V for the MBH. This onset potential must been taken into account for subsequent regeneration experiments as it affect the thermodynamics of NADH regeneration by H_2 oxidation. Figure 128 illustrates the relationship between thermodynamic potentials of NAD^+/NADH and $2H^+/H_2$ at different ratios of NADH/NAD^+ and 1 bar H_2 upon considering the E^{onset} of MBH. From this Figure, it can be shown that the driving force for NADH regeneration using MBH and HoxFU is much lower than with HoxFU modified with platinised particles. The conversion should only occur in the section highlighted in Figure 128 because at low NAD^+ concentrations, the $E(NAD^+/NADH)$ will be more positive than $E(2H^+/H_2)$ making NADH regeneration by H_2 with MBH as a catalyst unfeasible.

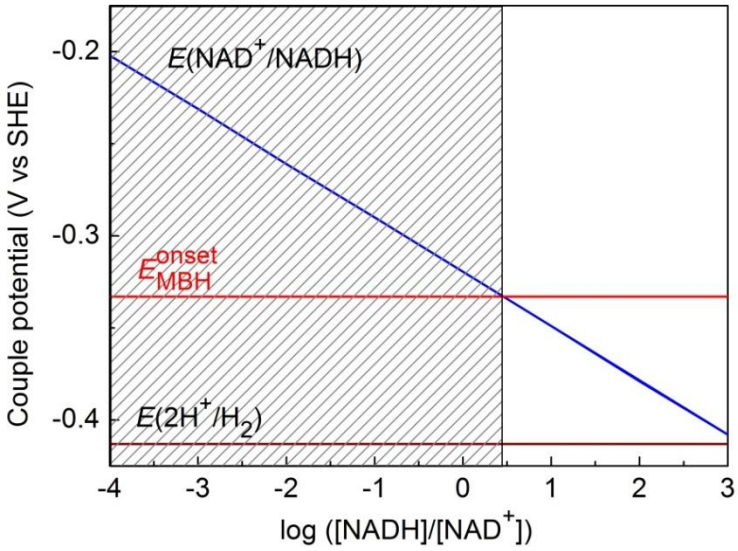

Figure 128. Thermodynamics of the reactions, considering the E^{onset} for MBH.

In place of the MBH, the HoxHY hydrogenase dimer of the SH could also be used for NADH regeneration. The moiety has been shown to catalyse H_2 oxidation and H^+ reduction with minimal overpotential (Figure 129).[77, 220] The moiety, however, is not used for coupling with HoxFU diaphorase for NADH regeneration due to several factors such as the low catalytic activity for H_2 oxidation compared to the MBH. Apart from that, the HoxHY moiety is also biased for H^+ reduction rather than H_2 oxidation at pH 7.0. This shows the preference for utilising MBH and HoxFU for the regeneration system.

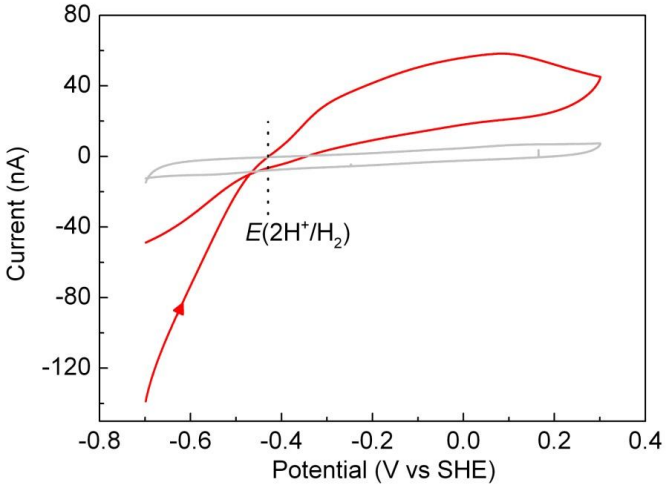

Figure 129. Cyclic voltammogram at an electrode modified with the HoxHY hydrogenase moiety of the SH. Scan recorded in solution saturated with H_2 at pH 7.0 phosphate buffer 50 mM at scan rate 1 mV/s on a stationary electrode. Adapted with permission from refs[77, 220]

Careful experimental procedures employing high concentrations of NAD^+ (1 mM; above the K_M of HoxFU for NAD^+), suitable pH (pH 7.0), 1 bar H_2 and equal amounts of both proteins applied to graphite were selected for the NADH regeneration system explored in the next Section.

6.2.4 Using graphite particles with MBH and HoxFU for NADH regeneration

Two attempts were employed for regeneration of NADH, either by using a graphite rod painted with MBH and HoxFU or by adsorbing the enzymes onto graphite particles. To the first technique, an equal mixture of HoxFU and MBH (10 µL each) was painted to freshly sanded graphite rod and left in a solution of H_2-saturated buffer containing 1 mM NAD^+. Aliquots of solution were taken at various time intervals and UV-Vis spectra were taken to see if any NADH was formed during the reactions. Figure 130 shows a UV-Vis spectrum taken after 120 minutes with a small broad peak at 340 nm confirming the system is able to produce some NADH.

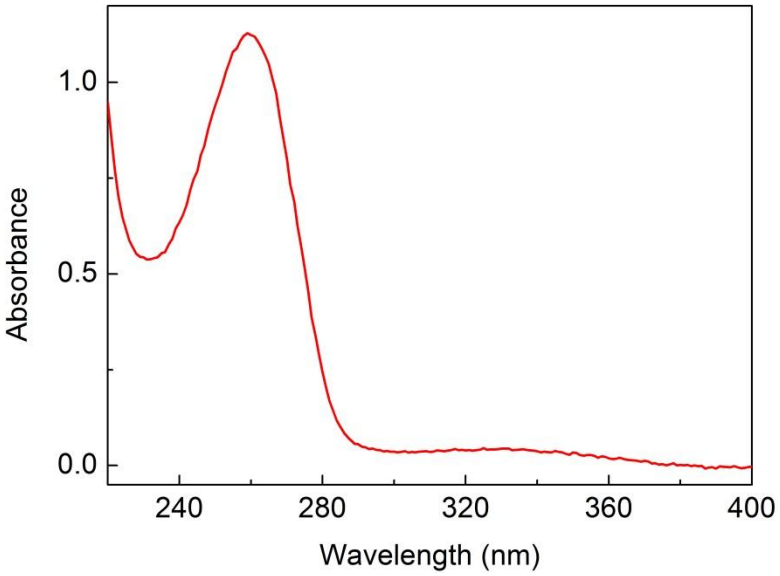

Figure 130. UV-Vis spectrum showing NADH is produced by after an enzyme modified rod was left in 300 µL solution of saturated H_2, 1 mM NAD^+ for 120 minutes.

For the second technique, a graphite block was first sanded with sand paper to get approximately 4 mg of PGE particles. The particles were sonicated for 10 seconds in a 50 µL buffer solution and 25 µL of the suspension was added to a mixture of HoxFU and MBH (2.5 µL each). The enzyme-particle mixture was left at approximately 4 ^oC for 30 minutes to aid enzyme adsorption before H_2 saturated buffer containing 1 mM NAD^+ was added to the vial. The vial was closed with a septum and left stirring for the duration of experiment. Aliquots of the solution were taken and UV-Vis spectra were run to check for NADH formation (Figure 131). As can been seen from the figure, there is an increase in the absorbance at 340 nm suggesting NADH generation from the reaction.

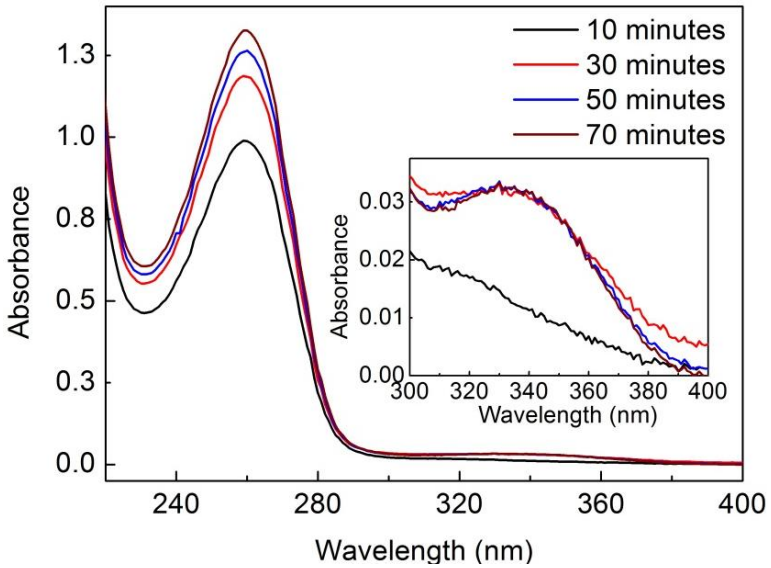

Figure 131. UV-Vis spectra showing peak at 340 nm rises against time, confirming the system works for NADH regeneration.

The systems demonstrated in this Section confirm that NADH generation from H_2 and NAD^+ utilising graphite particles or a graphite rod is possible, due to the ability of both enzymes to adsorb on to graphite. There is, however, a need for optimising the regeneration system to improve the amount of NADH generated. Several factors can be employed to improve the performance of the system such as using more enzyme and increasing the enzyme stability on the particles. The ratio of enzymes used in experiments can also be optimised so that the H_2 oxidation rate matches the NAD^+ reduction rate. A constant removal of NADH generated from the system might also help enhance the system as this will maintain a high relative amount of NAD^+, thus keeping the driving force high and minimising product inhibition of HoxFU. Since the MBH has quite a high overpotential, which in turn limits the driving force for the reaction, utilising a hydrogenase with a lower overpotential requirement would also be a good option. However, hydrogenases with a low $E(2H^+/H_2)$ overpotential are normally sensitive towards O_2 which would make the system ineffective in the presence of O_2. In

the next Section, the possibility of exploiting the NADH regeneration system in the presence of O_2 will be discussed.

6.2.5 NADH regeneration in the presence of O_2.

(Experiments described here were performed by Miss Holly Reeve former Part II student in the group under my supervision.)

Several factors have to be taken into consideration to make sure the regeneration system in the presence of O_2 will work. First of all, in the presence of O_2 the MBH will has a lower catalytic activity and the presence of O_2 will generate an inactive state of the enzyme. The inactive state requires electrons for reactivation which in the system will be provided by the graphite particles. Furthermore direct O_2 reduction will also occur on the graphite particles. These observations mean that fewer electrons will be available for NAD^+ reduction by HoxFU. Apart from that, introduction of 1% O_2 into the system will decrease the amount of H_2 present in the system, thus lowering the catalytic activity of MBH. The lower level of H_2 also means that the thermodynamic driving force for the reaction will change. To compensate for the lower catalytic activity of MBH under these conditions, the amount of MBH used in the experiments was doubled compared to the amount used in Section 6.2.4.

Similar methods of preparing the graphite particles were employed for this experiment as explained in Section 6.2.4. The vial containing enzymes, suspended particles and 1 mM NAD^+ was filled with 99% H_2 and 1% O_2 and sealed. The set up was left stirring continuously for 6 hours before the suspension was collected and centrifuged to obtain NADH that may have been regenerated. Figure 132 shows a UV-Vis spectrum recorded after 6 hours showing a small peak at 340 nm confirming that the regeneration system worked in the presence of O_2.

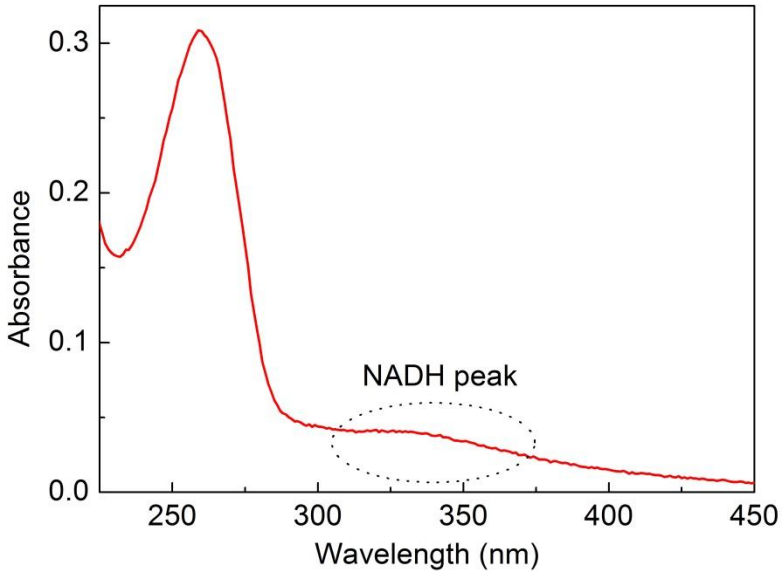

Figure 132. UV-Vis spectrum showing NADH regeneration in the presence of O_2. The set up was left for 6 hours before a UV-Vis spectrum was recorded.

The amount of NADH regenerated from this system was very low (< 1 %). This proof of concept demonstration of H_2-driven NADH production has since been further developed by H. A. Reeve and an improved result is shown in Figure 133.[270, 271]

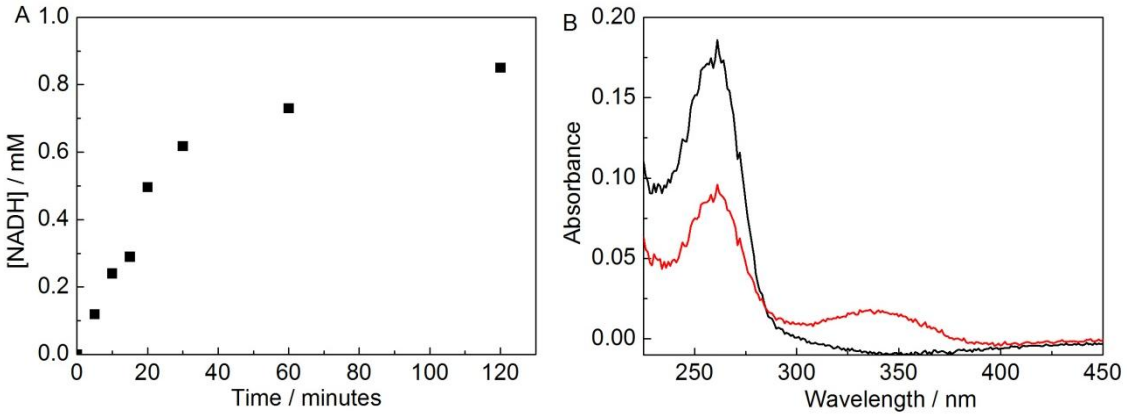

Figure 133. A. Time series of NADH regeneration using H_2 as an electron source, starting with 1 mM NAD^+. B. UV-Vis spectra of a solution of H_2-saturated 1 mM NAD^+ before (black) and after 4.5 hours (red) addition of HoxFU-*E.coli* Hyd2 hydrogenase modified particles. These figures are provided by Holly A. Reeve and modified accordingly.[271]

In the next Section, the concept of using electrochemistry to couple NAD^+ reduction by HoxFU with reduction of pyruvate to lactate by a lactate dehydrogenase will be explored.

6.3 Electrochemical NADH regeneration for coupling HoxFU and Lactate Dehydrogenase on electrode

This Section will discuss the possibilities of utilising HoxFU as an electrocatalyst for NADH regeneration in biotransformations. Results discussed in Chapter 3 confirmed that HoxFU adsorbs onto a graphite electrode, and exhibits excellent electrocatalytic of NAD^+ reduction and NADH oxidation in the presence of NAD^+ and NADH. Experiments discussed in this Section will exploit HoxFU to regenerate NADH for lactate dehydrogenase for the reduction of pyruvate to lactate.

6.3.1 Regeneration of NADH for lactate dehydrogenase

(Experiments described in this Section were initiated by Kate Simpson-Wells (Part II student under my supervision) and were further developed by Z. Idris.)

Lactate dehydrogenase (LDH) is a redox enzyme found in a wide variety of organisms. The LDH reduces pyruvate to lactate (a chiral species) while oxidising NADH simultaneously.[272] The requirement for continuous supply of NADH means that NADH regeneration is necessary and this Section will explore the possibility of exploiting HoxFU as an electrocatalyst for regenerating NADH coupled with LDH activity. Lactate, pyruvate and LDH are chosen as a test system because they are relatively cheap compared to other commercially available dehydrogenases and chemicals. Figure 134 shows a schematic presentation of the two redox enzymes adsorbed onto a graphite electrode. Since LDH requires electrons in the form of hydride ion (H^-) for reduction of pyruvate, direct electrochemical reduction of pyruvate on a

graphite electrode is not possible. The reduction of pyruvate will use NADH, thus producing NAD^+ which will then be recycled by HoxFU. The electrode potential is set at -0.412 V to give the driving force necessary for NADH production by HoxFU.

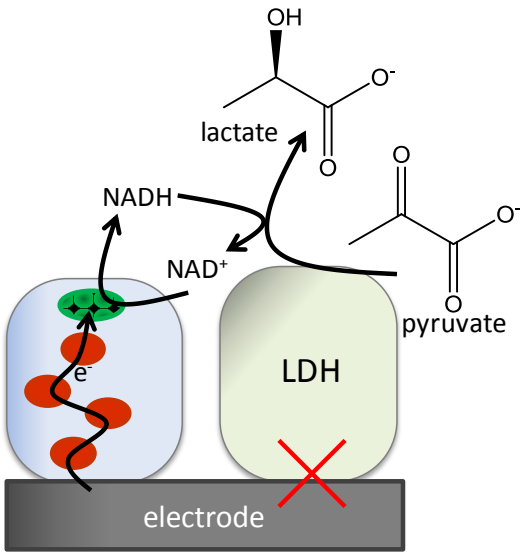

Figure 134. A scheme showing an ideal coupling of the diaphorase, HoxFU and lactate dehydrogenase onto a graphite electrode. The cross indicates that the LDH is unable to receive electrons from graphite electrode.

Chambers and coworkers recently reported the impact of high pyruvate concentrations on the catalytic activity of rabbit muscle LDH.[272] They showed that the presence of pyruvate at concentration higher than 4.3 mM will inhibit the formation of lactate; due to substrate inhibition, only 50% of the maximal catalytic activity was observed at 4.3 mM pyruvate concentration. It was initially proposed that pyruvate substrate inhibition results from the formation of 'dead-end' complex between pyruvate, LDH and NAD^+ making the reaction unable to proceed. Further studies suggested that the formation of a covalent bond between C2 atom of pyruvate with the C4 atom of nicotinamide ring of NAD^+ contributes to the inhibition observed. A very weak non-competitive inhibition of lactate during pyruvate reduction, with an inhibition constant of 126 mM was also reported by Chambers and coworkers for rabbit muscle

dehydrogenase. Therefore experiments in this Section were carefully designed to take into consideration the substrate and product inhibition reactions.

6.3.1.1 Feasibility Tests

Chronoamperometry experiments were used to check for HoxFU compatibility with pyruvate and lactate (Figure 135). In panel A, the working electrode was poised at -0.412 V and the HoxFU modified electrode was placed in a fresh buffer solution. No NAD^+ was present at the commencement of the experiment, and as expected, no catalytic current was recorded at first. An increase in the catalytic current magnitude was observed when an aliquot of NAD^+ was injected into the electrochemical cell solution to give a concentration of 0.2 mM at approximately 40 s, corresponding to NAD^+ reduction by HoxFU, confirming that the enzyme modified electrode is catalytically active. Injections of pyruvate containing 0.2 mM NAD^+ at several time intervals as shown in Figure 135A did not alter the catalytic current indicating that pyruvate does not inhibit HoxFU NAD^+ reduction over this concentration range, and pyruvate is not directly reduced by HoxFU.

A similar observation was recorded when lactate was introduced into the electrochemical cell (panel B), confirming that lactate does not inhibit NAD^+ reduction by HoxFU over this concentration range, and is not directly oxidised by HoxFU.

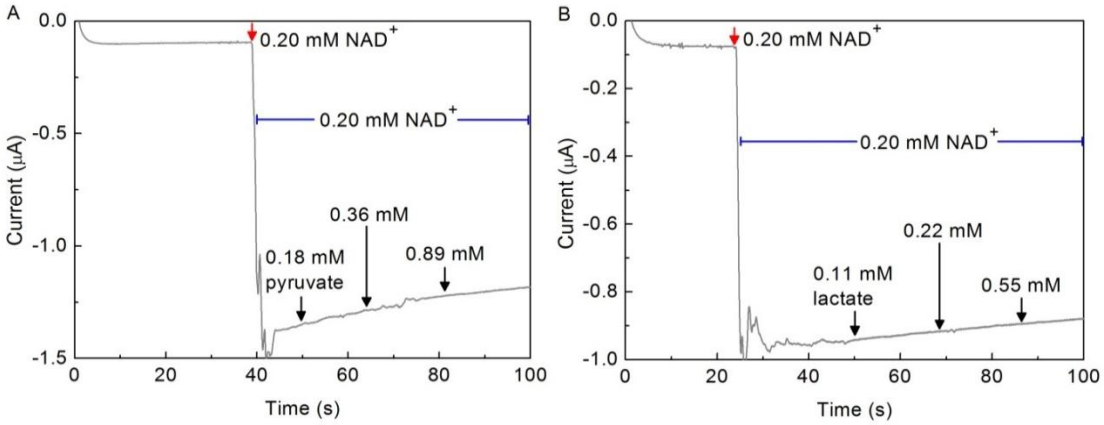

Figure 135. Chronoamperometry experiments designed to confirm compatibility of HoxFU with pyruvate (panel A) and lactate (panel B). In both panels, the working electrode was held at -0.412 V and the HoxFU modified electrode was placed in an electrochemical cell containing fresh buffer solution. Injection of NAD^+ stock solution to bring the cell concentration to 0.2 mM is indicated by the red arrows. Additions of pyruvate or lactate were performed as indicated in the figure. Other conditions: pH 6.0 BisTris-HCl buffer 50, mM, the electrode was rotated at 2000 rpm.

6.3.1.2 Control experiments

A set of control experiments was designed and the results are shown in Figure 136. The working electrode was held at -0.412 V for all experiments shown in the figure. The experiment in panel A was designed to check for pyruvate reduction on an unmodified graphite electrode. No significant change in the current magnitude was recorded upon addition of pyruvate to the electrochemical cell solution confirming that pyruvate is not reduced on the unmodified graphite electrode at this potential.

The chronoamperometry experiment shown in panel B was performed to check for the ability of LDH to reduce pyruvate with electrons directly supplied from the electrode. An aliquot of LDH (1 µL at concentration of 7 mg/mL) was spotted onto a graphite electrode and placed in the electrochemical cell containing fresh buffer solution. Additions of pyruvate solution as indicated in the panel did not lead to an increase the current magnitude suggesting LDH is unable to exchange electrons with the

electrode. The LDH modified electrode also did not show any catalytic response when aliquots of NAD^+ solution were injected into the electrochemical cell (panel C).

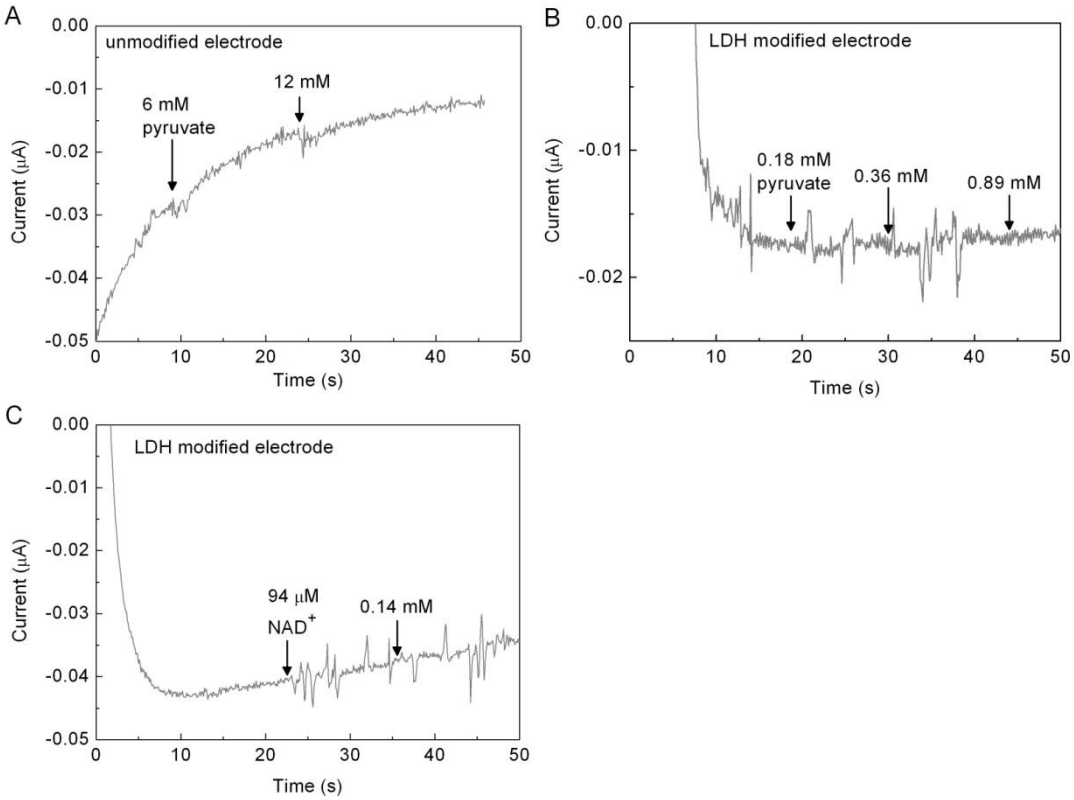

Figure 136. Control chronoamperometry experiments designed to check for possibility of pyruvate reduction on a bare graphite electrode (panel A), LDH ability to reduce pyruvate in the absence of NAD^+ (panel B) and LDH activity with NAD^+ (panel C). In all panels, the working electrode was held at -0.412 V and the electrode was placed in an electrochemical cell containing fresh buffer solution. Additions of pyruvate or NAD^+ were performed as indicated in the figure. Other conditions: pH 6.0 BisTris-HCl buffer 50, mM, the electrode was rotated at 2000 rpm.

Chronoamperometry experiments performed in this Section confirm that at -0.412 V, pyruvate reduction is not possible on the bare electrode, or on the HoxFU or LDH modified electrode without any supply of NADH. In the next Section, chronoamperometry used to monitor operation of a HoxFU-LDH electrode will be described. Infrared spectroelectrochemistry experiments used to monitor lactate formation *in situ* will also be described.

6.3.1.3 Using PFE to monitor NADH regeneration by HoxFU during pyruvate reduction by LDH

Figure 137 shows a diagram illustrating the experimental set up for monitoring NADH regeneration by HoxFU during pyruvate reduction by LDH. A solution of purified NADH was placed in the electrochemical cell and the electrode modified with HoxFU and LDH was poised at -0.412 V. Purified NADH solution was used instead of NAD^+ because NAD^+ is reduced by HoxFU at this potential giving rise to a negative current that will be difficult to differentiate with the current generated from the regeneration system.

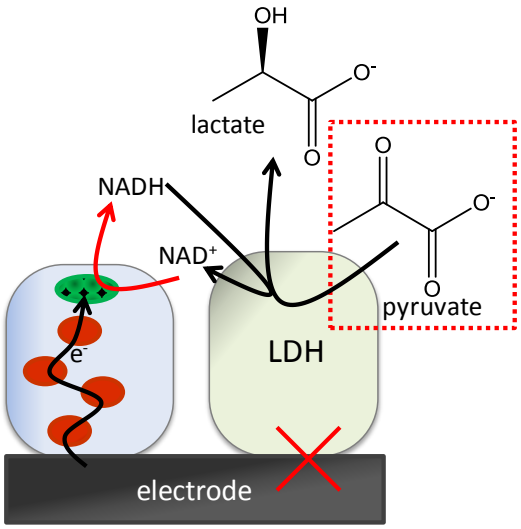

Figure 137. A cartoon representation showing how the NAD^+ reduction by HoxHU can be coupled to lactate dehydrogenase for reduction of pyruvate. The cross indicates that the LDH is unable to receive electrons from graphite electrode. In the electrochemical cell, purified NADH was present at the beginning of the experiment, and pyruvate (dotted red box) was added.

During the course of the experiment, the current response was monitored as aliquots of pyruvate solution were introduced into the cell. In the presence of NADH, pyruvate will be reduced to lactate while at the same time, NADH is oxidised to NAD^+. The NAD^+ produced by LDH should able to be taken up and re-reduced by HoxFU. If

HoxFU is able to successfully regenerate NADH, an increase in the current magnitude due to electrocatalytic NAD^+ reduction by HoxFU should be observed. Both enzymes were mixed in equal volume ratio prior to experiments (note that the concentration of HoxFU used was 0.4 mg/mL and concentration of LDH used was 0.7 mg/mL).

In the experiment shown in Figure 138A, 1 µL of the enzyme mixture was spotted onto an electrode and the enzyme modified electrode was placed in a solution containing 0.2 mM purified NADH. As there was no NAD^+ present in the electrochemical cell, no reductive current was recorded at the beginning of the experiment. At approximately 61 s, an aliquot of 36 µM pyruvate was injected into the cell solution and this lead to an increase in the reductive current. Further increase in the current magnitude was recorded as more pyruvate was introduced. In panel B where no NADH was present, injections of pyruvate did not lead to any increase in the current magnitude.

The increase in the current magnitude recorded in panel A upon introductions of pyruvate can be attributed to the ability of HoxFU to reduce NAD^+: produced during lactate formation by the LDH thus providing indirect evidence for LDH catalytic activity.

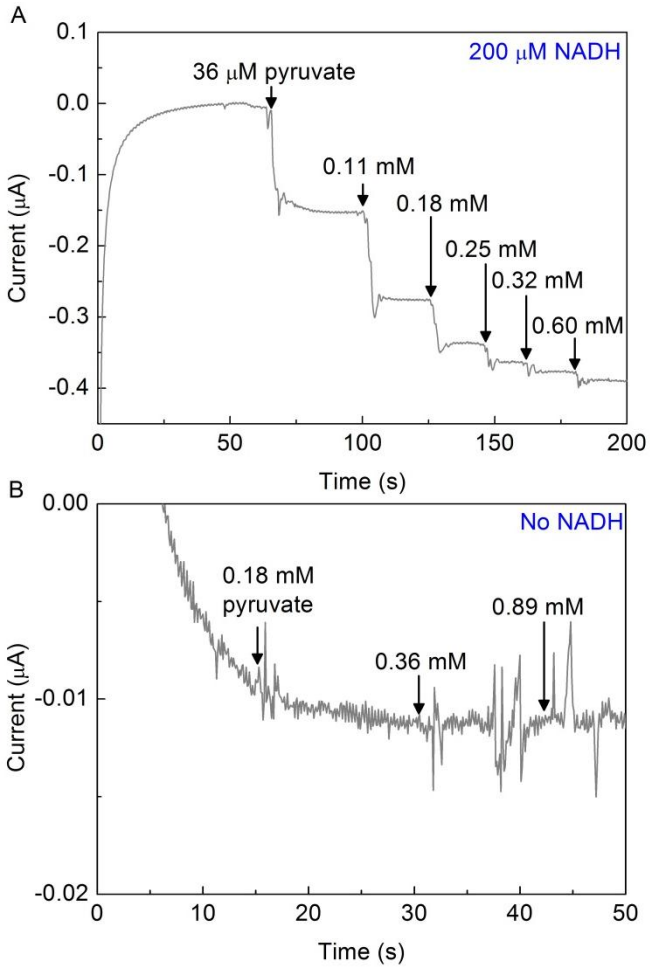

Figure 138. Typical chronoamperometry data obtained with an electrode modified with LDH and HoxFU. In panel A, the enzyme-modified electrode was placed in a solution containing 200 μM purified NADH and injections of pyruvate are indicated in the panel. In panel B, the enzyme-modified electrode was placed in a fresh buffer solution (No NADH) and injections of pyruvate are as indicated. Other conditions: working electrode was held at -0.412 V, experiments performed in a pH 6.0 BisTris-HCl buffer 50 mM, the electrode was rotated at 300 rpm.

Although these experiments confirm that LDH is able to channel NAD^+ to HoxFU for cofactor regeneration, chronoamperometry alone is unable to confirm the formation of lactate and disappearance of pyruvate during the course of experiments. Therefore in the next section, chronoamperometry coupled with IR spectroscopy will be used to monitor the formation of lactate by LDH using NADH supplied by HoxFU.

6.3.1.4 Using IR to monitor lactate formation

*These experiments were performed with assistance from Dr Philip Ash and Miss Holly Reeve

Figure 139 shows a diagram illustrating the experimental set up for monitoring lactate formation. A high surface area particle electrode modified with HoxFU and LDH was prepared according to the method described in Section 6.2.4. In contrast to the system used in Section 6.3.1.3 which utilised purified NADH in the starting solution, this experiment with particle electrode[1] uses NAD^+, meaning that any pyruvate reduction must arise from NADH produced electrochemically by the HoxFU.

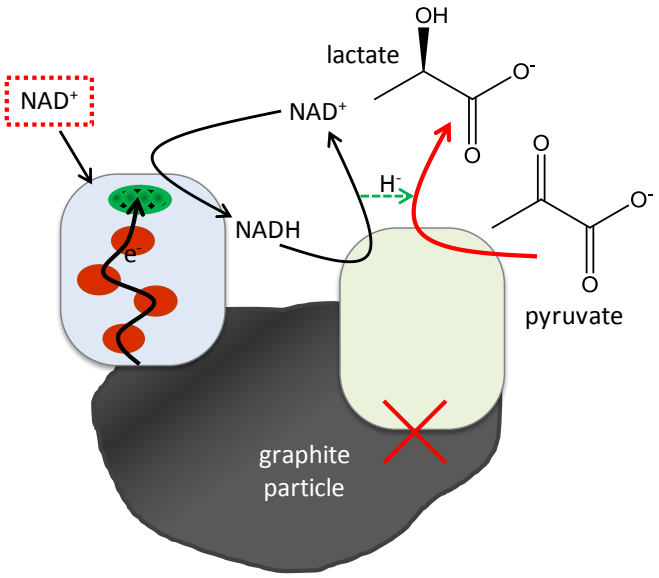

Figure 139. A cartoon representation showing how the NAD^+ reduction by HoxHU can be coupled to lactate dehydrogenase for reduction of pyruvate.

The particle electrode was held at -0.11 V at the beginning of the experiment (Figure 140A). At this potential, HoxFU is unable to reduce NAD^+ hence no catalytic current

[1] An aliquot of 10 µL from the mixture was pipetted on to a clean Si prism and left to partially-dry over around 90 seconds. A piece of carbon paper wetted with 1 mM NAD^+ and 5 mM pyruvate was applied on top of the partially-dry particles. To make the cell sealed, a rubber washer was put onto the carbon paper. The cell body is screwed on top and the cell is positioned in the sampling compartment of the spectrometer.

was recorded. An increase in the current magnitude was recorded upon stepping the electrode potential to -0.41 V and this increase can be attributed to NAD^+ reduction by HoxFU.

The IR spectra in panel B were recorded over time during the potential step at -0.41 V and are processed as difference spectra against an initial spectrum recorded at -0.11 V. Thus negative peaks show species lost during the experiment and positive peaks show species that increase in concentration during the experiment. An increase in the absorbance at 1118 cm^{-1} due to lactate formation is clearly visible at the expense of pyruvate absorbance at 1175 cm^{-1} (the absorbance at 1118 cm^{-1} can be assigned to a combination of CH_3 bending mode with the alcoholic stretching vibration, while the absorbance at 1175 cm^{-1} can be attributed to a combination of C-C and C-O stretching modes of pyruvate in solution).[273, 274] Spectra in panel B thus support the electrochemical result in panel A; the increase in current observed is due to HoxFU reducing NAD^+ which is the product of pyruvate reduction. Formation of lactate also confirms that the NADH produced by HoxFU is enzymatically active.

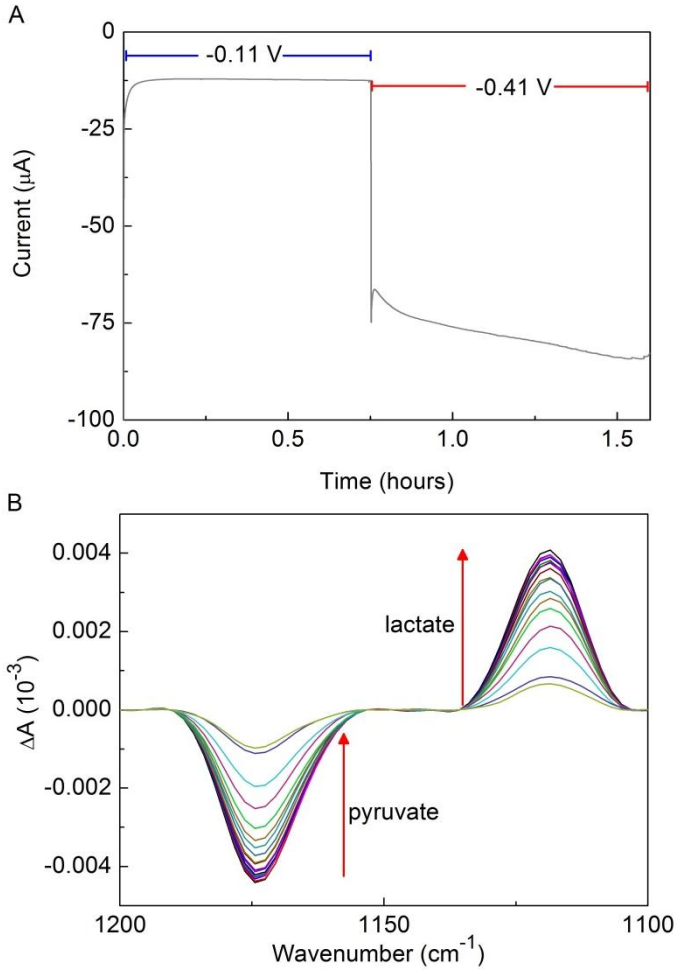

Figure 140. Electrochemically driven lactate formation. Panel A shows typical chronoamperometry data obtained with a particle electrode modified with LDH and HoxFU. The particle electrode was held at -0.11 V at the beginning of the experiment, before the potential was stepped to -0.41 V. Panel B shows IR spectra recorded during the course of experiment. Conditions: pH 6.0 BisTris-HCl 50 mM, 1 mM NAD^+ and 5 mM pyruvate.

Chapter 7: Summary

The work described in this Thesis utilised Protein Film Electrochemistry (PFE) as a tool to investigate the ability of different moieties of *R. eutropha* Soluble Hydrogenase to catalyse electro-enzymatic conversion of nicotinamide cofactors. In the first part of this Thesis, it was shown that the diaphorase moiety of the SH is able to oxidise NADH and reduce NAD^+ on a graphite electrode. The catalytic wave crosses the zero-current potential sharply suggesting a minimal overpotential requirement. The ability of the SH to catalyse NAD^+ reduction and NADH oxidation efficiently is very important because in the cell, the SH couples H_2 oxidation to NAD^+ reduction and these reactions are closely spaced to each other in potential. The diaphorase was also found to be biased towards NAD^+ reduction at all physiologically relevant NAD^+ and NADH concentrations investigated, consistent with the main function of the SH in the cell being NAD^+ reduction coupled to H_2 oxidation. Further experiments to investigate the binding and inhibition constants, inactivation at low potentials and the ability of HoxFU to function in the presence of O_2 were also conducted. The K_M of NADH acquired using electrochemical technique (58 μM) was very close to the one determined in biochemical assay experiments (56 μM) indicating that the diaphorase does not suffer from any damage to its catalytic properties upon detachment from its hydrogenase moiety and adsorption onto the electrode. The K_M^{NADH} value is also of the same order of magnitude as that of Complex I suggesting that the SH is equipped to be able to function in the reverse direction under certain physiological conditions. Electrochemical experiments on the hydrogenase moiety of the SH have shown that the inactive hydrogenase needs low potential electrons for reactivation, and in the cell, it is likely that these electrons can be supplied from NADH oxidation by the diaphorase moiety. It has not been possible to investigate NAD^+ reduction by HoxFU diaphorase in biochemical experiments because no suitable electron donor is available, however, a K_M value of 197

μM for NAD^+ was determined using electrochemistry. This value is 2.5 times lower than the affinity constant calculated for the whole SH (500 μM), indicating slight perturbation of the binding. Product inhibition was observed for NADH oxidation and NAD^+ reduction with inhibition constants found in the mM range. The affinity constants for NADH oxidation and NAD^+ reduction, together with product inhibitions constants, observed may serve as control mechanisms to balance these reactions. For instance, the low affinity of the SH for NAD^+ and product inhibition recorded for this reaction would slow the rate of H_2 oxidation coupled to NAD^+ reduction activity, perhaps assisting NADH oxidation under conditions when the NADH/NAD^+ pool has become too reduced by hindering the back reaction. This also suggests that the SH has been finely tuned by Nature to be a finely balanced catalyst for these reactions. PFE was also used to study a range of inhibitors of the related Complex I and it was discovered that NADH oxidation by HoxFU was also inhibited by these inhibitors. For example, NADH oxidation by HoxFU was found to be inhibited by ADP-Ribose, with a K_I in the μM range. Similarly, in Complex I, ADP-Ribose was found to inhibit NADH oxidation (K_I in μM range) suggesting that these two enzymes may share a similar substrate binding environment. Understanding these inhibition reactions is important if the SH is to be used in industrial processes, since compounds such as ADP-Ribose, ATP and ADP are often found in the commercially available NAD(P)H cofactors. However, judging from the high inhibition constants, and the low concentration of these inhibitors in the commercially available NAD(P)H, it is unlikely that these inhibitors will have a big impact on the reactions if the SH is to be used in industrial relevant processes, unless they are required as part of multi-step enzyme synthesis sequences.

The second part of this Thesis used PFE to explore the ability of the SH moieties and genetically engineered SH variants to catalyse $NADP^+$ reduction and NADPH

oxidation using PFE. The SH was shown to be able to catalyse $NADP^+$ reduction, with a K_M value of 8.0 mM. However, only a small catalytic current that could possibly be attributed to NADPH oxidation was observed, consistent with a very high K_M for NADPH oxidation. The engineered variants were found to be electrocatalytically active in $NADP^+$ reduction and some of the variants showed an increase in the affinity for $NADP^+$. For example, mutation of the Glutamic Acid residue at position 401 to Lysine in HoxF of the HoxHYFU decreased the K_M for $NADP^+$ from 8.0 mM to 1.7 mM. One of the variants investigated using PFE also showed bidirectional $NADP^+$ reduction and NADPH oxidation on a graphite electrode with no detectable overpotential. These findings suggest that the genetic modifications have been successful in increasing the affinity of the SH towards $NADP^+$. However, more work needs to be done before the engineered variants are ready for use in industrial processes. As the K_M is a measure of substrate concentration at which an enzyme has half of its maximal activity, a K_M in the range of mM is still considered high. In an industrial reaction, 1 mM is the maximum desirable concentration of NAD(P)H desired by industry, confirming the necessity for further improvements on the SH. However, any modification should also considered the stability of the SH on an electrode. Particularly for the genetic variants, it was found that the catalytic activity is sensitive to the storage time of the sample: samples stored for a long time had much lower catalytic activity than freshly purified samples, making the study of these variants challenging.

The third part of this Thesis illustrated some preliminary works towards regeneration of NADH by using the HoxFU diaphorase moiety. A H_2-driven regeneration system was first tested with platinised graphite particles modified with HoxFU and this system leads to clearly detectable regeneration of NADH. A similar regeneration system utilising HoxFU and the membrane bound hydrogenase (MBH) of *R. eutropha* was shown to

successfully regenerate NADH, although the amount of NADH regenerated this way was lower than with the platinised graphite particles. The low amount of NADH regenerated using the two-enzymes system compared to platinum was most likely because of the overpotential of the MBH which limits the thermodynamic driving force for the reaction. PFE was also used to demonstrate the ability of HoxFU to regenerate NADH required by lactate dehydrogenase. Efficient NADH regeneration for dehydrogenases has many possible applications, for example high surface area electrodes based on this principle could be used as electrodes for biotransformations as dehydrogenases are able to catalyse many important stereospecific reactions. Further work is now being carried out in the group to optimise the cofactor regeneration system and develop applications. As described in Chapter 5, some variants of HoxFU or the SH have been shown to function on an electrode as electrocatalysts for $NADP^+$ reduction, and this indicates that it should be possible to extend applications of the cofactor recycling particles or electrodes to NADP(H) dependent dehydrogenases and other enzymes for biotransformations. Stability will need to be improved in order to support applications of these cofactor recycling systems: films of HoxFU on a graphite electrode typically remained active over about 30 minutes, but would need to operate over at least 10 hours to be industrially viable. Improvements in this area will be necessary to make the electrodes or beads useful in industrial biotechnology.

Overall, this Thesis has provided insight into the diaphorase catalytic moiety of *Ralstonia eutropha* soluble hydrogenase, and has provided proof-of-concept demonstrations of the feasibility of using this enzyme moiety in cofactor recycling.

References

1. R. Cammack, M. Frey and R. Robson, *Hydrogen as a fuel: Learning from Nature*, Taylor and Francis, London and New York, 2001.
2. F. Tian, O. B. Toon, A. A. Pavlov and H. De Sterck, *Science*, 2005, **308**, 1014-1017.
3. B. P. Weiss, Y. L. Yung and K. H. Nealson, *Proc. Natl. Acad. Sci. U.S.A.*, 2000, **97**, 1395-1399.
4. R. Banerjee, in *Redox Biochemistry*, eds. R. Banerjee, D. Becker, M. Dickman, V. Gladyshev and S. Ragsdale, John Wiley & Sons, Inc., New Jersey, Editon edn., 2008, vol. 1, p. 11.
5. P. M. Vignais and B. Billoud, *Chem. Rev.*, 2007, **107**, 4206-4272.
6. R. Conrad, *Microb. Rev*, 1996, **60**, 609-640.
7. K. Schutz, T. Happe, O. Troshina, P. Lindblad, E. Leitao, P. Oliveira and P. Tamagnini, *Planta*, 2004, **218**, 350-359.
8. R. Conrad, C. Erkel and W. Liesack, *Curr. Opin. Biotechnol.*, 2006, **17**, 262-267.
9. M. W. W. Adams, *Biochim. Biophys. Acta*, 1990, **1020**, 115-145.
10. D. R. Lovley, D. E. Holmes and K. P. Nevin, *Adv. Microb. Physiol.*, 2004, **49**, 219-286.
11. R. Knowles, *Microb. Rev*, 1982, **46**, 43-70.
12. M. L. Ghirardi, M. C. Posewitz, P.-C. Maness, A. Dubini, J. Yu and M. Seibert, in *Annual Review of Plant Biology*, Editon edn., 2007, vol. 58, pp. 71-91.
13. T. Burgdorf, O. Lenz, T. Buhrke, E. van der Linden, A. K. Jones, S. P. J. Albracht and B. Friedrich, *J. Mol. Microbiol. Biotechnol.*, 2005, **10**, 181-196.
14. J. A. Cracknell, A. F. Wait, O. Lenz, B. Friedrich and F. A. Armstrong, *Proc. Natl. Acad. Sci. U.S.A.*, 2009, **106**, 20681-20686.
15. P. Constant, S. P. Chowdhury, L. Hesse, J. Pratscher and R. Conrad, *Appl. Environ. Microbiol.*, 2011, **77**, 6027-6035.
16. S. Srinivasan, G. C. Barnard and T. U. Gerngross, *Appl. Environ. Microbiol.*, 2002, **68**, 5925-5932.
17. B. Schink and H. G. Schlegel, *Biochim. Biophys. Acta*, 1979, **567**, 315-324.

18. J. Fritsch, P. Scheerer, S. Frielingsdorf, S. Kroschinsky, B. Friedrich, O. Lenz and C. M. T. Spahn, *Nature*, 2011, **479**, 249-252.
19. M. Bernhard, B. Benelli, A. Hochkoeppler, D. Zannoni and B. Friedrich, *Eur. J. Biochem.*, 1997, **248**, 179-186.
20. M. Horch, L. Lauterbach, O. Lenz, P. Hildebrandt and I. Zebger, *FEBS Lett.*, 2012, **586**, 545-556.
21. K. Schneider and H. G. Schlegel, *Biochim. Biophys. Acta*, 1976, **452**, 66-80.
22. A. Tranbetcke, U. Warnecke, C. Bocker, C. Zaborosch and B. Friedrich, *J. Bacteriol.*, 1990, **172**, 2920-2929.
23. T. Buhrke, O. Lenz, A. Porthun and B. Friedrich, *Mol. Microbiol.*, 2004, **51**, 1677-1689.
24. O. Lenz, M. Bernhard, T. Buhrke, E. Schwartz and B. Friedrich, *J. Mol. Microbiol. Biotechnol.*, 2002, **4**, 255-262.
25. O. Lenz and B. Friedrich, *Proc. Natl. Acad. Sci. U.S.A.*, 1998, **95**, 12474-12479.
26. M. Bernhard, T. Buhrke, B. Bleijlevens, A. L. De Lacey, V. M. Fernandez, S. P. J. Albracht and B. Friedrich, *J. Biol. Chem.*, 2001, **276**, 15592-15597.
27. J. M. Berg, J. L. Tymoczko and L. Stryer, *Biochemistry*, 6 edn., W. H. Freeman and Company, New York, 2006.
28. C. C. Page, C. C. Moser and P. L. Dutton, *Curr. Opin. Chem. Biol.*, 2003, **7**, 551-556.
29. L. A. Sazanov and P. Hinchliffe, *Science*, 2006, **311**, 1430-1436.
30. H. Beinert and S. P. J. Albracht, *Biochim. Biophys. Acta*, 1982, **683**, 245-277.
31. T. Ohnishi, *Biochim. Biophys. Acta-Bioenerg.*, 1998, **1364**, 186-206.
32. Z. L. Zhang, L. S. Huang, V. M. Shulmeister, Y. I. Chi, K. K. Kim, L. W. Hung, A. R. Crofts, E. A. Berry and S. H. Kim, *Nature*, 1998, **392**, 677-684.
33. V. Yankovskaya, R. Horsefield, S. Tornroth, C. Luna-Chavez, H. Miyoshi, C. Leger, B. Byrne, G. Cecchini and S. Iwata, *Science*, 2003, **299**, 700-704.
34. J. M. Berrisford and L. A. Sazanov, *J. Biol. Chem.*, 2009, **284**, 29773-29783.
35. J. W. Peters, W. N. Lanzilotta, B. J. Lemon and L. C. Seefeldt, *Science*, 1998, **282**, 1853-1858.
36. M. G. Bertero, R. A. Rothery, M. Palak, C. Hou, D. Lim, F. Blasco, J. H. Weiner and N. C. J. Strynadka, *Nat. Struct. Biol.*, 2003, **10**, 681-687.
37. A. Volbeda, M. H. Charon, C. Piras, E. C. Hatchikian, M. Frey and J. C. Fontecillacamps, *Nature*, 1995, **373**, 580-587.

38. A. Volbeda, L. Martin, C. Cavazza, M. Matho, B. W. Faber, W. Roseboom, S. P. J. Albracht, E. Garcin, M. Rousset and J. C. Fontecilla-Camps, *J. Biol. Inorg. Chem.*, 2005, **10**, 239-249.
39. H. Ogata, P. Kellers and W. Lubitz, *J. Mol. Biol.*, 2010, **402**, 428-444.
40. A. Volbeda, P. Amara, C. Darnault, J.-M. Mouesca, A. Parkin, M. M. Roessler, F. A. Armstrong and J. C. Fontecilla-Camps, *Proc. Natl. Acad. Sci. U.S.A.*, 2012, **109**, 5305-5310.
41. P. N. Bartlett, in *Bioelectrochemistry: Fundamentals, Experimental Techniques and Applications*, ed. P. N. Bartlett, John Wiley & Sons, Ltd, England, Editon edn., 2008, vol. 1, pp. 1-38.
42. A. Bansal, M. A. Dayton, H. Zalkin and R. F. Colman, *J. Biol. Chem.*, 1989, **264**, 9827-9835.
43. P. J. Baker, K. L. Britton, P. C. Engel, G. W. Farrants, K. S. Lilley, D. W. Rice and T. J. Stillman, *Proteins Struct. Funct. Bioinf.*, 1992, **12**, 75-86.
44. A. M. Lesk, *Curr. Opin. Struct. Biol.*, 1995, **5**, 775-783.
45. O. Carugo and P. Argos, *Proteins Struct. Funct. Bioinf.*, 1997, **28**, 10-28.
46. O. Carugo and P. Argos, *Proteins Struct. Funct. Bioinf.*, 1997, **28**, 29-40.
47. F. Fan, J. A. Lorenzen and B. V. Plapp, *Biochemistry*, 1991, **30**, 6397-6401.
48. I. Ohlsson, Nordstro.B and C. I. Branden, *J. Mol. Biol.*, 1974, **89**, 339-354.
49. P. A. Karplus, M. J. Daniels and J. R. Herriott, *Science*, 1991, **251**, 60-66.
50. O. S. Ksenzhek and S. A. Petrova, *Bioelectrochem. Bioenerg.*, 1983, **11**, 105-127.
51. M. W. Fraaije and A. Mattevi, *Trends Biochem. Sci*, 2000, **25**, 126-132.
52. P. Hinchliffe and L. A. Sazanov, *Science*, 2005, **309**, 771-774.
53. S. Shima and R. K. Thauer, *Chem. Rec.*, 2007, **7**, 37-46.
54. P. M. Vignais, B. Billoud and J. Meyer, *FEMS Microbiol. Rev.*, 2001, **25**, 455-501.
55. L. F. Wu and M. A. Mandrand, *FEMS Microbiol. Rev.*, 1993, **104**, 243-270.
56. K. A. Vincent, A. Parkin and F. A. Armstrong, *Chem. Rev.*, 2007, **107**, 4366-4413.
57. F. A. Armstrong, N. A. Belsey, J. A. Cracknell, G. Goldet, A. Parkin, E. Reisner, K. A. Vincent and A. F. Wait, *Chem. Soc. Rev.*, 2009, **38**, 36-51.
58. O. Pilak, B. Mamat, S. Vogt, C. H. Hagemeier, R. K. Thauer, S. Shima, C. Vonrhein, E. Warkentin and U. Ermler, *J. Mol. Biol.*, 2006, **358**, 798-809.

59. C. Zirngibl, R. Hedderich and R. K. Thauer, *FEBS Lett.*, 1990, **261**, 112-116.
60. J. Schleucher, C. Griesinger, B. Schworer and R. K. Thauer, *Biochemistry*, 1994, **33**, 3986-3993.
61. S. Shima, O. Pilak, S. Vogt, M. Schick, M. S. Stagni, W. Meyer-Klaucke, E. Warkentin, R. K. Thauer and U. Ermler, *Science*, 2008, **321**, 572-575.
62. B. Schworer, V. M. Fernandez, C. Zirngibl and R. K. Thauer, *Eur. J. Biochem.*, 1993, **212**, 255-261.
63. C. C. Page, C. C. Moser, X. X. Chen and P. L. Dutton, *Nature*, 1999, **402**, 47-52.
64. E. Garcin, X. Vernede, E. C. Hatchikian, A. Volbeda, M. Frey and J. C. Fontecilla-Camps, *Struct. Fold. Des.*, 1999, **7**, 557-566.
65. A. Volbeda, E. Garcin, C. Piras, A. L. deLacey, V. M. Fernandez, E. C. Hatchikian, M. Frey and J. C. FontecillaCamps, *J. Am. Chem. Soc.*, 1996, **118**, 12989-12996.
66. Y. Higuchi, H. Ogata, K. Miki, N. Yasuoka and T. Yagi, *Struct. Fold. Des.*, 1999, **7**, 549-556.
67. Y. Higuchi, T. Yagi and N. Yasuoka, *Structure*, 1997, **5**, 1671-1680.
68. Y. Montet, P. Amara, A. Volbeda, X. Vernede, E. C. Hatchikian, M. J. Field, M. Frey and J. C. FontecillaCamps, *Nat. Struct. Biol.*, 1997, **4**, 523-526.
69. P. M. Matias, C. M. Soares, L. M. Saraiva, R. Coelho, J. Morais, J. Le Gall and M. A. Carrondo, *J. Biol. Inorg. Chem.*, 2001, **6**, 63-81.
70. Y. Shomura, K.-S. Yoon, H. Nishihara and Y. Higuchi, *Nature*, 2011, **479**, 253-256.
71. S. J. Pilkington, J. M. Skehel, R. B. Gennis and J. E. Walker, *Biochemistry*, 1991, **30**, 2166-2175.
72. M. Long, J. Liu, Z. Chen, B. Bleijlevens, W. Roseboom and S. P. J. Albracht, *J. Biol. Inorg. Chem.*, 2007, **12**, 62-78.
73. E. van der Linden, T. Burgdorf, A. L. de Lacey, T. Buhrke, M. Scholte, V. M. Fernandez, B. Friedrich and S. P. J. Albracht, *J. Biol. Inorg. Chem.*, 2006, **11**, 247-260.
74. J. E. Walker, *Q. Rev. Biophys.*, 1992, **25**, 253-324.
75. T. Friedrich and D. Scheide, *FEBS Lett.*, 2000, **479**, 1-5.
76. M. Horch, L. Lauterbach, M. Saggu, P. Hildebrandt, F. Lendzian, R. Bittl, O. Lenz and I. Zebger, *Angew. Chem. Int. Ed.*, 2010, **49**, 8026-8029.

77. L. Lauterbach, J. A. Liu, M. Horch, P. Hummel, A. Schwarze, M. Haumann, K. A. Vincent, O. Lenz and I. Zebger, *Eur. J. Inorg. Chem.*, 2011, 1067-1079.
78. T. Burgdorf, E. van der Linden, M. Bernhard, Q. Y. Yin, J. W. Back, A. F. Hartog, A. O. Muijsers, C. G. de Koster, S. P. J. Albracht and B. Friedrich, *J. Bacteriol.*, 2005, **187**, 3122-3132.
79. E. van der Linden, B. W. Faber, B. Bleijlevens, T. Burgdorf, M. Bernhard, B. Friedrich and S. P. J. Albracht, *Eur. J. Biochem.*, 2004, **271**, 801-808.
80. J. Hirst, *Biochem. J*, 2010, **425**, 327-339.
81. U. Brandt, *Annu. Rev. Biochem.*, 2006, **75**, 69-92.
82. T. Yagi and A. Matsuno-Yagi, *Biochemistry*, 2003, **42**, 2266-2274.
83. A. H. V. Schapira, *Biochim. Biophys. Acta-Bioenerg.*, 1998, **1364**, 261-270.
84. A. H. V. Schapira, *Biochim. Biophys. Acta-Bioenerg.*, 1998, **1366**, 225-233.
85. M. T. Lin and M. F. Beal, *Nature*, 2006, **443**, 787-795.
86. S. DiMauro and E. A. Schon, *N. Engl. J. Med.*, 2003, **348**, 2656-2668.
87. M. P. Murphy, *Biochem. J*, 2009, **417**, 1-13.
88. T. M. Dawson and V. L. Dawson, *Science*, 2003, **302**, 819-822.
89. R. S. Balaban, S. Nemoto and T. Finkel, *Cell*, 2005, **120**, 483-495.
90. R. G. Efremov and L. A. Sazanov, *Nature*, 2011, **476**, 414-420.
91. R. G. Efremov, R. Baradaran and L. A. Sazanov, *Nature*, 2010, **465**, 441-U461.
92. L. A. Sazanov, *Biochemistry*, 2007, **46**, 2275-2288.
93. A. Volbeda and J. C. Fontecilla-Camps, in *A Structural Perspective on Respiratory Complex I: Structure and Function of NADH:Ubiquinone oxidoreductase*, ed. L. A. Sazanov, Springer Science, London, Editon edn., 2012, pp. 109-121.
94. L. Lauterbach, Z. Idris, K. A. Vincent and O. Lenz, *PLoS One*, 2011, **6(10). e25939**.
95. K. Schneider, R. Cammack and H. G. Schlegel, *Eur. J. Biochem.*, 1984, **142**, 75-84.
96. C. Grzeszik, M. Lubbers, M. Reh and H. G. Schlegel, *Microbiology-Uk*, 1997, **143**, 1271-1286.
97. C. Grzeszik, K. Ross, K. Schneider, M. Reh and H. G. Schlegel, *Arch. Microbiol.*, 1997, **167**, 172-176.
98. G. Rakhely, A. T. Kovacs, G. Maroti, B. D. Fodor, G. Csanadi, D. Latinovics and K. L. Kovacs, *Appl. Environ. Microbiol.*, 2004, **70**, 722-728.

99. J. Appel, S. Phunpruch, K. Steinmuller and R. Schulz, *Arch. Microbiol.*, 2000, **173**, 333-338.
100. J. Appel and R. Schulz, *J. Photochem. Photobiol., B*, 1998, **47**, 1-11.
101. B. Payen, M. Segui, P. Monsan, K. Schneider, C. G. Friedrich and H. G. Schlegel, *Biotechnol. Lett.*, 1983, **5**, 463-468.
102. K. Otsuka, S. Aono and I. Okura, *Chem. Lett.*, 1987, 2089-2090.
103. J. Cantet, A. Bergel and M. Comtat, *Enzyme Microb. Technol.*, 1996, **18**, 72-79.
104. J. Moiroux and P. J. Elving, *Journal of the American Chemical Society*, 1980, **102**, 6533-6538.
105. J. Moiroux and P. J. Elving, *J. Electroanal. Chem.*, 1979, **102**, 93-108.
106. H. Jaegfeldt, *J. Electroanal. Chem.*, 1980, **110**, 295-302.
107. W. J. Blaedel and R. A. Jenkins, *Anal. Chem.*, 1975, **47**, 1337-1343.
108. L. Gorton and E. Dominguez, in *Encyclopedia of electrochemistry: Bioelectrochemistry*, ed. G. S. Wilson, Wiley-VCH Verlag GmbH & Co. KGaA, Weinheim, Editon edn., 2002, vol. 9, p. 67 pages.
109. R. W. Coughlin, M. Aizawa, B. F. Alexander and M. Charles, *Biotechnol. Bioeng.*, 1975, **17**, 515-526.
110. C. O. Schmakel, K. S. V. Santhanam and P. J. Elving, *J. Am. Chem. Soc.*, 1975, **97**, 5083-5092.
111. P. J. Elving, W. T. Bresnahan, J. Moiroux and Z. Samec, *Bioelectrochem. Bioenerg.*, 1982, **9**, 365-378.
112. K. Takamura, A. Mori and F. Watanabe, *Bioelectrochem. Bioenerg.*, 1981, **8**, 125-136.
113. D. C. S. Tse and T. Kuwana, *Anal. Chem.*, 1978, **50**, 1315-1318.
114. F. Ni, H. Feng, L. Gorton and T. M. Cotton, *Langmuir*, 1990, **6**, 66-73.
115. T. Huang, A. Warsinke, T. Kuwana and F. W. Scheller, *Anal. Chem.*, 1998, **70**, 991-997.
116. A. A. Karyakin, Y. N. Ivanova and E. E. Karyakina, *Electrochem. Commun.*, 2003, **5**, 677-680.
117. Y. B. Zu, R. J. Shannon and J. Hirst, *J. Am. Chem. Soc.*, 2003, **125**, 6020-6021.
118. F. A. Armstrong, in *Encyclopedia of Electrochemistry: Bioelectrochemistry*, eds. A. J. Bard, M. Strattmann and H. J. Schafer, Wiley, Editon edn., 2002, vol. 9.

119. M. E. Pandelia, V. Fourmond, P. Tron-Infossi, E. Lojou, P. Bertrand, C. Leger, M. T. Giudici-Orticoni and W. Lubitz, *J. Am. Chem. Soc.*, 2010, **132**, 6991-7004.
120. A. Abou Hamdan, S. Dementin, P.-P. Liebgott, O. Gutierrez-Sanz, P. Richaud, A. L. De Lacey, M. Roussett, P. Bertrand, L. Cournac and C. Leger, *J. Am. Chem. Soc.*, 2012, **134**, 8368-8371.
121. C. Leger and P. Bertrand, *Chem. Rev.*, 2008, **108**, 2379-2438.
122. J. N. Butt, L. J. Anderson, L. M. Rubio, D. J. Richardson, E. Flores and A. Herrero, *Bioelectrochemistry*, 2002, **56**, 17-18.
123. J. N. Butt and F. A. Armstrong, in *Bioinorganic Electrochemstry*, eds. O. Hammerich and J. Ulstrup, Springer, Dordrecht, The Netherlands, Editon edn., 2008.
124. H. C. Angove, J. A. Cole, D. J. Richardson and J. N. Butt, *J. Biol. Chem.*, 2002, **277**, 23374-23381.
125. V. Fourmond, B. Burlat, S. Dementin, P. Arnoux, M. Sabaty, S. Boiry, B. Guigliarelli, P. Bertrand, D. Pignol and C. Leger, *J. Phys. Chem. B*, 2008, **112**, 15478-15486.
126. A. J. Gates, D. J. Richardson and J. N. Butt, *Biochem. J*, 2008, **409**, 159-168.
127. M. Firer-Sherwood, G. S. Pulcu and S. J. Elliott, *J. Biol. Inorg. Chem.*, 2008, **13**, 849-854.
128. M. G. Almeida, C. M. Silveira and J. J. G. Moura, *Biosens. Bioelectron.*, 2007, **22**, 2485-2492.
129. T. A. Clarke, G. L. Kemp, J. H. Van Wonderen, R.-M. A. S. Doyle, J. A. Cole, N. Tovell, M. R. Cheesman, J. N. Butt, D. J. Richardson and A. M. Hemmings, *Biochemistry*, 2008, **47**, 3789-3799.
130. A. K. Jones, E. Sillery, S. P. J. Albracht and F. A. Armstrong, *Chem. Commun.*, 2002, 866-867.
131. K. A. Vincent, A. Parkin, O. Lenz, S. P. J. Albracht, J. C. Fontecilla-Camps, R. Cammack, B. Friedrich and F. A. Armstrong, *J. Am. Chem. Soc.*, 2005, **127**, 18179-18189.
132. M. J. Lukey, A. Parkin, M. M. Roessler, B. J. Murphy, J. Harmer, T. Palmer, F. Sargent and F. A. Armstrong, *J. Biol. Chem.*, 2010, **285**, 3928-3938.
133. A. Parkin, L. Bowman, M. M. Roessler, R. A. Davies, T. Palmer, F. A. Armstrong and F. Sargent, *FEBS Letters*, 2011.

134. A. F. Wait, A. Parkin, G. M. Morley, L. dos Santos and F. A. Armstrong, *J. Phys. Chem. C*, 2010, **114**, 12003-12009.
135. S. Krishnan and F. A. Armstrong, *Chem. Sci.*, 2012, **3**, 1015-1023.
136. Y. Kamitaka, S. Tsujimura, N. Setoyama, T. Kajino and K. Kano, *Phys. Chem. Chem. Phys.*, 2007, **9**, 1793-1801.
137. D. R. Thevenot, K. Toth, R. A. Durst and G. S. Wilson, *Pure Appl. Chem.*, 1999, **71**, 2333-2348.
138. K. Cammann, *Fresenius J. Anal. Chem.*, 1977, **287**, 1-9.
139. L. C. Clark and C. Lyons, *Ann. N.Y. Acad. Sci.*, 1962, **102**, 29-&.
140. L. Gorton and P. N. Bartlett, in *Bioelectrochemistry: Fundamentals, Experimental Techniques and Applications*, ed. P. N. Bartlett, John Wiley & Sons, Ltd, England, Editon edn., 2008, vol. 1, pp. 157-198.
141. P. Yeh and T. Kuwana, *Chem. Lett.*, 1977, 1145-1148.
142. M. J. Eddowes and H. A. O. Hill, *Chem. Commun.*, 1977, 771-772.
143. L. J. C. Jeuken, *Nat. Prod. Rep.*, 2009, **26**, 1234-1240.
144. N. N. Daskalakis, A. Mueller, S. D. Evans and L. J. C. Jeuken, *Soft Matter*, 2011, **7**, 49-52.
145. A. J. Gates, G. L. Kemp, C. Y. To, J. Mann, S. J. Marritt, A. G. Mayes, D. J. Richardson and J. N. Butt, *Phys. Chem. Chem. Phys.*, 2011, **13**, 7720-7731.
146. A. J. Gates, C. S. Butler, D. J. Richardson and J. N. Butt, *Biochem. Soc. Trans.*, 2011, **39**, 236-242.
147. F. A. Armstrong, H. A. O. Hill and N. J. Walton, *Accounts Chem. Res.*, 1988, **21**, 407-413.
148. F. A. Armstrong, in *Encyclopedia of electrochemistry: Bioelectrochemistry*, ed. G. S. Wilson, Wiley-VCH Verlag GmbH & Co. KGaA, Weinheim, Editon edn., 2002, vol. 9, p. 17 pages.
149. D. E. Reed and F. M. Hawkridge, *Anal. Chem.*, 1987, **59**, 2334-2339.
150. T. M. Cotton, S. G. Schultz and R. P. Vanduyne, *J. Am. Chem. Soc.*, 1980, **102**, 7960-7962.
151. T. M. Cotton, D. Kaddi and D. Iorga, *J. Am. Chem. Soc.*, 1983, **105**, 7462-7464.
152. P. W. Atkins, *Physical Chemistry*, 6th edn., Oxford University Press, 1998.
153. C. F. Blanford and F. A. Armstrong, *J. Solid State Electrochem.*, 2006, **10**, 826-832.

154. N. Greenwood and A. Earnshaw, *Chemistry of the elements*, Heinemann, Butterworth 2002.
155. T. J. Davies, M. E. Hyde and R. G. Compton, *Angew. Chem. Int. Ed.*, 2005, **44**, 5121-5126.
156. F. A. Armstrong and A. M. Lannon, *J. Am. Chem. Soc.*, 1987, **109**, 7211-7212.
157. C. Leger, S. J. Elliott, K. R. Hoke, L. J. C. Jeuken, A. K. Jones and F. A. Armstrong, *Biochemistry*, 2003, **42**, 8653-8662.
158. F. A. Armstrong, H. A. Heering and J. Hirst, *Chem. Soc. Rev.*, 1997, **26**, 169-179.
159. V. Fourmond, T. Lautier, C. Baffert, F. Leroux, P.-P. Liebgott, S. Dementin, M. Rousset, P. Arnoux, D. Pignol, I. Meynial-Salles, P. Soucaille, P. Bertrand and C. Leger, *Anal. Chem.*, 2009, **81**, 2962-2968.
160. O. Rudiger, C. Gutierrez-Sanchez, D. Olea, I. A. C. Pereira, M. Velez, V. M. Fernandez and A. L. De Lacey, *Electroanalysis*, 2010, **22**, 776-783.
161. C. Gutierrez-Sanchez, D. Olea, M. Marques, V. M. Fernandez, I. A. C. Pereira, M. Velez and A. L. De Lacey, *Langmuir*, 2011, **27**, 6449-6457.
162. M. Pita, C. Gutierrez-Sanchez, D. Olea, M. Velez, C. Garcia-Diego, S. Shleev, V. M. Fernandez and A. L. De Lacey, *J. Phys. Chem. C*, 2011, **115**, 13420-13428.
163. X. Luo, M. Brugna, P. Tron-Infossi, M. T. Giudici-Orticoni and E. Lojou, *J. Biol. Inorg. Chem.*, 2009, **14**, 1275-1288.
164. O. Rudiger, J. M. Abad, E. C. Hatchikian, V. M. Fernandez and A. L. De Lacey, *J. Am. Chem. Soc.*, 2005, **127**, 16008-16009.
165. C. F. Blanford, R. S. Heath and F. A. Armstrong, *Chem. Commun.*, 2007, 1710-1712.
166. J. A. Cracknell, DPhil thesis. University of Oxford, 2008.
167. G. Goldet, A. F. Wait, J. A. Cracknell, K. A. Vincent, M. Ludwig, O. Lenz, B. Friedrich and F. A. Armstrong, *J. Am. Chem. Soc.*, 2008, **130**, 11106-11113.
168. C. Leger, S. Dementin, P. Bertrand, M. Rousset and B. Guigliarelli, *J. Am. Chem. Soc.*, 2004, **126**, 12162-12172.
169. F. Leroux, S. Dementin, B. Burlatt, L. Cournac, A. Volbeda, S. Champ, L. Martin, B. Guigliarelli, P. Bertrand, J. Fontecilla-Camps, M. Rousset and C. Leger, *Proc. Natl. Acad. Sci. U.S.A.*, 2008, **105**, 11188-11193.

170. M. Ludwig, J. A. Cracknell, K. A. Vincent, F. A. Armstrong and O. Lenz, *J. Biol. Chem.*, 2009, **284**, 465-477.
171. G. Goldet, C. Brandmayr, S. T. Stripp, T. Happe, C. Cavazza, J. C. Fontecilla-Camps and F. A. Armstrong, *J. Am. Chem. Soc.*, 2009, **131**, 14979-14989.
172. F. A. Armstrong and J. Hirst, *Proc. Natl. Acad. Sci. U.S.A.*, 2011, **108**, 14049-14054.
173. A. J. Bard and L. R. Faulkner, *Electrochemical Methods: Fundamentals and applications*, 2 edn., John Wiley & Sons, USA, 2001.
174. T. Sakata, *Bull. Chem. Soc. Jpn.*, 1996, **69**, 2435-2446.
175. A. C. Fisher, *Electrode Dynamics*, Oxford University Press, Oxford, 1996.
176. H. A. Heering, J. Hirst and F. A. Armstrong, *J. Phys. Chem. B*, 1998, **102**, 6889-6902.
177. M. S. Mondal, H. A. Fuller and F. A. Armstrong, *J. Am. Chem. Soc.*, 1996, **118**, 263-264.
178. C. Leger, K. Heffron, H. R. Pershad, E. Maklashina, C. Luna-Chavez, G. Cecchini, B. A. C. Ackrell and F. A. Armstrong, *Biochemistry*, 2001, **40**, 11234-11245.
179. A. Sucheta, R. Cammack, J. Weiner and F. A. Armstrong, *Biochemistry*, 1993, **32**, 5455-5465.
180. H. R. Pershad, J. L. C. Duff, H. A. Heering, E. C. Duin, S. P. J. Albracht and F. A. Armstrong, *Biochemistry*, 1999, **38**, 8992-8999.
181. J. M. Hudson, K. Heffron, V. Kotlyar, Y. Sher, E. Maklashina, G. Cecchini and F. A. Armstrong, *J. Am. Chem. Soc.*, 2005, **127**, 6977-6989.
182. K. Heffron, C. Leger, R. A. Rothery, J. H. Weiner and F. A. Armstrong, *Biochemistry*, 2001, **40**, 3117-3126.
183. G. A. Orr and J. S. Blanchard, *Anal. Biochem.*, 1984, **142**, 232-234.
184. C. D. Barker, T. Reda and J. Hirst, *Biochemistry*, 2007, **46**, 3454-3464.
185. M. Capone, D. Scanlon, J. Griffin and P. C. Engel, *FEBS J.*, 2011, **278**, 2460-2468.
186. A. Cornish-Bowden, *Fundamentals of enzyme kinetics*, Third Edition edn., Portland Press Ltd, 2004.
187. H. Lineweaver and D. Burk, *J. Am. Chem. Soc.*, 1934, **56**, 658-666.
188. A. Cornish-Bowden, *Biochem. J*, 1974, **137**, 143-144.
189. D. V. Dervartanian and C. Veeger, *Biochim. Biophys. Acta*, 1964, **92**, 233-247.

190. T. Burgdorf, S. Loscher, P. Liebisch, E. Van der Linden, M. Galander, F. Lendzian, W. Meyer-Klaucke, S. P. J. Albracht, B. Friedrich, H. Dau and M. Haumann, *J. Am. Chem. Soc.*, 2005, **127**, 576-592.
191. M. Kuhn, A. Steinbuchel and H. G. Schlegel, *J. Bacteriol.*, 1984, **159**, 633-639.
192. F. A. Armstrong, *Curr. Opin. Chem. Biol.*, 2005, **9**, 110-117.
193. T. Reda and J. Hirst, *J. Phys. Chem. B*, 2006, **110**, 1394-1404.
194. K. A. Vincent and F. A. Armstrong, *Inorg. Chem.*, 2005, **44**, 798-809.
195. B. D. Bennett, E. H. Kimball, M. Gao, R. Osterhout, S. J. Van Dien and J. D. Rabinowitz, *Nat. Chem. Biol.*, 2009, **5**, 593-599.
196. F. Kaplan, P. Setlow and N. O. Kaplan, *Arch. Biochem. Biophys.*, 1969, **132**, 91-98.
197. D. W. Reed, J. Millstein and P. L. Hartzell, *J. Bacteriol.*, 2001, **183**, 7007-7016.
198. V. Fourmond, K. Hoke, H. A. Heering, C. Baffert, F. Leroux, P. Bertrand and C. Leger, *Bioelectrochemistry*, 2009, **76**, 141-147.
199. E. V. Gavrikova, V. G. Grivennikova, V. D. Sled, T. Ohnishi and A. D. Vinogradov, *Biochim. Biophys. Acta-Bioenerg.*, 1995, **1230**, 23-30.
200. K. Simpson-Wells, Part II thesis. University of Oxford, 2011.
201. F. F. Delarosa and E. Palacian, *Plant Science Letters*, 1981, **21**, 1-8.
202. A. D. Vinogradov, *J. Bioenerg. Biomembr.*, 1993, **25**, 367-375.
203. A. B. Kotlyar, V. D. Sled and A. D. Vinogradov, *Biochim. Biophys. Acta*, 1992, **1098**, 144-150.
204. M. Dixon, *Biochem. J*, 1953, **55**, 170-171.
205. M. Dixon, *Biochem. J*, 1972, **129**, 197-202.
206. C. C. Wratten and W. W. Cleland, *Biochemistry*, 1963, **2**, 935-941.
207. A. D. Vinogradov and V. G. Grivennikova, *IUBMB Life*, 2001, **52**, 129-134.
208. I. S. Gostimskaya, G. Cecchini and A. D. Vinogradov, *Biochim. Biophys. Acta-Bioenerg.*, 2006, **1757**, 1155-1161.
209. T. V. Zharova and A. D. Vinogradov, *Biochim. Biophys. Acta-Bioenerg.*, 1997, **1320**, 256-264.
210. Y. Hatefi, K. E. Stempel and W. G. Hanstein, *J. Biol. Chem.*, 1969, **244**, 2358-2365.
211. G. Karp, *Cell and Molecular Biology*, Wiley, 2008.
212. R. M. Puranik and H. S. Srivastava, *Phytochemistry*, 1986, **25**, 803-805.
213. O. L. Francone and C. J. Fielding, *Biochemistry*, 1991, **30**, 10074-10077.

214. H. M. Zhao and W. A. van der Donk, *Curr. Opin. Biotechnol.*, 2003, **14**, 583-589.
215. T. Burgdorf, A. L. De Lacey and B. Friedrich, *J. Bacteriol.*, 2002, **184**, 6280-6288.
216. K. Schneider, R. Cammack, H. G. Schlegel and D. O. Hall, *Biochim. Biophys. Acta*, 1979, **578**, 445-461.
217. J. Ratzka, L. Lauterbach, O. Lenz and M. B. Ansorge-Schumacher, *Biocatal. Biotransform.*, 2011, **29**, 246-252.
218. M. Andersson, H. Holmberg and P. Adlercreutz, *Biotechnol. Bioeng.*, 1998, **57**, 79-86.
219. T. J. Deloggio and D. J. Graves, *Biotechnol. Bioeng.*, 1988, **32**, 295-300.
220. J. Liu, DPhil Thesis. University of Oxford, 2012.
221. K. Schneider and H. G. Schlegel, *Biochem. J*, 1981, **193**, 99-107.
222. E. F. Elstner and A. Heupel, *Anal. Biochem.*, 1976, **70**, 616-620.
223. L. Kussmaul and J. Hirst, *Proc. Natl. Acad. Sci. U.S.A.*, 2006, **103**, 7607-7612.
224. D. Esterhazy, M. S. King, G. Yakovlev and J. Hirst, *Biochemistry*, 2008, **47**, 3964-3971.
225. J. Hirst, M. S. King and K. R. Pryde, *Biochem. Soc. Trans.*, 2008, **36**, 976-980.
226. J. B. Jackson, *FEBS Lett.*, 2003, **555**, 176-177.
227. V. G. Grivennikova, R. Roth, N. V. Zakharova, C. Hagerhall and A. D. Vinogradov, *Biochim. Biophys. Acta-Bioenerg.*, 2003, **1607**, 79-90.
228. M. Katzberg, N. Skorupa-Parachin, M. F. Gorwa-Grauslund and M. Bertau, *Int. J. Mol. Sci.*, 2010, **11**, 1735-1758.
229. M. Mueller, M. Katzberg, M. Bertau and W. Hummel, *Org. Biomol. Chem.*, 2010, **8**, 1540-1550.
230. A. D. Vinogradov, *Biochim. Biophys. Acta-Bioenerg.*, 1998, **1364**, 169-185.
231. Y. Hatefi and W. G. Hanstein, *Biochemistry*, 1973, **12**, 3515-3522.
232. K. Morina, M. Schulte, F. Hubrich, K. Dorner, S. Steimle, S. Stolpe and T. Friedrich, *J. Biol. Chem.*, 2011, **286**, 34627-34634.
233. C. S. Hanes, *Biochem. J*, 1932, **26**, 1406-1421.
234. D. D. Keightley and N. A. C. Cressie, *J. Steroid Biochem. Mol. Biol.*, 1980, **13**, 1317-1323.
235. L. Lauterbach, *Personal Communication*, 2011.

236. O. Campapiano, E. Mundofrr, B. Borup and R. Voladri, *Chem. Abstr*, 2009, **150**, 416448.
237. C. Ching, J. M. Gruber, G. W. Huisman, E. Mundorff and L. M. Newman, *Chem. Abstr*, 2008, **149**, 326218.
238. A. J. Irwin and J. B. Jones, *J. Am. Chem. Soc.*, 1977, **99**, 1625-1630.
239. A. J. Irwin and J. B. Jones, *J. Am. Chem. Soc.*, 1976, **98**, 8476-8482.
240. N. S. Scrutton, A. Berry and R. N. Perham, *Nature*, 1990, **343**, 38-43.
241. R. Feeney, A. R. Clarke and J. J. Holbrook, *Biochem. Biophys. Res. Commun.*, 1990, **166**, 667-672.
242. L. Lauterbach and O. Lenz, *Personal Communication*, 2011.
243. K. S. Ma, R. Weiss and M. W. W. Adams, *J. Bacteriol.*, 2000, **182**, 1864-1871.
244. C. L. McIntosh, F. Germer, R. Schulz, J. Appel and A. K. Jones, *J. Am. Chem. Soc.*, 2011, **133**, 11308-11319.
245. J. Havel and D. Weuster-Botz, *Appl. Microbiol. Biotechnol.*, 2007, **75**, 1031-1037.
246. M. Eckstein, T. Daussmann and U. Kragl, *Biocatal. Biotransform.*, 2004, **22**, 89-96.
247. R. DevauxBasseguy, A. Bergel and M. Comtat, *Enzyme Microb. Technol.*, 1997, **20**, 248-258.
248. W. Hummel, *Trends Biotechnol.*, 1999, **17**, 487-492.
249. E. G. Hibbert and P. A. Dalby, *Microbial Cell Factories*, 2005, **4**.
250. E. G. Hibbert, F. Baganz, H. C. Hailes, J. M. Ward, G. J. Lye, J. M. Woodley and P. A. Dalby, *Biomol. Eng*, 2005, **22**, 11-19.
251. F. Hollmann, I. W. C. E. Arends and D. Holtmann, *Green Chem.*, 2011, **13**, 2285-2314.
252. C. Kohlmann, W. Maerkle and S. Luetz, *J. Mol. Catal. B: Enzym.*, 2008, **51**, 57-72.
253. J. Zhang, B. Witholt and Z. Li, *Chem. Commun.*, 2006, 398-400.
254. W. Liu and P. Wang, *Biotechnol. Adv.*, 2007, **25**, 369-384.
255. W. Hummel, in *Advances in Biochemical Engineering Biotechnology; New enzymes for organic synthesis: Screening, supply and engineering*, ed. T. Scheper, Springer, Editon edn., 1997, vol. 58. pp145-184.

256. F. H. Arnold and J. C. Moore, in *Advances in Biochemical Engineering Biotechnology; New enzymes for organic synthesis: Screening, supply and engineering*, ed. T. Scheper, Springer, Editon edn., 1997, vol. 58. pp1-14.
257. R. Ruinatscha, V. Hoellrigl, K. Otto and A. Schmid, *Adv. Synth. Catal.*, 2006, **348**, 2015-2026.
258. C. Wandrey, *Chem. Rec.*, 2004, **4**, 254-265.
259. A. Weckbecker, H. Groeger and W. Hummel, in *Biosystems Engineering I: Creating Superior Biocatalysts*, Editon edn., 2010, vol. 120, pp. 195-242.
260. S. Broussy, R. W. Cheloha and D. B. Berkowitz, *Org. Lett.*, 2009, **11**, 305-308.
261. R. Mertens, L. Greiner, E. C. D. van den Ban, H. Haaker and A. Liese, *J. Mol. Catal. B: Enzym.*, 2003, **24-5**, 39-52.
262. R. Mertens and A. Liese, *Curr. Opin. Biotechnol.*, 2004, **15**, 343-348.
263. K. Cheikhou and T. Tzedakis, *AlChE J.*, 2008, **54**, 1365-1376.
264. S. Kim, S. E. Yun and C. Kang, *Electrochem. Commun.*, 1999, **1**, 151-154.
265. B. Grundig, G. Wittstock, U. Rudel and B. Strehlitz, *J. Electroanal. Chem.*, 1995, **395**, 143-157.
266. J. Ratzka, L. Lauterbach, O. Lenz and M. B. Ansorge-Schumacher, *J. Mol. Catal. B: Enzym.*, 2012, **74**, 219-223.
267. Z. Shaked and G. M. Whitesides, *J. Am. Chem. Soc.*, 1980, **102**, 7104-7105.
268. M. R. Kula and C. Wandrey, *Methods Enzymol.*, 1987, **136**, 9-21.
269. K. A. Vincent, X. Li, C. F. Blanford, N. A. Belsey, J. H. Weiner and F. A. Armstrong, *Nat. Chem. Biol.*, 2007, **3**, 760-761.
270. H. A. Reeve, *Personal Communication*, 2012.
271. H. A. Reeve, L. Lauterbach, P. A. Ash, O. Lenz and K. A. Vincent, *Chem. Commun.*, 2012, **48**, 1589-1591.
272. M. W. Eggert, M. E. Byrne and R. P. Chambers, *Appl. Biochem. Biotechnol.*, 2011, **165**, 676-686.
273. K. Hanai, A. Kuwae, Y. Sugawa, K.-K. Kunimoto and S. Maeda, *J. Mol. Struct.*, 2007, **837**, 101-106.
274. G. Cassanas, M. Morssli, E. Fabregue and L. Bardet, *J. Raman Spectrosc.*, 1991, **22**, 409-413.

Appendix 1

Sequence alignment of Soluble Hydrogenases

Subunit HoxF		Subunit HoxF		Score (%)
Name	Length	Name	Length	
Thiocapsa roseopersicina	536	*Allochromatium vinosum*	538	80
Thiocapsa roseopersicina	536	*Rhodococcus opacus*	604	28
Thiocapsa roseopersicina	536	*Synechocystis sp* PCC 6803	533	60
Thiocapsa roseopersicina	536	*Ralstonia eutropha*	602	29
Allochromatium vinosum	538	*Rhodococcus opacus*	604	29
Allochromatium vinosum	538	*Synechocystis sp* PCC 6803	533	59
Allochromatium vinosum	538	*Ralstonia eutropha*	602	30
Rhodococcus opacus	604	*Synechocystis sp* PCC 6803	533	30
Rhodococcus opacus	604	*Ralstonia eutropha*	602	79
Synechocystis sp PCC 6803	533	*Ralstonia eutropha*	602	31

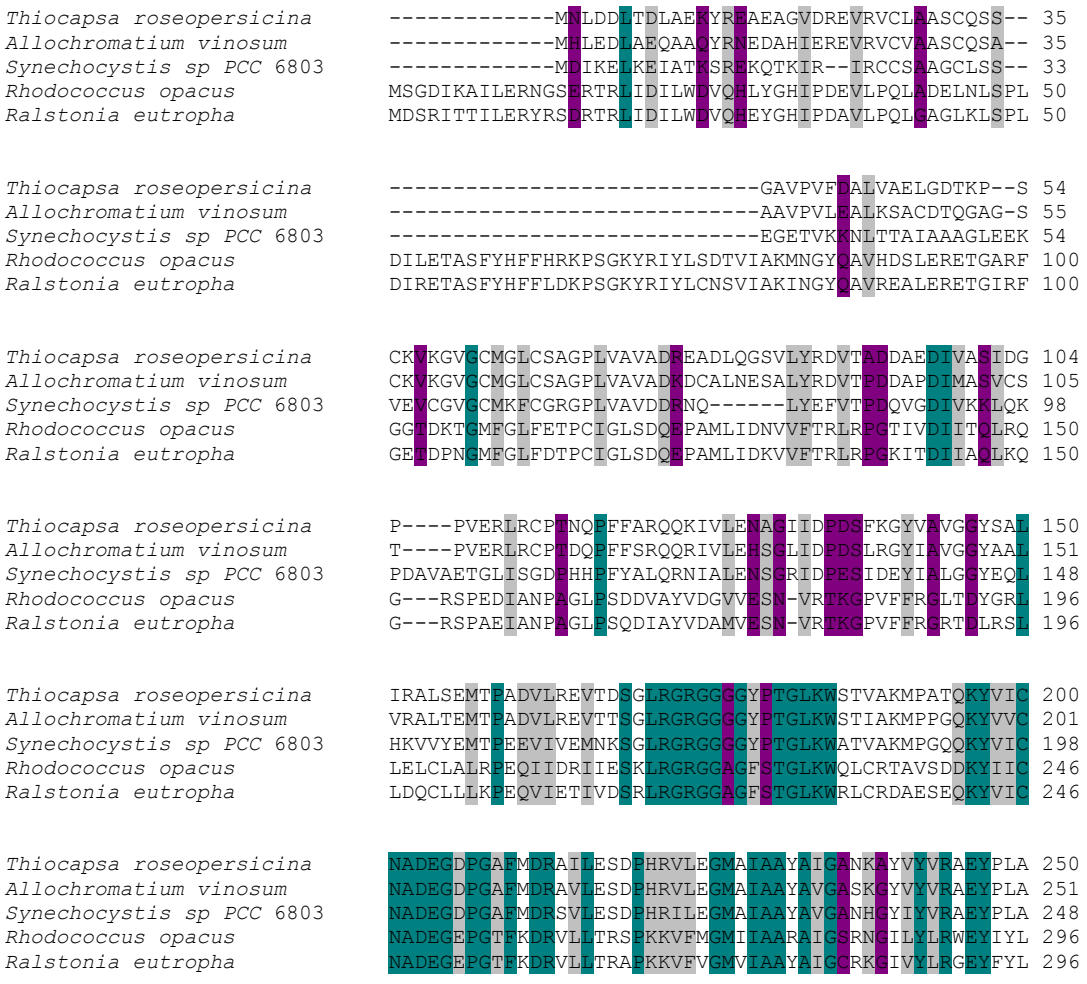

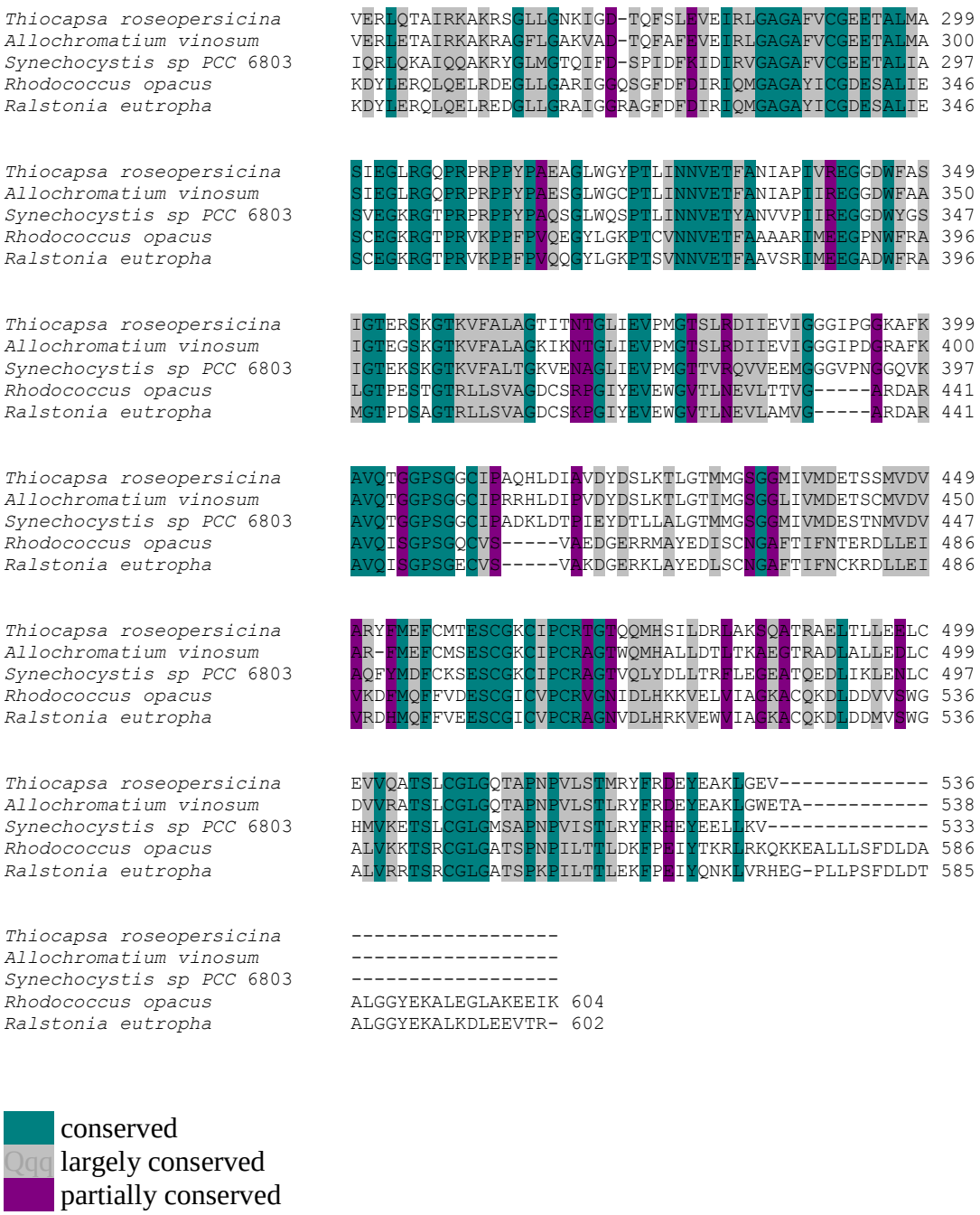
Thiocapsa roseopersicina VERLQTAIRKAKRSGLLGNKIGD-TQFSLEVEIRLGAGAFVCGEETALMA 299
Allochromatium vinosum VERLETAIRKAKRAGFLGAKVAD-TQFAFEVEIRLGAGAFVCGEETALMA 300
Synechocystis sp PCC 6803 IQRLQKAIQQAKRYGLMGTQIFD-SPIDFKIDIRVGAGAFVCGEETALIA 297
Rhodococcus opacus KDYLERQLQELRDEGLLGARIGGQSGFDFDIRIQMGAGAYICGDESALIE 346
Ralstonia eutropha KDYLERQLQELREDGLLGRAIGGRAGFDFDIRIQMGAGAYICGDESALIE 346
Thiocapsa roseopersicina SIEGLRGQPRPRPPYPAEAGLWGYPTLINNVETFANIAPIVREGGDWFAS 349
Allochromatium vinosum SIEGLRGQPRPRPPYPAESGLWGCPTLINNVETFANIAPIIREGGDWFAA 350
Synechocystis sp PCC 6803 SVEGKRGTPRPRPPYPAQSGLWQSPTLINNVETYANVVPIIREGGDWYGS 347
Rhodococcus opacus SCEGKRGTPRVKPPFPVQEGYLGKPTCVNNVETFAAAARIMEEGPNWFRA 396
Ralstonia eutropha SCEGKRGTPRVKPPFPVQQGYLGKPTSVNNVETFAAVSRIMEEGADWFRA 396
Thiocapsa roseopersicina IGTERSKGTKVFALAGTITNTGLIEVPMGTSLRDIIEVIGGGIPGGKAFK 399
Allochromatium vinosum IGTEGSKGTKVFALAGKIKNTGLIEVPMGTSLRDIIEVIGGGIPDGRAFK 400
Synechocystis sp PCC 6803 IGTEKSKGTKVFALTGKVENAGLIEVPMGTTVRQVVEEMGGGVPNGGQVK 397
Rhodococcus opacus LGTPESTGTRLLSVAGDCSRPGIYEVEWGVTLNEVLTTVG-----ARDAR 441
Ralstonia eutropha MGTPDSAGTRLLSVAGDCSKPGIYEVEWGVTLNEVLAMVG-----ARDAR 441
Thiocapsa roseopersicina AVQTGGPSGGCIPAQHLDIAVDYDSLKTLGTMMGSGGMIVMDETSSMVDV 449
Allochromatium vinosum AVQTGGPSGGCIPRRHLDIPVDYDSLKTLGTIMGSGGLIVMDETSCMVDV 450
Synechocystis sp PCC 6803 AVQTGGPSGGCIPADKLDTPIEYDTLLALGTMMGSGGMIVMDESTNMVDV 447
Rhodococcus opacus AVQISGPSGQQVS-----VAEDGERRMAYEDISCNGAFTIFNTERDLLEI 486
Ralstonia eutropha AVQISGPSGECVS-----VAKDGERKLAYEDLSCNGAFTIFNCKRDLLEI 486
Thiocapsa roseopersicina ARYFMEFCMTESCGKCIPCRIGIQQMHSILDRLAKSQATRAELTLLEELC 499
Allochromatium vinosum AR-FMEFCMSESCGKCIPCRAGTWQMHALLDTLTKAEGTRADLALLEDLC 499
Synechocystis sp PCC 6803 AQFYMDFCKSESCGKCIPCRAGTVQLYDLLTRLEGEATQEDLIKLENLC 497
Rhodococcus opacus VKDFMQFFVDESCGICVPCRVGNIDLHKKVELVIAGKACQKDLDDVVSWG 536
Ralstonia eutropha VRDHMQFFVEESCGICVPCRAGNVDLHRKVEWVIAGKACQKDLDDMVSWG 536
Thiocapsa roseopersicina EVVQATSLCGLGQTAPNPVLSTMRYFRDEYEAKLGEV---------- 536
Allochromatium vinosum DVVRATSLCGLGQTAPNPVLSTLRYFRDEYEAKLGWETA---------- 538
Synechocystis sp PCC 6803 HMVKETSLCGLGMSAPNPVISTLRYFRHEYEELLKV---------- 533
Rhodococcus opacus ALVKKTSRCGLGATSPNPILTTLDKFPEIYTKRLRKQKKEALLLSFDLDA 586
Ralstonia eutropha ALVRRTSRCGLGATSPKPILTTLEKFPEIYQNKLVRHEG-PLLPSFDLDT 585
Thiocapsa roseopersicina ----------
Allochromatium vinosum ----------
Synechocystis sp PCC 6803 ----------
Rhodococcus opacus ALGGYEKALEGLAKEEIK 604
Ralstonia eutropha ALGGYEKALKDLEEVTR- 602
conserved
Qqq largely conserved
partially conserved

Subunit HoxU		Subunit HoxU		Score (%)
Name	Length	Name	Length	
Thiocapsa roseopersicina	243	*Allochromatium vinosum*	243	87
Thiocapsa roseopersicina	243	*Rhodococcus opacus*	234	52
Thiocapsa roseopersicina	243	*Synechocystis sp* PCC 6803	238	29
Thiocapsa roseopersicina	243	*Ralstonia eutropha*	234	29
Allochromatium vinosum	243	*Rhodococcus opacus*	234	50
Allochromatium vinosum	243	*Synechocystis sp* PCC 6803	238	29
Allochromatium vinosum	243	*Ralstonia eutropha*	234	28
Rhodococcus opacus	234	*Synechocystis sp* PCC 6803	238	31
Rhodococcus opacus	234	*Ralstonia eutropha*	234	82
Synechocystis sp PCC 6803	238	*Ralstonia eutropha*	234	33

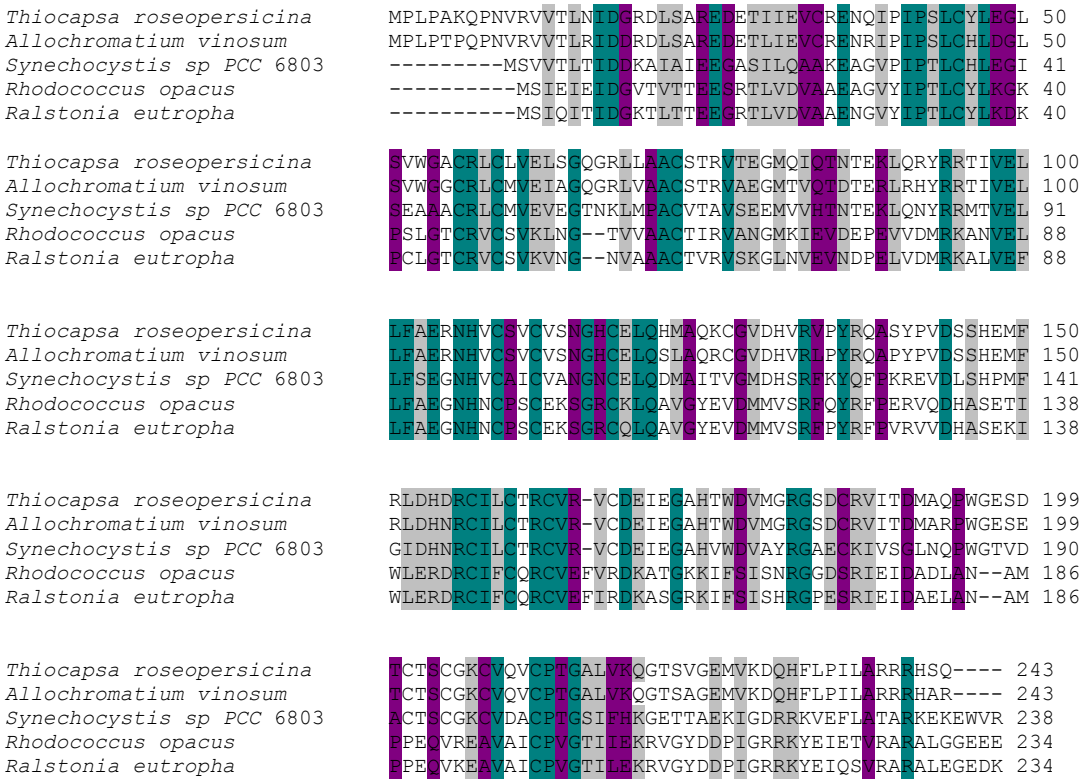

Subunit HoxH		Subunit HoxH		Score (%)
Name	Length	Name	Length	
Thiocapsa roseopersicina	475	*Allochromatium vinosum*	349	84
Thiocapsa roseopersicina	475	*Rhodococcus opacus*	488	40
Thiocapsa roseopersicina	475	*Synechocystis sp* PCC 6803	474	56
Thiocapsa roseopersicina	475	*Ralstonia eutropha*	488	41
Allochromatium vinosum	349	*Rhodococcus opacus*	488	36
Allochromatium vinosum	349	*Synechocystis sp* PCC 6803	474	55
Allochromatium vinosum	349	*Ralstonia eutropha*	488	37
Rhodococcus opacus	488	*Synechocystis sp* PCC 6803	474	43
Rhodococcus opacus	488	*Ralstonia eutropha*	488	85
Synechocystis sp PCC 6803	474	*Ralstonia eutropha*	488	44

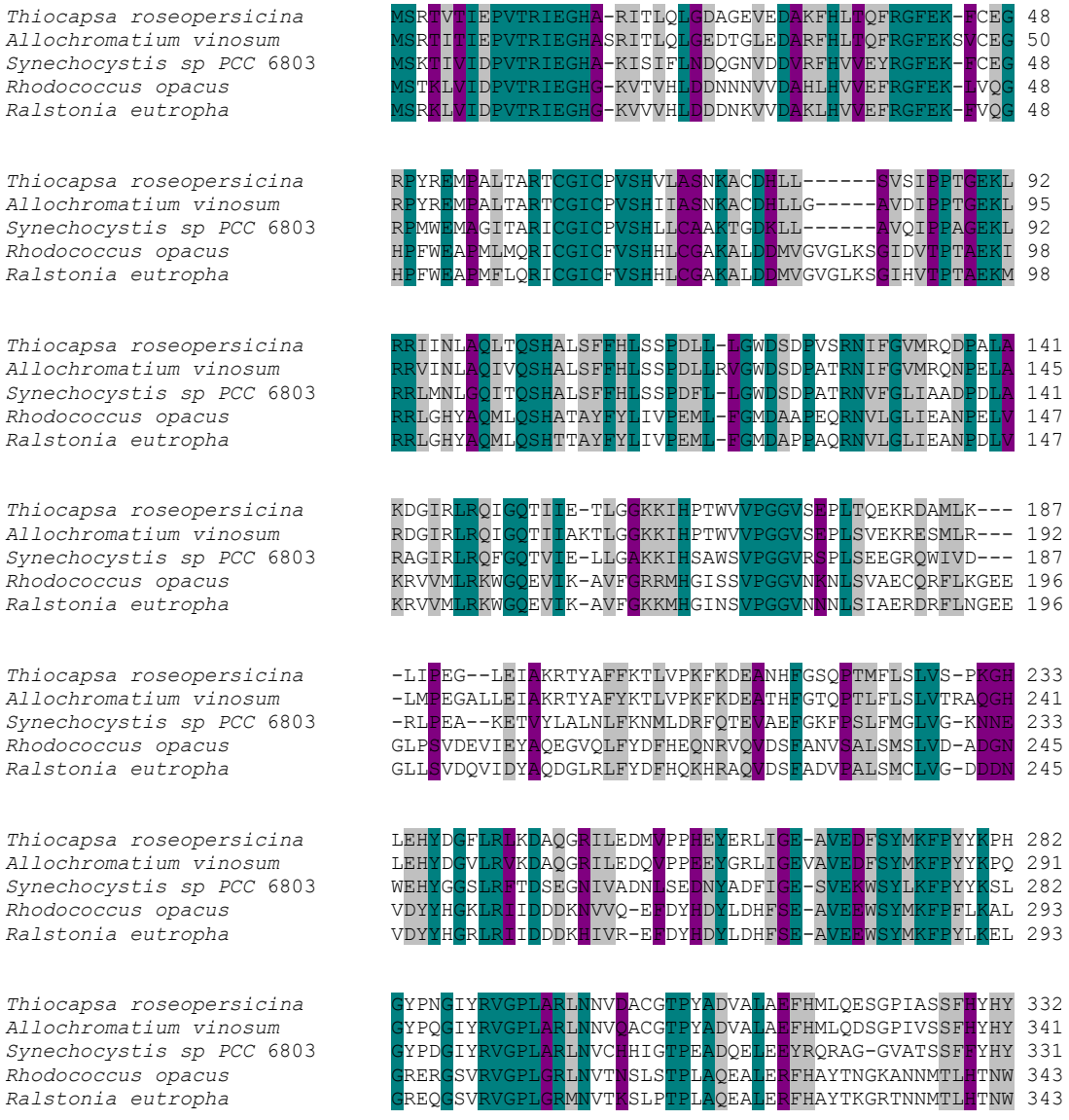

```
Thiocapsa roseopersicina        ARLVEIIYALEMMERLLKDPTILDARVRARARSNRY--EGIGVAEAPRGI 380
Allochromatium vinosum          ARLVEIIY---------------------------------------- 349
Synechocystis sp PCC 6803       ARLVEILACLEAIELLMADPDILSKNCRAKAEINCT--EAVGVSEAPRGT 379
Rhodococcus opacus              ARAIEILHAAELIKELLNDPDLQKEQLLLTPADNAWTGEGVGVVEAPRGT 393
Ralstonia eutropha              ARAIEILHAAEVVKELLHDPDLQKDQLVLTPPPNAWTGEGVGVVEAPRGT 393

Thiocapsa roseopersicina        LMHHYRIDDEGLITWVNLIIATGHNNLAMNQSIRQVADAYVDGN-NLQEG 429
Allochromatium vinosum          ------------------------------------------------- 
Synechocystis sp PCC 6803       LFHHYKIDEDGLIKKVNLIIATGNNNLAMNKTVAQIAKHYIRNH-DVQEG 428
Rhodococcus opacus              LLHHYRADQEGDITFANLVVATTQNNQVMNRTVRSVAEDYLGGQGEVTEG 443
Ralstonia eutropha              LLHHYRADERGNITFANLVVATTQNNQVMNRTVRSVAEDYLGGHGEITEG 443

Thiocapsa roseopersicina        MLNRVEAVIRCFDPCLSCASHAFGEMPLAIELKDATGRVVDTLRRG 475
Allochromatium vinosum          ---------------------------------------------- 
Synechocystis sp PCC 6803       FLNRVEAGIRCYDPCLSCSTHAAGQMPLMIDLVNPQGELIKSIQRD 474
Rhodococcus opacus              MMNAIEVGIRAYDPCLSCATHALGQMPLIVSVHDTEGHVINERVR- 488
Ralstonia eutropha              MMNAIEVGIRAYDPCLSCATHALGQMPLVVSVFDAAGRLIDERAR- 488
```

conserved
largely conserved
partially conserved

Subunit HoxY		Subunit HoxY		Score (%)
Name	Length	Name	Length	
Thiocapsa roseopersicina	180	*Allochromatium vinosum*	180	82
Thiocapsa roseopersicina	180	*Rhodococcus opacus*	209	40
Thiocapsa roseopersicina	180	*Synechocystis sp* PCC 6803	182	48
Thiocapsa roseopersicina	180	*Ralstonia eutropha*	209	43
Allochromatium vinosum	180	*Rhodococcus opacus*	209	40
Allochromatium vinosum	180	*Synechocystis sp* PCC 6803	182	47
Allochromatium vinosum	180	*Ralstonia eutropha*	209	44
Rhodococcus opacus	209	*Synechocystis sp* PCC 6803	182	39
Rhodococcus opacus	209	*Ralstonia eutropha*	209	85
Synechocystis sp PCC 6803	182	*Ralstonia eutropha*	209	37

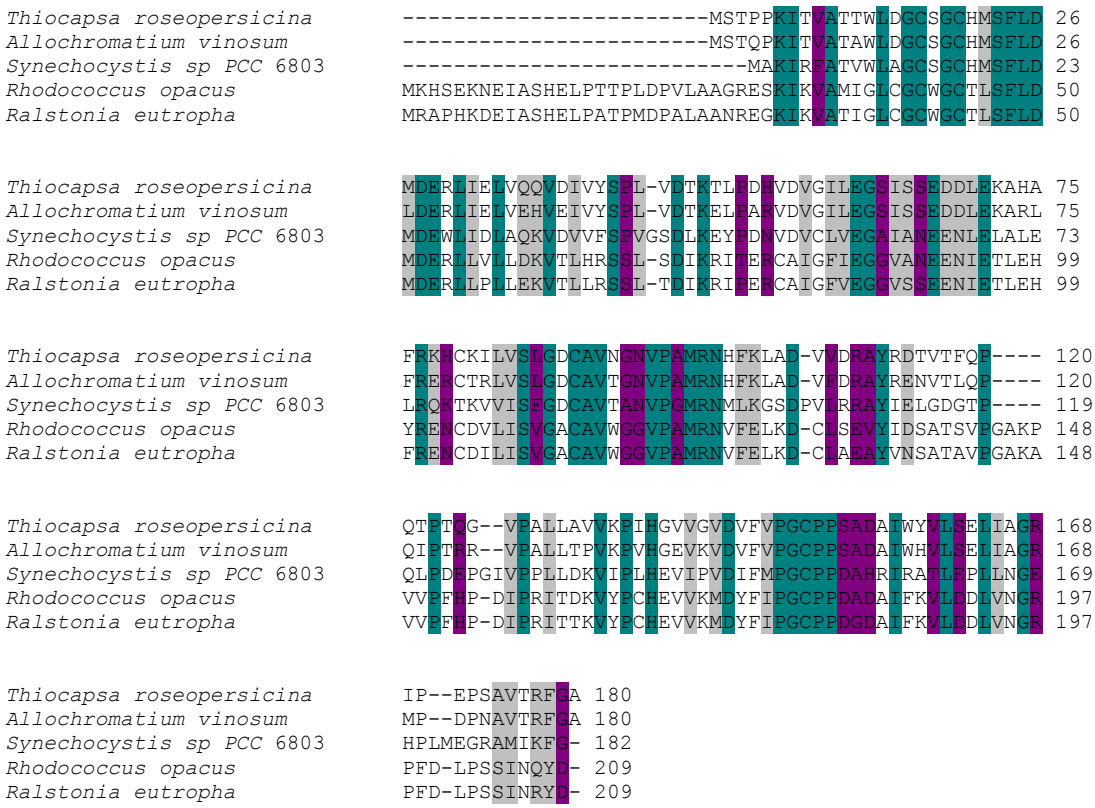

Appendix 2

Electrochemical results of D467S HoxHYFU

NADH oxidation and NAD^+ reduction by D467S HoxHYFU on an electrode.

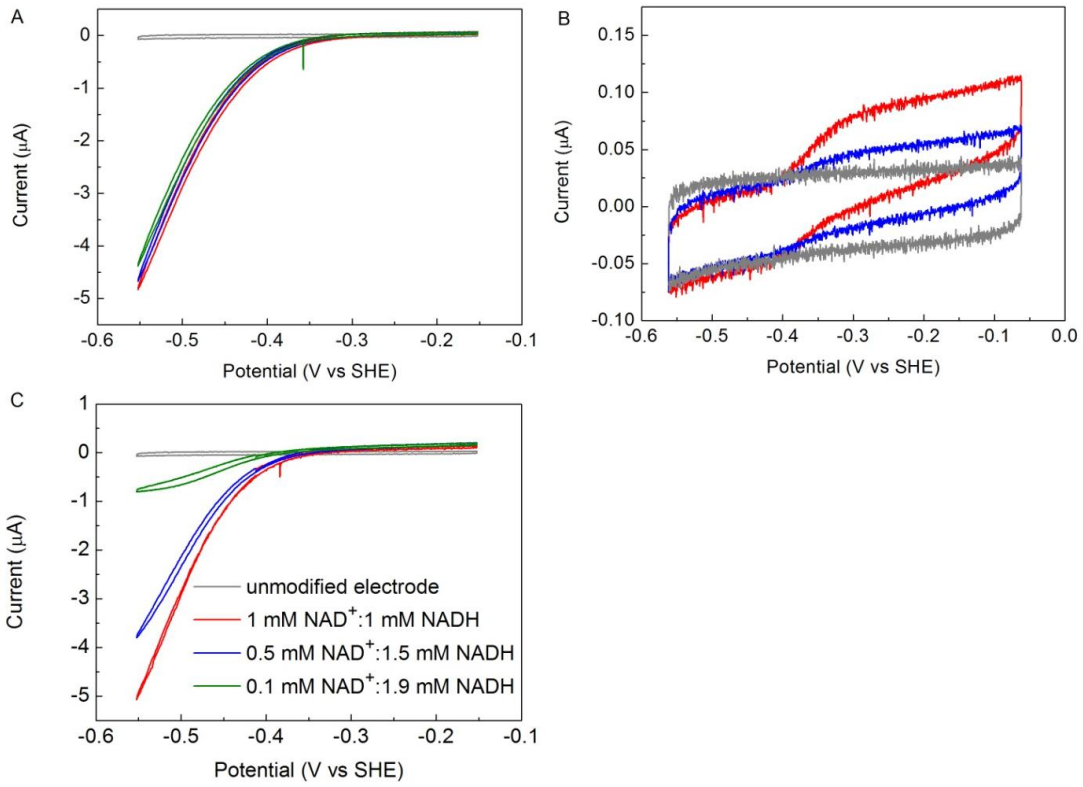

Figure 141. Electrocatalytic NAD^+ reduction and NADH oxidation by D467S HoxHYFU variant. Experiments in panels A and B were performed in a solution of 2 mM NAD^+ and 2 mM NADH respectively. Panel C shows cyclic voltammograms of HoxHYFU D467S variant in a mixture of NAD^+ and NADH, the concentrations used are as labelled in the figure. Other conditions: Tris-HCl buffer 50 mM, pH 8.0, 30 ^oC, electrode was rotated at 2500 rpm, scan rate 10 mV/s.

Low potential inactivation observed for D467S HoxHYFU.

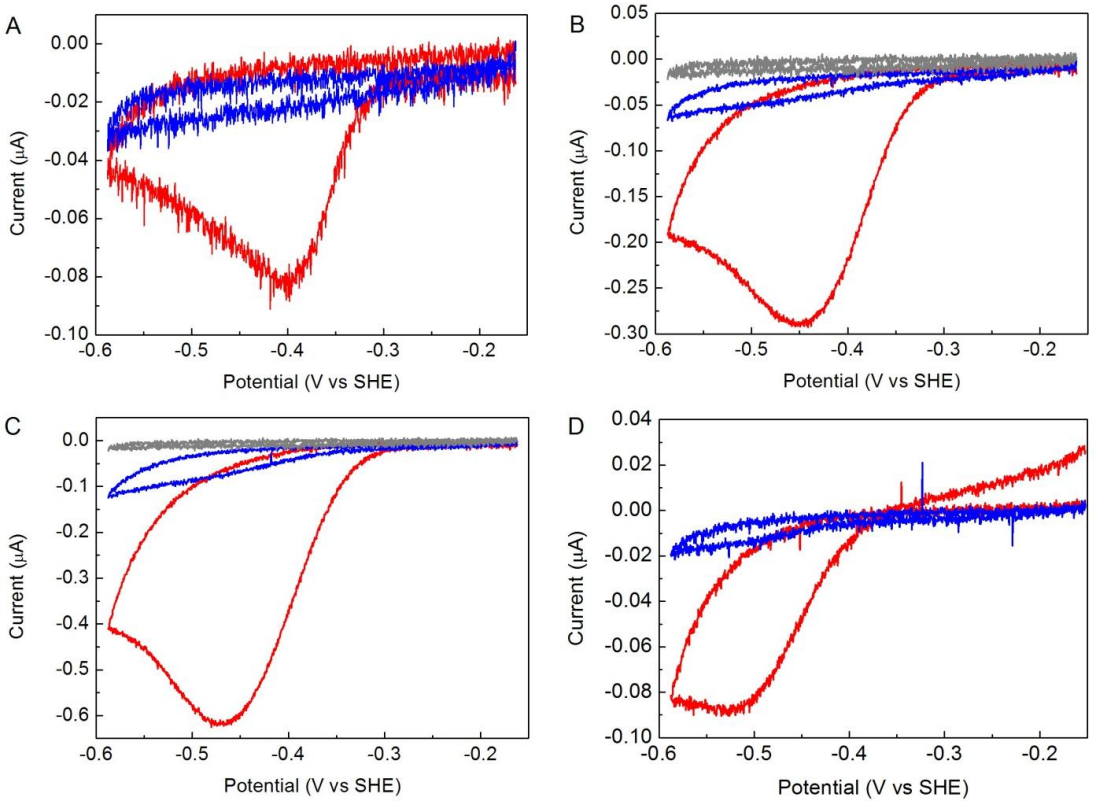

Figure 142. Cyclic voltammetry experiments to check for low potential inactivation by HoxHYFU D467S variant at different NAD^+ and NADH concentrations: 50 μM NAD^+ (A), 2 mM NAD^+ (B), 5 mM NAD^+ (C) and 1 mM NAD^+: 1 mM NADH (D). Experimental conditions: Tris-HCl buffer 50 mM at pH 8.0, 30 ^oC. The experiments were performed at a slow scan rate of 1 mV/s while the electrode was rotated at 2500 rpm. The first cycle of each scan is shown as a red line and the second cycle is shown as a blue line.

Michaelis-Menten constant for NAD^+

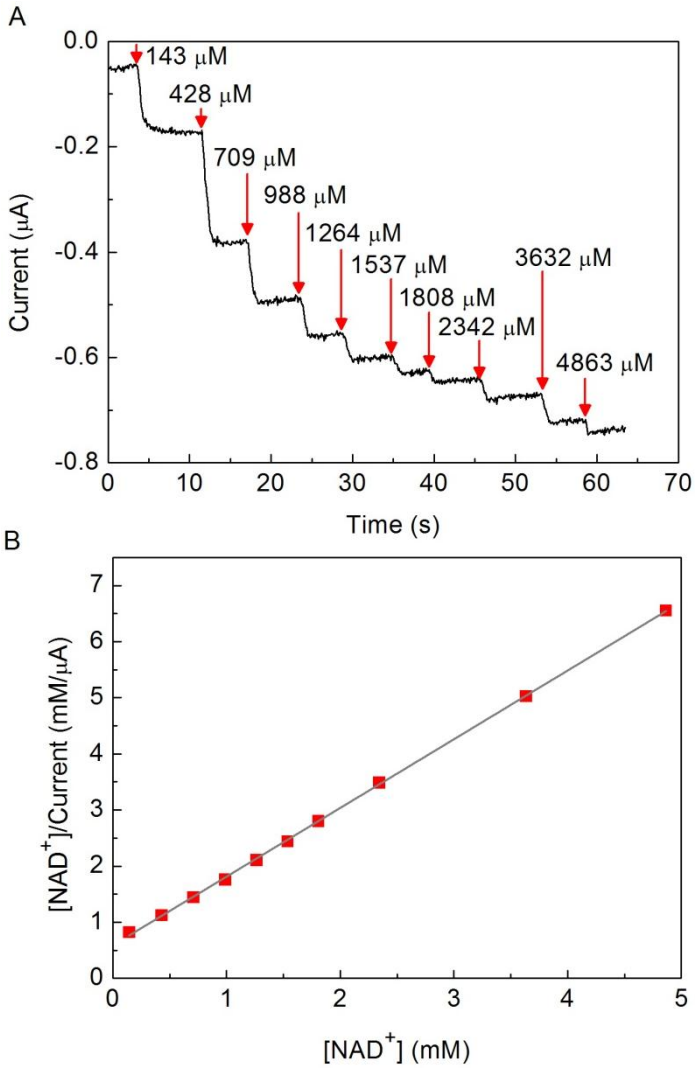

Figure 143. Panel A shows a typical chronoamperometry experiment designed to determine the D467S HoxHYFU variant affinity constant for NAD^+. The experiment was performed in a 50 mM Tris-HCl buffer, pH 8.0, titrated to 30 ^oC and the electrode was poised at -0.412 V and rotated at 2500 rpm. In panel B, a typical Hanes-Woolf plot is shown.

Michaelis-Menten constant for NADH

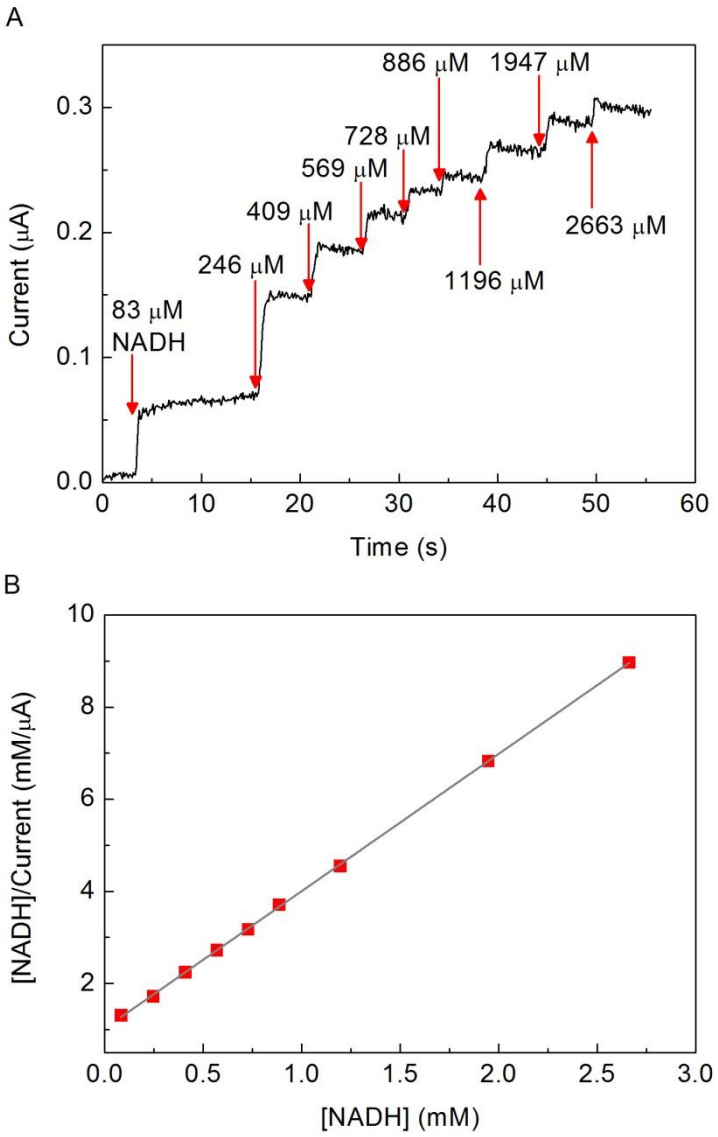

Figure 144. Panel A shows a typical chronoamperometry experiment designed to determine the D467S HoxHYFU variant affinity constant for NADH. The experiment was performed in a 50 mM Tris-HCl buffer, pH 8.0, titrated to 30 ^{o}C and the electrode was poised at -0.062 V and rotated at 2500 rpm. In panel B, a typical Hanes-Woolf plot is shown.

Michaelis-Menten constant for $NADP^+$

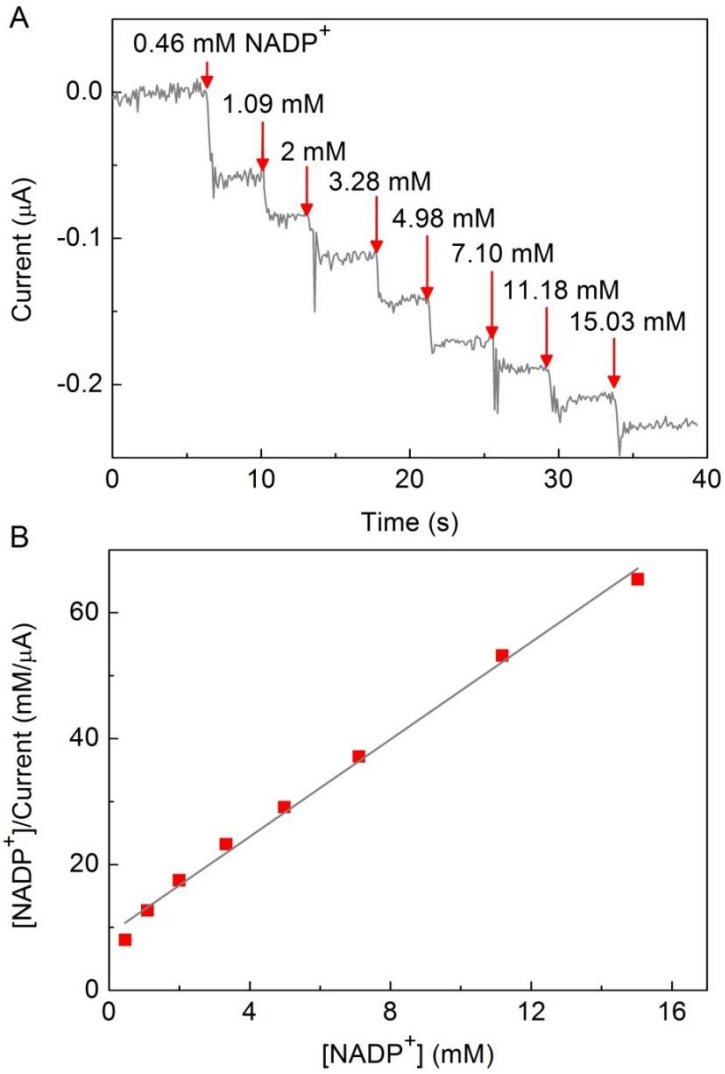

Figure 145. Panel A shows a typical chronoamperometry experiment designed to determine the D467S HoxHYFU variant affinity constant for $NADP^+$. The experiment was performed in a 50 mM Tris-HCl buffer, pH 8.0, titrated to 30 ^oC and the electrode was poised at -0.412 V and rotated at 2500 rpm. In panel B, a typical Hanes-Woolf plot is shown.

Inhibition constant for NADH oxidation

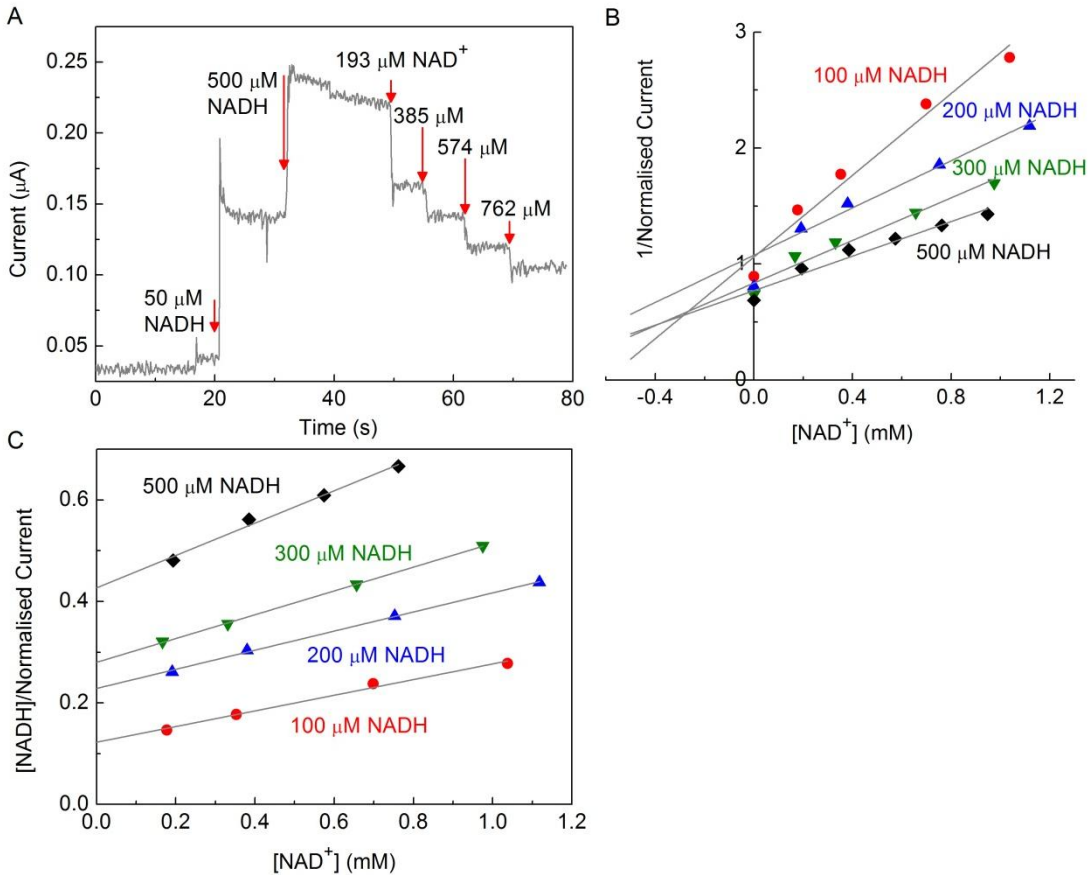

Figure 146. A. Current time plot from chronoamperometry experiment designed to determine the D467S HoxHYFU product inhibition constant for NADH oxidation. No NADH was present at the beginning of the experiment, then 50 μM NADH was introduced into the cell to give a 'control' current for normalising to other data sets. Further injection of NADH was performed to a final concentration of 500 μM NADH. Inhibitor containing the same final concentration of NADH was then introduced into the electrochemical cell to give concentrations as indicated by red arrows. The electrode was poised at -0.062 V vs SHE, and rotated at 2500 rpm. Experiments were performed at 30 ^{o}C, in a 50 mM Tris-HCl pH 8 buffer solution. Panels B and C show the Dixon and Cornish-Bowden plots to determine the inhibition constant and type of inhibition.

Inhibition constant for NAD^+ reduction

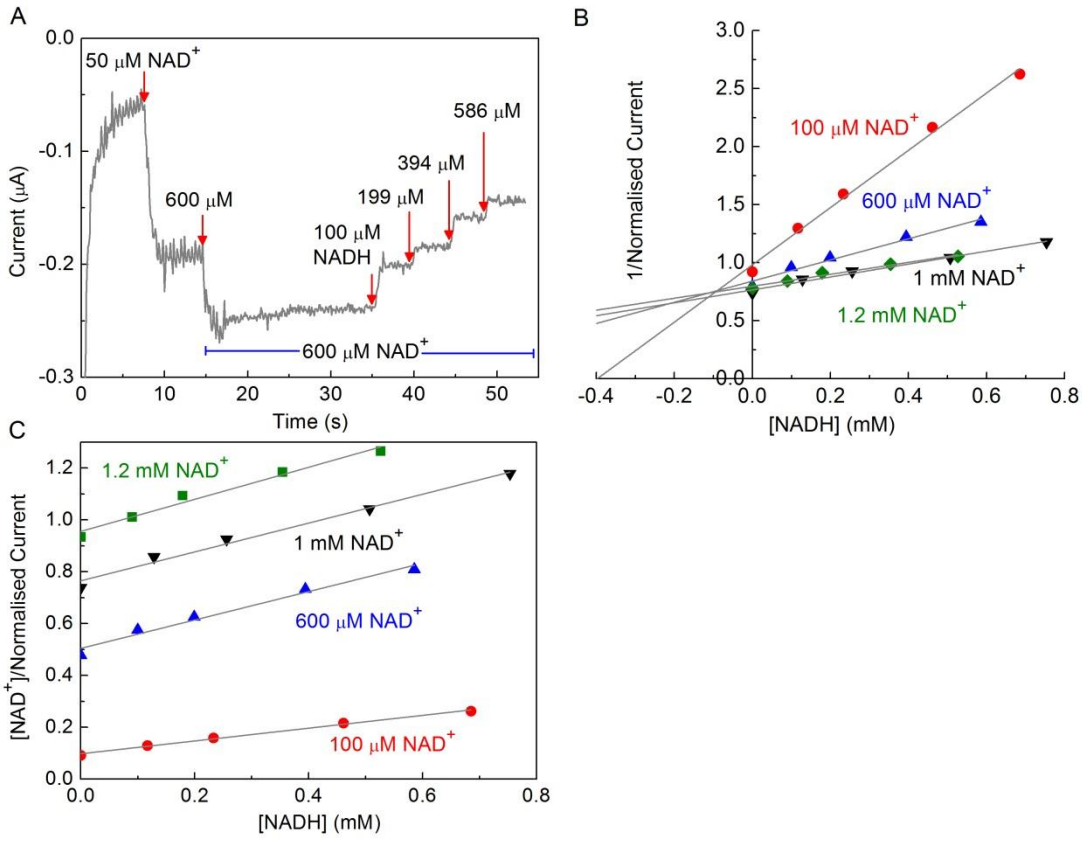

Figure 147. A. Current time plot from chronoamperometry experiment designed to determine the D467S HoxHYFU product inhibition constant for NAD^+ reduction. No NAD^+ was present at the beginning of the experiment, then 50 μM NAD^+ was introduced into the cell to give a 'control' current for normalising to other data sets. Further injection of NAD^+ was performed to a final concentration of 600 μM NAD^+. Inhibitor containing the same final concentration of NAD^+ was then introduced into the electrochemical cell to give concentrations as indicated by red arrows. The electrode was poised at -0.412 V vs SHE, and rotated at 2500 rpm. Experiments were performed at 30 ^oC, in a 50 mM Tris-HCl pH 8 buffer solution. Panels B and C show the Dixon and Cornish-Bowden plots to determine the inhibition constant and type of inhibition.

Appendix 3

Electrochemical results of HoxHYFU D326K

NADH oxidation and NAD^+ reduction by D326K HoxHYFU on an electrode

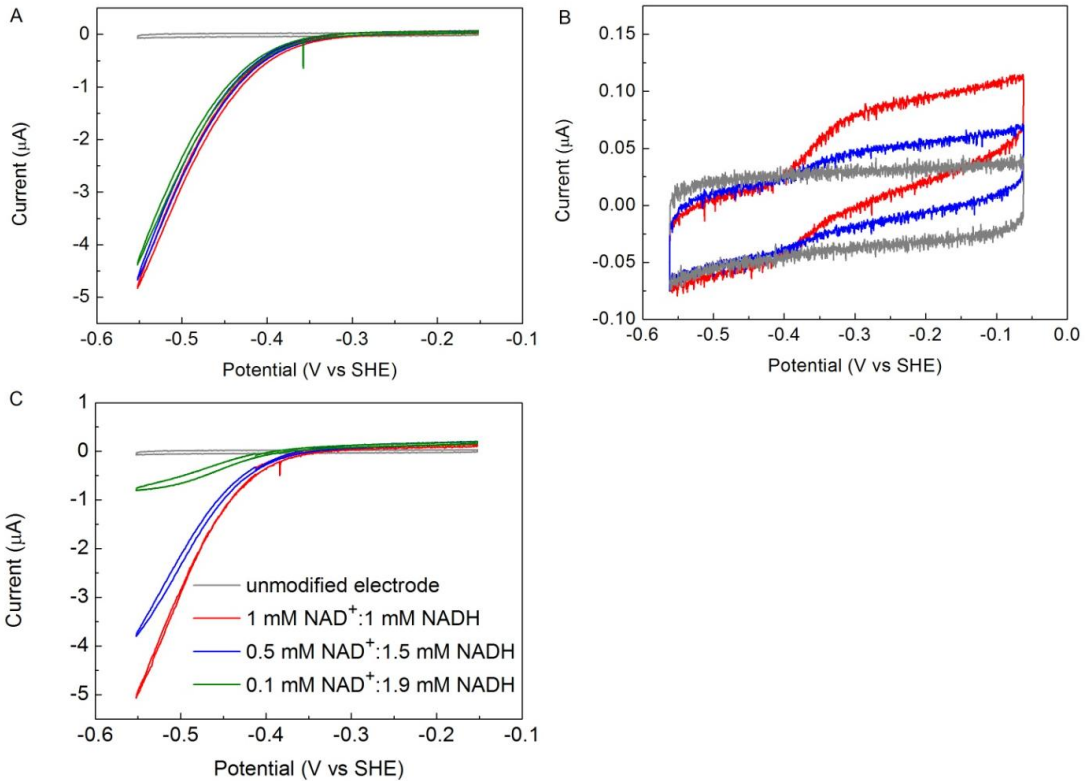

Figure 148. Electrocatalytic NAD^+ reduction and NADH oxidation by HoxHYFU D326K variant. Experiments in panels A and B were performed in a solution of 2 mM NAD^+ and 2 mM NADH respectively. Panel C shows cyclic voltammograms of HoxHYFU D326K variant in a mixture of NAD^+ and NADH, the concentrations used are as labelled in the figure. Other conditions: Tris-HCl buffer 50 mM, pH 8.0, 30 ^oC, electrode was rotated at 2500 rpm, scan rate 10 mV/s.

Low potential inactivation observed for D326K HoxHYFU

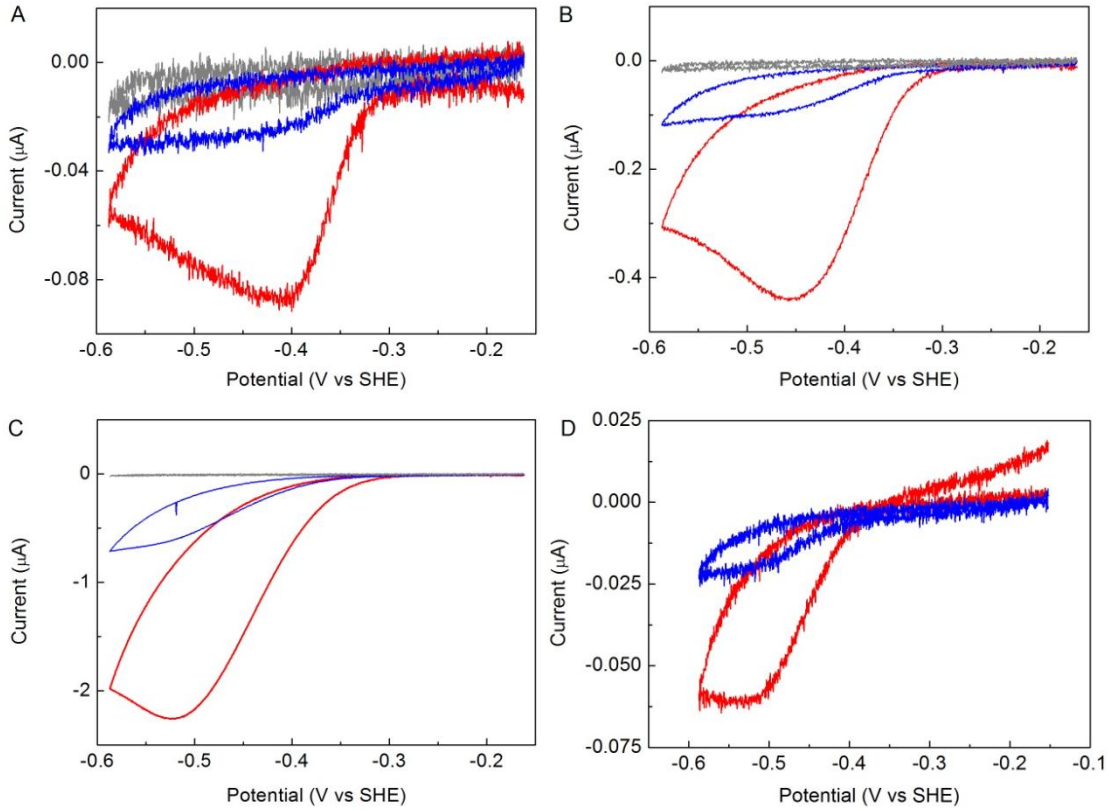

Figure 149. Cyclic voltammetry experiments to check for low potential inactivation by D326K HoxHYFU variant at different NAD^+ and NADH concentrations: 50 μM NAD^+ (A), 2 mM NAD^+ (B), 5 mM NAD^+ (C) and 1 mM NAD^+: 1 mM NADH (D). Experimental conditions: Tris-HCl buffer 50 mM at pH 8.0, 30 ^oC. The experiments were performed at a slow scan rate of 1 mV/s while the electrode was rotated at 2500 rpm. The first cycle of each scan is shown as a red line and the second cycle is shown as a blue line.

Michaelis-Menten constant for NAD^+

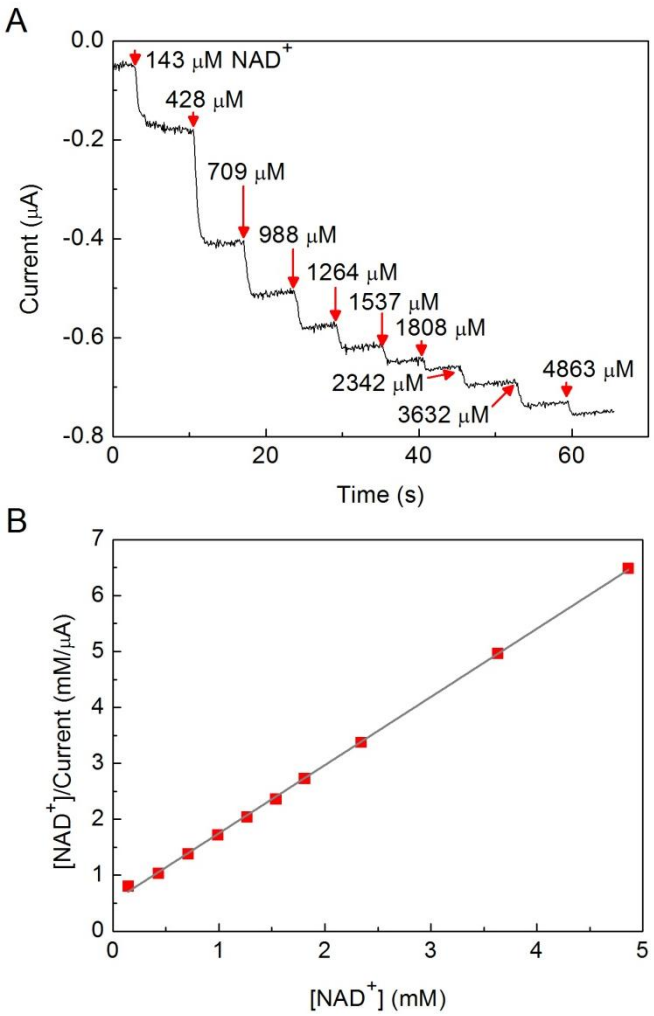

Figure 150. Panel A shows a typical chronoamperometry experiment designed to determine the D326K HoxHYFU variant affinity constant for NAD^+. The experiment was performed in a 50 mM Tris-HCl buffer, pH 8.0, titrated to 30 ^oC and the electrode was poised at -0.412 V and rotated at 2500 rpm. In panel B, a typical Hanes-Woolf plot is shown.

Michaelis-Menten constant for NADH

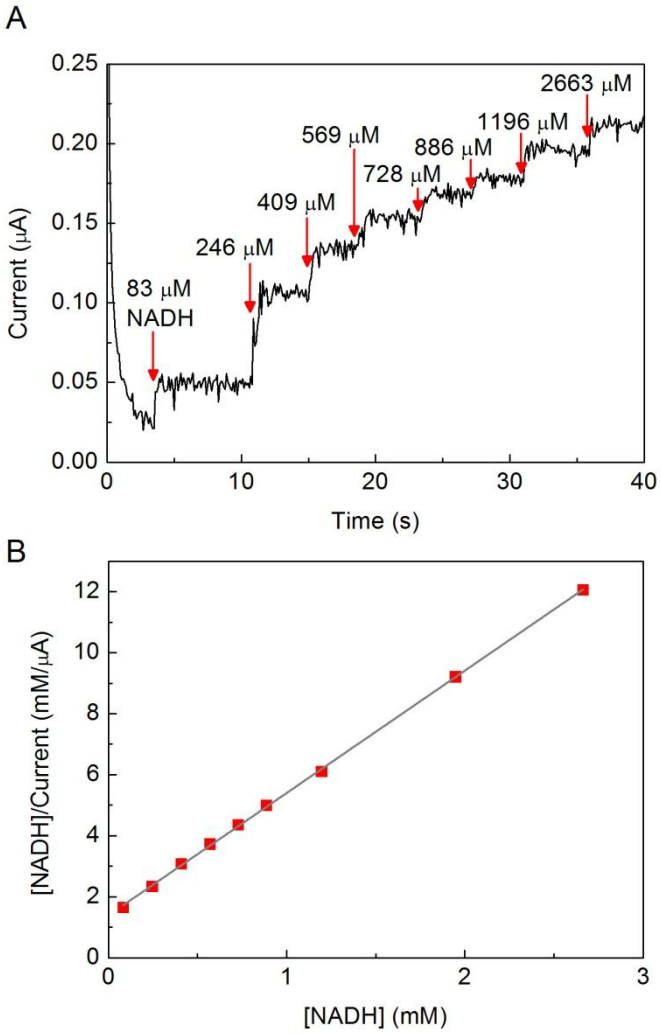

Figure 151. Panel A shows a typical chronoamperometry experiment designed to determine the D326K HoxHYFU variant affinity constant for NADH. The experiment was performed in a 50 mM Tris-HCl buffer, pH 8.0, titrated to 30 ^{o}C and the electrode was poised at -0.062 V and rotated at 2500 rpm. In panel B, a typical Hanes-Woolf plot is shown.

Michaelis-Menten constant for $NADP^+$

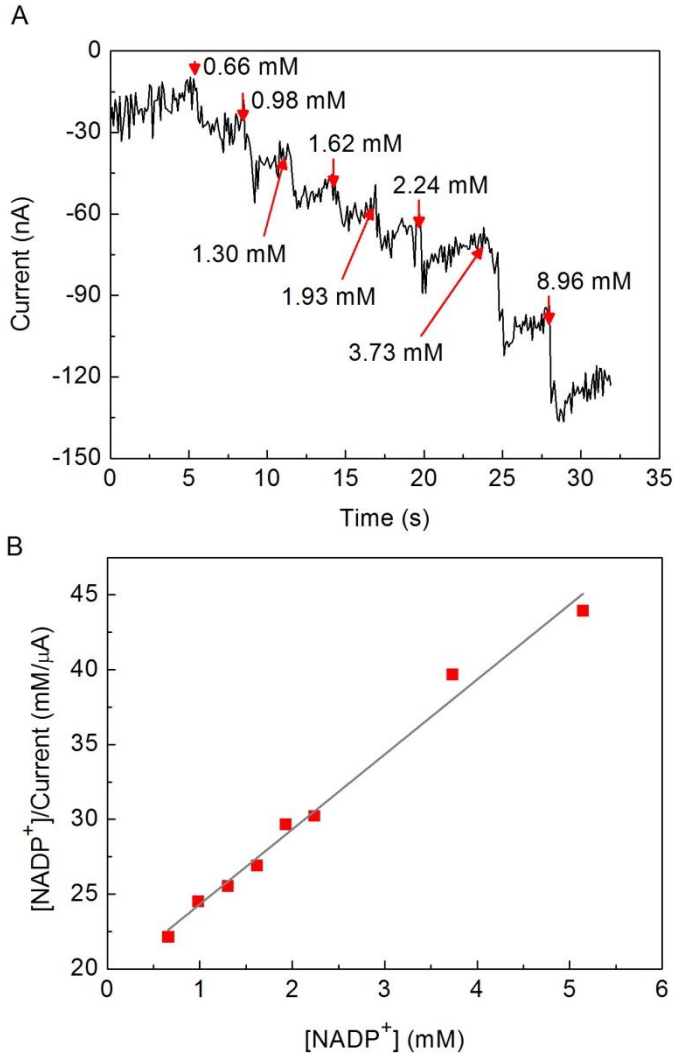

Figure 152. Panel A shows a typical chronoamperometry experiment designed to determine the D326K HoxHYFU variant affinity constant for $NADP^+$. The experiment was performed in a 50 mM Tris-HCl buffer, pH 8.0, titrated to 30 ^oC and the electrode was poised at -0.412 V and rotated at 2500 rpm. In panel B, a typical Hanes-Woolf plot is shown.

Inhibition constant for NADH oxidation

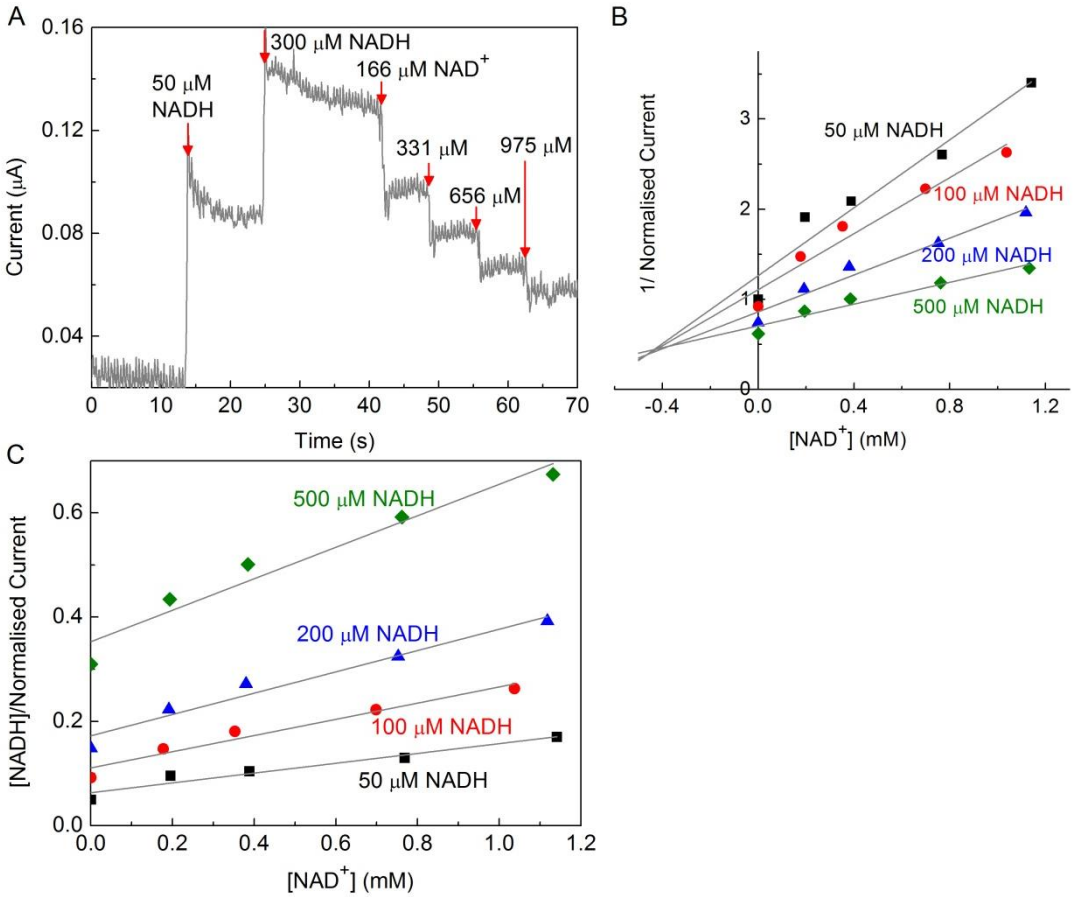

Figure 153. A. Current time plot from chronoamperometry experiment designed to determine the D326K HoxHYFU product inhibition constant for NADH oxidation. No NADH was present at the beginning of the experiment, then 50 μM NADH was introduced into the cell to give a 'control' current for normalising to other data sets. Further injection of NADH was performed to a final concentration of 300 μM NADH. Inhibitor containing the same final concentration of NADH was then introduced into the electrochemical cell to give concentrations as indicated by red arrows. The electrode was poised at -0.062 V vs SHE, and rotated at 2500 rpm. Experiments were performed at 30 ^{o}C, in a 50 mM Tris-HCl pH 8 buffer solution. Panels B and C show the Dixon and Cornish-Bowden plots to determine the inhibition constant and type of inhibition.

Inhibition constant for NAD^+ reduction

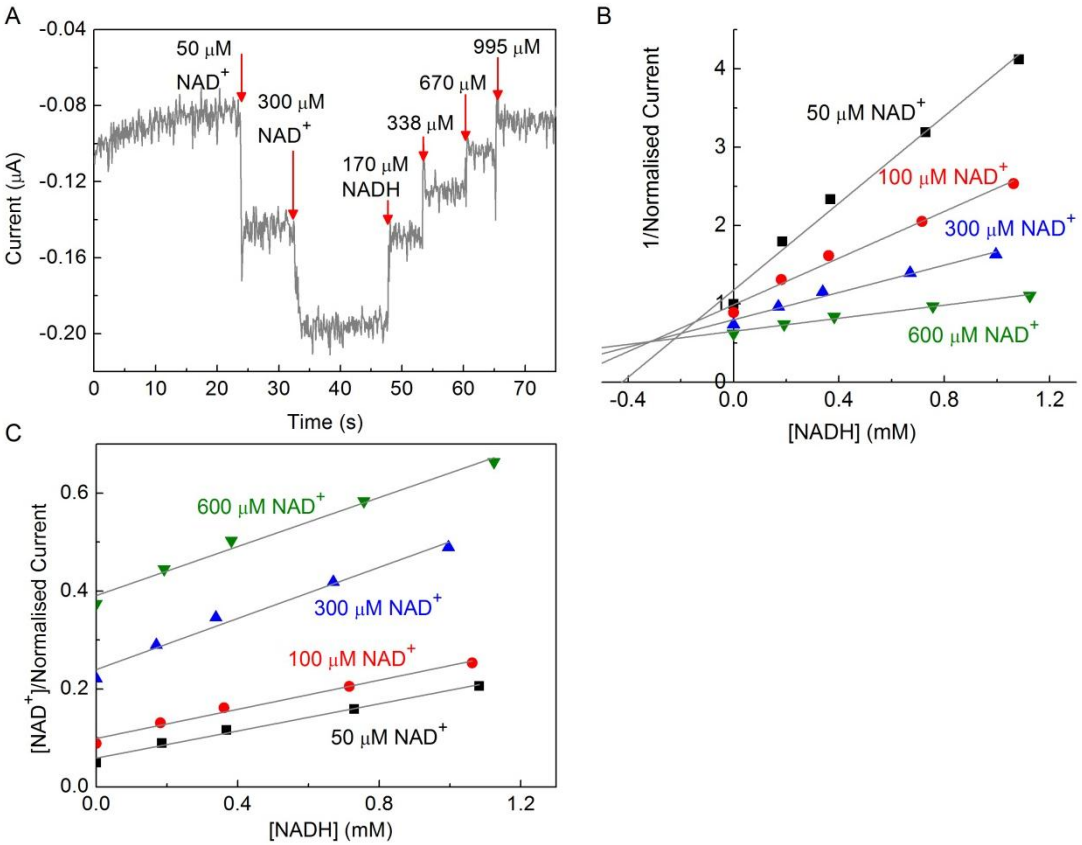

Figure 154. A. Current time plots from chronoamperometry experiments designed to determine the D326K HoxHYFU product inhibition constant for NAD^+ reduction. No NAD^+ was present at the beginning of the experiment, then 50 μM NAD^+ was introduced into the cell to give a 'control' current for normalising to other data sets. Further injection of NAD^+ was performed to a final concentration of 300 μM NAD^+. Inhibitor containing the same final concentration of NAD^+ was then introduced into the electrochemical cell to give concentrations as indicated by red arrows. The electrode was poised at -0.412 V vs SHE, and rotated at 2500 rpm. Experiments were performed at 30 ^oC, in a 50 mM Tris-HCl pH 8 buffer solution. Panels B and C show the Dixon and Cornish-Bowden plots to determine the inhibition constant and type of inhibition.

Appendix 4

Electrochemical results of HoxHYFU D401K D340A

NADH oxidation and NAD^+ reduction by D401K D340A HoxHYFU on an electrode.

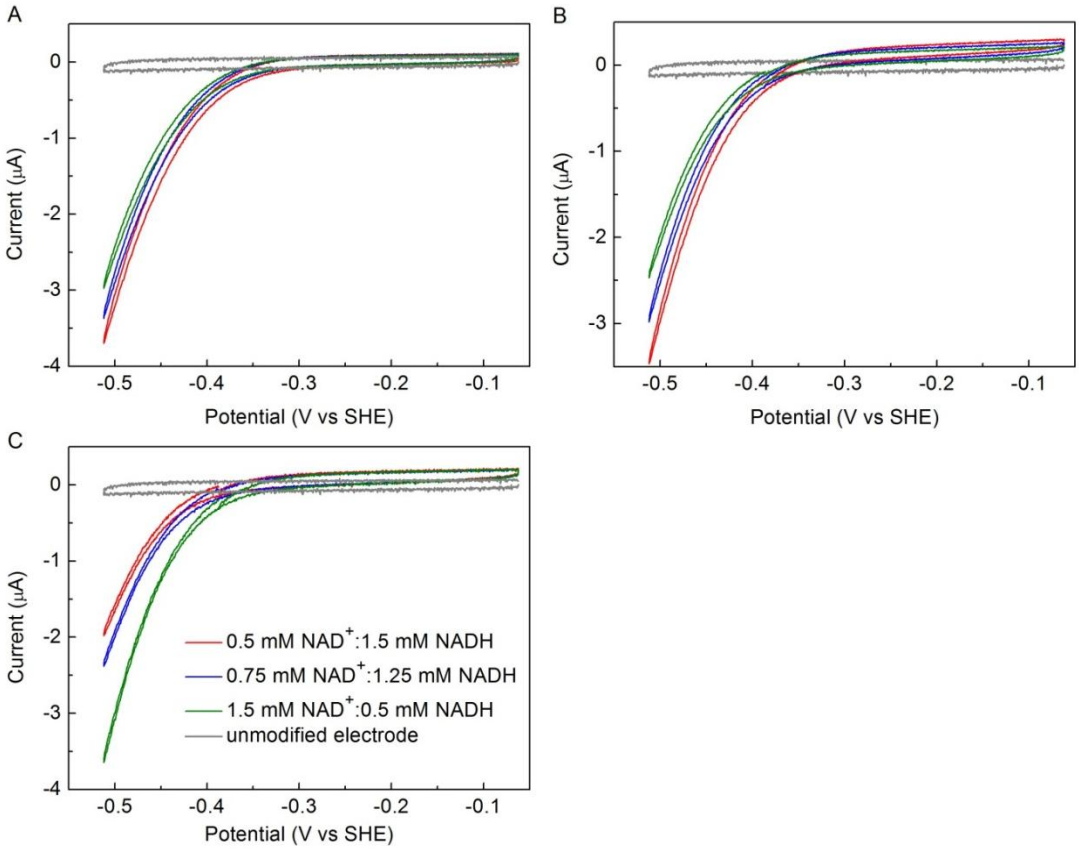

Figure 155. Electrocatalytic NAD^+ reduction and NADH oxidation by D401K D340A HoxHYFU variant. Experiments in panels A and B were performed in a solution of 2 mM NAD^+ and 1 mM NADH: 1 mM NAD^+ respectively. Panel C shows cyclic voltammograms of D401K D340A HoxHYFU variant in a mixture of NAD^+ and NADH, the concentrations used are as labelled in the figure. Other conditions: Tris-HCl buffer 50 mM, pH 8.0, 30 ^oC, electrode was rotated at 2500 rpm, scan rate 10 mV/s.

Low potential inactivation observed for D401K D340A

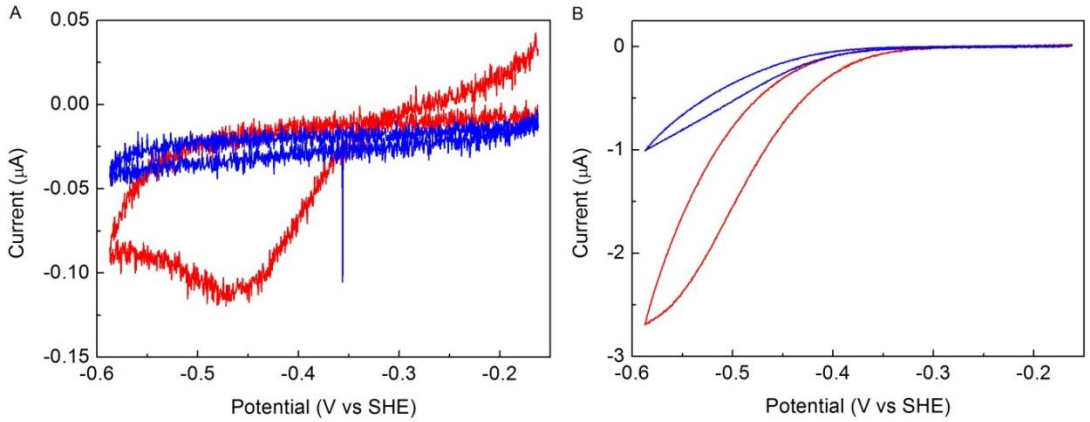

Figure 156. Cyclic voltammetry experiments to check for low potential inactivation by D401K D340A HoxHYFU variant at different NAD^+ concentrations: 50 µM NAD^+ (A) and 2 mM NAD^+ (B). Experimental conditions: Tris-HCl buffer 50 mM at pH 8.0, 30 ^oC. The experiments were performed at a slow scan rate of 1 mV/s while the electrode was rotated at 2500 rpm. The first cycle of each scan is shown as a red line and the second cycle is shown as a blue line.

Michaelis-Menten constant for NAD^+

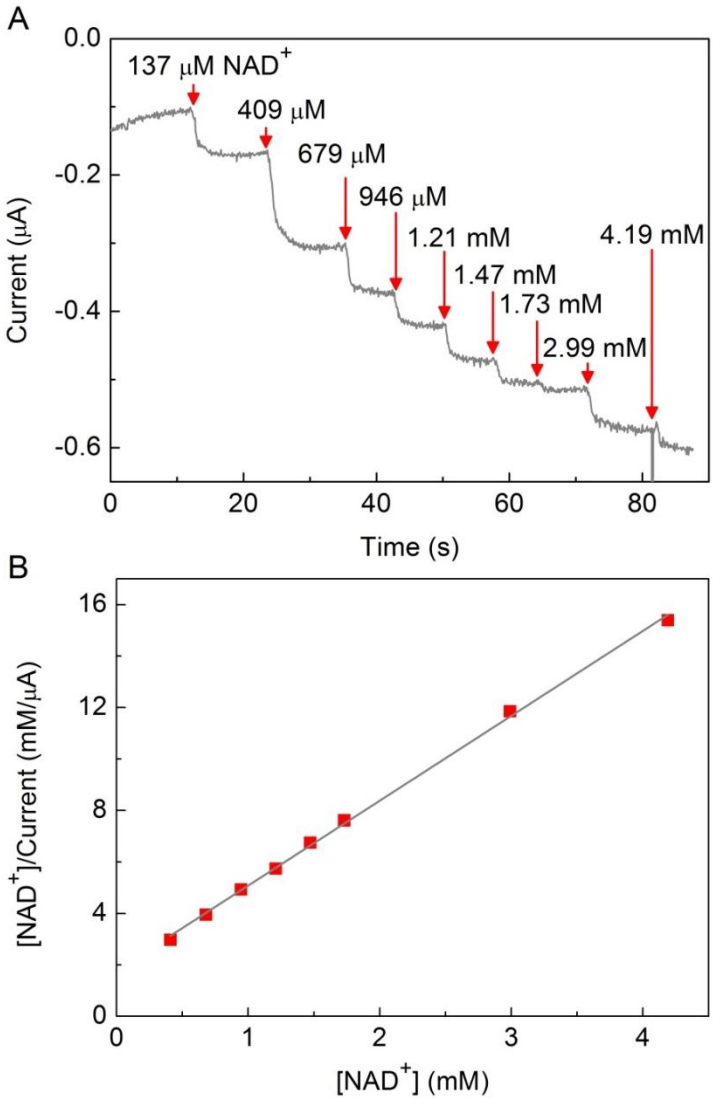

Figure 157. Panel A shows a typical chronoamperometry experiment designed to determine the D401K D340A HoxHYFU variant affinity constant for NAD^+. The experiment was performed in a 50 mM Tris-HCl buffer, pH 8.0, titrated to 30 ^oC and the electrode was poised at -0.412 V and rotated at 2500 rpm. In panel B, a typical Hanes-Woolf plot is shown.

Michaelis-Menten constant for NADH

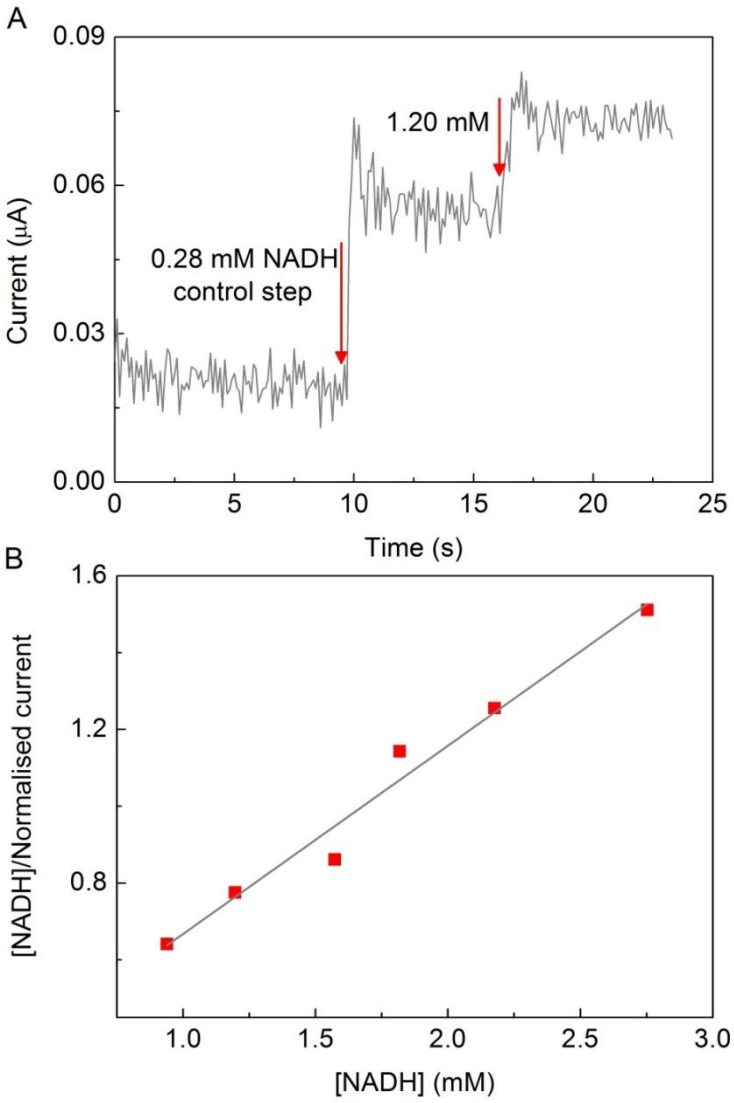

Figure 158. Panel A shows a typical chronoamperometry experiment designed to determine the D401K D340A HoxHYFU variant affinity constant for NADH. The experiment was performed in a 50 mM Tris-HCl buffer, pH 8.0, titrated to 30 ^{o}C and the electrode was poised at -0.063 V and rotated at 2500 rpm. In panel B, a typical Hanes-Woolf plot is shown.

Michaelis-Menten constant for $NADP^+$

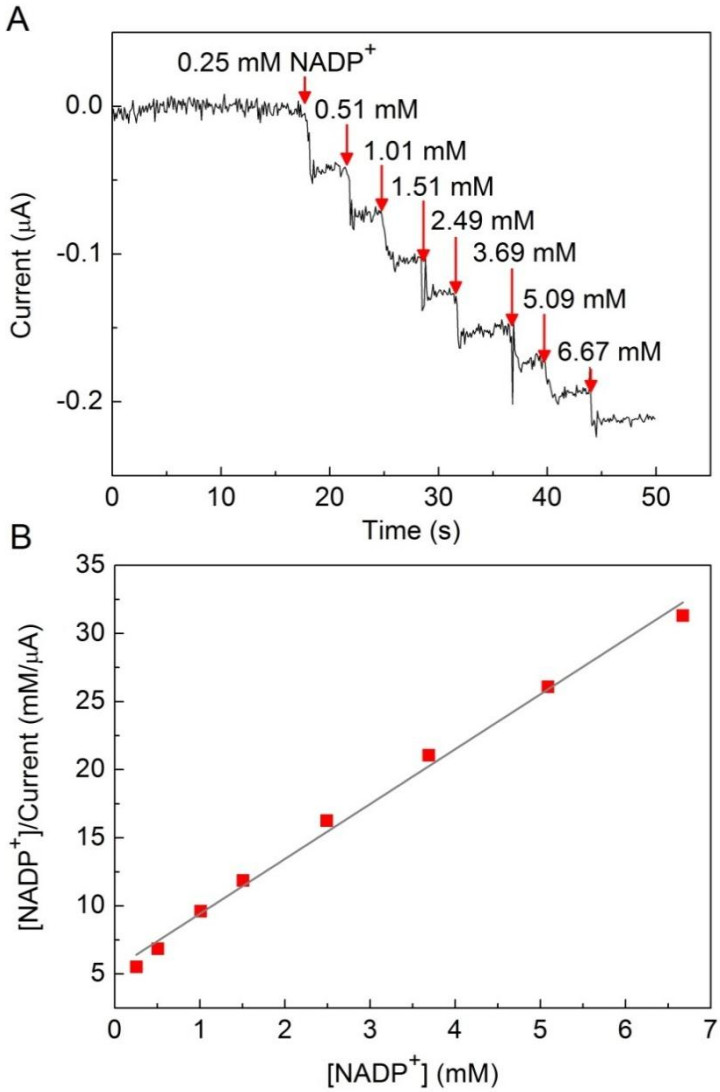

Figure 159. Panel A shows a typical chronoamperometry experiment designed to determine the D401K D340A HoxHYFU variant affinity constant for $NADP^+$. The experiment was performed in a 50 mM Tris-HCl buffer, pH 8.0, titrated to 30 ^oC and the electrode was poised at -0.412 V and rotated at 2500 rpm. In panel B, a typical Hanes-Woolf plot is shown.

Inhibition constant for NADH oxidation

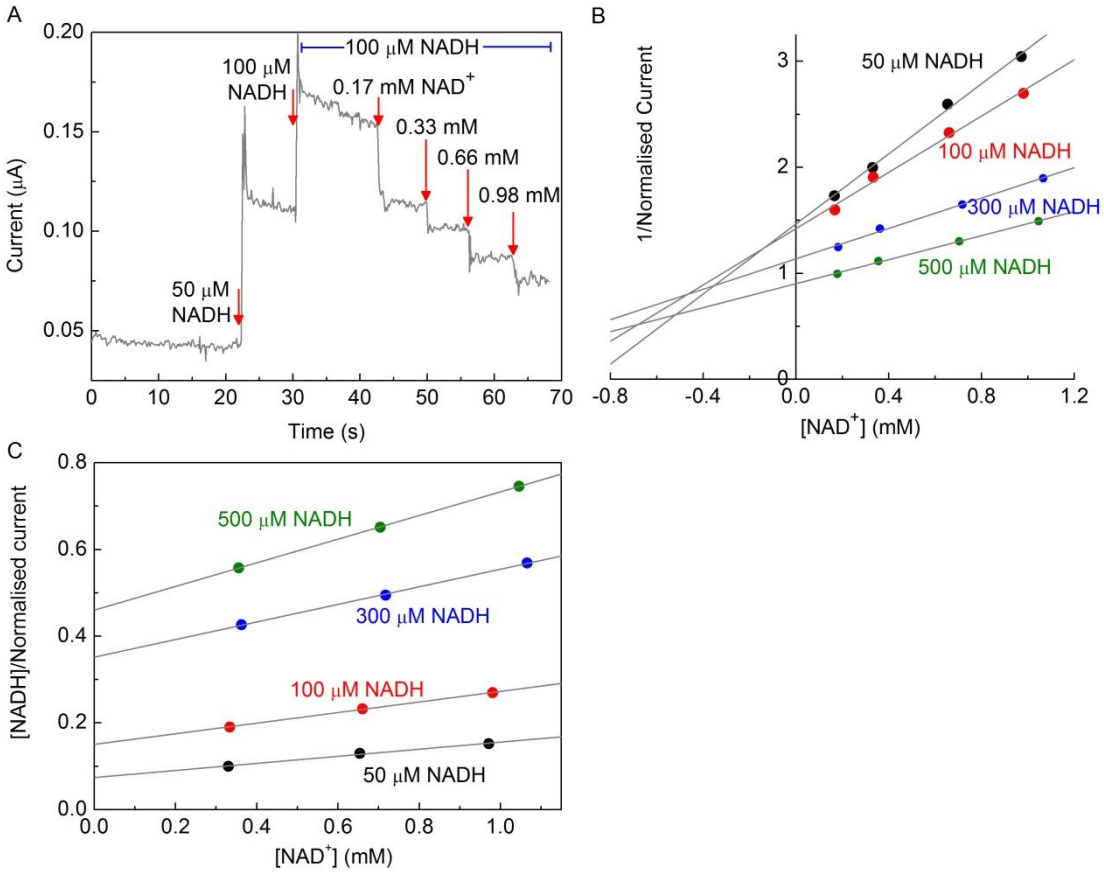

Figure 160. A. Current time plots from chronoamperometry experiments designed to determine the D401K D340A HoxHYFU product inhibition constant for NADH oxidation. No NADH was present at the beginning of the experiment, then 50 μM NADH was introduced into the cell to give a 'control' current for normalising to other data sets. Further injection of NADH was performed to a final concentration of 100 μM NADH. Inhibitor containing the same final concentration of NADH was then introduced into the electrochemical cell to give concentrations as indicated by red arrows. The electrode was poised at -0.062 V vs SHE, and rotated at 2500 rpm. Experiments were performed at 30 ^{o}C, in a 50 mM Tris-HCl pH 8 buffer solution. Panels B and C show the Dixon and Cornish-Bowden plots to determine the inhibition constant and type of inhibition.

Inhibition constant for NAD^+ reduction

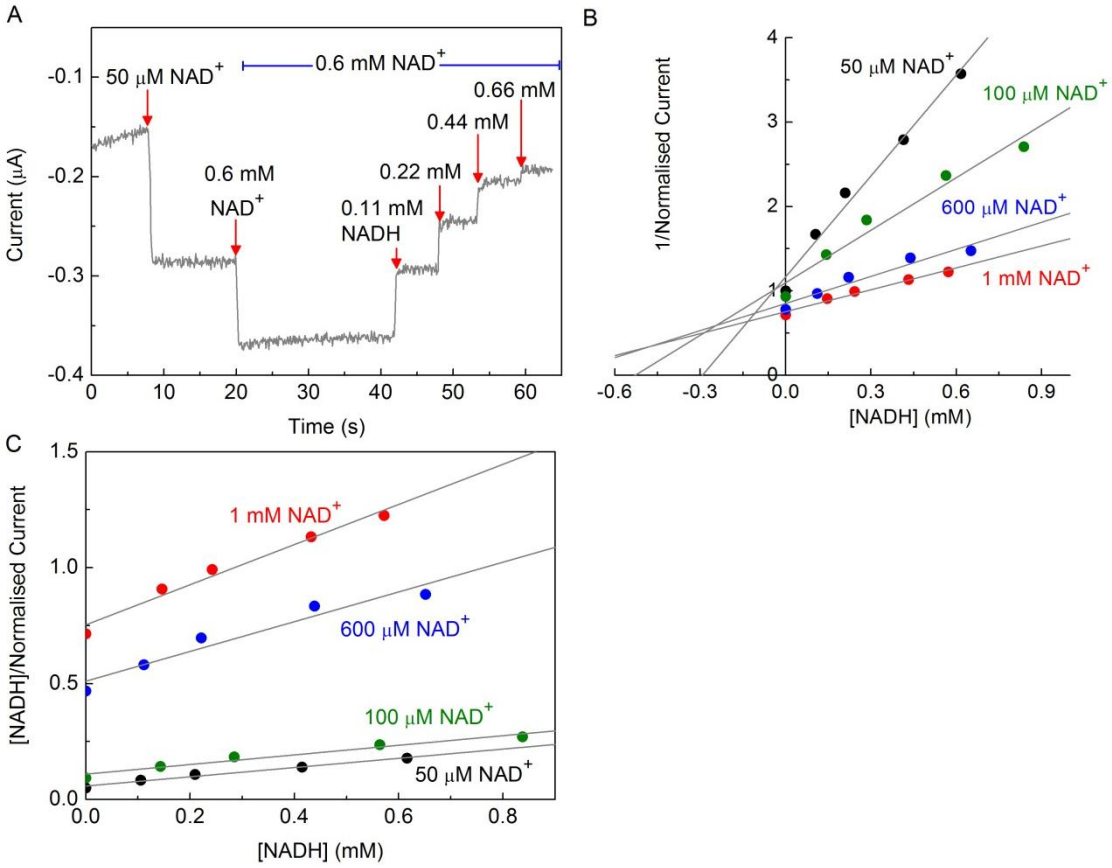

Figure 161. A. Current time plots from chronoamperometry experiments designed to determine the D401K D340A HoxHYFU product inhibition constant for NAD^+ reduction. No NAD^+ was present at the beginning of the experiment, then 50 μM NAD^+ was introduced into the cell to give a 'control' current for normalising to other data sets. Further injection of NAD^+ was performed to a final concentration of 0.6 mM NAD^+. Inhibitor containing the same final concentration of NAD^+ was then introduced into the electrochemical cell to give concentrations as indicated by red arrows. The electrode was poised at -0.412 V vs SHE, and rotated at 2500 rpm. Experiments were performed at 30 ^oC, in a 50 mM Tris-HCl pH 8 buffer solution. Panels B and C show the Dixon and Cornish-Bowden plots to determine the inhibition constant and type of inhibition.